

# **Rydberg-dressed Bose-Einstein condensates**

DISSERTATION

zur Erlangung des akademischen Grades

Doctor rerum naturalium  
(Dr. rer. nat.)

vorgelegt

der Fakultät Mathematik und Naturwissenschaften  
der Technischen Universität Dresden

von

Nils Henkel

aus Bad Lauterberg im Harz  
geboren am 11.07.1983 in Osterode am Harz

**Eingereicht am 17.01.2013**

Eingereicht am 17.01.2013

1. Gutachter: Prof. Dr. Jan-Michael Rost
2. Gutachter: Prof. Dr. Walter T. Strunz

Verteidigt am 10.12.2013

# Contents

<b>1. Introduction</b>	<b>1</b>
<b>2. Ultracold gases and Bose-Einstein condensates</b>	<b>5</b>
2.1. Bose-Einstein condensation of a homogeneous gas . . . . .	5
2.2. Experimental preparation of ultra-cold atomic gases and BECs . . . . .	6
2.3. Mean-field approximation and Gross-Pitaevskii equation . . . . .	8
2.3.1. First Born approximation . . . . .	10
2.3.2. Second Born approximation for short-range interactions . . . . .	10
2.3.3. Combination of different interactions . . . . .	14
2.3.4. Thermodynamic limit . . . . .	15
2.4. Bogoliubov excitation spectrum . . . . .	15
2.5. Superfluidity . . . . .	18
<b>3. Rydberg atoms and their interaction</b>	<b>21</b>
3.1. Rydberg states and their energies . . . . .	21
3.1.1. The hydrogen atom . . . . .	22
3.1.2. Alkali atoms . . . . .	23
3.2. Calculation of the interaction between alkali atoms . . . . .	24
3.2.1. Dipole approximation . . . . .	25
3.2.2. Minimal example: a three-state atom . . . . .	26
3.2.3. The physically realistic situation . . . . .	29
3.2.4. Application to Rubidium . . . . .	33
<b>4. Rydberg dressing</b>	<b>39</b>
4.1. Setup . . . . .	39
4.2. Dressing to non-degenerate states . . . . .	39
4.2.1. Interaction between a two-level atom and a laser . . . . .	40
4.2.2. The rotating wave approximation . . . . .	41
4.2.3. Reduction of a three-level atom to two levels . . . . .	43
4.2.4. Two-atom dressing scheme, Born-Oppenheimer approximation . . . . .	48
4.2.5. Dressing interaction between many atoms . . . . .	51
4.2.6. The lifetime of a dressed state . . . . .	56
4.2.7. Validity of the perturbation expansion . . . . .	58
4.3. Dressing to degenerate states . . . . .	59
4.4. Length and energy scaling . . . . .	60
4.4.1. Non-degenerate states . . . . .	61
4.4.2. Degenerate states . . . . .	63
<b>5. Supersolids in a dressed gas</b>	<b>65</b>
5.1. Dressing to Rubidium-87 $s$ -states . . . . .	66

5.2.	Bogoliubov-spectrum and Roton instability . . . . .	67
5.3.	Supersolid ground states . . . . .	71
5.4.	Time evolution . . . . .	75
5.5.	Beyond mean-field . . . . .	79
5.5.1.	Calculation of superfluidity: Monte-Carlo and mean-field . . . . .	80
5.5.2.	Comparison between Monte-Carlo and mean-field results . . . . .	82
5.5.3.	Validity of the mean-field approximation . . . . .	83
5.5.4.	The physical mechanism of supersolidity . . . . .	85
5.6.	Supersolid crystals and Abrikosov lattices in rotating dressed gases . . . . .	85
<b>6.</b>	<b>Solitons and matter-wave bullets of a dressed-gas</b>	<b>91</b>
6.1.	Self-trapping and collapse-instability . . . . .	92
6.2.	Physical realization of an attractive dressing-interaction . . . . .	95
6.3.	Self-trapped ground states . . . . .	96
6.4.	Anisotropy of trapped states . . . . .	100
6.5.	Physical mechanism of self-trapping . . . . .	102
6.6.	Soliton robustness . . . . .	104
<b>7.</b>	<b>Rydberg-dressing beyond perturbation theory</b>	<b>107</b>
7.1.	Higher-order perturbation theory terms . . . . .	108
7.2.	The Born-Oppenheimer approximation beyond perturbation theory . . . . .	110
7.3.	Application to self-trapping . . . . .	112
7.3.1.	Interaction energy of a BEC . . . . .	113
7.3.2.	Variational method for minimization of the energy . . . . .	117
7.4.	Modification of the self-trapping condition . . . . .	118
7.5.	Implications for experiments . . . . .	120
<b>8.</b>	<b>Conclusions</b>	<b>123</b>
<b>A.</b>	<b>Solving the Gross-Pitaevskii equation on a discrete spatial grid</b>	<b>129</b>
A.1.	Split-operator method . . . . .	129
A.2.	Mean-field potential, convolution theorem and periodicity . . . . .	130
A.3.	Generalization to rotating systems . . . . .	132
A.4.	Imaginary time evolution . . . . .	134
<b>B.</b>	<b>Clebsch-Gordan coefficients</b>	<b>137</b>
<b>C.</b>	<b>Superfluidity</b>	<b>139</b>
C.1.	Leggett's estimator for rotating motion . . . . .	139
C.2.	Leggett's estimator for linear motion . . . . .	141
	<b>Bibliography</b>	<b>143</b>
	<b>Acknowledgements</b>	<b>161</b>

# 1. Introduction

Most of the atoms making up our everyday world exist in or close to their electronic ground state and therefore have sizes below one nanometer. However, laser technology allows the creation of highly excited atoms with large principal quantum numbers  $n$ . Since the extent of the electron orbit increases rapidly ( $\propto n^2$ ), such so-called Rydberg atoms can take on sizes in the micrometer-range. As a result, they have many fascinating properties that set them apart from ground state atoms. In particular, their high polarizability ( $\propto n^7$ ) makes them very sensitive to external fields and leads to enormous van-der-Waals interactions ( $\propto n^{11}$ ). For typical quantum numbers, the interaction strength exceeds that of ground-state atoms by more than 10 orders of magnitude. Due to these exotic properties, the physics of Rydberg atoms has attracted significant interest in many fields, ranging from quantum information science [96, 128, 175], non-linear quantum optics [78, 155, 158, 163, 180], molecular physics [15, 16, 35, 124], plasma physics [159, 196] and radio astronomy [75]. On the other hand, the high susceptibility to external fields makes them very fragile with respect to environmental perturbations which is why they rarely occur in nature except in very dilute and extremely cold environments such as interstellar space [75]. In fact, the largest Rydberg atom ever recorded ( $n \approx 1009$ ) has been observed via radio spectroscopy [185].

Recent experimental advances have made it possible to create conditions similar to interstellar space in laboratories by laser cooling atomic gases down to ultra-cold temperatures. This has made it possible to create Rydberg atoms on earth and make them the subject of targeted manipulation.

In particular, this thesis will be concerned with Rydberg atoms in the ultimate cold gas, a Bose-Einstein condensate (BEC). BECs are gases that are so close to absolute zero temperature that all of their particles reside in their motional ground state and all fluctuations, quantum and thermal alike, are negligible. The first BEC was created in 1995 [7], 70 years after its theoretical conjecture [58, 59], and for this breakthrough the Nobel Prize was awarded in 2001. In the years since, BECs have been widely studied and are now routinely created in many laboratories. Altogether, condensates of thirteen different elements have been created [4, 31, 48, 51, 66, 81, 112, 127, 143, 152, 184, 190, 200]. Generally, BECs of ground-state atoms interact via short-range  $s$ -wave scattering. However, since particle densities are low, the interactions are usually relatively weak. Thus, the possibility of strongly increasing the interaction strength by creating Feshbach resonances via magnetic fields [45, 94, 136] created a significant boost for the importance of the field. The stronger interactions enabled in this manner paved the way for the use of BECs as quantum simulators for several paradigmatic condensed matter phenomena, including the phase transition between superfluid and Mott insulator [79, 95], spinor system in optical lattices [52, 85] and the quantum Hall effect [203]. A drawback of the enhancement of interaction strengths via Feshbach resonances is the ensuing strong decrease of the condensate lifetime [61, 153]. An alternative approach that avoids this is the confinement of a BEC in an optical lattice [22, 23]. This has led to a number of inter-

esting observations, such as a Kosterlitz-Thouless crossover [87] and a Tonks-Girardeau gas [105, 148, 150, 154] in a one-dimensional quasi-BEC.

Additional perspectives arise if it is possible to introduce longer-range interactions into a BEC. Many interesting systems in the field of condensed matter are governed by such interactions. Hence, a long-range interacting BEC would make an even better quantum simulator than a short-range interacting BEC in an optical lattice. This is where Rydberg atoms come in as suitable sources of a long-range interaction. The investigation of Bose-Einstein condensates with Rydberg-induced long-range interactions constitutes the main part of this thesis.

### Outline

In chapter 2, a short textbook level introduction into the theory of Bose-Einstein condensation will be given, including the description of dynamics in BECs. In chapter 3, Rydberg atoms will be discussed. In particular, it will be shown how the strong van-der-Waals interaction comes about and it will be calculated numerically for the  $s$ -,  $p$ - and  $d$ -Rydberg states of Rubidium.

In chapter 4, our proposal of how to use Rydberg atoms in order to create a long-range interacting BEC will be introduced. The idea consists in the off-resonant coupling of the atomic ground-state to a Rydberg state, a so-called “Rydberg dressing” scheme. This admixes a small fraction of Rydberg character to the new dressed ground-state [91, 177]. We will show by many-body perturbation theory that the scheme leads to the emergence of a new ground-state interaction which is van-der-Waals like at large distances but converges to a finite value for small distances. This is a consequence of the so-called interaction blockade [96, 128]: when two or more atoms are very close, the mutual van-der-Waals interaction between their Rydberg states makes it impossible to excite more than one of them since all multiply excited many-body states are shifted far out of resonance with the exciting laser. Hence, atoms become non-interacting below a certain blockade radius. In our Rydberg dressing scheme, this blockade radius is also the characteristic length scale of the interaction and is typically on the order of micrometers. The particle density in typical BECs is on the order of  $10^{19} - 10^{20} \text{ m}^{-3}$ , implying an interparticle distance that is also on the order of micrometers. Hence, the interaction cannot be approximated as a short-range scattering interaction.

Since only a small fraction of Rydberg character is admixed, the dressed ground-state has a lifetime sufficiently long so that decay is negligible on the typical timescale of the atomic dynamics.

The peculiar form of the interaction has a number of interesting implications for the motional degrees of freedom of the atoms and the atomic dynamics which will be discussed in the subsequent chapters.

In chapter 5, we will demonstrate that a repulsive dressing interaction induces a roton

---

instability of the dressed BEC. This leads to the dynamical creation of so-called supersolid states. A supersolid is an exotic state of matter which was first conjectured 40 years ago [10, 37]. It is a state of matter that is, at the same time, superfluid and solid. These two properties seem antithetic since they imply that the atoms making up the supersolid must simultaneously provide the rigidity of the solid state, yet must also be highly mobile in order to induce superfluidity. After its conjecture, supersolidity has been pursued intensively, mostly in the context of solid helium. The history of the pursuit was volatile. Early experiments showed no supersolidity [9, 20, 57, 80, 140, 189, 193]. This changed in 2004, with experiments suggesting that a supersolid ground state might indeed exist [38, 102–104]. Theoretical evidence, on the other hand, continually rejected the supersolidity of the helium ground-state [27]. Recently, a new experiment [101] showed that the previously claimed supersolidity was in error. Hence, the theoretical and experimental evidence now suggests that helium is, indeed, not supersolid. This makes the dressed gas even more important as an alternative candidate system where supersolidity may be realized. There is now already considerable interest in the experimental validation of our predictions.

Another long-sought-after phenomenon, namely a matter-wave bullet, can be found in an attractive dressed BEC. A matter-wave bullet, the matter-equivalent of a light-bullet is defined as a three-dimensional self-trapped soliton, i.e., a state that remains confined despite diffraction solely due to its internal interaction. Solitons in general have fascinated researchers since 1834, when Russel observed a solitary water wave traveling through a canal [174]. The experimental creation of true three-dimensional light- or matter-wave bullets have remained elusive.

The main problem in the creation of solitons and self-trapped states lies in the properties of typical interactions. They are either too weak or they diverge strongly at low distances which leads to the collapse of the BEC to a single point. In contrast, the dressing interaction does not lead to collapse, due to its soft core.

In the final chapter 7, we will go beyond the perturbation theory of chapter 4 and explore many-body effects of the dressing scheme. These begin to manifest themselves due to the inherent many-body nature of the interaction blockade when the density of Rydberg excitations becomes too high. In this regime, the interaction can no longer be expressed as a sum of binary interactions but contains three-body and higher contributions. Such true many-body interactions are of high fundamental interest [34, 179]. Furthermore, it is important to check whether the many-body contributions jeopardize self-trapping at stronger dressing. Finally, the method developed there can be used to check the validity of the perturbative calculation.



## 2. Ultracold gases and Bose-Einstein condensates

A Bose-Einstein condensate (BEC) is a state of matter of bosons (i.e., particles with integer spin) below a critical temperature  $T_c$  (in typical experiments on the order of 100nK, as we will see), where a macroscopic number of particles populates the ground state. It is named after its discoverers Satyendra Nath Bose and Albert Einstein. In 1924, Bose was the first to find a derivation of Planck's law on black body radiation in thermal equilibrium that did not rely on classical arguments [30]. His idea was extended by Einstein from photons to massive particles [59], leading to the prediction of the phenomenon that is now known as Bose-Einstein condensation.

### 2.1. Bose-Einstein condensation of a homogeneous gas

A gas of non-interacting bosonic particles with the density  $\rho$ , the chemical potential  $\mu$  and the inverse temperature  $\beta = 1/k_B T$  obeys the Bose-Einstein distribution [157]

$$N(\mathbf{k}) = \frac{1}{\exp(\beta(\varepsilon(\mathbf{k}) - \mu)) - 1}, \quad (2.1)$$

where the momentum  $\mathbf{k}$  labels the one-particle eigenstates that each particle can reside in, and their energies are

$$\varepsilon(\mathbf{k}) = \frac{\hbar^2 k^2}{2m}. \quad (2.2)$$

The average density of particles in the momentum space region  $V$  is

$$\rho_V = \int_V \frac{d^3k}{(2\pi)^3} N(\mathbf{k}). \quad (2.3)$$

For  $\mu = 0$ , the total density of the gas can be calculated analytically:

$$\rho = \int_{\mathbb{R}^3} \frac{d^3k}{(2\pi)^3} \frac{1}{\exp\left(\frac{\hbar^2 k^2}{2mT}\right) - 1} = \left(\frac{mT}{2\pi\hbar^2}\right)^{\frac{3}{2}} \underbrace{\zeta\left(\frac{3}{2}\right)}_{\approx 2.612}. \quad (2.4)$$

For a strictly negative chemical potential  $\mu < 0$ , the density would be smaller than this. Therefore, and since  $\mu$  is non-positive for bosons, the lowest temperature that can be reached for a gas of the density  $\rho$ , is the so-called critical temperature for Bose-Einstein

condensation

$$T_c = \left( \frac{\rho_0}{\zeta\left(\frac{3}{2}\right)} \right)^{\frac{2}{3}} \frac{2\pi\hbar^2}{m} \approx 3.313 \frac{\hbar^2 \rho^{\frac{2}{3}}}{m}. \quad (2.5)$$

When trying to cool a gas below  $T_c$ , a macroscopic number of particles condenses into the ground state [58,59] and the rest of the particles remains in a thermal cloud with the temperature  $T_c$ . The thermal cloud is still governed by the Bose-Einstein distribution (2.1). The condensate fraction, i.e., the fraction of particles in the condensate, is

$$f_c(T) = 1 - \left( \frac{T}{T_c} \right)^{3/2}, \quad (2.6)$$

for  $T \leq T_c$ .  $f_c$  can be used as an order parameter of the phase transition from an ideal Bose gas to a Bose-Einstein condensate.

A different way of expressing the condensation condition given by Eq. (2.5) is by defining the thermal de Broglie wavelength

$$\Lambda = \sqrt{\frac{2\pi}{mk_B T}} \hbar \quad (2.7)$$

and the phase space density

$$\rho_{\text{PS}} = \rho \Lambda^3. \quad (2.8)$$

Then, Eq. (2.5) is equivalent to

$$\rho_{\text{PS}} \geq \zeta\left(\frac{3}{2}\right) \approx 2.6124. \quad (2.9)$$

In real gases, the critical temperature often significantly deviates from this due to the presence of interactions [11, 99, 183].

## 2.2. Experimental preparation of ultra-cold atomic gases and BECs

Every scientific theory has to be judged according to how well it describes the real world. In the words of Richard Feynman [63]:

It does not make any difference how beautiful your guess is. It does not make any difference how smart you are, who made the guess, or what his name is – if it disagrees with experiment it is wrong.

In this spirit, we will try to make predictions that can be verified with current experimental capabilities. Nevertheless, this thesis is a theoretical work and only very little will be said about experimental methods. The rest of this section will contain a brief

overview over the route to the creation of BECs and the necessary techniques [100]. Since condensation is only expected to occur at extremely low temperatures, efficient cooling techniques are tremendously important. The two most important techniques are laser cooling (more specifically: Doppler cooling and sub-Doppler cooling<sup>1</sup> and evaporative cooling. Doppler cooling utilizes two collinear lasers of the same frequency in opposite directions, creating a standing wave. They are slightly red-detuned with respect to a suitable atomic transition, i.e., the laser frequency is lower than the transition frequency  $\omega_a$ . Thus, an atom moving towards one of the lasers will, through the Doppler shift affecting  $\omega_a$ , have a higher probability of getting excited by this laser than by the opposite one. Hence, every moving atom will on average experience a force slowing its motion, leading to a lower temperature. The Doppler cooling limit is given by  $T_D = \hbar\gamma/2k_B$ , where  $\gamma$  is the line-width of the used transition. For alkali atoms,  $T_D$  is typically on the order of  $100\ \mu\text{K}$  [47].

While  $T_D$  had been accepted as the minimum temperature achievable by laser cooling for some time, it was later observed that there are possibilities to go below this limit via Sisyphus cooling [122], an effect that is now well-understood [47]. The lowest temperature thus achievable is the recoil energy of an atom absorbing a single photon which is on the order of a few  $\mu\text{K}$ . While this is a significant improvement over Doppler cooling it is not yet sufficient to reach Bose-Einstein condensation.

To this end, additional evaporative cooling [47] is necessary. In this method, fast atoms are selectively removed by slowly lowering the strength of the trapping potential. Thus, only those atoms with small kinetic energy remain, leading to a lower temperature of the remaining gas.

Even well after these techniques were known, the experimental creation of a BEC was still seen by many as a goal that might forever remain elusive [191]. It had been believed that, as a gas is cooled down, Bose-Einstein condensation would always be preempted by the transition to a solid or liquid. This transition occurs because of inelastic three-body collisions, where two particles form a bound state and the third particle carries away the excess energy. In principle, the three-body collision rate can be decreased by reducing the density of the gas so that the transition time can be scaled up to values on the order of seconds or minutes [100]. Then, in principle, the BEC could exist as a metastable state. However, there are two problems: First, according to Eq. (2.5) the reduction of the density also reduces the critical temperature. Second, evaporative cooling relies heavily on two-body collisions which also become less frequent as the density decreases. It was by far not evident that any system exists where a temperature and density could be achieved that suffice for condensation but where, at the same time, the usual transition to a solid is inhibited.

The question was finally answered in 1995 with the creation of the first BEC in a  $^{87}\text{Rb}$ -gas at a temperature of  $T = 170\text{nK}$  [7]. For this achievement, Wolfgang Ketterle, Eric Cornell and Carl Wieman were awarded the Nobel prize in 2001.

In the years since this first realization, BECs have been created in twelve more atomic

---

<sup>1</sup>also known as Sisyphus cooling

species: Lithium [31], Sodium [48], Hydrogen [66], Potassium [143], Helium [152], Cesium [200], Ytterbium [190], Chromium [81], Calcium [112], Strontium [51,184], Dysprosium [127] and Erbium [4]. Recently, condensation of photons in a cavity has also been achieved [108], closing the circle to Planck's law whence the whole theory originated.

### 2.3. Mean-field approximation and Gross-Pitaevskii equation

Solving a full  $N$ -body Schrödinger equation (SE) is numerically very demanding. However, in many dilute gases, the SE can be well approximated by a so-called mean-field (MF) approximation. Therein, the  $N$ -body system is described in a one-particle picture with an effective potential (the “mean-field potential”). We will start by deriving the first Born approximation which is valid for weak interactions. Then, we will move to a description of realistic potentials between ground state atoms. These are short-ranged but very strong at small distances so that the first Born approximation is invalid. Nevertheless, a dilute gas with those interactions can still be described in a one-particle picture if the short-range correlations are taken into account. This is done in the second Born approximation, by solving the two-body SE describing a two-body scattering process. We start from the Hamiltonian in second quantization,

$$\hat{H} = \hat{H}_1 + \hat{W} \quad (2.10)$$

$$= \int d^3r \hat{\Psi}^\dagger(\mathbf{r}) H_1(\mathbf{r}) \hat{\Psi}(\mathbf{r}) + \int d^3r \int d^3r' \hat{\Psi}^\dagger(\mathbf{r}) \hat{\Psi}^\dagger(\mathbf{r}') W(\mathbf{r} - \mathbf{r}') \hat{\Psi}(\mathbf{r}') \hat{\Psi}(\mathbf{r}), \quad (2.11)$$

where

$$H_1(\mathbf{r}) = -\frac{\hbar^2}{2m} \nabla^2 + V_{\text{ext}}(\mathbf{r}) \quad (2.12)$$

is a one-body term including the kinetic energy and external potential.  $W$  is a two-body interaction, i.e., it depends only on the relative positions of all particle pairs. The time evolution is described by the Heisenberg equation for the field operator:

$$i\hbar\partial_t \hat{\Psi}(\mathbf{r}) = [\hat{\Psi}(\mathbf{r}), \hat{H}] \quad (2.13)$$

$$= \left( H_1(\mathbf{r}) + \int d^3r' \hat{\Psi}^\dagger(\mathbf{r}') W(\mathbf{r} - \mathbf{r}') \hat{\Psi}(\mathbf{r}') \right) \hat{\Psi}(\mathbf{r}, t) \quad (2.14)$$

In order to derive the mean-field approximation, we apply the Bogoliubov ansatz [172]

$$\hat{\Psi}(\mathbf{r}) = \sqrt{N} \psi(\mathbf{r}) + \hat{\varphi}(\mathbf{r}), \quad (2.15)$$

where  $\psi(\mathbf{r}) = \langle \hat{\Psi}(\mathbf{r}) \rangle$  is the so-called condensate wave-function, a classical field that (in its simplest interpretation which is justified for very weak interactions) represents the

wave-function that every single particle in the BEC resides in. It is normalized to

$$\langle \psi | \psi \rangle = \int d^3r |\psi(\mathbf{r})|^2 = 1. \quad (2.16)$$

$\hat{\varphi}(\mathbf{r})$  describes fluctuations and vanishes on average:  $\langle \hat{\varphi}(\mathbf{r}) \rangle = 0$ . We insert this into Eq. (2.14) and then form the expectation value of both sides:

$$i\hbar\partial_t\psi(\mathbf{r}) = H_1(\mathbf{r})\psi(\mathbf{r}) + \int d^3r' W(\mathbf{r} - \mathbf{r}') \langle \hat{\Psi}^\dagger(\mathbf{r}') \hat{\Psi}(\mathbf{r}') \hat{\Psi}(\mathbf{r}) \rangle \quad (2.17)$$

$$\begin{aligned} &= H_1(\mathbf{r})\psi(\mathbf{r}) + \int d^3r' W(\mathbf{r} - \mathbf{r}') \left( N|\psi(\mathbf{r}')|^2\psi(\mathbf{r}) + \overline{\psi(\mathbf{r}')} \langle \hat{\varphi}(\mathbf{r}') \hat{\varphi}(\mathbf{r}) \rangle \right. \\ &\quad \left. + \psi(\mathbf{r}') \langle \hat{\varphi}^\dagger(\mathbf{r}') \hat{\varphi}(\mathbf{r}) \rangle + \psi(\mathbf{r}) \langle \hat{\varphi}^\dagger(\mathbf{r}') \hat{\varphi}(\mathbf{r}') \rangle + \langle \hat{\varphi}^\dagger(\mathbf{r}') \hat{\varphi}(\mathbf{r}') \hat{\varphi}(\mathbf{r}) \rangle \right) \end{aligned} \quad (2.18)$$

$$\begin{aligned} &= \left( H_1(\mathbf{r}) + \int d^3r' W(\mathbf{r} - \mathbf{r}') \left( N|\psi(\mathbf{r}')|^2 + \langle \hat{\varphi}^\dagger(\mathbf{r}') \hat{\varphi}(\mathbf{r}') \rangle \right) \right) \psi(\mathbf{r}) \\ &\quad + \int d^3r' W(\mathbf{r} - \mathbf{r}') \left( \overline{\psi(\mathbf{r}')} \langle \hat{\varphi}(\mathbf{r}') \hat{\varphi}(\mathbf{r}) \rangle + \psi(\mathbf{r}') \langle \hat{\varphi}^\dagger(\mathbf{r}') \hat{\varphi}(\mathbf{r}) \rangle \right) \\ &\quad + \int d^3r' W(\mathbf{r} - \mathbf{r}') \langle \hat{\varphi}^\dagger(\mathbf{r}') \hat{\varphi}(\mathbf{r}') \hat{\varphi}(\mathbf{r}) \rangle. \end{aligned} \quad (2.19)$$

In the Popov approximation [82], the “anomalous” term involving  $\langle \hat{\varphi}(\mathbf{r}') \hat{\varphi}(\mathbf{r}) \rangle$  is neglected. Since fluctuations are small, we can also neglect the term that is cubic in  $\hat{\varphi}$ . Thus, we find

$$\begin{aligned} i\hbar\partial_t\psi(\mathbf{r}) &= \left( H_1(\mathbf{r}) + \int d^3r' W(\mathbf{r} - \mathbf{r}') \left( \rho_c(\mathbf{r}') + \rho_f(\mathbf{r}', \mathbf{r}') \right) \right) \psi(\mathbf{r}) \\ &\quad + \int d^3r' W(\mathbf{r} - \mathbf{r}') \psi(\mathbf{r}') \rho_f(\mathbf{r}', \mathbf{r}). \end{aligned} \quad (2.20)$$

$\rho_f(\mathbf{r}', \mathbf{r}) = \langle \hat{\varphi}^\dagger(\mathbf{r}') \hat{\varphi}(\mathbf{r}) \rangle$  is the one-particle density matrix of the non-condensate part of the system and  $\rho_c(\mathbf{r}) = N|\psi(\mathbf{r})|^2$  is the one-particle density of the condensate.

A similar equation can be found for  $\hat{\varphi}(\mathbf{r})$ .

### 2.3.1. First Born approximation

In the first Born approximation, fluctuations are completely neglected, i.e.,  $\hat{\varphi} = 0$ . Therefore,  $\rho_f = 0$  and Eq. (2.20) is reduced to the single-particle equation

$$\left( -\frac{\hbar^2}{2m}\nabla^2 + V_{\text{ext}}(\mathbf{r}) + V_{MF}[\psi](\mathbf{r}) \right) \psi(\mathbf{r}) = i\hbar\partial_t\psi(\mathbf{r}) \quad (2.21)$$

which is known as the Hartree equation with the mean-field potential

$$V_{MF}[\psi](\mathbf{r}) = N \int d^3r' W(\mathbf{r} - \mathbf{r}') |\psi(\mathbf{r}')|^2. \quad (2.22)$$

The mean-field potential can easily be understood as the effective potential on the first particle, generated by all the other particles. The first Born approximation is valid as long as the temperature is very low and the interaction  $W$  is sufficiently weak to neglect correlations between the particles. However, the interactions between ground state atoms are very strong at short ranges and correlations become highly relevant. Therefore, Eq. (2.21) is not justified, even for dilute gases, and the second Born approximation is necessary in order to describe them.

### 2.3.2. Second Born approximation for short-range interactions

The interaction between ground state atoms is typically a very short-ranged and partially attractive (roughly Lennard-Jones-like) potential (see Fig. 2.1) which supports bound states.<sup>2</sup> Hence, as mentioned before, the BEC is not the ground state of an ensemble of atoms but only a meta-stable state which can be created for a finite time if the atoms in the gas phase are cooled quickly enough. This also means that the BEC cannot be described using the actual potential (any calculation of the ground state of the Hamiltonian with that interaction would yield a crystal). Furthermore, the interaction is too strong to be treated in the first Born approximation.

Both problems can be solved by using the second Born approximation for short-range interactions. Here, it is assumed that the interaction is very short-ranged compared to the typical inter-particle separation in the gas, i.e.  $r_m^3\rho \ll 1$ . Hence, the gas is so dilute that the interaction can be described purely by elastic two-body collisions, without the formation of bound states. In experimental situations where a BEC is actually formed, this condition is obviously fulfilled because it is necessary for the formation of the BEC (as we already discussed in section 2.3). We now derive the so-called Gross-Pitaevskii equation (GPE) that describes a gas with such interactions. We follow the outline in [157].

Since we assume that the gas is governed solely by elastic two-body collisions, we can describe it *exactly* (i.e., without invoking any mean-field approximation yet) by the

---

<sup>2</sup>This is the reason why the ground state of, e.g., Rubidium is a solid.

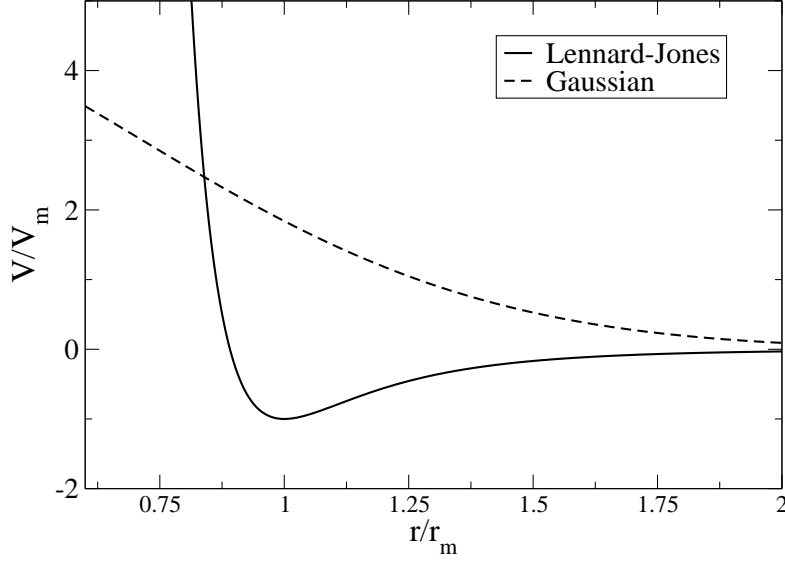


**Figure 2.1.:** Generic Lennard-Jones potential, supporting a bound state around  $r = r_m$  and a generic example for a Gaussian potential by which it can be approximated if bound states are not of interest. The first Born approximation is justified for the Gaussian potential, but not for the Lennard-Jones potential because of its high strength for  $r \rightarrow 0$ .

Schrödinger equation describing such two-body collisions. In relative coordinates  $\mathbf{r}$  with the reduced mass  $\mu = m/2$  the SE is

$$E\psi(\mathbf{r}) = \left(-\frac{\hbar^2}{2\mu}\nabla^2 + W(r)\right)\psi(\mathbf{r}) \quad (2.23)$$

$$\Leftrightarrow f_l''(r) + \frac{2}{r}f_l'(r) = \left(U(r) + \frac{l(l+1)}{r^2} - \varepsilon\right)f_l(r) \quad (2.24)$$

where  $\psi(\mathbf{r}) = f_l(r)Y_l^m(\vartheta, \varphi)$ ,  $\varepsilon = \frac{2\mu E}{\hbar^2}$  and  $U(r) = \frac{2\mu}{\hbar^2}W(r)$ .

Since we want to isolate the effect of the interaction, we need to compare the solution of this equation to that of the corresponding *non-interacting* SE

$$f_l''(r) + \frac{2}{r}f_l'(r) = \left(\frac{l(l+1)}{r^2} - k^2\right)f_l(r), \quad (2.25)$$

which can be transformed by  $s = kr$ ,  $f_l(r) = g_l(s)$  to

$$g_l''(s) + \frac{2}{s}g_l'(s) = \left(\frac{l(l+1)}{s^2} - 1\right)g_l(s). \quad (2.26)$$

This is the Bessel differential equation and its solutions are linear combinations of Bessel functions

$$g_l(s) = c_1 J_l(s) + c_2 Y_l(s). \quad (2.27)$$

$J_l$  is singular for  $s \rightarrow 0$ , so that  $c_2 = 0$  ( $g_l$  must be defined everywhere). Furthermore,  $Y_l(s) \approx \frac{1}{s} \sin\left(s - \frac{l}{2}\pi\right)$  for  $s \gg 1$ , so we have for large distances (which is all that we are interested in)

$$g_l(s) = c_1 \frac{\sin\left(s - \frac{l}{2}\pi\right)}{s}. \quad (2.28)$$

If we now reintroduce the short-ranged interaction  $W$ , the system is, at large distances, described by the same SE as before and the solutions must also be given by Eq. (2.27). However, the condition that  $g_l$  must be defined everywhere does not apply because the solution needs to be valid only at large distances). For  $s \gg 1$ ,  $Y_l(s) \approx -\frac{1}{s} \cos\left(s - \frac{l}{2}\pi\right)$ , so that

$$g_l(s) = c_1 \frac{\sin\left(s - \frac{l}{s}\right)}{s} - c_2 \frac{\cos\left(s - \frac{l}{s}\right)}{s} \quad (2.29)$$

$$= \frac{c}{s} \sin(s + \eta_l) \quad (2.30)$$

$$\Rightarrow f_l(r) = \frac{c}{kr} \sin(kr + \eta_l) \quad (2.31)$$

with  $c \cos(\eta_l + \frac{l}{2}\pi) = c_1$ ,  $c \sin(\eta_l + \frac{l}{2}\pi) = -c_2$ . The quantity  $\eta_l = -ka_s$  is called the phase shift and  $a_s$  is called the scattering length. In the non-interacting case both  $a_s$  and  $\eta_l$  vanish. Evidently, the phase shift is the only implication of the interaction at large distances.

This is the crucial point which makes the second Born approximation possible: since the exact form of the interaction is irrelevant, we can replace it with any other function, if and only if it yields the correct phase shift. In particular, following the approach in [157], we can choose an interaction which lacks regions where it is very strong and for which therefore the *first* Born approximation can be applied. E.g., we can choose the Gaussian interaction

$$U_{\text{gauss}}(r) = U_0 \exp\left(-\frac{r^2}{\sigma^2}\right) \quad (2.32)$$

depicted in Fig. 2.1 ( $U_0$  and  $\sigma$  have to be chosen such that the interaction yields the correct phase shift). For *this* interaction the first Born approximation is valid, so that we can describe the gas by the Hartree equation (2.21) with the particular mean-field potential

$$V_{MF}[\psi](\mathbf{r}) = N \int d^3r' U_0 \exp\left(-\frac{|\mathbf{r} - \mathbf{r}'|^2}{\sigma^2}\right) |\psi(\mathbf{r}')|^2. \quad (2.33)$$

Due to the short range of the true interaction,  $U_{\text{gauss}}$  is short-ranged, too. Therefore, for the purpose of calculating the integral (2.33), it can in turn be approximated by a delta-like pseudo-potential

$$U(r) = G\delta(\mathbf{r})\partial_r r \quad (2.34)$$

with a suitably chosen parameter  $G$ . This particular pseudo-potential describes  $s$ -wave scattering. For  $p$ -wave and  $d$ -wave-scattering and so on, other pseudo-potentials exist. In order to show that the pseudo-potential indeed properly approximates the true interaction and in order to find the correct choice for  $G$ , we substitute  $U$  into the three-dimensional form of Eq. (2.24):

$$\left(\nabla^2 + k^2 - G\delta(\mathbf{r})\partial_r r - \frac{l(l+1)}{r^2}\right)\psi(\mathbf{r})Y_l^m(\vartheta, \varphi) = 0 \quad (2.35)$$

$$\Leftrightarrow \left(\nabla^2 + k^2 - \frac{l(l+1)}{r^2}\right)\frac{1}{r}\sin(kr + \eta_0)Y_l^m(\vartheta, \varphi) = G\delta(\mathbf{r})k\cos(kr + \eta_0)Y_l^m(\vartheta, \varphi). \quad (2.36)$$

The equation needs to be integrated over a small ball  $B_\varepsilon$  around  $\mathbf{0}$  in order to properly account for the influence of the delta function:

$$\int_{B_\varepsilon} d^3r \left(\nabla^2 + k^2 - \frac{l(l+1)}{r^2}\right)\frac{\sin(kr + \eta_0)}{r}Y_l^m = Gk \int_{B_\varepsilon} d^3r \delta(\mathbf{r})\cos(kr + \eta_0)Y_l^m. \quad (2.37)$$

Both sides vanish<sup>3</sup> if  $l \neq 0$  since

$$\int_0^\pi d\vartheta \sin \vartheta \int_0^{2\pi} d\varphi Y_l^m(\vartheta, \varphi) = 0 \quad (2.38)$$

for  $l \neq 0$ , so we only need to consider the case  $l = 0$ :

$$\int_{B_\varepsilon} d^3r \left[\nabla^2 \frac{\sin(kr + \eta_0)}{r}\right] + \int_{B_\varepsilon} d^3r k^2 \frac{1}{r} \sin(kr + \eta_0) = Gk \cos(\eta_0). \quad (2.39)$$

For  $\varepsilon \rightarrow 0$ , the second summand on the left hand side approaches zero, but the first one does not ( $\partial B_\varepsilon$  denotes the surface of  $B_\varepsilon$ ):

$$\int_{B_\varepsilon} d^3r \nabla^2 \frac{\sin(kr + \eta_0)}{r} = \oint_{\partial B_\varepsilon} d^2\mathbf{r} \cdot \nabla \frac{\sin(kr + \eta_0)}{r} \quad (2.40)$$

$$= \oint_{\partial B_\varepsilon} d^2\mathbf{r} \cdot \left[\frac{1}{r}\nabla \sin(kr + \eta_0) + \sin(kr + \eta_0)\nabla \frac{1}{r}\right] \quad (2.41)$$

$$= \oint_{\partial B_\varepsilon} d^2\mathbf{r} \cdot \left[\frac{k}{r}\cos(kr + \eta_0)\frac{\mathbf{r}}{r} - \sin(kr + \eta_0)\frac{\mathbf{r}}{r^3}\right] \quad (2.42)$$

<sup>3</sup>Here, the necessity of choosing different pseudo-potentials for different  $l$  manifests itself.

$$= \oint_{\partial B_\varepsilon} d^2r \left[ \frac{k}{r} \cos(kr + \eta_0) - \sin(kr + \eta_0) \frac{1}{r^2} \right] \quad (2.43)$$

$$= 4\pi\varepsilon^2 \left[ \frac{k}{\varepsilon} \cos(k\varepsilon + \eta_0) - \sin(k\varepsilon + \eta_0) \frac{1}{\varepsilon^2} \right] \quad (2.44)$$

$$\xrightarrow{\varepsilon \rightarrow 0} -4\pi \sin(\eta_0). \quad (2.45)$$

So we find:

$$G = -\frac{4\pi \tan(\eta_0)}{k}. \quad (2.46)$$

Now we undo the original transformation and obtain:

$$W(\mathbf{r}) = \frac{\hbar^2}{2\mu} U(\mathbf{r}) = \frac{\hbar^2}{2\mu} G \delta(\mathbf{r}) = \frac{2\pi \tan(ka_s) \hbar^2}{k\mu} \delta(\mathbf{r}). \quad (2.47)$$

For low energy collisions with  $ka_s \ll 1$  this reduces to

$$W(\mathbf{r}) = g \delta(\mathbf{r}), \quad (2.48)$$

where

$$g = \frac{2\pi \hbar^2 a_s}{\mu} = \frac{4\pi \hbar^2 a_s}{m} \quad (2.49)$$

is the short-range interaction strength and  $a_s$  is the scattering length of the atomic collision process. The value of  $g$ , or equivalently  $a_s$ , can be calculated by numerically solving the SE with the true (roughly Lennard-Jones-like) inter-atomic potential, or by measurement. For Rubidium, one finds  $a_s \approx 100$  a.u. [24, 202].

By substituting the pseudo-potential (2.48) into the Hartree equation (2.21), it finally becomes the Gross-Pitaevskii equation (GPE)

$$i\hbar \partial_t \psi(\mathbf{r}) = \left( -\frac{\hbar^2}{2m} \nabla^2 + V_{\text{ext}}(\mathbf{r}) + Ng|\psi(\mathbf{r})|^2 \right) \psi(\mathbf{r}). \quad (2.50)$$

### 2.3.3. Combination of different interactions

In this thesis, we will consider BECs that exhibit short-ranged as well as long-ranged interactions. To treat such systems, we can combine Eqs. (2.21) and (2.50) into the non-local Gross-Pitaevskii equation

$$i\hbar \partial_t \psi(\mathbf{r}) = \left( -\frac{\hbar^2}{2m} \nabla^2 + V_{\text{ext}}(\mathbf{r}) + Ng|\psi(\mathbf{r})|^2 + V_{MF}[\psi](\mathbf{r}) \right) \psi(\mathbf{r}). \quad (2.51)$$

with

$$V_{MF}[\psi](\mathbf{r}) = N \int d^3r' W(\mathbf{r} - \mathbf{r}') |\psi(\mathbf{r}')|^2, \quad (2.52)$$

as before. Note that this treats the two interactions at different levels of approximation. In particular, the validity of the first Born approximation for the long-range interaction  $W$  will need to be justified for every specific problem. If a system has an interaction that is both long-ranged and strong, it cannot be treated at the mean-field level. Instead, a method that takes correlations fully into account (such as Path-Integral Monte Carlo) needs to be used. However, (2.51) is justified for all situations considered in this thesis, as we will see later.

### 2.3.4. Thermodynamic limit

Previously, we considered a gas with a finite number of particles  $N < \infty$ . Let us now discuss the limit of an unconfined ( $V_{\text{ext}} = 0$ ), thermodynamically large gas. In this limit, we let  $N$  approach infinity.  $N$  then ceases to be a reasonable observable and must be replaced by the average density  $\rho$ . Similarly, all extensive or super-extensive variables need to be replaced by their densities. Moreover, the former normalization condition  $\langle \psi | \psi \rangle = 1$  becomes impossible and must be replaced by the condition that the average density, i.e., the average value of  $|\psi|^2$  over large volumes is 1:

$$\int_V d^3r |\psi(\mathbf{r})|^2 = V \quad \text{for sufficiently large volumes } V. \quad (2.53)$$

Then, the GPE for the system is

$$i\hbar\partial_t\psi(\mathbf{r}) = \left( -\frac{\hbar^2}{2m}\nabla^2 + \rho g|\psi(\mathbf{r})|^2 + V_{MF}[\psi](\mathbf{r}) \right) \psi(\mathbf{r}). \quad (2.54)$$

$$V_{MF}[\psi](\mathbf{r}) = \rho \int dr' W(\mathbf{r} - \mathbf{r}') |\psi(\mathbf{r}')|^2. \quad (2.55)$$

The ground state of a gas with the fixed average density  $\rho$  that has only a repulsive short-range interaction ( $W = 0, g > 0$ ) is the homogeneous state  $|\psi_{\text{hom}}\rangle$  with

$$\psi_{\text{hom}}(\mathbf{r}) = 1, \quad (2.56)$$

since this state minimizes both the kinetic energy density (to zero) and the interaction energy density (to  $g\rho/2$ ). Additionally,  $\psi_{\text{hom}}$  is also always a stationary state of the GPE (2.54), regardless of  $W$ . However, it is not necessarily the ground state but can be an excited state. If this is the case, it can be unstable with respect to small perturbations. This will be discussed in the next section.

## 2.4. Bogoliubov excitation spectrum

Given any stationary state of the GPE (2.55), we can study its elementary excitations, i.e., the low-lying excited states and their energies. It is possible to derive it using the

Bogoliubov ansatz (2.15) and writing the field operator  $\hat{\varphi}(\mathbf{r})$  in momentum representation. We choose another route. We will derive it based on the GPE with a classical field  $\psi$ . In a homogeneous condensate, the elementary excitations are plane waves with wave vectors  $\mathbf{k}$ . A wave function with such an excitation is given by [157]

$$\psi(\mathbf{r}) = \left(1 + u_k e^{i\mathbf{k}\mathbf{r}-i\omega t} + \overline{v_k} e^{-i\mathbf{k}\mathbf{r}+i\omega t}\right) e^{-i\mu t/\hbar} \quad (2.57)$$

with  $|u_k|, |v_k| \ll 1$ . We insert  $\psi$  into the GPE (2.54) and the MF potential (2.55). Since we only consider small perturbations, we can neglect terms proportional to  $|u_k|^2$ ,  $|v_k|^2$  and  $|u_k v_k|$ . Thus, we find for the terms in the GPE:

$$\begin{aligned} i\hbar\partial_t\psi(\mathbf{r}) &= \hbar\omega \left(u_k e^{i\mathbf{k}\mathbf{r}-i\omega t} - \overline{v_k} e^{-i\mathbf{k}\mathbf{r}+i\omega t}\right) e^{-i\mu t} + \mu\psi(\mathbf{r}), \\ -\frac{\hbar^2}{2m}\nabla^2\psi(\mathbf{r}) &= \frac{\hbar^2 k^2}{2m} \left(u_k e^{i\mathbf{k}\mathbf{r}-i\omega t} + \overline{v_k} e^{-i\mathbf{k}\mathbf{r}+i\omega t}\right) e^{-i\mu t}, \end{aligned}$$

$$\begin{aligned} V_{MF}[\psi](\mathbf{r})\psi(\mathbf{r}) &= \rho \int d^3r' W(\mathbf{r}-\mathbf{r}') \left| \left(1 + u_k e^{i\mathbf{k}\mathbf{r}'-i\omega t} + \overline{v_k} e^{-i\mathbf{k}\mathbf{r}'+i\omega t}\right) \right|^2 \psi(\mathbf{r}) \\ &\approx \rho \int d^3r' W(\mathbf{r}-\mathbf{r}') \left(1 + (u_k + v_k) e^{i\mathbf{k}\mathbf{r}'-i\omega t} + (\overline{v_k} + \overline{u_k}) e^{-i\mathbf{k}\mathbf{r}'+i\omega t}\right) \psi(\mathbf{r}) \\ &= \rho \left(\tilde{W}(\mathbf{0}) + (u_k + v_k)\tilde{W}(\mathbf{k})e^{i\mathbf{k}\mathbf{r}-i\omega t} + (\overline{v_k} + \overline{u_k})\tilde{W}(-\mathbf{k})e^{-i\mathbf{k}\mathbf{r}+i\omega t}\right) \psi(\mathbf{r}) \\ &\approx \rho \left(\tilde{W}(\mathbf{0}) + (u_k + v_k)\tilde{W}(\mathbf{k})e^{i\mathbf{k}\mathbf{r}-i\omega t} + (\overline{v_k} + \overline{u_k})\tilde{W}(-\mathbf{k})e^{-i\mathbf{k}\mathbf{r}+i\omega t}\right. \\ &\quad \left.+ \left[u_k e^{i\mathbf{k}\mathbf{r}-i\omega t} + \overline{v_k} e^{-i\mathbf{k}\mathbf{r}+i\omega t}\right] \tilde{W}(\mathbf{0})\right), \end{aligned}$$

where  $\tilde{W}$  is the Fourier transform of  $W$ .

$$\begin{aligned} \rho g |\psi(\mathbf{r})|^2 \psi(\mathbf{r}) &\approx \rho g \left(1 + (u_k + v_k) e^{i\mathbf{k}\mathbf{r}-i\omega t} + (\overline{v_k} + \overline{u_k}) e^{-i\mathbf{k}\mathbf{r}+i\omega t}\right) \psi(\mathbf{r}) \\ &\approx \rho g \left(1 + (u_k + v_k) e^{i\mathbf{k}\mathbf{r}-i\omega t} + (\overline{v_k} + \overline{u_k}) e^{-i\mathbf{k}\mathbf{r}+i\omega t}\right. \\ &\quad \left.+ u_k e^{i\mathbf{k}\mathbf{r}-i\omega t} + \overline{v_k} e^{-i\mathbf{k}\mathbf{r}+i\omega t}\right). \end{aligned}$$

These expressions contain three types of different phase factors: 1,  $e^{-i\mathbf{k}\mathbf{r}+i\omega t}$  and  $e^{i\mathbf{k}\mathbf{r}-i\omega t}$ . We can split up the GPE with respect to these factors and find as the first equation:

$$\mu = \rho\tilde{W}(\mathbf{0}) + \rho g. \quad (2.58)$$

This equation corresponds to the unperturbed zero momentum part (hence the phase factor 1). It reflects that  $|\psi\rangle$  is a stationary state of the GPE and determines the

chemical potential  $\mu$ . The relevant equations are those for the excitations:

$$\begin{aligned}(\hbar\omega + \mu)u_k &= \frac{\hbar^2 k^2}{2m}u_k + (u_k + v_k)\rho\tilde{W}(\mathbf{k}) + \rho g(u_k + v_k) + u_k\rho(\tilde{W}(\mathbf{0}) + g) \\(-\hbar\omega + \mu)\bar{v}_k &= \frac{\hbar^2 k^2}{2m}\bar{v}_k + (\bar{u}_k + \bar{v}_k)\rho\tilde{W}(-\mathbf{k}) + \rho g(\bar{u}_k + \bar{v}_k) + \bar{v}_k\rho(\tilde{W}(\mathbf{0}) + g),\end{aligned}$$

or equivalently (using Eq. (2.58)):

$$\hbar\omega u_k = \left(\frac{\hbar^2 k^2}{2m}\right) u_k + (u_k + v_k)\rho\tilde{W}(\mathbf{k}) + \rho g(u_k + v_k) \quad (2.59)$$

$$\hbar\omega v_k = \left(-\frac{\hbar^2 k^2}{2m}\right) v_k - (u_k + v_k)\rho\tilde{W}(\mathbf{k}) - \rho g(u_k + v_k). \quad (2.60)$$

These are known as the Bogoliubov-de-Gennes equations [157]. To solve them, we write them in matrix form

$$\hbar\omega \begin{pmatrix} u_k \\ v_k \end{pmatrix} = \begin{pmatrix} \frac{\hbar^2 k^2}{2m} + \rho(g + \tilde{W}(\mathbf{k})) & \rho(g + \tilde{W}(\mathbf{k})) \\ -\rho(g + \tilde{W}(\mathbf{k})) & -\frac{\hbar^2 k^2}{2m} - \rho(g + \tilde{W}(\mathbf{k})) \end{pmatrix} \begin{pmatrix} u_k \\ v_k \end{pmatrix}. \quad (2.61)$$

Finally, by diagonalizing the above matrix, we obtain the simple expression for the so-called Bogoliubov spectrum [157]

$$\varepsilon(\mathbf{k}) = \hbar\omega(\mathbf{k}) = \sqrt{\frac{\hbar^2 k^2}{2m} \left( \frac{\hbar^2 k^2}{2m} + 2\rho g + 2\rho\tilde{W}(\mathbf{k}) \right)}, \quad (2.62)$$

As we will see, the spectrum is useful for the study of certain properties of a BEC, such as superfluidity and stability under small perturbations. For a short-range interaction, the spectrum is:

$$\varepsilon(k) = \sqrt{\frac{\hbar^2 k^2}{2m} \left( \frac{\hbar^2 k^2}{2m} + 2\rho g \right)} \quad (2.63)$$

This expression can be made parameterless by scaling lengths with the healing length  $\xi = \hbar/\sqrt{m\rho g}$  and energies with the short-range interaction energy  $\rho g$ , so that it can be represented as one curve (see Fig. 2.2):

$$\frac{\varepsilon(k)}{\rho g} = \sqrt{\frac{(k\xi)^2}{2} \left( \frac{(k\xi)^2}{2} + 2 \right)} \quad (2.64)$$

For large  $k$  (more specifically, for  $k\xi \gg 1$ ), one finds the free-particle dispersion

$$\varepsilon(k) = \frac{\hbar^2 k^2}{2m}, \quad (2.65)$$

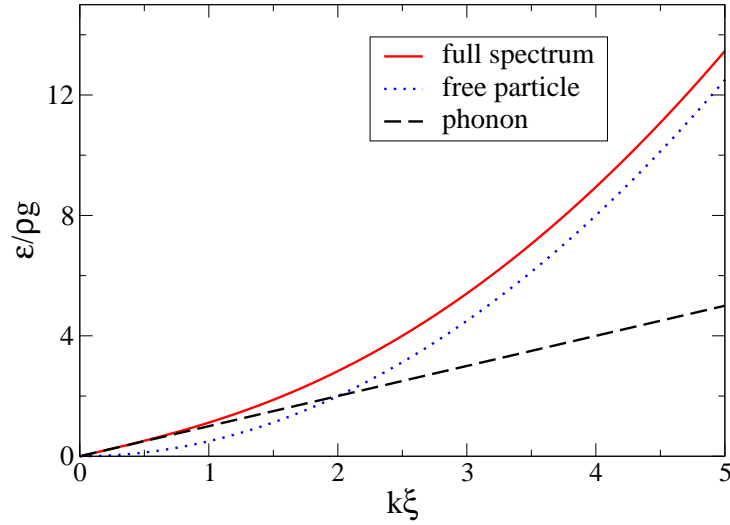


**Figure 2.2.:** Bogoliubov spectrum for a short-range interaction. Energies are scaled by the short-range interaction energy  $\rho g$ , lengths by the healing length  $\xi = \frac{\hbar}{\sqrt{m\rho g}}$ . The exact spectrum (2.63) and the limiting cases of a phonon (for small momenta  $k$ ) and the free-particle spectrum (for large  $k$ ) are shown.

while at small  $k$ , the spectrum has phonon-character

$$\varepsilon(k) = \sqrt{\frac{\rho g}{m}} \hbar k. \quad (2.66)$$

with the speed of sound

$$c = \sqrt{\rho g/m}. \quad (2.67)$$

We will come back to investigate these properties for a *long-range* interaction in chapter 5.

## 2.5. Superfluidity

A superfluid is an exotic state of matter where a liquid loses all of its viscosity and flows without dissipation [119]. It was first found experimentally in 1938 [5,98]. As shown by Landau [116,117,157], superfluidity is closely connected to the spectrum of elementary excitations of a zero-temperature BEC that we derived above: When a particle with the mass  $m$  moves with the velocity  $\mathbf{v}$  in a reference frame  $S$ , then its energy in another

reference frame  $S'$  (that moves with the velocity  $\mathbf{V}$  with respect to  $S$ ) is

$$E' = \frac{m}{2}(\mathbf{v} - \mathbf{V})^2 = \frac{m}{2}(\mathbf{v}^2 + \mathbf{V}^2 - 2\mathbf{v} \cdot \mathbf{V}) = E + \frac{m}{2}\mathbf{V}^2 - \mathbf{p} \cdot \mathbf{V}. \quad (2.68)$$

Now we consider a BEC flowing through a stationary capillary with the velocity of flow  $\mathbf{V}$ . Friction is created by the spontaneous formation of elementary excitations. Therefore, we consider an excitation with the momentum  $\mathbf{p}$  and the energy  $\varepsilon(\mathbf{p})$  appearing in the frame moving with the stream. According to Eq. (2.68), the change of energy in the frame of the capillary due to the appearance of the excitation is  $\varepsilon(\mathbf{p}) + \mathbf{p} \cdot \mathbf{V}$ . However, such a process can occur only if it is energetically favorable, i.e., there must be a  $\mathbf{p}$  such that

$$\varepsilon(\mathbf{p}) + \mathbf{p} \cdot \mathbf{V} < 0, \quad (2.69)$$

which is equivalent to

$$V > v_c := \min_p \left( \frac{\varepsilon(p)}{p} \right). \quad (2.70)$$

Hence, if the velocity  $V$  is smaller than  $v_c$ , no excitations can form and no friction can occur so that we have a superfluid.  $v_c$  is called the Landau critical velocity.

We can calculate the critical velocity of a short-range interacting BEC in the homogeneous state:

$$\begin{aligned} v_c &= \min_p \left( \frac{\varepsilon(p)}{p} \right) = \min_p \left( \frac{\sqrt{\frac{p^2}{2m} \left( \frac{p^2}{2m} + 2\rho g \right)}}{p} \right) = \min_p \left( \sqrt{\frac{1}{m} \left( \frac{p^2}{4m} + \rho g \right)} \right) \\ &= \sqrt{\rho g / m}. \end{aligned} \quad (2.71)$$

Hence, the critical velocity coincides with the speed of sound (2.4). This is always true for short-range interactions because  $v_c$  is then determined by the limit  $k \rightarrow 0$ . Since the elementary excitations are phonons, the connection between the two speeds is not surprising.

Even though this model of superfluidity is very simple, there is evidence [178] that it describes, e.g., the dynamics in helium nano-droplets quite well.

For long-range interactions, the spectrum can differ and the Landau critical velocity can be different from the speed of sound. We will investigate an example for such a long-range interaction in chapter 5.



### 3. Rydberg atoms and their interaction

Rydberg atoms are atoms with an electron in a Rydberg state, i.e., a highly excited atomic eigenstate (high principal quantum number  $n$ ). They exhibit various extreme properties [70]:

- Large size (average distance between Rydberg electron and nucleus), scaling as  $n^2$ . For  $n = 100$  this leads to a typical size scale of  $0.5\mu\text{m}$ .
- Long radiative lifetime, scaling as  $n^3$ , e.g., the  $80s$  state of Rubidium has a lifetime of about  $700\mu\text{s}$  [19, 32].
- High polarizability  $\propto n^7$ .
- Strong van-der-Waals interaction  $C_6/r^6$  with  $C_6$  scaling roughly as  $n^{11}$ . This interaction is the most important property for this thesis. The rest of the chapter is dedicated to the accurate numerical calculation of these interactions for arbitrary alkali atoms.
- The dipole coupling between neighboring states scales with  $n^2$  as the size does.

Rydberg atoms have applications in quantum information [96, 128, 175], quantum optics [78, 158], non-linear optics [155, 163, 180], plasma formation [159, 196], astronomy [75] and in other fields.

Experimentally, they are now routinely created in a controlled way as well as detected in ultra-cold gases in many laboratories [130].

In this chapter, we will first show how to calculate the Rydberg states of alkali atoms and their energies. Then, we will construct the Hamiltonian describing a system of two alkali atoms, each with its valence electron in a Rydberg state. Finally, we will calculate the resulting interaction between the Rydberg atoms by diagonalizing the Hamiltonian. Throughout the chapter, Hartree atomic units will be used, i.e., the following constants are unity: the electron mass  $m_e$ , the elementary charge  $e$ , the reduced Planck constant  $\hbar$  and the coulomb constant  $4\pi\epsilon_0$ . Therefore, the Bohr radius  $a_0$  and the Hartree energy  $E_H$ , as derived quantities, are also unity.

#### 3.1. Rydberg states and their energies

In this section, we will show how to calculate the Rydberg eigenstates and eigenenergies of alkali atoms (which have only one valence electron). To introduce all necessary fundamental ideas, we start from the simplest example, hydrogen, whose states and energies can be calculated analytically. Then, we generalize the problem to arbitrary alkali atoms. There, approximate numerical solutions are necessary.

### 3.1.1. The hydrogen atom

The hydrogen atom consists of a nucleus and an electron, interacting with the Coulomb interaction

$$U_c(r) = -\frac{1}{r}. \quad (3.1)$$

Its eigenenergies and eigenstates can be calculated analytically (including the fine structure, but neglecting its effect on the *radial* wave-function) [67]:

$$E_{nljm} = E_{nj} = -\frac{1}{2n^2} \left( 1 + \frac{\alpha^2}{n^2} \left[ \frac{n}{j + \frac{1}{2}} - \frac{3}{4} \right] \right), \quad (3.2)$$

$$\psi_{nljm}(\mathbf{r}) = \sqrt{\left(\frac{2}{n}\right)^3 \frac{(n-l-1)!}{2n(n+l)!}} e^{-\rho/2} \rho^l L_{n-l-1}^{2l+1}(\rho) \mathcal{Y}_{ljm}(\vartheta, \varphi), \quad (3.3)$$

where  $\rho = 2r/n$  and  $L_{n-l-1}^{2l+1}$  is a generalized Laguerre polynomial.  $\mathcal{Y}_{ljm}$  is the generalized spherical harmonic spinor [67]

$$\mathcal{Y}_{ljm}(\vartheta, \varphi) = \frac{1}{\sqrt{2l+1}} \begin{pmatrix} \pm \sqrt{l + \frac{1}{2} \pm m} Y_l^{m-\frac{1}{2}}(\vartheta, \varphi) \\ \sqrt{l + \frac{1}{2} \mp m} Y_l^{m+\frac{1}{2}}(\vartheta, \varphi) \end{pmatrix} \quad \text{for } j = l \pm \frac{1}{2} \quad (3.4)$$

Eq. (3.2) is known as the Rydberg formula. The indices  $n, l, j, m$  are called quantum numbers:

- $n \in \mathbb{N}$ : principal quantum number,
- $l \in \{0, \dots, n-1\}$ : orbital angular momentum,
- $j \in \{l - \frac{1}{2}, l + \frac{1}{2}\}$ : total angular momentum (including the electron spin which is accounted for by the  $\pm \frac{1}{2}$  term.),
- $m \in \{-j, -(j-1), \dots, j-1, j\}$ : magnetic quantum number (corresponding to projection of the total angular momentum  $j$  on the  $z$  direction).

The quantum numbers label all eigenstates so that every eigenstate can be written as

$$|\psi_{nljm}\rangle = |n, l, j, m\rangle. \quad (3.5)$$

For historic reasons, states have common names based on the value of  $l$ :

- $l = 0$ : *s*-states,
- $l = 1$ : *p*-states,
- $l = 2$ : *d*-states,
- $l = 3$ : *f*-states,
- $l = 4$ : *g*-states,

and so on.

### 3.1.2. Alkali atoms

Rydberg electrons are, on average, far away from the nucleus and the core electrons. Since alkali atoms have only one valence electron, the Rydberg states that we have to consider always consist of the core with all the core electrons and one and only one electron in a Rydberg state. Hence, the atom can be described very well as an atom with only one electron and with an effective potential  $U_{\text{eff}}$  that is Coulomb-like for large distances (as in hydrogen) but is modified close to the nucleus due to the presence of the core electrons [133]:

$$U_{\text{eff}}^{(l)}(r) = -\frac{Z_l(r)}{r} - \frac{\alpha}{2r^4} \left(1 - e^{-(r/r_0)^6}\right). \quad (3.6)$$

$\alpha$  is the static dipole polarizability of the whole core (nucleus and core electrons) and the radial charge  $Z_l$  is

$$Z_l(r) = 1 + (z - 1)e^{-a_1 r} - r(a_3 + a_4 r)e^{-a_2 r}, \quad (3.7)$$

where  $z$  is the charge of the nucleus.

The five free parameters ( $a_1, a_2, a_3, a_4, r_0$ ) in the formula have to be fitted such that the potential yields the correct eigenenergies, so it is important for this method to know them with high precision. While it is very hard to calculate the eigenenergies theoretically<sup>1</sup>, experiments have succeeded in measuring them extremely precisely [88, 123]. Using the experimental values, it is possible to obtain the fitting parameters. We will use the values determined in [133].

Apart from their role for the calculation of the wave-functions, the energies will also be important for the calculation of the van-der-Waals interaction between Rydberg atoms. They can be written as [70]

$$E_{nlj} = -\frac{1}{(n - \delta_{l,j}(n))^2}, \quad (3.8)$$

where  $\delta_{l,j}(n) = \delta_{l,j,0} + \delta_{l,j,2}/(n - \delta_{l,j,0})^2$  is the so-called quantum defect.  $\delta_{l,j,0}$  and  $\delta_{l,j,2}$  are constants that can be determined experimentally. Their experimental values for Rubidium are shown in Table 3.1. Since electrons with higher angular momentum  $l$  have a smaller probability of presence near the nucleus they are less influenced by the deviation of the modified potential (3.6) from the Coulomb potential. Hence, their quantum defects are smaller. The numbers in the table make it evident that the dependence on  $j$  is negligible. In other words, spin-orbit coupling can have only a very small effect on the radial wave-functions  $f_l$ . This justifies our approximation that  $f_l$  is not dependent on  $j$  (for given  $l$ ).

Since the potential is still spherically symmetric, the angular structure of the eigenstates

<sup>1</sup>This would entail solving the full many-electron problem thus making the whole modified-potential method superfluous.

$l$	$j$	$\delta_{l,j,0}$	$\delta_{l,j,2}$
0	1/2	3.1311804	0.1784
1	1/2	2.6548849	0.2900
1	3/2	2.6416737	0.2950
2	3/2	1.34809171	-0.60286
2	5/2	1.34646572	-0.596
3	5/2	0.0165192	-0.085
3	7/2	0.0165437	-0.086

**Table 3.1.:** Rubidium quantum defect parameters from [88, 123]. The quantum defect is  $\delta_{l,j}(n) = \delta_{l,j,0} + \delta_{l,j,2}/(n - \delta_{l,j,0})^2$ . The dependence on  $j$  is very small, justifying our neglect of the  $j$ -dependence of the radial wave-function.

remains identical to that of hydrogen. As for hydrogen, we define the wave-function as

$$\psi_{nljm}(\mathbf{r}) = f_{nl}(r)\mathcal{Y}_{ljm}(\vartheta, \varphi), \quad (3.9)$$

so that we only have to numerically solve the radial Schrödinger equation

$$\left(-\frac{1}{2}\partial_r^2 + \frac{l(l+1)}{2r^2} + U_{\text{eff}}^{(l)}(r)\right)g_{nl}(r) = E_{nl}g_{nl}(r) \quad (3.10)$$

with  $g_{nl}(r) = rf_{nl}(r)$ , separately for every value of the quantum number  $l$ . We do this by discretizing position space with the grid spacing  $dr$ , writing the Hamiltonian

$$H(r) = -\frac{1}{2}\partial_r^2 - \frac{l(l+1)}{2r^2} + U_{\text{eff}}^{(l)}(r) \quad (3.11)$$

in matrix form:

$$H = \frac{1}{dr^2} \begin{pmatrix} 1 & -\frac{1}{2} & \dots & & \\ -\frac{1}{2} & 1 & -\frac{1}{2} & \dots & \\ 0 & -\frac{1}{2} & 1 & -\frac{1}{2} & \dots \\ \vdots & & \ddots & & \end{pmatrix} + \begin{pmatrix} U_{\text{eff}}^{(l)}(1) & 0 & \dots & \\ 0 & U_{\text{eff}}^{(l)}(2) & 0 & \dots \\ 0 & 0 & U_{\text{eff}}^{(l)}(3) & \\ \vdots & & \ddots & \end{pmatrix} \quad (3.12)$$

and diagonalizing it. Thereby, we obtain approximations for all eigenstates  $|n, l, j, m\rangle$  that we will need for the calculation of the interaction between two atoms in a Rydberg state.

## 3.2. Calculation of the interaction between alkali atoms

We will now use the Rydberg states and their energies as obtained from the previous section in order to construct the Hamiltonian of a system consisting of two Rydberg atoms, including their interaction. Then, we can derive the Born-Oppenheimer potential

describing the inter-atomic interaction, after the electron dynamics have been eliminated. We will see that it is a van-der-Waals potential at sufficiently large distances and a dipole potential at smaller distances.

### 3.2.1. Dipole approximation

We consider two nuclei 1 and 2 of the same species, with positions  $\mathbf{R}_1$  and  $\mathbf{R}_2$  and the distance vector  $\mathbf{R} = \mathbf{R}_2 - \mathbf{R}_1$ . Each of them has one Rydberg electron with the position operator  $\hat{\mathbf{r}}_i$  that describes the distance between that electron and its corresponding nucleus. Each of the isolated atoms is thus governed by a Hamiltonian

$$\hat{H}_0^{(i)} = -\frac{1}{2}\nabla_i^2 + U_{\text{eff}}^{(l)}(\hat{\mathbf{r}}_i). \quad (3.13)$$

The interaction between the two atoms is given by

$$V(\mathbf{R}, \mathbf{r}_1, \mathbf{r}_2) = \frac{1}{|\mathbf{R}|} - \frac{1}{|\mathbf{R} - \mathbf{r}_1|} - \frac{1}{|\mathbf{R} + \mathbf{r}_2|} + \frac{1}{|\mathbf{R} - (\mathbf{r}_1 - \mathbf{r}_2)|}. \quad (3.14)$$

We are interested in the situation where the atoms are far enough apart for the wavefunctions of the Rydberg electrons not to overlap, i.e.,  $r_i \ll R$ . So, we will calculate the multipole expansion of  $V(\mathbf{R}, \mathbf{r}_1, \mathbf{r}_2)$  by performing a multidimensional Taylor expansion. We set

$$f(\mathbf{x}) = \frac{1}{|\mathbf{R} - \mathbf{x}|}, \quad (3.15)$$

so that

$$V(\mathbf{R}, \mathbf{r}_1, \mathbf{r}_2) = f(\mathbf{0}) - f(\mathbf{r}_1) - f(-\mathbf{r}_2) + f(\mathbf{r}_1 - \mathbf{r}_2). \quad (3.16)$$

Now we Taylor expand  $f$ :

$$f(\mathbf{0}) = \frac{1}{R}, \quad (3.17)$$

$$\partial_i f(\mathbf{x}) = \frac{R_i - x_i}{|\mathbf{R} - \mathbf{x}|^3} \quad (3.18)$$

$$\Rightarrow \partial_i f(\mathbf{0}) = \frac{R_i}{R^3} \quad (3.19)$$

$$\partial_{ij} f(\mathbf{x}) = -\frac{\delta_{ij}}{|\mathbf{R} - \mathbf{x}|^3} + \frac{3(x_i - R_i)(x_j - R_j)}{|\mathbf{R} - \mathbf{x}|^5} \quad (3.20)$$

$$\Rightarrow \partial_{ij} f(\mathbf{0}) = -\frac{\delta_{ij}}{R^3} + \frac{3R_i R_j}{R^5}. \quad (3.21)$$

We insert these derivatives into the multidimensional Taylor expansion

$$f(\mathbf{x}) = f(\mathbf{0}) + \sum_{i=1}^3 x_i \partial_i f(\mathbf{0}) + \frac{1}{2} \sum_{i,j=1}^3 x_i x_j \partial_{ij} f(\mathbf{0}) + \mathcal{O}(\mathbf{x}^3), \quad (3.22)$$

to yield to second approximation

$$f(\mathbf{x}) = \frac{1}{R} + \frac{1}{R^3} \sum_{i=1}^3 x_i R_i + \frac{1}{2} \sum_{i,j=1}^3 x_i x_j \left( -\frac{\delta_{ij}}{R^3} + \frac{3R_i R_j}{R^5} \right) \quad (3.23)$$

$$= \frac{\mathbf{x} \cdot \mathbf{R}}{R^3} + \frac{3}{2R^5} (\mathbf{x} \cdot \mathbf{R})^2 - \frac{x^2}{2R^3}. \quad (3.24)$$

With Eq. (3.16) this gives the final result

$$\begin{aligned} V(\mathbf{R}, \mathbf{r}_1, \mathbf{r}_2) &= - \left( \frac{\mathbf{r}_1 \cdot \mathbf{R}}{R^3} + \frac{3}{2R^5} (\mathbf{r}_1 \cdot \mathbf{R})^2 - \frac{r_1^2}{2R^3} \right) \\ &\quad - \left( \frac{-\mathbf{r}_2 \cdot \mathbf{R}}{R^3} + \frac{3}{2R^5} (\mathbf{r}_2 \cdot \mathbf{R})^2 - \frac{r_2^2}{2R^3} \right) \end{aligned} \quad (3.25)$$

$$\begin{aligned} &+ \frac{(\mathbf{r}_1 - \mathbf{r}_2) \cdot \mathbf{R}}{R^3} + \frac{3}{2R^5} ((\mathbf{r}_1 - \mathbf{r}_2) \cdot \mathbf{R})^2 - \frac{(\mathbf{r}_1 - \mathbf{r}_2)^2}{2R^3} \\ &= \frac{\mathbf{r}_1 \cdot \mathbf{r}_2}{R^3} - \frac{3}{R^5} (\mathbf{r}_1 \cdot \mathbf{R})(\mathbf{r}_2 \cdot \mathbf{R}). \end{aligned} \quad (3.26)$$

Hence, the two-atom Hamiltonian (which depends parametrically on  $\mathbf{R}$ ) is

$$\hat{H}(\mathbf{R}) = \hat{H}_1 + \hat{H}_2 + \hat{V}_d(\mathbf{R}). \quad (3.27)$$

with the dipole-dipole interaction operator

$$\hat{V}_d(\mathbf{R}) = \frac{\hat{\mathbf{r}}_1 \cdot \hat{\mathbf{r}}_2}{R^3} - \frac{3(\hat{\mathbf{r}}_1 \cdot \mathbf{R})(\hat{\mathbf{r}}_2 \cdot \mathbf{R})}{R^5}. \quad (3.28)$$

### 3.2.2. Minimal example: a three-state atom

In order to get a feeling for the qualitative properties of the resulting interactions we first consider a simple example of two atoms, numbered by  $i \in \{1, 2\}$ . Each one has only three states  $|s_i\rangle$ ,  $s \in \{-, 0, +\}$  (See Fig. 3.1).

The single-atom Hamiltonians are  $\hat{H}_i$ . We assume  $\langle \mathbf{r} | s_1 \rangle = \langle \mathbf{r} | s_2 \rangle$  for all  $s$ , i.e., we consider the same three states for both atoms, the only difference between  $|s_1\rangle$  and  $|s_2\rangle$  being that they are centered around the different atoms. Therein, the  $|0_i\rangle$  can be thought of as  $s$ -states and the others as  $p$ -states (except that we do not consider states of different  $m$ ). Conforming to this example, we assume that

$$\langle +_i | \hat{\mathbf{r}}_i | -_i \rangle = \langle -_i | \hat{\mathbf{r}}_i | +_i \rangle = 0, \quad (3.29)$$

$$\langle 0_i | \hat{\mathbf{r}}_i | +_i \rangle = \langle +_i | \hat{\mathbf{r}}_i | 0_i \rangle = d_+ \neq 0, \quad (3.30)$$

$$\langle 0_i | \hat{\mathbf{r}}_i | -_i \rangle = \langle -_i | \hat{\mathbf{r}}_i | 0_i \rangle = d_- \neq 0. \quad (3.31)$$

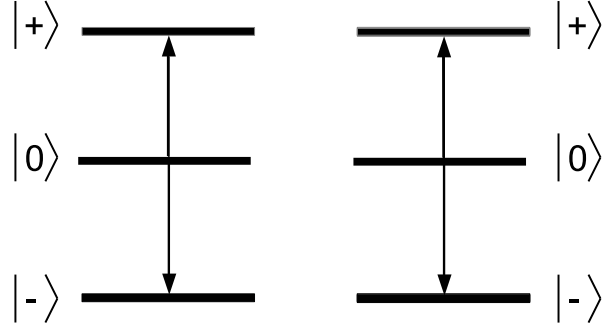


**Figure 3.1.:** Simple example of two three-state atoms.

The one particle energies are

$$\varepsilon_0 = \langle 0_i | \hat{H}_i | 0_i \rangle = 0, \quad (3.32)$$

$$\varepsilon_+ = \langle +_i | \hat{H}_i | +_i \rangle > 0, \quad (3.33)$$

$$\varepsilon_- = \langle -_i | \hat{H}_i | -_i \rangle < 0. \quad (3.34)$$

There are 9 two-atom states that we denote as  $|+-\rangle = |+_1\rangle \otimes |-_2\rangle$  and so on. They have the *unperturbed* energies

$$\varepsilon_{00} = \langle 00 | \hat{H}_1 + \hat{H}_2 | 00 \rangle = 0, \quad (3.35)$$

$$\varepsilon_{+-} = \varepsilon_{-+} = \langle +- | \hat{H}_1 + \hat{H}_2 | +- \rangle = \varepsilon_+ + \varepsilon_-, \quad (3.36)$$

$$\varepsilon_{++} = \langle ++ | \hat{H}_1 + \hat{H}_2 | ++ \rangle = 2\varepsilon_+, \quad (3.37)$$

$$\varepsilon_{--} = \langle -- | \hat{H}_1 + \hat{H}_2 | -- \rangle = 2\varepsilon_-. \quad (3.38)$$

Since  $\varepsilon_+ > 0$  and  $\varepsilon_- < 0$ , we assume that  $|\varepsilon_{++}|, |\varepsilon_{--}| \gg |\varepsilon_{+-}|$ . Then, the states  $|++\rangle$  and  $|--\rangle$  only give negligible contributions because they are energetically far away and can be ignored. Hence, only  $|+-\rangle$  and  $| -+\rangle$  need to be taken into account.

It is convenient to choose the symmetrized and anti-symmetrized states

$$|m\rangle = \frac{|+-\rangle - |-+\rangle}{\sqrt{2}}, \quad (3.39)$$

$$|p\rangle = \frac{|+-\rangle + |-+\rangle}{\sqrt{2}}. \quad (3.40)$$

as basis states. We also consider only a simplified dipole interaction operator

$$\hat{V}_d(R) = \frac{\hat{\mathbf{r}}_1 \cdot \hat{\mathbf{r}}_2}{R^3}, \quad (3.41)$$

so that

$$\langle 00 | \hat{V}_d(R) | m \rangle = 0, \quad (3.42)$$

$$\langle 00 | \hat{V}_d(R) | p \rangle = \frac{\sqrt{2}d_+d_-}{R^3} = \frac{d^2}{R^3} \quad (3.43)$$

with  $d^2 = \sqrt{2}d_+d_-$ . So  $|m\rangle$  can be eliminated and we find the total Hamiltonian

$$\hat{H}(R) = \begin{pmatrix} 0 & \frac{d^2}{R^3} \\ \frac{d^2}{R^3} & -\Delta \end{pmatrix} \quad (3.44)$$

with  $-\Delta = \varepsilon_{+-}$ . The eigenvalues of  $\hat{H}(R)$  are

$$E_{\pm}(R) = -\frac{\Delta}{2} \pm \sqrt{\frac{\Delta^2}{4} + \frac{d^4}{R^6}}, \quad (3.45)$$

with corresponding eigenvectors  $\mathbf{e}_{\pm}(R)$  whose specific form is not relevant here. For  $\Delta \geq 0$ , the eigenstate  $\mathbf{e}_{\pm}$  connects asymptotically to  $|00\rangle$ , so the inter-atomic potential of atoms in the  $|0\rangle$ -state is given by (see also Fig. 3.2)

$$W(R) = -\frac{\Delta}{2} + \text{sgn}(\Delta) \sqrt{\frac{\Delta^2}{4} + \frac{d^4}{R^6}} = \frac{\Delta}{2} \left( -1 + \sqrt{1 + \frac{4d^4}{\Delta^2 R^6}} \right). \quad (3.46)$$

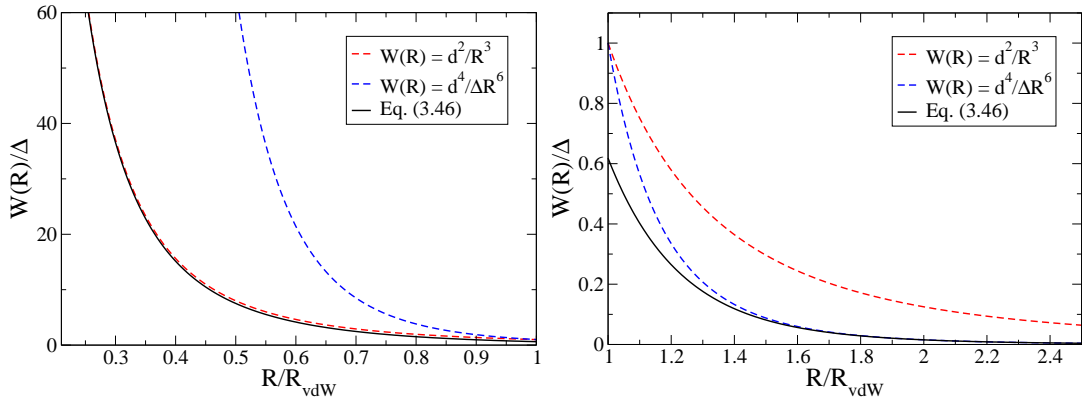


**Figure 3.2.:** Eqs. (3.46), (3.48), (3.51) for small distances  $R < R_{\text{vdW}}$  (left) and for large distances  $R > R_{\text{vdW}}$  (right). For small distances,  $W(R)$  is a dipole-dipole interaction  $\propto R^{-3}$ , for large distances it is van der-Waals like  $\propto R^{-6}$ .

Hence,  $W$  is repulsive for  $\Delta > 0$  and attractive for  $\Delta < 0$ ; the sign of the interaction depends only on the atomic eigenenergies. Qualitatively, this remains true for the realistic cases. There, the sign is typically determined by a few two-body states that are energetically very close to  $|00\rangle$  because their contributions are large. The many other

states that exist yield corrections to the interaction but do not usually change the sign. An exception is the case where the contributions of the states energetically close to  $|00\rangle$  cancel, so-called Förster-zeros [198, 199].

In order to understand  $W(R)$  better, it is helpful to develop it in two limiting cases:

For

$$D = \frac{4d^4}{\Delta^2 R^6} \ll 1. \quad (3.47)$$

Calculating the Taylor series of Eq. (3.46) in  $D$  yields

$$W(R) = \frac{d^4}{\Delta R^6} + \mathcal{O}(R^{-12}), \quad (3.48)$$

which is a van-der-Waals potential with the coefficient

$$C_6 = \frac{d^4}{\Delta}. \quad (3.49)$$

Since  $d \propto n^2$  and  $\Delta \propto n^{-3}$  (see the beginning of the chapter), we expect a scaling of  $C_6 \propto n^{11}$ .

According to Eq. (3.47) the description as a van-der-Waals potential is valid if  $R$  is much larger than the critical radius

$$R_{\text{vdW}} = \left( \frac{2d^2}{\Delta} \right)^{1/3}. \quad (3.50)$$

In the other limiting case of  $R \ll R_{\text{vdW}}$ , we have  $D \gg 1$  so that Eq. (3.46) becomes

$$W(R) = \frac{d^2 \Delta}{|\Delta| R^3} = \text{sgn}(\Delta) \frac{d^2}{R^3}, \quad (3.51)$$

a dipole-dipole interaction whose sign is again determined by  $\Delta$  alone.

### 3.2.3. The physically realistic situation

While the previous simple example already contains all important ideas about how to proceed, in realistic scenarios many more states have to be included. This necessitates the numerical diagonalization of the two-atom Hamiltonian. Furthermore, we need to put some effort into the calculation of all the matrix elements of the Hamiltonian:

We denote the atomic eigenstate with the quantum numbers  $n_a, l_a, j_a, m_a$ , centered at the nucleus  $i$  by

$$|a^i\rangle = |n_a, l_a, j_a, m_a\rangle_i, \quad (3.52)$$

with  $a$  running from 0 to  $\infty$ . We assume that the nuclei are sufficiently far apart so that there is no overlap between their wave-functions:

$$\langle a^1 | a^2 \rangle = 0 \quad \forall a. \quad (3.53)$$

### 3. Rydberg atoms and their interaction

---

Two-body states will be written as

$$|ab\rangle = |a^1\rangle \otimes |b^2\rangle \quad (3.54)$$

We will calculate the interaction between two Rydberg atoms that are both in the state

$$|0\rangle = |n_0, l_0, j_0, m_0\rangle, \quad (3.55)$$

and, without loss of generality, we define all energies relative to the unperturbed energy of  $|0\rangle$ , so that

$$\varepsilon_0 = \langle 0 | \hat{H}_1 | 0 \rangle = \langle 0 | \hat{H}_2 | 0 \rangle = 0. \quad (3.56)$$

We recall that the one-particle wave-functions are given by Eq. (3.9):

$$\langle \mathbf{r}_i | a^i \rangle = f_{n_a l_a}(r_i) \mathcal{Y}_{l_a j_a m_a}(\vartheta_i, \varphi_i), \quad (3.57)$$

Hence, we find for the dipole matrix elements

$$\langle 00 | \hat{V}_d(\mathbf{R}) | ab \rangle = \mathcal{V}_0^a \mathcal{V}_0^b \left( \frac{\mathbf{C}_0^a \cdot \mathbf{C}_0^b}{R^3} - 3 \frac{(\mathbf{C}_0^a \cdot \mathbf{R})(\mathbf{C}_0^b \cdot \mathbf{R})}{R^5} \right), \quad (3.58)$$

where

$$\mathcal{V}_0^a = \mathcal{V}_{n_0 l_0}^{n_a l_a} = \int dr r^3 f_{n_0 l_0}(r) f_{n_a l_a}(r) \quad (3.59)$$

$$(3.60)$$

is the radial contribution which can be calculated numerically and

$$\mathbf{C}_0^a = \mathbf{C}_{l_0, j_0, m_0}^{l_a, j_a, m_a} = \int d\varphi d(\cos \vartheta) \overline{\mathcal{Y}_{l_0, j_0, m_0}(\vartheta, \varphi)} \begin{pmatrix} \sin \vartheta \cos \varphi \\ \sin \vartheta \sin \varphi \\ \cos \vartheta \end{pmatrix} \mathcal{Y}_{l_a, j_a, m_a}(\vartheta, \varphi) \quad (3.61)$$

is the so-called Clebsch–Gordan coefficient [67]. It is the angular contribution to the matrix elements and it can be evaluated component-by-component in terms of Wigner-3j-symbols. It is convenient to express them in the position space basis

$$(\mathbf{e}_1, \mathbf{e}_2, \mathbf{e}_3) = \left( \frac{\mathbf{e}_x + i\mathbf{e}_y}{\sqrt{2}}, \frac{\mathbf{e}_x - i\mathbf{e}_y}{\sqrt{2}}, \mathbf{e}_z \right) \quad (3.62)$$

The coordinates  $\xi_i$  in that basis are given by

$$\xi_1 \mathbf{e}_1 + \xi_2 \mathbf{e}_2 + \xi_3 \mathbf{e}_3 = x \mathbf{e}_x + y \mathbf{e}_y + z \mathbf{e}_z. \quad (3.63)$$

If we define the spin sign  $s_a = 2(j_a - l_a) \in \{-1, 1\}$ , the prefactors  $c_i$  and the change in the magnetic quantum number  $\mu_i$ , the results can be written as

$$\begin{aligned} & \mathbf{e}_i \cdot \mathbf{C}_{l_0, j_0, m_0}^{l_a, j_a, m_a} \\ &= c_i (-1)^{m_0 + \frac{1}{2}} \left[ s_0 s_a \sqrt{(l_0 + \frac{1}{2} + s_0 m_0)(l_a + \frac{1}{2} + s_a m_a)} \begin{pmatrix} l_0 & 1 & l_a \\ \frac{1}{2} - m_0 & \mu_i & m_a - \frac{1}{2} \end{pmatrix} \right. \\ & \quad \left. - \sqrt{(l_0 + \frac{1}{2} - s_0 m_0)(l_a + \frac{1}{2} - s_a m_a)} \begin{pmatrix} l_0 & 1 & l_a \\ -m_0 - \frac{1}{2} & \mu_i & m_a + \frac{1}{2} \end{pmatrix} \right] \begin{pmatrix} l_0 & 1 & l_a \\ 0 & 0 & 0 \end{pmatrix} \end{aligned}$$

with  $\mu_1 = 1$ ,  $\mu_2 = -1$  and  $\mu_3 = 0$  and  $c_2 = c_3 = 1$  and  $c_1 = -1$ . The calculation is given in Appendix B.

Due to properties of the Wigner-3j-symbols, this formula reflects the well-known one-electron dipole selection rules:

- $l$ -selection rule:

$$\begin{pmatrix} l_0 & 1 & l_a \\ 0 & 0 & 0 \end{pmatrix} \neq 0$$

only if  $|l_0 - 1| \leq l_a \leq l_0 + 1$  and  $l_0 + 1 + l_a$  is an even integer. For  $l_0 = 0$  it is easy to see that this implies  $l_a = 1$ . For  $l_0 > 0$ , we find

$$\begin{aligned} & l_0 - 1 \leq l_a \leq l_0 + 1 \text{ and } l_0 + l_a \text{ is odd.} \\ \Leftrightarrow & l_0 - 1 \leq l_a \leq l_0 + 1 \text{ and one and only one of } l_0 \text{ and } l_a \text{ is odd.} \\ \Rightarrow & l_a = l_0 \pm 1. \end{aligned}$$

Hence, the orbital angular momentum can only change from  $l$  to  $l + 1$  or to  $l - 1$  in any transition. It cannot remain constant. This is very useful for the numerical treatment of the realistic situation since it strongly restricts the number of states that have to be taken into account: when we calculate the interaction of  $s$ -states ( $l = 0$ ) in first order we only need to consider couplings to  $p$ -states ( $l = 1$ ). For  $p$ -states, only  $s$ -states and  $d$ -states need to be considered and so on. A priori, it would be conceivable that second order couplings needed to be taken into account: while  $d$ -states do not couple to  $s$ -states, they do couple to  $p$ -states which, in turn, couple to the  $s$ -states. Hence,  $d$ -states might be important for the calculation of the  $s$ -state-interactions. However, in practice we found no situations where such second-order effects were relevant to the result.

- $m$ -selection rule:

$$\begin{pmatrix} l_0 & 1 & l_a \\ \frac{1}{2} - m_0 & \mu_i & m_a - \frac{1}{2} \end{pmatrix} \neq 0, \quad \begin{pmatrix} l_0 & 1 & l_a \\ -m_0 - \frac{1}{2} & \mu_i & m_a + \frac{1}{2} \end{pmatrix} \neq 0$$

only if  $m_0 - \mu_i = m_a$ . Since  $\mu_i \in \{0, \pm 1\}$ , this is equivalent to  $m_a = m_0$  or  $m_a = m_0 \pm 1$ .

### 3. Rydberg atoms and their interaction

---

- *j*-selection rule:

Since  $l_a = l_0 \pm 1$  and  $j_i = l_i \pm \frac{1}{2}$  it is immediately clear that  $j_a - j_0 \in \{0, \pm 1, \pm 2\}$ . To prove the actual selection rule  $j_a - j_0 \in \{0, \pm 1\}$ , one stills need to exclude the case  $j_a - j_0 = \pm 2$ . This can be shown by explicitly calculating

$$\mathbf{e}_i \cdot \mathbf{C}_{l_0, j_0, m_0}^{l_0 \pm 1, j_0 \pm 2, m_a} = 0.$$

Furthermore, there is a two-electron selection rule as long as  $\mathbf{R}$  points in the  $z$ -direction: since the total angular momentum is conserved, the sum of the  $m$ -quantum numbers  $M$  cannot be changed by  $\hat{V}_d(\mathbf{R})$ . In other words,  $\hat{V}_d(\mathbf{R})$  can couple two-body states

$$|ab\rangle = |n_a l_a j_a m_a\rangle \otimes |n_b l_b j_b m_b\rangle \quad (3.64)$$

and

$$|a'b'\rangle = |n'_a l'_a j'_a m'_a\rangle \otimes |n'_b l'_b j'_b m'_b\rangle \quad (3.65)$$

only if

$$M = m_a + m_b = m'_a + m'_b = M', \quad (3.66)$$

which can be seen by evaluating  $\langle ab | \hat{V}_d(\mathbf{R}) | a'b'\rangle$ . Since the terms involving the  $z$ -direction do not even change the (one-electron)- $m$ , we can ignore them. Only the  $x$ - and  $y$ -directions need to be considered. We transform the relevant term  $\hat{x}_1 \hat{x}_2 + \hat{y}_1 \hat{y}_2$  into the basis (3.62) in which we calculated the Clebsch-Gordan coefficients by using the inverse transformation  $x = \frac{1}{\sqrt{2}}(\xi^1 + \xi^2)$  and  $y = \frac{1}{i\sqrt{2}}(\xi^1 - \xi^2)$ :

$$\begin{aligned} \frac{1}{R^3} \langle ab | \hat{x}_1 \hat{x}_2 + \hat{y}_1 \hat{y}_2 | a'b'\rangle &= \frac{1}{2R^3} \langle ab | (\hat{\xi}_1^1 + \hat{\xi}_1^2)(\hat{\xi}_2^1 + \hat{\xi}_2^2) - (\hat{\xi}_1^1 - \hat{\xi}_1^2)(\hat{\xi}_2^1 - \hat{\xi}_2^2) | a'b'\rangle \\ &= \frac{1}{R^3} \langle ab | \hat{\xi}_1^1 \hat{\xi}_2^2 + \hat{\xi}_2^1 \hat{\xi}_1^2 | a'b'\rangle. \end{aligned} \quad (3.67)$$

Since  $\hat{\xi}_1^i$  decreases the  $m$  of the  $i$ -th electron by one and  $\hat{\xi}_2^i$  increases it by one,  $\hat{\xi}_1^1 \hat{\xi}_2^2 + \hat{\xi}_2^1 \hat{\xi}_1^2$  cannot change  $M$  and, hence, neither can  $\hat{V}_d(\mathbf{R})$ .

Therefore,  $M$  is still a “good quantum number” (i.e, the corresponding observable, here  $\hat{L}_z$ , commutes with the Hamiltonian  $\hat{H}$  including  $\hat{V}_d$ ). Hence,  $\hat{H}$  is separable with respect to  $M$ . This has an implication for the numerical treatment: instead of diagonalizing the full Hamiltonian at once, one can partition the two-body Hilbert space with respect to  $M$  and define Hamiltonians

$$\hat{H}_M = \hat{H} \upharpoonright_M \quad (3.68)$$

as the restrictions of  $\hat{H}$  to the subspace with total magnetic quantum number  $M$ . These can then be diagonalized independently of each other. Due to the smaller matrix sizes this accelerates the diagonalization.

We now return to the task of numerically calculating the inter-atomic interaction. In practice, the Wigner-3j-symbols can be computed using the Racah formula [166]. Once

the matrix for a given  $\mathbf{R}$  has been constructed, it is diagonalized using the Lapack library [6]. This procedure is then repeated for a discretized grid of distance vectors  $\mathbf{R}$ . We have checked that the eigenvalues actually depend only on the distance  $R$ , not on its direction – this is how it should be due to the Hamiltonian’s symmetry and this check serves as validation of the numerical code.  $W(R)$  can then be identified as that eigenvalue curve which asymptotically connects to the two-atom state of interest  $|00\rangle$ . Finally,  $C_6$  can be extracted by fitting the interaction to

$$W(r) = \frac{C_6}{R^6} \quad (3.69)$$

for sufficiently large  $R \gg R_{\text{vdW}}$ , where  $R_{\text{vdW}}$  is the critical radius above which the interaction is purely van-der-Waals like. It can be estimated based on Eq. (3.50).

### 3.2.4. Application to Rubidium

We now apply the method to the Rydberg states of Rubidium-87. The results are important for the later chapters because the effects discussed there depend crucially on the exact form of the interaction and, in particular, its sign (attractive or repulsive). Rubidium was chosen as example because Rubidium BECs are now routinely created in many laboratories. We are particularly interested in finding states where all curves have the same sign since they will be useful in the later chapters. The interactions have been investigated before [182], but in that work spin-orbit was neglected. All results have been checked for convergence with respect to the number of basis states. The total number of two-body states in the basis that was necessary to reach convergence lies between 2500 ( $s$ -states) and 30000 ( $d_{5/2}$ -states).

#### **s-states**

For  $s$ -states ( $l = 0$ ) the interactions are always repulsive which was also found in [182]. The results are depicted in Fig. 3.3. Shown are the coefficients scaled by  $n^{11}$  because this is the scaling that is expected from the simplified example in section 3.2.2.

Since we take spin-orbit coupling into account, there are two  $m$ -degenerate atomic  $s$ -states  $|\uparrow\rangle$  and  $|\downarrow\rangle$  per  $n$ . Hence, we find four two-body interaction curves corresponding asymptotically to the four two-body states  $|\uparrow\uparrow\rangle, |\downarrow\downarrow\rangle$  and  $\frac{1}{\sqrt{2}}(|\uparrow\downarrow\rangle \pm |\downarrow\uparrow\rangle)$ . Due to spatial mirror symmetry ( $z \rightarrow -z$ ), the first two must be identical. In general, the others are different. This is confirmed by the numerical results that show exactly this behavior. We also find that all the curves are very similar (deviations  $< 4\%$ ). This shows that the neglect of spin-orbit coupling in [182] for  $s$ -states is justified.

In chapters 5 and 7, the  $s$ -states will become very important due to the purely repulsive nature of their interactions and because they can be efficiently excited in experiment by a two-photon transition as will be discussed there.

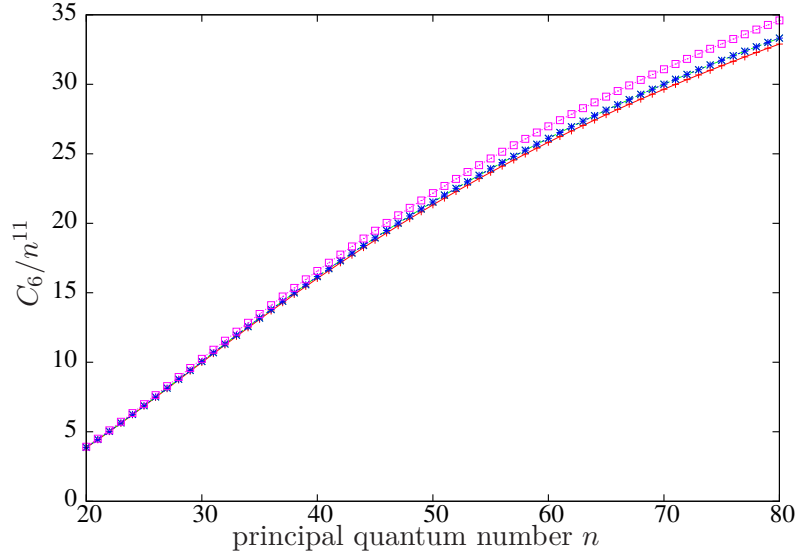


**Figure 3.3.:** Dependence of the van-der-Waals coefficient  $C_6$  on the principal quantum number  $n$  for  $s_{1/2}$  states.  $C_6$  is scaled by  $n^{11}$  since this is the scaling predicted by a simplified perturbative argument (see main text). All curves are repulsive and almost identical so that spin-orbit coupling can typically be neglected for  $s$ -states (cf. [182]).

#### ***p*-states**

For  $p$ -states ( $l = 1$ ) the situation is somewhat more complicated. For  $l = 1$  and  $j = 1/2$  ( $p_{1/2}$  states; see Fig. 3.4) there are again four curves, two of which are identical. One of them is always attractive, one always repulsive. The two identical ones switch sign between  $n = 42$  and  $n = 43$ .

For  $l = 1$  and  $j = 3/2$  ( $p_{3/2}$  states; see Fig. 3.5) we have  $4^2 = 16$  curves, 12 of which are pairwise identical. Hence, there are 10 different curves. Four curves (two of which are identical) show “resonances” between  $n = 37$  and  $n = 38$ . The other curves are repulsive for all  $n$ . In this context, the word “resonance” refers not to a resonance in position space (the resulting interaction curves are always non-singular for  $r \neq 0$ ), but to a significant increase in the van-der-Waals coefficient  $C_6(n)$  as  $n$  approaches certain values (37 and 38 in this case). In other words, the interaction becomes very strong near a resonance and switches from repulsive to attractive or vice versa.

#### ***d*-states**

$d$ -states ( $l = 2$ ) will also be important later on in chapter 6. In  $d_{3/2}$  states ( $j = 3/2$ , Fig. 3.6), there are two resonances, one between  $n = 39$  and  $n = 40$  and one between  $n = 58$  and  $n = 59$ . Below the first resonance and above the second one, all curves are attractive; between them there are always attractive and repulsive curves. This makes

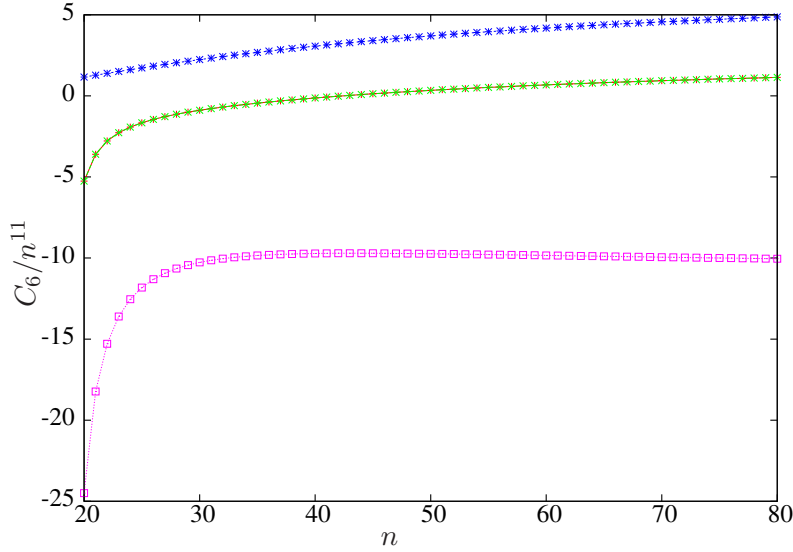


**Figure 3.4.:** Dependence of the van-der-Waals coefficient  $C_6$  on the principal quantum number  $n$  for  $p_{1/2}$  states

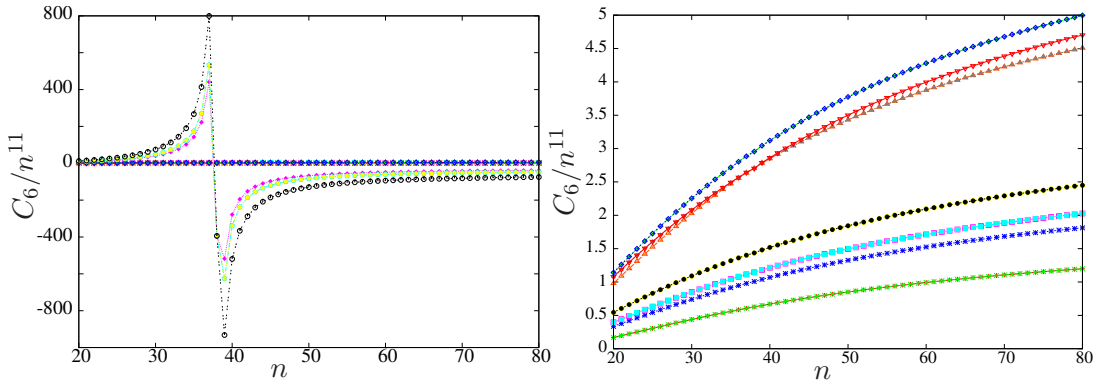


**Figure 3.5.:** Dependence of the van-der-Waals coefficient  $C_6$  on the principal quantum number  $n$  for  $p_{3/2}$  states. Left side: all curves; right side: only non-resonant curves (all of which are repulsive).

$d_{3/2}$  states with  $n \geq 59$  a very useful example of attractive Rydberg states (cf. chapter 6).

The  $d_{5/2}$  states ( $j = 5/2$ , Fig. 3.7) exhibit a total number of  $6^2 = 36$  curves, and for most  $n$  curves of different signs exist. Only in the interval  $n \in \{44 \dots 51\}$  all curves are attractive. A resonance exists directly below this interval (but not all curves resonate at the exact same  $n$ ).

In general, it should be noted that the calculations become unreliable in the close vicinity of resonances, since an extremely large number of states is needed to achieve convergence. Furthermore, the interaction can no longer be described in good approximation as van-

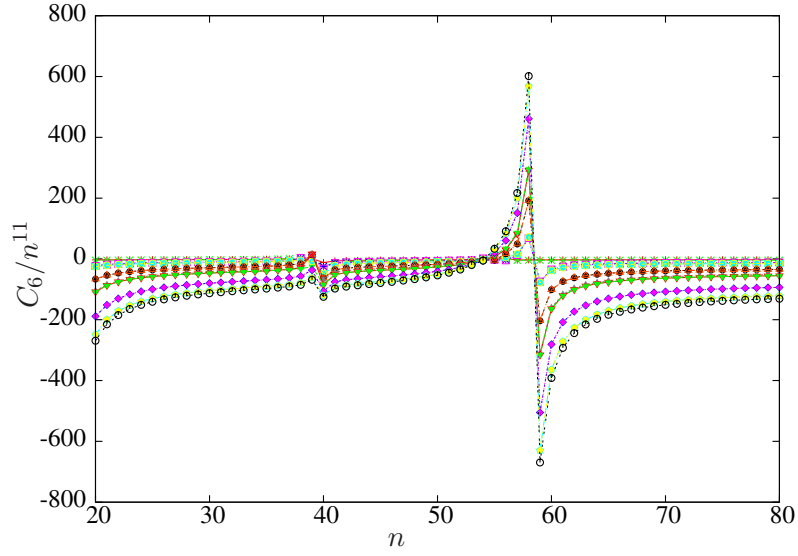


**Figure 3.6.:** Dependence of the van-der-Waals coefficient  $C_6$  on the principal quantum number  $n$  for  $d_{3/2}$  states. For  $n \geq 59$  all curves are attractive.

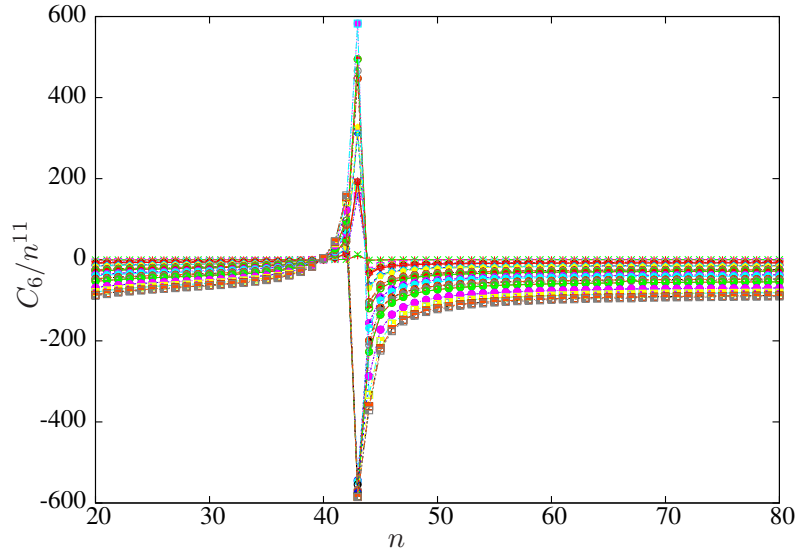


**Figure 3.7.:** Dependence of the van-der-Waals coefficient  $C_6$  on the principal quantum number  $n$  for  $d_{5/2}$  states. All curves are attractive in the interval  $44 \leq n \leq 51$ . For higher  $n$ , attractive as well as repulsive curves exist.

der-Waals like. Instead, it has a significant  $1/R^3$  contribution which is consistent with the simple picture we developed in the previous section (cf. Eqs. (3.48), (3.50) and (3.51)). In the later chapters we will only use states that are far from resonance, so this is not an issue for us and we can always assume a pure van-der-Waals interaction. Still, we needed to find out where the resonances are to avoid using states in their vicinity.

Our results are consistent with earlier calculations [169].

Summarizing, we have found for Rubidium that

- $s$ -states are always repulsive. This will be important in chapters 5 and 7.
- $p_{1/2}$ -states have attractive as well as repulsive curves at all  $n$ .
- $p_{3/2}$ -states exhibit only repulsive curves for  $n \leq 37$ . At  $n = 37$  some of them go through a resonance and become attractive.
- $d_{3/2}$ -states have two resonances and are always attractive for  $n \geq 59$ . This (together with Strontium  $s$ -states) will become important in chapter 6.
- $d_{5/2}$ -states are fully attractive for  $n \in [44, 51]$ ; at all other  $n$ , there are always curves with different signs.



## 4. Rydberg dressing

Rydberg states have long radiative lifetimes on the order of  $100\ \mu\text{s}$  to  $1\text{ms}$  as we discussed in the beginning of chapter 3. However, even this long lifetime is still too short to observe the atomic dynamics we are interested in.

In this chapter, we will introduce the dressing scheme [91, 177]. In this scheme, the atomic ground state is off-resonantly coupled to a Rydberg state. We will show that this leads to a new ground state of the laser-perturbed atom that still has a strong effective interaction but a significantly longer lifetime than the Rydberg state. We will derive the interaction of the perturbed state using perturbation theory for the scenario of non-degenerate Rydberg-states (i.e.,  $s$ -states) as well as degenerate ones (all other Rydberg states). Interesting properties of a gas with dressing-interaction will be discussed in the subsequent chapters in detail.

### 4.1. Setup

We consider a BEC of alkali atoms (typically Rubidium) each of which has an atomic ground state  $|g\rangle$  and at least one Rydberg state  $|e\rangle = |n, l, j, m\rangle$ . These states are off-resonantly coupled by a laser or combination of lasers. We will explicitly consider the two situations where  $|e\rangle$  is either an  $s$ -state or a  $d$ -state. Since  $|g\rangle$  is an  $s$ -state in Rubidium, two lasers are needed in each case and the excitation will proceed via an intermediate  $p$ -state (cf. Fig. 4.1). In section 4.2.3, we will show that this intermediate state can be adiabatically eliminated if it is far-detuned and that the system can be treated considering only two states  $|g\rangle$  and  $|e\rangle$ . We denote the total Rabi frequency of the transition by  $\Omega$  and the total detuning by  $\Delta = \omega_L - \omega_a$ , where  $\omega_a = (E_e - E_g)/\hbar$  is the atomic transition frequency and  $\omega_L$  is the laser frequency. We assume that the coupling is off-resonant in the sense that  $\Delta \gg \Omega$ . As we will see, this procedure combined with the strong van-der-Waals interaction between Rydberg states (see previous chapter) leads to a peculiar form of interaction in the BEC.

### 4.2. Dressing to non-degenerate states

We will first consider the case with only one Rydberg state. In reality, this corresponds to  $s$ -states because there are only two  $s$ -states for each quantum number  $n$  and all four of their interaction curves are either exactly identical (if spin-orbit coupling is ignored) or so similar (see Fig. 3.3) that the deviation can safely be ignored. Later (section 4.3), we will move to the generalized situation where there is a number of  $m$ -degenerate Rydberg states (e.g.,  $d$ -states which we will consider explicitly).

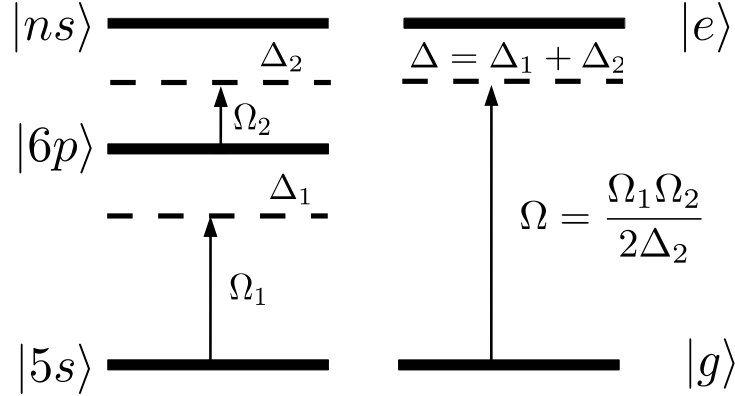


**Figure 4.1.:** Left: nondegenerate dressing scheme for a Rubidium atom. The  $5s$ -ground state is off-resonantly coupled to the  $6p$ -state, which in turn is coupled to a highly excited  $s$ -state. Right: effective two-state scheme, where the intermediate  $p$ -state has been adiabatically eliminated. (cf. section 4.2.3). The scheme is identical for other alkali atoms, except that the  $5s$ -state has to be replaced by the respective ground state.

#### 4.2.1. Interaction between a two-level atom and a laser

We start by considering a single atom with the atomic eigenstates  $|g\rangle$  and  $|e\rangle$ , corresponding eigenenergies  $E_g = 0$  (which can be chosen without loss of generality) and  $E = \hbar\omega_a$ , under the influence of a laser field which is given by

$$\mathbf{E}(\mathbf{r}, t) = \mathbf{E}_0 \cos(\omega_L t - \mathbf{k} \cdot \mathbf{r}) = \frac{1}{2} \mathbf{E}_0 \left( e^{i(\omega_L t - \mathbf{k} \cdot \mathbf{r})} + e^{-i(\omega_L t - \mathbf{k} \cdot \mathbf{r})} \right), \quad (4.1)$$

The Hamiltonian of the system is

$$\hat{H}_0 = \hat{H}_{\text{atom}} + \hat{h}_{\text{int}} \quad (4.2)$$

$$= \hbar\omega_a \hat{\sigma}_{ee} + q\hat{\mathbf{r}} \cdot \mathbf{E}(\hat{\mathbf{r}}, t) \quad (4.3)$$

$$= \hbar\omega_a \hat{\sigma}_{ee} + \frac{1}{2} q\hat{\mathbf{r}} \cdot \mathbf{E}_0 \left( e^{i(\omega_L t - \mathbf{k} \cdot \hat{\mathbf{r}})} + e^{-i(\omega_L t - \mathbf{k} \cdot \hat{\mathbf{r}})} \right) \quad (4.4)$$

where  $q = -e$  is the electron charge.  $q\hat{\mathbf{r}}e^{\pm i\mathbf{k} \cdot \hat{\mathbf{r}}}$  can be expressed in the two-state basis  $\{|g\rangle, |e\rangle\}$ :

$$q\hat{\mathbf{r}}e^{\pm i\mathbf{k} \cdot \hat{\mathbf{r}}} = \langle g|q\hat{\mathbf{r}}e^{\pm i\mathbf{k} \cdot \hat{\mathbf{r}}}|e\rangle |g\rangle \langle e| + \langle e|q\hat{\mathbf{r}}e^{\pm i\mathbf{k} \cdot \hat{\mathbf{r}}}|g\rangle |e\rangle \langle g| \quad (4.5)$$

$$+ \langle g|q\hat{\mathbf{r}}e^{\pm i\mathbf{k} \cdot \hat{\mathbf{r}}}|g\rangle |g\rangle \langle g| + \langle e|q\hat{\mathbf{r}}e^{\pm i\mathbf{k} \cdot \hat{\mathbf{r}}}|e\rangle |e\rangle \langle e|. \quad (4.6)$$

We can now perform a dipole approximation, neglecting the spatial dependence of the electric field. The Rydberg state  $|e\rangle$  typically has a large size on the order of hundreds of nanometers (see previous chapter), which is the same order of magnitude as the laser wavelength  $2\pi/k$ . Hence, on first glance, the possibility of a dipole approximation is precluded. However, if the scalar products in the previous expression are written as

integrals of the form

$$\int d^3r \overline{\psi_g(\mathbf{r})} q\mathbf{r} e^{\pm i\mathbf{k}\cdot\mathbf{r}} \psi_e(\mathbf{r}), \quad (4.7)$$

we see that they have significant contributions only from positions where the product  $|\psi_g(\mathbf{r})\psi_e(\mathbf{r})|$  is large. Since the ground state  $|g\rangle$  has a size of only a few atomic units ( $< 1\text{nm} \ll 2\pi/k$ ), also the product  $|\psi_g(\mathbf{r})\psi_e(\mathbf{r})|$  has a size much smaller than the wavelength so that only from with  $\mathbf{k}\cdot\mathbf{r} \ll 1$  contribute significantly. Therefore, we can apply the dipole approximation and, by using  $\langle g|\hat{\mathbf{r}}|g\rangle = \langle e|\hat{\mathbf{r}}|e\rangle = 0$ , we find

$$q\hat{\mathbf{r}}e^{\pm i\mathbf{k}\cdot\hat{\mathbf{r}}} \approx q\hat{\mathbf{r}} = \langle g|q\hat{\mathbf{r}}|e\rangle |g\rangle \langle e| + \langle e|q\hat{\mathbf{r}}|g\rangle |e\rangle \langle g| = \mathbf{d}(\hat{\sigma}_{eg} + \hat{\sigma}_{ge}), \quad (4.8)$$

where  $\mathbf{d} = \langle g|q\hat{\mathbf{r}}|e\rangle$  is the dipole matrix element (which can be chosen to be real without loss of generality). Here, we have also defined the operators  $\hat{\sigma}_{ee} = |e\rangle \langle e|$ ,  $\hat{\sigma}_{eg} = |e\rangle \langle g|$  and  $\hat{\sigma}_{ge} = |g\rangle \langle e|$ .

The Hamiltonian is

$$\hat{H}_0 = \hbar\omega_a \hat{\sigma}_{ee} + \frac{1}{2} \mathbf{E}_0 \cdot \mathbf{d} (\hat{\sigma}_{eg} + \hat{\sigma}_{ge}) (e^{i\omega_L t} + e^{-i\omega_L t}). \quad (4.9)$$

It is useful to transform the problem to the interaction picture by applying the unitary transformation

$$\hat{U} = e^{-i\hbar\omega_a \hat{\sigma}_{ee} t}, \quad (4.10)$$

from which we obtain the Hamiltonian

$$\hat{H}_0^I = \hat{U}^\dagger \hat{H}_0 \hat{U} - \hbar\omega_a \hat{\sigma}_{ee} \quad (4.11)$$

$$= \frac{1}{2} \mathbf{E}_0 \cdot \mathbf{d} (\hat{\sigma}_{eg} e^{i\omega_a t} + \hat{\sigma}_{ge} e^{-i\omega_a t}) (e^{i\omega_L t} + e^{-i\omega_L t}) \quad (4.12)$$

$$= \frac{\hbar\Omega}{2} (\hat{\sigma}_{eg} e^{i(\omega_a + \omega_L)t} + \hat{\sigma}_{ge} e^{i\Delta t} + \hat{\sigma}_{eg} e^{-i\Delta t} + \hat{\sigma}_{ge} e^{-i(\omega_a + \omega_L)t}), \quad (4.13)$$

where  $\Delta = \omega_L - \omega_a$  is the so-called detuning and  $\Omega = \mathbf{E}_0 \cdot \mathbf{d}/\hbar$  is the (resonant) Rabi frequency.

### 4.2.2. The rotating wave approximation

First, we perform another unitary transformation  $\hat{U} = e^{-i\hbar\Delta \hat{\sigma}_{ee} t}$  to partially remove the time dependence and find

$$\hat{H} = \hat{U}^\dagger \hat{H}_0^I \hat{U} - \hbar\Delta \hat{\sigma}_{ee} \quad (4.14)$$

$$= -\hbar\Delta \hat{\sigma}_{ee} + \frac{\hbar\Omega}{2} (\hat{\sigma}_{ge} + \hat{\sigma}_{eg} + \hat{\sigma}_{eg} e^{i(\omega_a + \omega_L + \Delta)t} + \hat{\sigma}_{ge} e^{-i(\omega_a + \omega_L + \Delta)t}) \quad (4.15)$$

$$= -\hbar\Delta \hat{\sigma}_{ee} + \frac{\hbar\Omega}{2} (\hat{\sigma}_{ge} + \hat{\sigma}_{eg} + \hat{\sigma}_{eg} e^{2i\omega_L t} + \hat{\sigma}_{ge} e^{-2i\omega_L t}). \quad (4.16)$$

We use the Hilbert space basis  $(|e\rangle, |g\rangle)$ , i.e.,

$$|\psi\rangle = c_g |g\rangle + c_e |e\rangle \quad (4.17)$$

and numerically find the solution of the Schrödinger equation

$$i\hbar\partial_t |\psi(t)\rangle = \hat{H} |\psi(t)\rangle \quad (4.18)$$

with the initial condition  $|\psi(0)\rangle = |g\rangle$ . It is depicted in Fig. 4.2. For large values of  $\omega_L$ , the solution is a combination of slow oscillations (the so-called ‘‘Rabi-oscillations’’) and small, fast oscillations. The latter vanish for  $\omega_L \rightarrow \infty$ . This is due to the quickly oscillating nature of the terms  $e^{\pm i(\omega_a + \omega_L + \Delta)t}$  in the Hamiltonian (4.16). Hence, if  $\omega_a + \omega_L$  becomes large enough ( $\omega_a + \omega_L \gg \Delta, \Omega$ ), they average out over very short timescales  $\sim (\omega_L + \omega_a)^{-1} \ll \Delta^{-1}, \Omega^{-1}$  and it is justified to neglect them. This is known as the

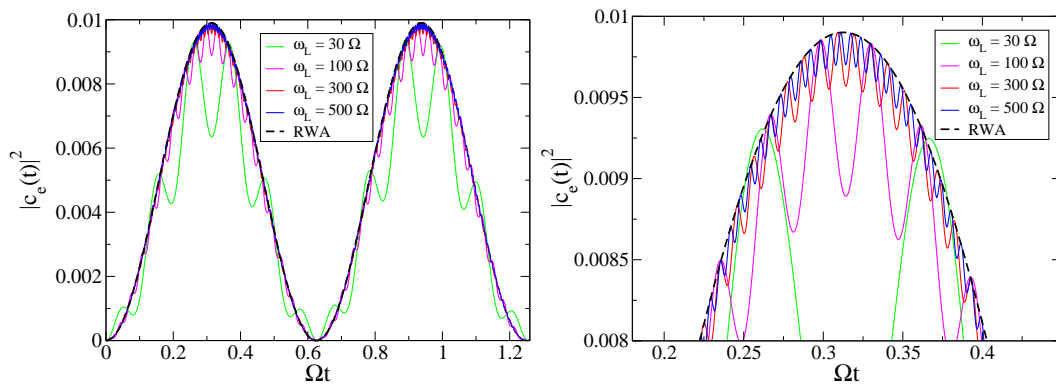


**Figure 4.2.:** Time evolution of the population  $|c_e(t)|^2$  of the excited state  $|e\rangle$  for  $\Delta = 10\Omega$  and various values of  $\omega_L$  according to Eqs. (4.16) and (4.18). For  $\omega_L \rightarrow \infty$ , the small, fast oscillations vanish and all curves converge to the curve given by Eq. (4.20) (‘‘RWA’’). The left panel shows two full Rabi periods, the right panel shows an enlarged section, where the convergence of the curves towards the result of the RWA can be seen.

rotating wave approximation (RWA)<sup>1</sup>. This leaves us with

$$\hat{H} = -\hbar\Delta\hat{\sigma}_{ee} + \frac{\hbar\Omega}{2} (\hat{\sigma}_{ge} + \hat{\sigma}_{eg}), \quad (4.19)$$

which is our final Hamiltonian describing the atom-laser interaction. For this time-independent Hamiltonian, the SE can be solved analytically and yields

$$c_e(t) = i\frac{\Omega}{\tilde{\Omega}} e^{\frac{1}{2}i\Delta t} \cos\left(\frac{1}{2}\tilde{\Omega}t\right), \quad (4.20)$$

<sup>1</sup>Another way of justifying the approximation is in Fourier space where it means to neglect states that are energetically far away from the others.

where  $\tilde{\Omega} = \sqrt{\Delta^2 + \Omega^2}$  is the “generalized” or “off-resonant” Rabi frequency. This is precisely the limit to which the exact dynamical results of the Schrödinger equation (4.18) converge for  $\omega_L/\Omega \rightarrow \infty$  (see Fig. 4.2).

### 4.2.3. Reduction of a three-level atom to two levels

All of the previous considerations involved two-level atoms. In practice, however, some of the states that have the most useful van-der-Waals interactions ( $s$ -states and  $d$ -states) are only accessible via a two-photon transition. In this section, we will show that a three-state atom with the states

$$|g\rangle, |p\rangle, |e\rangle,$$

can be described as an effective two state system if the intermediate state  $|p\rangle$  is far detuned.

$|g\rangle$  is the atomic ground state ( $|5s\rangle$  for Rubidium, and generally  $|n_0s\rangle$  for alkali atoms),  $|p\rangle$  is an intermediate state and  $|e\rangle$  is a Rydberg state whose van-der-Waals interaction and long lifetime we would like to utilize (see left part of Fig. 4.1). The Hamiltonian in the RWA can be derived analogously to the two-level RWA Hamiltonian (4.19) and it is

$$\hat{H} = \hbar \begin{pmatrix} 0 & \frac{1}{2}\Omega_1 & 0 \\ \frac{1}{2}\Omega_1 & -\Delta_1 & \frac{1}{2}\Omega_2 \\ 0 & \frac{1}{2}\Omega_2 & -\Delta \end{pmatrix} \quad (4.21)$$

with  $\Delta = \Delta_1 + \Delta_2$ , so  $\Delta_1$  is the detuning between  $|g\rangle$  and  $|p\rangle$ .  $\Delta_2$  is the detuning between  $|p\rangle$  and  $|e\rangle$ . We assume, without loss of generality, the Rabi frequencies  $\Omega_i$  to be real. Furthermore, the decay of the states  $|e\rangle$  and, more importantly,  $|p\rangle$  has to be taken into account ( $|p\rangle$  decays much faster than  $|e\rangle$ ).

Including the decay, the system can be described by the Lindblad equation [72, 121]

$$i\partial_t \hat{\rho}(t) = \frac{1}{\hbar} [\hat{H}, \hat{\rho}(t)] + i\mathcal{L}(\hat{\rho}), \quad (4.22)$$

where the so-called Lindblad super operator

$$\mathcal{L}(\hat{\rho}) = -\frac{1}{2} \sum_{i \in \{p,e\}} \left( \hat{C}_i^\dagger \hat{C}_i \hat{\rho}(t) + \hat{\rho}(t) \hat{C}_i^\dagger \hat{C}_i \right) + \sum_{i \in \{p,e\}} \hat{C}_i \hat{\rho}(t) \hat{C}_i^\dagger \quad (4.23)$$

with the operators

$$\hat{C}_p = \sqrt{\Gamma_p} |g\rangle \langle p|, \quad (4.24)$$

$$\hat{C}_e = \sqrt{\Gamma_e} |p\rangle \langle e| \quad (4.25)$$

describes the decay from  $|p\rangle$  to  $|g\rangle$  and from  $|e\rangle$  to  $|p\rangle$  with decay rates  $\gamma_p$  and  $\gamma_e$ . Since we would like to minimize the total decay rate, we assume that  $|\Delta_1|$  and  $|\Delta_2|$  are large

compared to the other frequencies. This ensures that  $|p\rangle$  is only weakly populated, and (as the derivation will show) minimizes the total decay.

In the basis  $(|g\rangle, |p\rangle, |e\rangle)$ , we write the density matrix as

$$\hat{\rho} = \begin{pmatrix} a_g & c_{gp} & c_{ge} \\ c_{pg} & a_p & c_{pe} \\ c_{eg} & c_{ep} & a_e \end{pmatrix} \quad (4.26)$$

with  $c_{ji} = \overline{c_{ij}}$  and  $a_g + a_p + a_e = 1$ .

Then, the Lindblad term reads

$$\mathcal{L}(\hat{\rho}) = \begin{pmatrix} a_p\Gamma_p & -\frac{1}{2}c_{gp}\Gamma_p & -\frac{1}{2}c_{ge}\Gamma_e \\ -\frac{1}{2}c_{pg}\Gamma_p & a_e\Gamma_e - a_p\Gamma_p & -\frac{1}{2}c_{pe}(\Gamma_e + \Gamma_p) \\ -\frac{1}{2}c_{eg}\Gamma_e & -\frac{1}{2}c_{ep}(\Gamma_e + \Gamma_p) & -a_e\Gamma_e \end{pmatrix}. \quad (4.27)$$

Hence, the Lindblad equation can be written component-by-component as

$$i\dot{a}_g = \frac{1}{2}\Omega_1(c_{pg} - c_{gp}) + ia_p\Gamma_p, \quad (4.28)$$

$$i\dot{c}_{gp} = \frac{1}{2}\Omega_1(a_p - a_g) + c_{gp}\Delta_1 - \frac{1}{2}\Omega_2c_{ge} - \frac{1}{2}ic_{gp}\Gamma_p, \quad (4.29)$$

$$i\dot{c}_{ge} = \frac{1}{2}\Omega_1c_{pe} - \frac{1}{2}\Omega_2c_{gp} + c_{ge}\Delta - \frac{1}{2}ic_{ge}\Gamma_e, \quad (4.30)$$

$$i\dot{a}_p = \frac{1}{2}\Omega_1(c_{gp} - c_{pg}) + \frac{1}{2}\Omega_2(c_{ep} - c_{pe}) + ia_e\Gamma_e - ia_p\Gamma_p, \quad (4.31)$$

$$i\dot{c}_{pe} = \frac{1}{2}\Omega_1c_{ge} + \frac{1}{2}\Omega_2(a_e - a_p) + c_{pe}\Delta_2 - \frac{1}{2}ic_{pe}(\Gamma_e + \Gamma_p), \quad (4.32)$$

$$i\dot{a}_e = \frac{1}{2}\Omega_2(c_{pe} - c_{ep}) - ia_e\Gamma_e. \quad (4.33)$$

The relevant condition that has to be fulfilled so that the intermediate state  $|p\rangle$  can be eliminated is that the intermediate detuning  $\Delta_1$  is large compared to the other frequencies:

$$\Delta_1 \gg \Delta, \Omega_1, \Omega_2, \Gamma_e, \Gamma_p. \quad (4.34)$$

Then, the oscillations of the population  $a_p$  and the coherences  $c_{gp}$  and  $c_{pe}$  occur on short timescales and have small amplitudes. Thus, we can eliminate the intermediate state  $|p\rangle$  by setting

$$\dot{a}_p = \dot{c}_{gp} = \dot{c}_{pe} = 0. \quad (4.35)$$

This yields, by solving Eqs. (4.30), (4.31) and (4.32):

$$a_p = \frac{\Omega_1(c_{gp} - c_{pg}) + \Omega_2(c_{ep} - c_{pe})}{2i\Gamma_p} + a_e \frac{\Gamma_e}{\Gamma_p} \quad (4.36)$$

$$c_{gp} = \frac{1}{\Delta_1 - \frac{1}{2}i\Gamma_p} \left( \frac{1}{2}\Omega_1(a_g - a_p) + \frac{1}{2}\Omega_2c_{ge} \right) \quad (4.37)$$

$$= \frac{\Delta_1 + \frac{1}{2}i\Gamma_p}{\Delta_1^2 + \frac{1}{4}\Gamma_p^2} \left( \frac{1}{2}\Omega_1(a_g - a_p) + \frac{1}{2}\Omega_2c_{ge} \right), \quad (4.38)$$

$$c_{pe} = \frac{1}{\Delta_2 - \frac{1}{2}i(\Gamma_e + \Gamma_p)} \left( \frac{1}{2}\Omega_2(a_p - a_e) - \frac{1}{2}\Omega_1c_{ge} \right) \quad (4.39)$$

$$= \frac{\Delta_2 + \frac{1}{2}i(\Gamma_e + \Gamma_p)}{\Delta_2^2 + \frac{1}{4}(\Gamma_e + \Gamma_p)^2} \left( \frac{1}{2}\Omega_2(a_p - a_e) - \frac{1}{2}\Omega_1c_{ge} \right). \quad (4.40)$$

We now perform a number of approximations. We neglect:

- $a_p$  compared to  $a_e$  and  $a_g$ ,
- $\Gamma_e$  compared to  $\Gamma_p$ ,
- $\Gamma_p^2$  compared to  $\Delta_1^2$  and  $\Delta_2^2$

Since  $\Delta \ll |\Delta_1|, |\Delta_2|$ , we also assume that  $\Delta_1 \approx -\Delta_2$ . Thus, the previous two equations simplify to

$$c_{gp} = \left( \frac{1}{\Delta_1} + \frac{i\Gamma_p}{2\Delta_1^2} \right) \left( \frac{1}{2}\Omega_1a_g + \frac{1}{2}\Omega_2c_{ge} \right), \quad (4.41)$$

$$c_{pe} = \left( -\frac{1}{\Delta_1} + \frac{i\Gamma_p}{2\Delta_1^2} \right) \left( -\frac{1}{2}\Omega_2a_e - \frac{1}{2}\Omega_1c_{ge} \right). \quad (4.42)$$

We will shortly need the following two expressions:

$$\begin{aligned} c_{pg} - c_{gp} &= \left( \frac{1}{\Delta_1} - \frac{i\Gamma_p}{2\Delta_1^2} \right) \left( \frac{\Omega_1}{2}a_g + \frac{\Omega_2}{2}c_{eg} \right) - \left( \frac{1}{\Delta_1} + \frac{i\Gamma_p}{2\Delta_1^2} \right) \left( \frac{\Omega_1}{2}a_g + \frac{\Omega_2}{2}c_{ge} \right) \\ &= \frac{\Omega_2}{2\Delta_1}(c_{eg} - c_{ge}) - \frac{i\Gamma_p\Omega_1}{2\Delta_1^2}a_g - \frac{i\Omega_2\Gamma_p}{4\Delta_1^2}(c_{eg} + c_{ge}), \end{aligned} \quad (4.43)$$

$$c_{pe} - c_{ep} = -\frac{\Omega_1}{2\Delta_1}(c_{eg} - c_{ge}) - \frac{i\Gamma_p\Omega_2}{2\Delta_1^2}a_e - \frac{i\Omega_1\Gamma_p}{4\Delta_1^2}(c_{ge} + c_{eg}). \quad (4.44)$$

Combined with Eq. (4.36), they imply:

$$\begin{aligned}
 a_p &= \frac{-\frac{\Omega_1\Omega_2}{2\Delta_1}(c_{eg} - c_{ge}) + \frac{i\Gamma_p\Omega_1^2}{2\Delta_1^2}a_g + \frac{i\Omega_1\Omega_2\Gamma_p}{4\Delta_1^2}(c_{eg} + c_{ge})}{2i\Gamma_p} \\
 &\quad + \frac{\frac{\Omega_1\Omega_2}{2\Delta_1}(c_{eg} - c_{ge}) + \frac{i\Gamma_p\Omega_2^2}{2\Delta_1^2}a_e + \frac{i\Omega_1\Omega_2\Gamma_p}{4\Delta_1^2}(c_{ge} + c_{eg})}{2i\Gamma_p} + a_e \frac{\Gamma_e}{\Gamma_p} \\
 &= \frac{\Omega_1^2}{4\Delta_1^2}a_g + \frac{\Omega_2^2}{4\Delta_1^2}a_e + \frac{\Omega_1\Omega_2}{4\Delta_1^2}(c_{ge} + c_{eg}) + a_e \frac{\Gamma_e}{\Gamma_p}. \tag{4.45}
 \end{aligned}$$

Substituting Eqs. (4.41)–(4.45) into the component-by-component Lindblad equation (Eqs. (4.28), (4.30) and (4.33)) and introducing the two-photon Rabi frequency

$$\Omega = \frac{\Omega_1\Omega_2}{2\Delta_1}, \tag{4.46}$$

we obtain the three equations for  $a_g$ ,  $a_e$  and  $c_{ge}$ :

$$\begin{aligned}
 i\dot{a}_g &= \frac{1}{2}\Omega_1 \left[ \frac{\Omega_2}{2\Delta_1}(c_{eg} - c_{ge}) - \frac{i\Gamma_p\Omega_1}{2\Delta_1^2}a_g - \frac{i\Omega_2\Gamma_p}{4\Delta_1^2}(c_{eg} + c_{ge}) \right] \\
 &\quad + i \left[ \frac{\Omega_1^2}{4\Delta_1^2}a_g + \frac{\Omega_2^2}{4\Delta_1^2}a_e + \frac{\Omega_1\Omega_2}{4\Delta_1^2}(c_{ge} + c_{eg}) + a_e \frac{\Gamma_e}{\Gamma_p} \right] \Gamma_p \\
 &= \frac{\Omega}{2}(c_{eg} - c_{ge}) + \frac{i\Omega\Gamma_p}{4\Delta_1}(c_{ge} + c_{eg}) + ia_e \left( \Gamma_e + \frac{\Omega_2^2}{4\Delta_1^2}\Gamma_p \right), \tag{4.47}
 \end{aligned}$$

$$\begin{aligned}
 i\dot{a}_e &= \frac{1}{2}\Omega_2 \left[ -\frac{\Omega_1}{2\Delta_1}(c_{eg} - c_{ge}) - \frac{i\Gamma_p\Omega_2}{2\Delta_1^2}a_e - \frac{i\Omega_1\Gamma_p}{4\Delta_1^2}(c_{ge} + c_{eg}) \right] - ia_e\Gamma_e \\
 &= -\frac{\Omega}{2}(c_{eg} - c_{ge}) - \frac{i\Omega\Gamma_p}{4\Delta_1}(c_{ge} + c_{eg}) - ia_e \left( \Gamma_e + \frac{\Omega_2^2}{4\Delta_1^2}\Gamma_p \right) \tag{4.48}
 \end{aligned}$$

$$\begin{aligned}
 i\dot{c}_{ge} &= \frac{1}{2}\Omega_1 \left[ \left( -\frac{1}{\Delta_1} + \frac{i\Gamma_p}{2\Delta_1^2} \right) \left( -\frac{1}{2}\Omega_2 a_e - \frac{1}{2}\Omega_1 c_{ge} \right) \right] \\
 &\quad - \frac{1}{2}\Omega_2 \left[ \left( \frac{1}{\Delta_1} + \frac{i\Gamma_p}{2\Delta_1^2} \right) \left( \frac{1}{2}\Omega_1 a_g + \frac{1}{2}\Omega_2 c_{ge} \right) \right] + c_{ge}\Delta - \frac{1}{2}ic_{ge}\Gamma_e \\
 &= \frac{\Omega}{2}(a_e - a_g) + \left( \Delta + \frac{\Omega_1^2 - \Omega_2^2}{4\Delta_1} \right) c_{ge} - \frac{i\Gamma_p\Omega}{4\Delta_1}(a_g + a_e) \\
 &\quad - \frac{1}{2}ic_{ge} \left( \Gamma_e + \frac{\Omega_1^2 + \Omega_2^2}{4\Delta_1^2}\Gamma_p \right). \tag{4.49}
 \end{aligned}$$

We can rewrite them in the form

$$i\dot{a}_g = \left(\frac{\Omega}{2} + \frac{i\Omega\Gamma_p}{4\Delta_1}\right) c_{eg} - \left(\frac{\Omega}{2} - \frac{i\Omega\Gamma_p}{4\Delta_1}\right) c_{ge} + ia_e \left(\Gamma_e + \frac{\Omega_2^2}{4\Delta_1^2}\Gamma_p\right), \quad (4.50)$$

$$i\dot{a}_e = -\left(\frac{\Omega}{2} + \frac{i\Omega\Gamma_p}{4\Delta_1}\right) c_{eg} + \left(\frac{\Omega}{2} - \frac{i\Omega\Gamma_p}{4\Delta_1}\right) c_{ge} - ia_e \left(\Gamma_e + \frac{\Omega_2^2}{4\Delta_1^2}\Gamma_p\right), \quad (4.51)$$

$$\begin{aligned} i\dot{c}_{ge} = & \left(\frac{\Omega}{2} - \frac{i\Gamma_p\Omega}{4\Delta_1}\right) a_e - \left(\frac{\Omega}{2} + \frac{i\Gamma_p\Omega}{4\Delta_1}\right) a_g + \left(\Delta + \frac{\Omega_1^2 - \Omega_2^2}{4\Delta_1}\right) c_{ge} \\ & - \frac{1}{2}ic_{ge} \left(\Gamma_e + \frac{\Omega_1^2 + \Omega_2^2}{4\Delta_1^2}\Gamma_p\right), \end{aligned} \quad (4.52)$$

and we can replace the effective Rabi frequencies

$$\Omega' = \Omega \pm \frac{i\Omega\Gamma_p}{4\Delta_1} \quad (4.53)$$

by  $\Omega$ . This is justified since only the modulus of  $\Omega'$  is relevant and

$$|\Omega'| = \Omega \sqrt{1 + \frac{\Gamma_p^2}{4\Delta_1^2}} \approx \Omega. \quad (4.54)$$

This and  $\Delta + \frac{\Omega_1^2 - \Omega_2^2}{4\Delta_1} \approx \Delta$  simplify the equations to

$$i\dot{a}_g = \frac{\Omega}{2} (c_{eg} - c_{ge}) + ia_e \left(\Gamma_e + \frac{\Omega_2^2}{4\Delta_1^2}\Gamma_p\right), \quad (4.55)$$

$$i\dot{a}_e = \frac{\Omega}{2} (c_{ge} - c_{eg}) - ia_e \left(\Gamma_e + \frac{\Omega_2^2}{4\Delta_1^2}\Gamma_p\right), \quad (4.56)$$

$$i\dot{c}_{ge} = \frac{\Omega}{2} (a_e - a_g) + \left(\Delta + \frac{\Omega_1^2 - \Omega_2^2}{4\Delta_1}\right) c_{ge} - \frac{1}{2}ic_{ge} \left(\Gamma_e + \frac{\Omega_1^2 + \Omega_2^2}{4\Delta_1^2}\Gamma_p\right). \quad (4.57)$$

This set of equations can be written as a generalized *two-state* Lindblad equation:

$$i\partial_t \hat{\rho}(t) = \frac{1}{\hbar} [\hat{H}, \hat{\rho}(t)] + i\mathcal{L}(\hat{\rho}) + i\mathcal{L}'(\hat{\rho}) \quad (4.58)$$

with

$$\hat{H} = \hbar \begin{pmatrix} 0 & \frac{1}{2}\Omega \\ \frac{1}{2}\Omega & -\Delta \end{pmatrix}, \quad (4.59)$$

$$\hat{\rho} = \begin{pmatrix} a_g & c_{ge} \\ c_{eg} & a_e \end{pmatrix}, \quad (4.60)$$

$$(4.61)$$

where the decay consists of two parts: There is a standard decay channel, given by

$$\mathcal{L}(\hat{\rho}) = -\frac{1}{2} \left( \hat{C}^\dagger \hat{C} \hat{\rho}(t) + \hat{\rho}(t) \hat{C}^\dagger \hat{C} \right) + \hat{C} \hat{\rho}(t) \hat{C}^\dagger, \quad (4.62)$$

$$\hat{C} = \sqrt{\Gamma} |g\rangle \langle e|, \quad (4.63)$$

and the decay rate

$$\Gamma = \Gamma_e + \left( \frac{\Omega_2}{2\Delta_1} \right)^2 \Gamma_p. \quad (4.64)$$

Furthermore, there is the additional decay of the coherence given by

$$\mathcal{L}'(\hat{\rho}) = -\frac{\Omega_1^2}{8\Delta_1^2} \Gamma_p \begin{pmatrix} 0 & c_{ge} \\ c_{eg} & 0 \end{pmatrix}. \quad (4.65)$$

Because of this term, Eq. (4.58) cannot be written as a standard Lindblad equation ( $\mathcal{L}'(\hat{\rho})$  cannot be expressed as a Lindblad super-operator). However, in the later chapters, we will only be interested in the rough magnitude of the decay so that we can ensure that any decay can be ignored.

#### 4.2.4. Two-atom dressing scheme, Born-Oppenheimer approximation

In the next section, we will formally consider the  $N$ -body Hamiltonian and calculate an effective interaction. But before that, it is useful to study a simplified system of only two atoms in some detail.

We denote the distance between the atoms by  $R$  and we assume that they interact with a van-der-Waals interaction  $W(R) = C_6/R^6$  if both are in the Rydberg state  $|e\rangle$ . We will apply a Born-Oppenheimer (BO) approximation, relying on the very different time scales of the electron dynamics and the atom dynamics. In this approximation one diagonalizes the electronic Hamiltonian under the assumption that the interatomic distance  $R$  is fixed. This yields a number of  $R$ -dependent eigenvalues, so-called ‘‘potential surfaces’’. These are the potentials that drive the dynamics of the nuclei.

Each atom in isolation is described by the electronic Hamiltonian

$$\hat{H}_i = \hbar \begin{pmatrix} 0 & \frac{1}{2}\Omega \\ \frac{1}{2}\Omega & -\Delta \end{pmatrix} \quad (4.66)$$

in the one-atom basis ( $|g\rangle, |e\rangle$ ). The Hamiltonian describing the electron dynamics is

$$\hat{H}_{\text{el}} = \begin{pmatrix} 0 & \frac{\hbar\Omega}{\sqrt{2}} & 0 \\ \frac{\hbar\Omega}{\sqrt{2}} & -\hbar\Delta & \frac{\hbar\Omega}{\sqrt{2}} \\ 0 & \frac{\hbar\Omega}{\sqrt{2}} & -2\hbar\Delta + W(R) \end{pmatrix}, \quad (4.67)$$

in the two-atom basis

$$\left( |gg\rangle, |eg\rangle^+, |ee\rangle \right) = \left( |gg\rangle, \frac{|eg\rangle + |ge\rangle}{\sqrt{2}}, |ee\rangle \right). \quad (4.68)$$

The anti-symmetric state  $|eg\rangle^-$  does not couple to the others and can be ignored. Diagonalizing  $\hat{H}_{\text{el}}$  for fixed values of  $\Delta$  and  $\Omega$  yields three potential surfaces

$$U_{\tilde{g}\tilde{g}}(R), U_{\tilde{e}\tilde{g}}(R), U_{\tilde{e}\tilde{e}}(R).$$

Here,  $|\tilde{g}\rangle$  and  $|\tilde{e}\rangle$  denote the eigenstates of the single-atom Hamiltonians  $\hat{H}_i$ . Accordingly,  $|\tilde{g}\tilde{g}\rangle$ ,  $|\tilde{e}\tilde{g}\rangle^+$  and  $|\tilde{e}\tilde{e}\rangle$  are the eigenstates of  $\hat{H}_{\text{el}}(\infty)$ .

A few examples of the potentials are shown in Fig. 4.3. The BO approximation is justified if all the potential surfaces are well-separated for all  $R$ . Then, diabatic transitions between the surfaces are inhibited (cf. the adiabatic theorem of quantum mechanics [29] and the Landau-Zener problem [115, 131, 188, 209]). We observe in Fig. 4.3 that this is fulfilled whenever  $\Delta$  and  $C_6$  have different signs.

We will be interested in the atomic dynamics of a gas of atoms initially in their ground state  $|g\rangle$  that are subjected to a dressing laser. If the laser is initially switched on slowly<sup>2</sup>, this system will be described by the potential  $W_{\tilde{g}\tilde{g}}(R)$ .

$W_{\tilde{g}\tilde{g}}(R)$  is van-der-Waals-like for large  $R$  but has a soft core, i.e., for  $R \rightarrow 0$  it approaches a finite value  $W_{\tilde{g}\tilde{g}}(0) < \infty$ . This behavior can be understood within a so-called blockade picture:

If the atoms are very far apart, the interaction  $W(R)$  is much smaller than the detuning  $\hbar\Delta$  and both atoms will, separately, perform Rabi oscillations as described in the previous section. Their effective interaction  $W_{\text{eff}}$  will be the van-der-Waals interaction scaled by the two-particle excitation probability  $p_{\text{exc}}^2$ , i.e.

$$U_{\text{eff}}(R) = p_{\text{exc}}^2 \frac{C_6}{R^6}. \quad (4.69)$$

However, the situation changes at distances where  $W(R) \lesssim \hbar\Delta$ . In that case, the interaction leads to a shift of the effective detuning (see Fig. 4.4). More precisely, the effective two-particle detuning becomes  $\Delta_{\text{eff}}(R) = -2\hbar\Delta + W(R)$ . Hence, if  $\Delta$  and  $W$  have the same sign (attractive interaction with a red detuned laser or repulsive

<sup>2</sup>Here we invoke the adiabatic theorem a second time. Switching the laser on slowly ensures that the non-dressed eigenstate  $|g\rangle$  evolves adiabatically towards the dressed eigenstate  $|\tilde{g}\rangle$ .

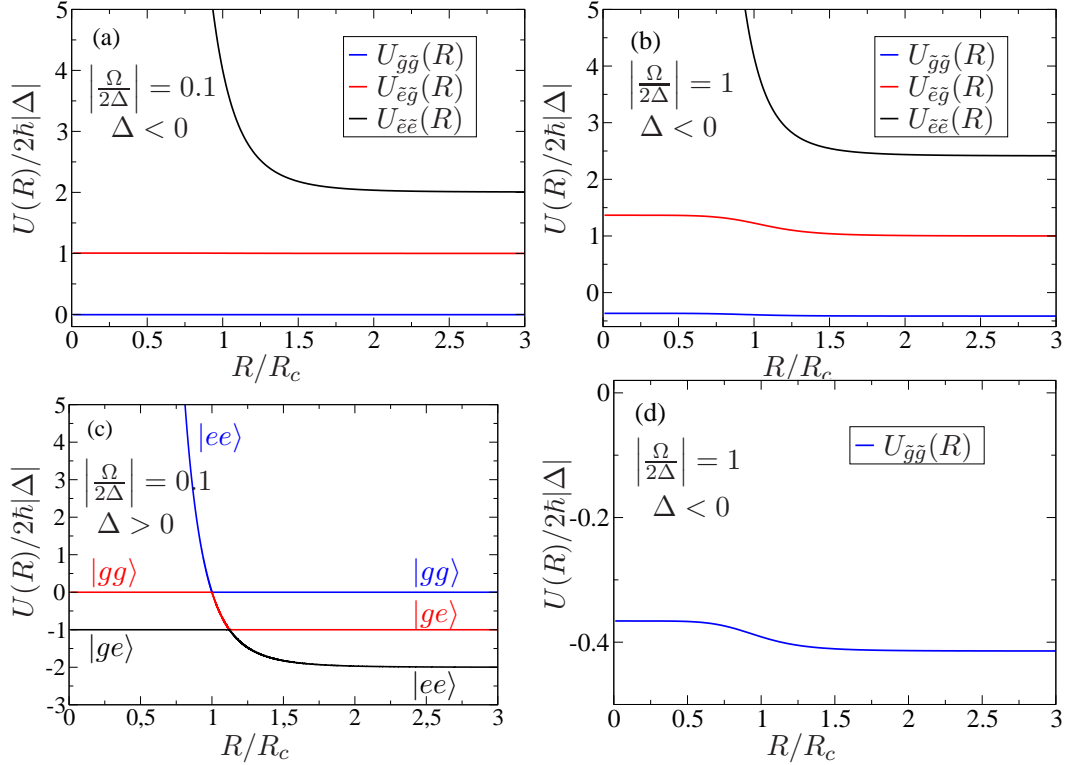


**Figure 4.3.:** (a)–(b) BO potential curves for  $C_6 > 0$  and  $\Delta < 0$  and (a)  $\Omega/2\Delta = 0.1$  and (b)  $\Omega/2\Delta = 1$ . The potential surfaces are always well separated, justifying the BO approximation. In (c) we chose  $\Delta > 0$  (and still  $C_6 > 0$ ). This leads to avoided crossings between  $|\tilde{e}\tilde{e}\rangle$  and the other curves, implying the breakdown of the BO approximation. Panel (d) shows a zoomed view of the potential  $U_{\tilde{g}\tilde{g}}(R)$  for  $\Omega/2\Delta = 1$ . For different values of  $\Omega/2\Delta$  it remains qualitatively identical. All distances are scaled by the characteristic length scale  $R_c = |C_6/2\hbar\Delta|^{1/6}$ .

interaction with blue detuning), then the laser will become resonant with the atomic transition at

$$R = \left( \frac{C_6}{2\hbar\Delta} \right)^{1/6} \quad (4.70)$$

which leads to the breakdown of the BO approximation. Furthermore it may lead to a large number of Rydberg excitations, extremely strong interactions and subsequent destruction of the condensate through heating. Hence, these cases are *not* the ones we are interested in.

We will study the cases where  $\Delta$  and  $W$  have opposite signs (repulsive interaction with red detuning laser or attractive interaction with blue detuning). This is the case for which we have seen the BO approximation to be valid. Then, for small distances the interaction leads to an increase of the effective detuning and, therefore, to a decrease of the Rydberg fraction. This effect is known as “interaction blockade” [96, 128] because it is the interaction-induced shift in the energy of the Rydberg state that inhibits excita-

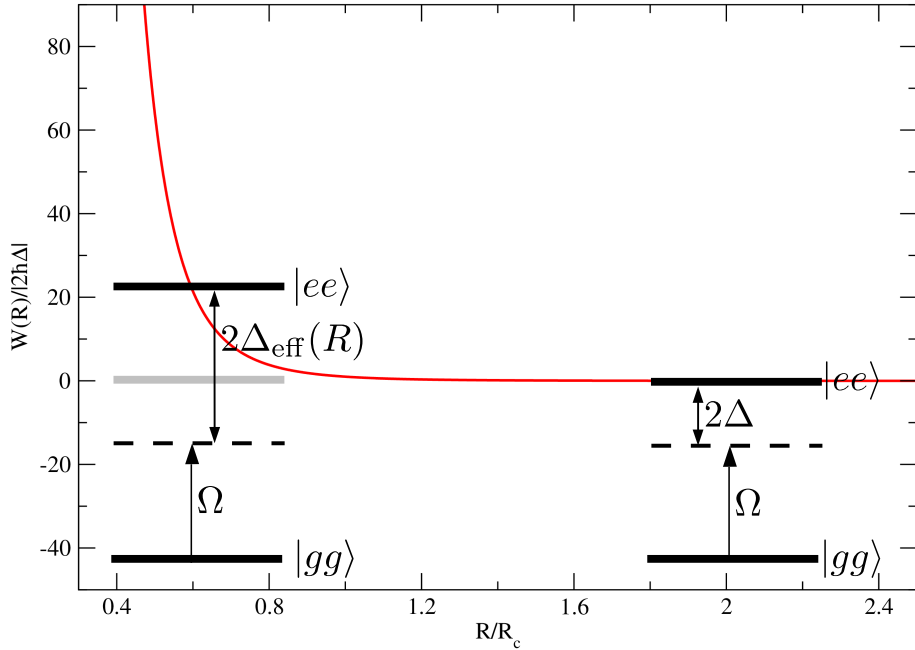


**Figure 4.4.:** Visualization of the blockade effect for a pair of atoms (energies not to scale). For  $R \rightarrow \infty$ , the system is one of two unperturbed atoms, each with two eigenstates  $|g\rangle$  and  $|e\rangle$ . Depicted are the eigenstates  $|gg\rangle$ ,  $|ee\rangle$  for a large and a small distance. The detuning between the laser and the atomic transition is  $\Delta$ . Hence, in the rotating frame, the energy difference  $|ee\rangle$  and  $|gg\rangle$  is  $2\Delta$  at large  $R$ . For smaller  $R$ , the van-der-Waals interaction  $W(R) = C_6/R^6$  shifts the detuning to the larger value  $2\Delta_{\text{eff}}(R) = 2\Delta - W(R)/\hbar$ , so that the excitation probability is reduced.

tion into that very state.

Consequently, the effective interaction at small distances will be smaller than the simple Eq. (4.69) would predict. We will see in the following section what the effective interaction exactly is.

#### 4.2.5. Dressing interaction between many atoms

Now we turn to a whole BEC of  $N$  atoms, with distance vectors  $\mathbf{r}_{ij} = \mathbf{r}_i - \mathbf{r}_j$ , where  $\mathbf{r}_i$  is the position of the  $i$ -th atom. If both the atoms  $i$  and  $j$  are in the Rydberg state  $|e\rangle$ , they have an interaction energy  $W_{ij} = W(r_{ij}) = C_6/r_{ij}^6$ . The detuning and interaction are chosen such that  $C_6/\Delta < 0$ . This is in line with our insight from the previous section about how to avoid going resonant (and destroying the BEC).

Then, the full Hamiltonian of the system is

$$\hat{H}_F = \hat{T} + \sum_{i<j} \hat{W}_{ij} \otimes \hat{\sigma}_{ee}^i \hat{\sigma}_{ee}^j + \sum_{i=1}^N \hat{H}_0^i \quad (4.71)$$

$$= \hat{T} + \sum_{i<j} \hat{W}_{ij} \otimes \hat{\sigma}_{ee}^i \hat{\sigma}_{ee}^j - \hbar\Delta \sum_{i=1}^N \sigma_{ee}^i + \frac{\hbar\Omega}{2} \sum_{i=1}^N (\sigma_{ge}^i + \sigma_{eg}^i) \quad (4.72)$$

$$= \hat{T} + \hat{H}_{\text{el}}(\mathbf{r}_1 \dots \mathbf{r}_N). \quad (4.73)$$

where  $\hat{T} = \frac{1}{2m} \sum_i \hat{\mathbf{p}}_i^2$  is the kinetic energy of all atoms. We now apply the Born-Oppenheimer approximation to the  $N$ -body problem.

### Perturbation theory

The operator  $\hat{H}_{\text{el}}$  acts on the  $2^N$ -dimensional Hilbert space comprised of the internal states of the atoms and depends parametrically on the positions  $\mathbf{r}_i$ . In the BO approximation, it is replaced by a BO potential  $U(\mathbf{r}_1 \dots \mathbf{r}_N)$  (which is a multiplication operator in position space). It is given by the eigenvalue equation

$$U(\mathbf{r}_1 \dots \mathbf{r}_N) |G(\mathbf{r}_1 \dots \mathbf{r}_N)\rangle = \hat{H}_{\text{el}}(\mathbf{r}_1 \dots \mathbf{r}_N) |G(\mathbf{r}_1 \dots \mathbf{r}_N)\rangle, \quad (4.74)$$

such that

$$\lim_{r_i \rightarrow \infty} |G(\mathbf{r}_1 \dots \mathbf{r}_N)\rangle = |G_0\rangle = |g \dots g\rangle, \quad (4.75)$$

i.e.,  $|G(\mathbf{r}_1 \dots \mathbf{r}_N)\rangle$  is the eigenstate that connects asymptotically to the state  $|G_0\rangle = |g \dots g\rangle$  where all atoms are in their ground state.

Then, the system is described by the BO Hamiltonian

$$\hat{H} = \hat{T} + \hat{U}. \quad (4.76)$$

Note that (even for  $r_i \rightarrow \infty$  and  $\Omega = 0$ )  $|G_0\rangle$  is not always the ground state of the *overall* system:

$|G_0\rangle$  is the ground state if  $\Delta < 0$  (and where the interaction must be repulsive in order to avoid resonant excitations). If  $\Delta > 0$ ,  $|G_0\rangle$  is the highest-energy state.

We now treat the eigenvalue problem (4.74) in perturbation theory and we will use the result in most of the subsequent chapters. In chapter 7, we will go beyond this additional approximation. The perturbative treatment is justified if  $\left|\frac{\Omega}{2\Delta}\right|^2 N \ll 1$  as we will discuss more precisely in chapter 7). To calculate the perturbation expansion we write

$$\hat{u} = \frac{\hat{U}}{\hbar\Delta} = \underbrace{-\sum_{i=1}^N \sigma_{ee}^i + \frac{1}{\hbar\Delta} \sum_{i<j} \hat{W}_{ij} \otimes \hat{\sigma}_{ee}^i \hat{\sigma}_{ee}^j}_{=\hat{h}_0} + \underbrace{\frac{\Omega}{2\Delta} \sum_{i=1}^N (\sigma_{ge}^i + \sigma_{eg}^i)}_{=\hat{w}}. \quad (4.77)$$

We want to find the effective interaction of the state that asymptotically connects to  $|G_0\rangle = |g \dots g\rangle$ , so we need to consider the following expansion in  $\lambda = \Omega/2\Delta$ :

$$u(\mathbf{r}_1 \dots \mathbf{r}_N) = \sum_{l=1}^{\infty} \left( \frac{\Omega}{2\Delta} \right)^l u^{(l)}(\mathbf{r}_1 \dots \mathbf{r}_N), \quad (4.78)$$

or

$$U(\mathbf{r}_1 \dots \mathbf{r}_N) = \hbar\Delta u(\mathbf{r}_1 \dots \mathbf{r}_N) = \sum_{l=1}^{\infty} \left( \frac{\Omega}{2\Delta} \right)^l U^{(l)}(\mathbf{r}_1 \dots \mathbf{r}_N). \quad (4.79)$$

The various orders  $u^{(l)}$  can be calculated by the usual perturbation formulae [42], involving sums over all other eigenstates of  $\hat{h}_0$ . Those eigenstates can be divided up as follows:

- singly excited states  $|e_i\rangle$ ,  $i = 1 \dots N$  with energy  $\langle e_i | \hat{h}_0 | e_i \rangle = -1$ ,
- doubly excited states  $|e_{ij}\rangle$ , with energy  $\langle e_{ij} | \hat{h}_0 | e_{ij} \rangle = -2 + W_{ij}/\hbar\Delta$ ,
- and so on.

The original state  $|G_0\rangle$  has the energy  $\langle G_0 | \hat{h}_0 | G_0 \rangle = 0$ .

We abbreviate all eigenstates by  $|a\rangle$ , with  $a \in \{1 \dots 2^N\}$ , numbered such that

$$\begin{aligned} |0\rangle &= |G_0\rangle, \\ |1\rangle &= |e, g, \dots, g\rangle, \\ &\dots \\ |N+1\rangle &= |e, e, g, \dots, g\rangle, \\ &\dots \\ |2^N\rangle &= |e, \dots, e\rangle. \end{aligned}$$

Their couplings to  $|G_0\rangle$  and each other are denoted by  $w_{ab} = \langle a | \hat{w} | b \rangle$ . All of those couplings are either 1 or 0. The eigenenergies will be denoted by  $\varepsilon_a = \langle a | \hat{h}_0 | a \rangle$  and the energy differences by  $\varepsilon_{ab} = \varepsilon_a - \varepsilon_b$ . In the spirit of the above definitions, the indices  $a, b, c$  will run over all states, while indices  $i, j, k$  run over atoms.

The  $l$ -th order of the perturbation series describes the contribution of virtual processes that consist of exactly  $l$  basic processes of the perturbation operator  $\hat{w}$  (here, those are simple one-electron excitations/relaxations) and that lead back to  $|G_0\rangle$ . Therefore, all odd orders must vanish, since in order to finally return to  $|G_0\rangle$  there must be one and only one relaxation for every excitation. One can also see this by explicitly calculating the low odd orders:

$$u^{(1)} = w_{G_0 G_0} = \langle G_0 | \hat{w} | G_0 \rangle = 0. \quad (4.80)$$

$$u^{(3)} = \sum_{ab} \frac{w_{G_0 a} w_{ab} w_{b G_0}}{\varepsilon_{G_0 a} \varepsilon_{G_0 b}} - w_{G_0 G_0} \sum_b \frac{|w_{G_0 b}|^2}{\varepsilon_{G_0 b}^2} = \sum_a \frac{w_{G_0 a} w_{aa} w_{a G_0}}{\varepsilon_{G_0 a} \varepsilon_{G_0 a}} = 0. \quad (4.81)$$

The even orders, on the other hand, are non-vanishing:

$$u^{(2)} = \sum_a \frac{|w_{G_0a}|^2}{\varepsilon_{G_0a}} = \sum_{i=1}^N \frac{|\langle e_i | \hat{w} | G_0 \rangle|^2}{0 - (-1)} = N, \quad (4.82)$$

such that

$$\left(\frac{\Omega}{2\Delta}\right)^2 U^{(2)} = \frac{\hbar\Omega^2}{4\Delta} N. \quad (4.83)$$

This energy is called the first-order light-shift. The single-atom light-shift

$$E_L = \frac{\hbar\Delta}{2} \left( -1 + \sqrt{1 + 4 \left(\frac{\Omega}{2\Delta}\right)^2} \right) \quad (4.84)$$

is the difference in energy between a dressed and a non-dressed atom. Its Taylor series is

$$E_L = \frac{\hbar\Omega^2}{4\Delta} - \frac{\hbar\Omega^4}{16\Delta^3} + \frac{\hbar\Omega^6}{32\Delta^5} + \mathcal{O}\left(\left(\frac{\Omega}{2\Delta}\right)^8\right). \quad (4.85)$$

We recognize that Eq. (4.83) is exactly  $N$  times the first term of this series and, hence, the first-order light-shift of  $N$  atoms.

Since the second order only includes processes where *one* atom is excited and then decays it is clear that it cannot lead to an interaction. For the description of the atomic dynamics that we are interested in, constant terms in the energy are irrelevant so that we do not need to include this term in the resulting interaction curve. Since the fourth order includes up to two excited atoms, a position-dependent term appears:

$$\begin{aligned} u^{(4)} &= \sum_{abc} \frac{w_{G_0a} w_{ab} w_{bc} w_{cG_0}}{\varepsilon_{G_0a} \varepsilon_{G_0b} \varepsilon_{G_0c}} - u^{(2)} \sum_a \frac{|w_{G_0a}|^2}{\varepsilon_{G_0a}^2} - 2w_{G_0G_0} \sum_{ab} \frac{w_{G_0a} w_{ab} w_{bG_0}}{\varepsilon_{G_0a}^2 \varepsilon_{G_0b}} \\ &\quad + w_{G_0G_0}^2 \sum_a \frac{|w_{G_0a}|^2}{\varepsilon_{G_0a}^3} \\ &= \sum_{abc} \frac{w_{G_0a} w_{ab} w_{bc} w_{cG_0}}{\varepsilon_{G_0a} \varepsilon_{G_0b} \varepsilon_{G_0c}} - N \sum_a \frac{|w_{G_0a}|^2}{\varepsilon_{G_0a}^2} \\ &= \sum_{i \neq j}^N \frac{2}{(-1)(2 - W_{ij}/\hbar\Delta)(-1)} - N^2 \\ &= \hbar\Delta \sum_{i < j}^N \frac{4}{2\hbar\Delta - W_{ij}} - N^2. \end{aligned} \quad (4.86)$$

$$(4.87)$$

Hence,

$$\left(\frac{\Omega}{2\Delta}\right)^4 U^{(4)} = \left(\frac{\Omega}{2\Delta}\right)^4 \hbar\Delta u^{(4)} = \frac{\hbar^2\Omega^4}{4\Delta^2} \sum_{i < j}^N \frac{1}{2\hbar\Delta - W_{ij}} - \left(\frac{\Omega}{2\Delta}\right)^4 \hbar\Delta N^2. \quad (4.88)$$

For non-interacting atoms (or atoms that are infinitely far apart), this becomes

$$\left(\frac{\Omega}{2\Delta}\right)^4 U^{(4)} = \frac{\hbar^2\Omega^4}{4\Delta^2} \frac{N(N-1)}{2} \frac{1}{2\hbar\Delta} - \left(\frac{\Omega}{2\Delta}\right)^4 \hbar\Delta N^2 = -N \frac{\hbar\Omega^4}{16\Delta^3}. \quad (4.89)$$

This is  $N$  times the second term in Eq. (4.84) and, hence, the second-order light-shift of  $N$  atoms.

We can normalize  $\left(\frac{\Omega}{2\Delta}\right)^4 U^{(4)}$  to vanish at infinity by subtracting the second-order light-shift. Hence, if we truncate the perturbation expansion after the fourth order, we retain a Born-Oppenheimer potential:

$$U(\mathbf{r}_1 \dots \mathbf{r}_N) = \frac{\hbar^2\Omega^4}{4\Delta^2} \sum_{i<j}^N \frac{W(\mathbf{r}_{ij})}{2\hbar\Delta - W(\mathbf{r}_{ij})}. \quad (4.90)$$

Finally, we can insert the van-der-Waals interaction  $W(\mathbf{r}_{ij}) = C_6/r_{ij}^6$  to find the important result

$$U(\mathbf{r}_1 \dots \mathbf{r}_N) = \sum_{i<j}^N \frac{\tilde{C}_6}{R_c^6 + r_{ij}^6}, \quad (4.91)$$

where

$$\tilde{C}_6 = \left(\frac{\Omega}{2\Delta}\right)^4 C_6, \quad (4.92)$$

$$R_c = \left(-\frac{C_6}{2\hbar\Delta}\right)^{1/6}. \quad (4.93)$$

We see that the many-body interaction  $U$  is a sum of two-body interactions

$$U_{ij}(r_{ij}) = \frac{\tilde{C}_6}{r_{ij}^6 + R_c^6} \quad (4.94)$$

which have soft-core form, i.e., for  $r_{ij} \rightarrow 0$ , they do not diverge, but approach a finite value

$$U_{ij}(0) = \frac{\tilde{C}_6}{R_c^6} = -2\hbar\Delta \left(\frac{\Omega}{2\Delta}\right)^4, \quad (4.95)$$

independent of the van-der-Waals coefficient  $C_6$  (see also Fig. 4.5).

This soft core is the most significant property of the dressing interaction. It means that particles at low distances are non-interacting. Hence, it is possible (and even energetically favorable under the right circumstances) for particles to stick together to a certain extent. This is in stark contrast to typical solids, where there is one and only one particle per lattice site. Hence, it is the soft-core nature that leads to all of the interesting effects which we will investigate in the subsequent chapters.

The soft core comes about through a blockade effect, as we have explained in the previous section with two atoms. The range of the interaction is given by  $R_c$  which is typically

on the order of a few micrometers, such that at typical BEC densities  $\sim 10^{19} - 10^{20} \text{m}^{-3}$ , the interaction can not be described in the second Born approximation (section 2.3.2). Instead, we will use the first Born approximation.

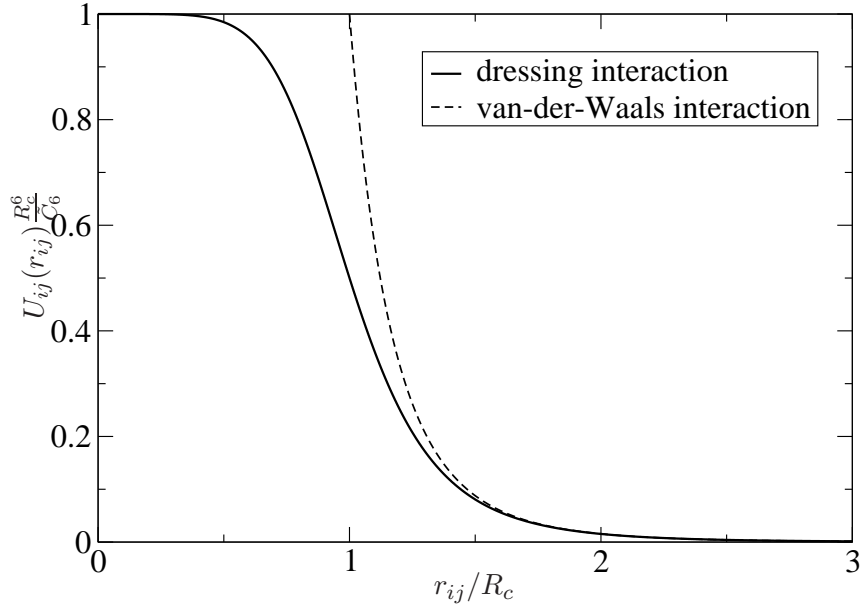


**Figure 4.5.:** Two-body interaction potential  $U_{ij}(\mathbf{r})$  (Eq. (4.94)) for dressing to  $s$ -states, and comparison to pure van-der-Waals interaction. For large distances they are identical but for  $r_{ij} \lesssim R_c$ , the dressing interaction's soft-core nature becomes important.

#### 4.2.6. The lifetime of a dressed state

The most important motivation for the introduction of the dressing scheme is the enhancement of the lifetime of Rydberg states. This is achieved by only weakly admixing the Rydberg state to the ground state. In section 4.2.3, we found that the weak admixing (with the factor  $\frac{\Omega_2}{2\Delta_1}$ ) of the intermediate state  $|p\rangle$  with the decay rate  $\Gamma_p$  led to an additional decay

$$\left(\frac{\Omega_2}{2\Delta_1}\right)^2 \Gamma_p. \quad (4.96)$$

Analogously, the weak admixing of the Rydberg state  $|e\rangle$  (with the factor  $\frac{\Omega}{2\Delta}$ ) to the ground state  $|g\rangle$  will lead to the additional decay

$$\left(\frac{\Omega}{2\Delta}\right)^2 \Gamma_e, \quad (4.97)$$

$l, j$	$\Gamma_s$ [GHz]	$\tau_s$ [ns]	$\varepsilon$
$s_{1/2}$	0.731	1.368	3.0008
$p_{1/2}$	0.411	2.4360	2.9989
$p_{3/2}$	0.395	2.5341	3.0019
$d_{3/2}$	0.929	1.0761	2.9898
$d_{5/2}$	0.936	1.0687	2.9897

**Table 4.1.:** Parameters (see Eqs. (4.99), (4.100)) for the decay rates  $\Gamma = \Gamma_s n^{-\varepsilon}$  and lifetimes  $\tau = \Gamma^{-1} = \tau_s n^\varepsilon$  of Rubidium Rydberg states, from [19]

so that the total decay rate is

$$\Gamma_{\text{eff}} = \left(\frac{\Omega}{2\Delta}\right)^2 \Gamma_e + \left(\frac{\Omega_2}{2\Delta_1}\right)^2 \Gamma_p. \quad (4.98)$$

The decay rates and lifetimes of Rubidium Rydberg states can be written as [19, 32]

$$\Gamma_e = \frac{\Gamma_s}{n^\varepsilon} \quad (4.99)$$

$$\tau_e = \tau_s n^\varepsilon \quad (4.100)$$

with the parameters (from reference [19]) in table 4.1. Furthermore, the lifetimes of the  $5p$ - and  $6p$ -states are relevant, because these can be convenient choices for the intermediate state  $|p\rangle$  from the previous sections. Those lifetimes are [76, 86]

$$\tau(5p_{1/2}) = 27.8 \text{ ns} \quad (4.101)$$

$$\tau(5p_{3/2}) = 26.3 \text{ ns} \quad (4.102)$$

$$\tau(6p) = 120.7 \text{ ns}. \quad (4.103)$$

Hence, the decay rates are

$$\Gamma_p(5p) \approx 36 \text{ MHz} \quad (4.104)$$

$$\Gamma_p(6p) \approx 8.3 \text{ MHz}. \quad (4.105)$$

In the following chapters, we will typically use parameters  $\Omega$  and  $\Delta$  with

$$\frac{\Omega}{2\Delta} \sim \frac{1}{100}, \quad (4.106)$$

$$\frac{\Omega_2}{2\Delta_1} \sim \frac{1}{2500}, \quad (4.107)$$

yielding effective decay rates of (e.g., for the  $50s$ -state with  $\Gamma_e = 5.83$  kHz)

$$\Gamma_{\text{eff}}(5p) = \left(\frac{\Omega}{2\Delta}\right)^2 \cdot 5.83\text{kHz} + \left(\frac{\Omega_2}{2\Delta_1}\right)^2 \cdot 36\text{ MHz} \quad (4.108)$$

$$\Gamma_{\text{eff}}(6p) = \left(\frac{\Omega}{2\Delta}\right)^2 \cdot 5.83\text{kHz} + \left(\frac{\Omega_2}{2\Delta_1}\right)^2 \cdot 8.3\text{ MHz}. \quad (4.109)$$

Therefore,

$$\Gamma_{\text{eff}}(5p) \approx 6\text{ Hz} \quad (4.110)$$

$$\Gamma_{\text{eff}}(6p) \approx 2\text{ Hz}. \quad (4.111)$$

Hence, the lifetimes of the dressed states will be on the order of 100 ms to 1 s. As the following chapters will show this is long enough to observe the ensuing dynamics.

#### 4.2.7. Validity of the perturbation expansion

The perturbative treatment is only valid if the dressing is “weak enough”. In chapter 7, we will investigate what exactly the correct criterion is. But we can already speculate by considering the above calculation and the general form of the perturbation series: The  $(2l)$ th-order of the perturbation expansion has the form

$$U^{(2l)} \propto \left(\frac{\Omega}{2\Delta}\right)^{2l} \sum_{i_1=1}^N \cdots \sum_{i_l=1}^N f_l(\mathbf{r}_{i_1} \dots \mathbf{r}_{i_l}), \quad (4.112)$$

with a function  $f$  that approaches a constant value on the length scale  $R_c$ . Hence, it scales like

$$U^{(l)} \propto \left(\frac{\Omega}{2\Delta}\right)^{2l} N_{\text{loc}}^l = \left(\frac{\Omega_e}{2\Delta}\right)^{2l}, \quad (4.113)$$

where  $\Omega_e = \sqrt{N_{\text{loc}}}\Omega$  is the so-called bosonically enhanced Rabi frequency.  $N_{\text{loc}}$  is the local number of particles, i.e., the number of particles within a radius  $R_c$ . For a gas with constant density  $\rho$  this number is

$$N_{\text{loc}} = \frac{4}{3}\pi R_c^3 \rho. \quad (4.114)$$

The relative weight of the  $(l+1)$ -th order, compared to the  $l$ -th order is

$$N_R = \left(\frac{\Omega}{2\Delta}\right)^2 N_{\text{loc}}. \quad (4.115)$$

Notably,  $N_R$  has a simple interpretation: the dressed ground state of a *single* atom can be calculated in perturbation theory just as we calculated the interaction:

$$|G\rangle = |g\rangle + \frac{\Omega}{2\Delta} |e\rangle, \quad (4.116)$$

leading to a probability of  $\left(\frac{\Omega}{2\Delta}\right)^2$  of finding the atom in its Rydberg state. Hence,  $N_R$  is the average number of Rydberg excitations within one radius  $R_c$  for a *non-interacting* gas.

In chapter 7 we will show that this is indeed the relevant parameter.

### 4.3. Dressing to degenerate states

The two-level dressing scheme can be generalized to a dressing scheme with  $n_d > 1$  excited states  $\{|e_m\rangle\}_{m=1}^{n_d}$ . This is particularly relevant for the dressing to  $d$ -states which are (in the absence of an external magnetic field) degenerate with respect to the magnetic quantum number  $m$ .

The derivation is very similar to the one before, with two differences:

- there are now  $n_d = 2j + 1$  Rabi frequencies  $\Omega_m = \mathbf{d}_m \cdot \mathbf{E}_0 / \hbar$ , where  $\mathbf{d}_m = q \langle g | \hat{\mathbf{r}} | e_m \rangle$  is the dipole matrix element coupling ground state and the  $m$ -th excited state
- there are now  $n_d^2$  Born-Oppenheimer potentials  $C_6^{(\mathbf{m})} / r^6$ .  $\mathbf{m} = (m_1, m_2)$  labels the potential whose state asymptotically connects to  $|e_{m_1}\rangle \otimes |e_{m_2}\rangle$ .

Then, by choosing the laser polarization appropriately, one particular state  $|e\rangle$  of the  $n_d$  degenerate one-particle-states can be chosen by exploiting the selection rules. For example, starting from an  $s$ -state with  $m = 1/2$ , dipole selection rules allow one to excite  $p_{1/2}$ -states as well as  $p_{3/2}$ -states. However, at low principal quantum numbers, these states have significantly different energies so that one can be chosen via the laser frequency. Furthermore, the laser polarization controls the change in  $m$ , so that this can be chosen, too. If a  $p_{1/2}$ -state has been chosen, a second laser can then (due to the  $j$ -selection rule) excite only  $d_{3/2}$ -states, not  $d_{5/2}$ -states. Again, the polarization can be used to select one of the  $m$ -degenerate states. Hence, among others, the following excitation schemes are possible:

$$s_{1/2}(m = 1/2) \rightarrow p_{1/2}(m = 1/2) \rightarrow d_{3/2}(m = 1/2), \quad (4.117)$$

$$s_{1/2}(m = 1/2) \rightarrow p_{1/2}(m = 1/2) \rightarrow d_{3/2}(m = 3/2). \quad (4.118)$$

Note that it is not possible to select a single  $d_{3/2}$ -state in this manner. It would be necessary to first excite a  $p_{3/2}$ -state; but from there, one can not control whether a  $d_{3/2}$ - or  $d_{5/2}$  is excited with the second laser since, at high  $n$  (which we are interested in), are energetically very similar. Fortunately, as we saw in the previous chapter, it is

$d_{3/2}$ -states that are relevant for us, so this is not a problem. The resulting effective dressing-potential is

$$U(\mathbf{r}_1 \dots \mathbf{r}_N) = \sum_{i < j} U_{ij}(\mathbf{r}_{ij}) = \sum_{i < j} \sum_{\beta=1}^{n_d^2} |\langle ee | \mu_\beta(\mathbf{r}_{ij}) \rangle|^2 \frac{\tilde{C}_6^{(\beta)}}{\left(R_c^{(\beta)}\right)^6 + r_{ij}^6}. \quad (4.119)$$

As before,

$$\tilde{C}_6^{(\beta)} = \left(\frac{\Omega}{2\Delta}\right)^4 C_6^{(\beta)}, \quad (4.120)$$

$$R_c^{(\beta)} = \left(\frac{C_6^{(\beta)}}{2\hbar\Delta}\right)^{1/6} \quad (4.121)$$

and  $\Omega$  and  $\Delta$  are the two-photon Rabi frequency and detuning for coupling to the one *chosen* Rydberg state.  $|\mu_\beta(\mathbf{r})\rangle$  is the two-body eigenstate of  $\hat{H}(\mathbf{r})$  (the Hamiltonian we used in chapter 3 to calculate the van-der-Waals coefficients  $C_6^{(\beta)}$ ). In general, the interaction is not spherically symmetric because it also depends on the eigenstates. These are not spherically symmetric, in contrast to the *eigenvalues*. However,  $|\langle ee | \mu_\beta(\mathbf{r}) \rangle|^2$  is still symmetric with respect to rotation around the  $z$ -axis (i.e., the quantization axis of the lasers) so  $U_{ij}$  exhibits a cylindrical symmetry.

#### 4.4. Length and energy scaling

By the calculation of the Born-Oppenheimer potential  $U(\mathbf{r}_1 \dots \mathbf{r}_N) = \sum_{i < j} U_{ij}(\mathbf{r}_i - \mathbf{r}_j)$ , the Hilbert space concerning the electrons has been eliminated and we are now only dealing with a system of atoms without internal structure. Then, the many-body Hamiltonian describing a dressed gas is

$$\hat{H} = \frac{1}{2m} \sum_{i=1}^N \hat{\mathbf{p}}_i^2 + U(\hat{\mathbf{r}}_1 \dots \hat{\mathbf{r}}_N). \quad (4.122)$$

Additionally, depending on the situation, there can be an external potential  $\sum_{i=1}^N V_{\text{ext}}(\hat{\mathbf{r}}_i)$ : where  $V_{\text{ext}}$  is the external potential. The corresponding Schrödinger equations (SE) are.

$$\hat{H} |\Psi(t)\rangle = i\hbar \partial_t |\Psi(t)\rangle, \quad (4.123)$$

$$\hat{H} |\Psi\rangle = E |\Psi\rangle. \quad (4.124)$$

We will later solve the stationary SE with the Path-Integral Monte Carlo (PIMC) method, and by comparison with its results we will show that a mean-field approximation is justified. We will apply the mean-field approximation (i.e. a Gross-Pitaevskii equation) to the time-dependent SE to study the dynamics of the gas. Let us consider

how the Gross-Pitaevskii equation for the dressed gas can be simplified. In both cases (dressing to a non-degenerate state and to degenerate states), we start from the GPE

$$i\hbar\partial_t\psi(\mathbf{r}) = \left( -\frac{\hbar^2}{2m}\nabla^2 + \rho g|\psi(\mathbf{r})|^2 + V_{MF}[\psi](\mathbf{r}) \right) \psi(\mathbf{r}) \quad (4.125)$$

#### 4.4.1. Non-degenerate states

The MF potential is

$$V_{MF}[\psi](\mathbf{r}) = \rho \int d^3r' U(\mathbf{r} - \mathbf{r}') |\psi(\mathbf{r}')|^2 = \rho \int d^3r' \frac{\tilde{C}_6 |\psi(\mathbf{r}')|^2}{R_c^6 + |\mathbf{r} - \mathbf{r}'|^6}. \quad (4.126)$$

We have renamed  $U_{ij}$  to  $U$  for convenience. Note that this equation describes the short-ranged  $s$ -wave scattering interaction and the long-ranged dressing interaction in different approximations. The short-range interaction is described in the second Born approximation (see section 2.3.2). However, this approximation cannot be used for long-ranged interactions since it assumes that only two-body effects are relevant. Hence, the long-ranged interaction is described in the first Born approximation. However, it is not yet clear at this point that this approximation is actually justified. We will see later that this is indeed the case by comparing it to exact Monte Carlo simulations.

It is useful to rescale this equation with the length scale  $R_c$  and the time scale  $\frac{mR_c^2}{\hbar}$ . This is equivalent to scaling the stationary GPE by the energy scale  $\frac{\hbar^2}{mR_c^2}$ . Furthermore, we scale the wave function by the square root of the density  $\sqrt{\rho}$ . In the case of a bulk system,  $\rho$  is defined as the average density of the system. In a finite (three-dimensional) system we use  $\rho = N/R_c^3$ . This simplifies the GPE to

$$i\partial_t\psi(\mathbf{r}) = \left( -\frac{1}{2}\nabla^2 + \gamma|\psi(\mathbf{r})|^2 + \alpha \int d^3r' \frac{|\psi(\mathbf{r}')|^2}{1 + |\mathbf{r} - \mathbf{r}'|^6} \right) \psi(\mathbf{r}), \quad (4.127)$$

where

$$\alpha = \frac{\tilde{C}_6 m \rho}{\hbar^2 R_c}, \quad (4.128)$$

$$\gamma = \frac{m R_c^2 \rho}{\hbar^2} g = 4\pi a_s R_c^2 \rho \quad (4.129)$$

are the effective strengths of the dressing interaction and the contact interaction (due to  $s$ -wave scattering), respectively. In the case of a finite system, using  $\rho = N/R_c^3$ , they

can also be written as

$$\alpha = \frac{\tilde{C}_6 m N}{\hbar^2 R_c^4}, \quad (4.130)$$

$$\gamma = \frac{m N}{\hbar^2 R_c} g = \frac{4\pi a_s N}{R_c}. \quad (4.131)$$

The same scaling can be applied if lower-dimensional systems are considered. These can be realized by confining the system very strongly in one or two directions, e.g., using a harmonic trap. The treatment as a lower-dimensional system is justified if the trapping frequencies  $\omega_z$  and/or  $\omega_y$  in the directions that are to be strongly confined are much larger than the typical one-particle energy in the system, or, equivalently, if the corresponding oscillator lengths  $l_y, l_z$  are much smaller than typical length scales. Then, one has to take into account that  $g$  is modified. For example, if a Gaussian profile in the tightly confined direction is assumed, one has

$$g^{3D} = g, \quad (4.132)$$

$$g^{2D} = \frac{g}{\sqrt{2\pi} l_z}, \quad (4.133)$$

$$g^{1D} = \frac{g^{2D}}{\sqrt{2\pi} l_y} = \frac{g}{2\pi l_y l_z}. \quad (4.134)$$

$$(4.135)$$

The system is then still described by Eq. (4.127), no matter the dimension. However, in  $d$  dimensions with density  $\rho_d$  the interaction strengths are

$$\alpha = \frac{\tilde{C}_6 m \rho_d}{\hbar^2 R_c^{4-d}}, \quad (4.136)$$

$$\gamma = \frac{m R_c^2 \rho_d}{\hbar^2} g^{dD}. \quad (4.137)$$

The same scaling can also be applied to the Hamiltonian itself without first invoking a mean-field approximation, yielding the rescaled Hamiltonian

$$\hat{H} = \frac{1}{2} \sum_{i=1}^N \hat{\mathbf{p}}_i^2 + \sum_{i<j} \frac{\alpha_{MC}}{1 + |\hat{\mathbf{r}}_i - \hat{\mathbf{r}}_j|^6} + \gamma_{MC} \sum_{i<j} \delta(\hat{\mathbf{r}}_i - \hat{\mathbf{r}}_j). \quad (4.138)$$

The interaction strengths differ from the ones in the GPE for a finite system only by a factor of  $N$ :

$$\alpha = N \alpha_{MC}, \quad (4.139)$$

$$\gamma = N \gamma_{MC}. \quad (4.140)$$

This reflects that, in the MF simulations there is no particle number since it considers only one active particle in the field of many other indistinguishable particles in the same state. Hence, a change in the number of particles is equivalent to a change in the pair interaction strength since the interaction potential felt by any one particle is identical in both situations. In contrast, the MC simulations take the particle number explicitly into account so that it cannot be included in the interaction parameter.

#### 4.4.2. Degenerate states

For dressing to a degenerate Rydberg manifold, the situation is more complicated and cannot be simplified as nicely due to the existence of multiple length scales  $R_c^{(\beta)}$  in the interaction. The MF potential is (Eq. (4.119))

$$V_{MF}[\psi](\mathbf{r}) = \int d^3 r' U(\mathbf{r} - \mathbf{r}') |\psi(\mathbf{r}')|^2 \quad (4.141)$$

$$= \sum_{\beta=1}^{n_d^2} \int d^3 r' |\langle ee | \mu_{\beta}(\mathbf{r} - \mathbf{r}') \rangle|^2 \frac{\tilde{C}_6^{(\beta)}}{(R_c^{(\beta)})^6 + |\mathbf{r} - \mathbf{r}'|^6}. \quad (4.142)$$

Fig. 4.6 shows the two-body interaction  $U(\mathbf{r}) = U(x, y, z)$  for the two particular exam-

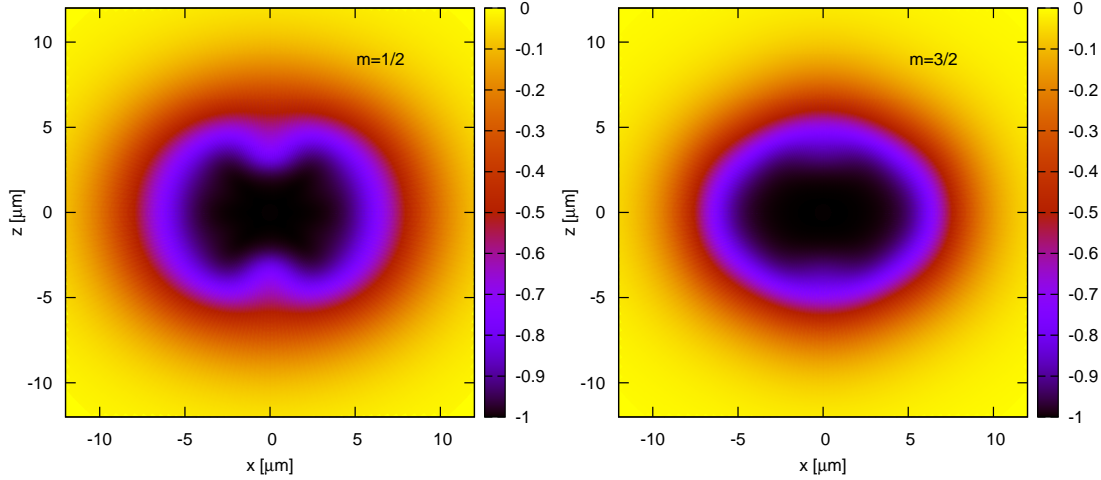


**Figure 4.6.:** Interaction potential  $U(\mathbf{r})$  for dressing to the  $65d$ -state (left:  $m = 1/2$ , right:  $m = 3/2$ ), with  $\Delta = 2\pi \cdot 32\text{MHz}$ ; scaled by its maximum absolute value  $|U(0)| = \frac{\hbar\Omega^4}{8\Delta^3}$ . The quantization axis is the  $z$ -axis. Shown is a cut through the  $xz$ -plane which determines the whole interaction since it is symmetric w.r.t. rotation around the  $z$ -axis.

ples of dressing to the  $65d_{3/2}(m = 1/2)$  or the  $65d_{3/2}(m = 3/2)$ -state. The quantization axis is the  $z$ -axis and in experiment it is determined by the laser polarization. Since the interactions are always still symmetric with respect to rotation around the  $z$ -axis (as was noted before), it is sufficient to show a slice through the  $xz$ -plane. The small

anisotropy of the interaction can be clearly seen.

One can apply a length scaling to remove one of the length scales  $R_c^{(\beta)}$ . Clearly, this will not simplify the equation as significantly as in the isotropic case since many length scales remain. However, since the anisotropy in the interaction is small, it is possible to find an isotropic approximation by defining  $R_c(\vartheta)$  as the full width at half maximum (FWHM) of  $U$  at the angle  $\vartheta = \angle(x, z)$  and by introducing the approximate parameters

$$R_c = \frac{1}{2\pi} \int_0^{2\pi} d\vartheta \sin(\vartheta) R_c(\vartheta), \quad (4.143)$$

$$C_6 = -2\hbar\Delta R_c^6. \quad (4.144)$$

The ensuing approximate isotropic potential is

$$U_{\text{iso}}(\mathbf{r}) = U_{\text{iso}}(r) = \left(\frac{\Omega}{2\Delta}\right)^4 \frac{C_6}{R_c^6 + r^6} = \frac{\tilde{C}_6}{R_c^6 + r^6}. \quad (4.145)$$

For this potential the isotropic rescaling can be applied as before. Hence, the isotropic interaction strength  $\alpha$  approximately characterizes the strength of the anisotropic potential, too. This will be useful to compare the strengths of two potentials of which at least one is anisotropic.

## 5. Supersolids in a dressed gas

A supersolid is an exotic state of matter that is at the same time superfluid (see section 2.5) and solid. Its possible existence was first conjectured in 1969/1970 by Andreev and Lifshitz [10] and Chester [37]. The concept of supersolidity is rather unintuitive because the two properties of superfluidity and solidity seem antithetic: A perfect superfluid can be pictured as a gas of atoms, all of which are free to move throughout the system. This is exactly in contrast to a classical solid. There, particles are strongly localized on lattice positions. Depending on whether the solid is crystalline or amorphous, the particle positions might more or less follow a symmetry pattern, but in all cases there is a rigid structure. The rigidity is brought about by inter-particle interactions. Hence, in a supersolid the same particles whose interactions provide the rigidity must also provide for superfluid flow. Whether supersolidity is, indeed, possible has been controversially discussed for many decades [27,146,151,205]. One system that seemed a good candidate and has been investigated extensively is solid Helium-4. Unless pressurized, it remains liquid down to zero temperature [126] and shows strong superfluid behavior [5,64,98,116]. By and large, this originates from its small mass, such that quantum effects are more strongly pronounced than in most other elements.

Early on, Leggett proposed an experimental way to measure superfluidity [120]. In the same paper, he also showed that, even at zero temperature, the superfluid fraction (the order parameter of superfluidity) of any *perfect* crystal should be either zero or very small. Nevertheless, as conjectured by Andreev, Lifshitz and Chester [10,37], superfluidity might still arise from delocalized lattice defects in the ground state. Such defects are called zero-point defects to clarify that they do not constitute excitations but that the ground state is a crystal with a non-integer number of particles per lattice site. Since they are delocalized, the defects can provide superfluid flow. However, it remained unclear whether the ground state of solid helium indeed exhibits any zero-point defects.

At first, experimental findings seemed to rule out the existence of supersolids [9,20,57,80,140,189,193]. However, several explanations were brought forth why experiments might have failed to observe a supersolid phase. In particular, the possibility that supersolidity sets in only below experimentally achievable temperatures could not be ruled out.

The situation changed in 2004, when an experiment by Kim and Chan [102] was the first to find evidence of a supersolid. Following the idea of Leggett [120], they measured the oscillation period of a torsional oscillator filled with solid He-4. At temperatures below 250 mK, they found a decrease of the period implying a drop of the rotational inertia of the helium sample. This can be interpreted as a part of the system becoming superfluid and no longer participating in the rotation. This effect is called non-classical rotational inertia (NCRI), as introduced by Leggett. A number of subsequent experiments [38,103,104] confirmed the finding.

On the theoretical side, it was shown [164] that the aforementioned zero-point defects are, indeed, the only way how a crystal can become superfluid. Thus, the crucial question was whether the ground state of solid helium has zero-point defects, or not. Numerous

theoretical calculations based on Monte-Carlo methods [12,25,41,71,173] were performed to address this question and they all found that the helium ground state has no defects, suggesting that it cannot be supersolid. Such calculations yield very good agreement with experimental measurements in condensed helium [36]. On the other hand, arguments were put forward, e.g. by Anderson [8] and Bali bar [14], that a supersolid state might yet exist in helium. This ushered in an ongoing theoretical debate.

At the same time, there have been suggestions how to explain the experimentally found NCRI without having to assume superfluidity [134,162,170,207]. Finally, very recent experiments by D.Y. Kim and Chan [101] found *no* decrease of the oscillation period. They suggested that the previously found decrease could be explained purely mechanically by shear modulus stiffening which occurs at low temperatures [50,171]. This new observation brings the experimental findings in agreement with the theory.

In this thesis, we will not discuss solid helium but we will show that a Rydberg-dressed BEC, as introduced in the previous chapter, provides a promising alternative route towards an unambiguous realization of supersolidity. The mechanism for supersolidity here is different from the one described above. The essential idea was introduced by Gross [83,84] in 1957.

First, we will investigate the dressed BEC in the mean-field approximation, starting with the Bogoliubov spectrum. Furthermore, the ground state of a dressed BEC will be investigated and a possible scheme for the dynamical preparation of a supersolid will be discussed.

In the second part of this chapter, we will demonstrate the validity of the mean-field approximation by comparing it to exact results from Quantum-Monte-Carlo simulations. In particular, both methods agree that, for a certain range of interaction strengths, the modulated states that we found are superfluid, thus making them supersolids.

## 5.1. Dressing to Rubidium-87 *s*-states

Throughout this chapter, we will consider Rydberg-*s*-states of Rubidium, since their interaction is always repulsive and almost isotropic.

For a given principal quantum number  $n$  there are two degenerate *s*-states (spin-up  $|\uparrow\rangle$  and spin-down  $|\downarrow\rangle$ ). However, as we have seen in chapter 3, the corresponding four interaction curves are practically identical so that the spin-multiplicity can safely be neglected and the atom can be treated as having only one *s*-state with a van-der-Waals interaction  $W(r)$ . Hence, the analysis in section 4.4 applies and the rescaled GPE reads

$$i\partial_t\psi(\mathbf{r}) = \left( -\frac{1}{2}\nabla^2 + \gamma|\psi(\mathbf{r})|^2 + \alpha \int_V dr' \frac{|\psi(\mathbf{r}')|^2}{1 + |\mathbf{r} - \mathbf{r}'|^6} \right) \psi(\mathbf{r}) \quad (5.1)$$

with the effective interaction strengths (see section 4.4)

$$\alpha = \frac{\tilde{C}_6 m \rho}{\hbar^2 R_c}, \quad (5.2)$$

$$\gamma = \frac{m R_c^2 \rho}{\hbar^2} g = 4\pi a_s R_c^2 \rho. \quad (5.3)$$

## 5.2. Bogoliubov-spectrum and Roton instability

We start the investigation of the dressed BEC's properties by calculating the Bogoliubov spectrum of the homogeneous state (2.62)

$$\varepsilon(\mathbf{k}) = \sqrt{\frac{\hbar^2 k^2}{2m} \left( \frac{\hbar^2 k^2}{2m} + 2\rho g + 2\rho \tilde{W}(\mathbf{k}) \right)}, \quad (5.4)$$

which describe the energy of elementary excitations of the form

$$\chi_{\mathbf{k}}(\mathbf{r}) = u_{\mathbf{k}} e^{i\mathbf{k}\cdot\mathbf{r} - i\varepsilon(\mathbf{k})t} + \overline{v_{\mathbf{k}}} e^{-i\mathbf{k}\cdot\mathbf{r} + i\varepsilon(\mathbf{k})t}. \quad (5.5)$$

Using the length and energy scaling introduced in Section 4.4, the spectrum can be expressed solely in terms of the interaction parameters (5.2) and (5.3):

$$\varepsilon(k) = \sqrt{\frac{k^2}{2} \left( \frac{k^2}{2} + 2\gamma + 2\alpha \tilde{W}(k) \right)}, \quad (5.6)$$

where  $k$  is now given in terms of  $1/R_c$ .

Depending on the dimensionality of the system, the Fourier transformed interaction  $\tilde{W}$  is given by (see Fig. 5.1(a)):

$$\tilde{W}^{1D}(k) = \frac{\pi}{3} \left( e^{-k} + e^{-\frac{1}{2}k} \cos\left(\frac{1}{2}k\sqrt{3}\right) + \sqrt{3}e^{-\frac{1}{2}k} \sin\left(\frac{1}{2}k\sqrt{3}\right) \right), \quad (5.7)$$

$$\tilde{W}^{2D}(k) = \frac{2\pi}{k} G_{0,6}^{4,0} \left( \frac{5}{6}, \frac{5}{6}, \frac{1}{2}, \frac{1}{6}, \frac{1}{2}, \frac{1}{6} \mid \left(\frac{k}{6}\right)^6 \right), \quad (5.8)$$

$$\tilde{W}^{3D}(k) = \frac{2\pi^2}{3k} e^{-\frac{k}{2}} \left( e^{-\frac{k}{2}} - \cos\left(\frac{\pi}{3} + \frac{1}{2}k\sqrt{3}\right) - \cos\left(\frac{5\pi}{3} - \frac{1}{2}k\sqrt{3}\right) \right). \quad (5.9)$$

The function  $G$  in Eq. (5.8) denotes Meijer's G-function [139].

All of the spectra  $\varepsilon(k)$  have ‘‘roton-maxon’’ form (see Fig. 5.1(b)–(d)) for sufficiently large  $\alpha$ . A roton-maxon spectrum is a spectrum that has at least one local maximum (the maxon) and a local minimum at  $k_{\text{rot}} \neq 0$  (the roton). This feature yields a formal connection to the physics of helium which also exhibits roton-excitations [55, 62, 92, 113, 149, 206].

Whether an interaction  $W$  gives rise to a roton-maxon spectrum depends on its Fourier Transform  $\tilde{W}$ : if  $\tilde{W}$  has any negative values then it has a roton-maxon spectrum if

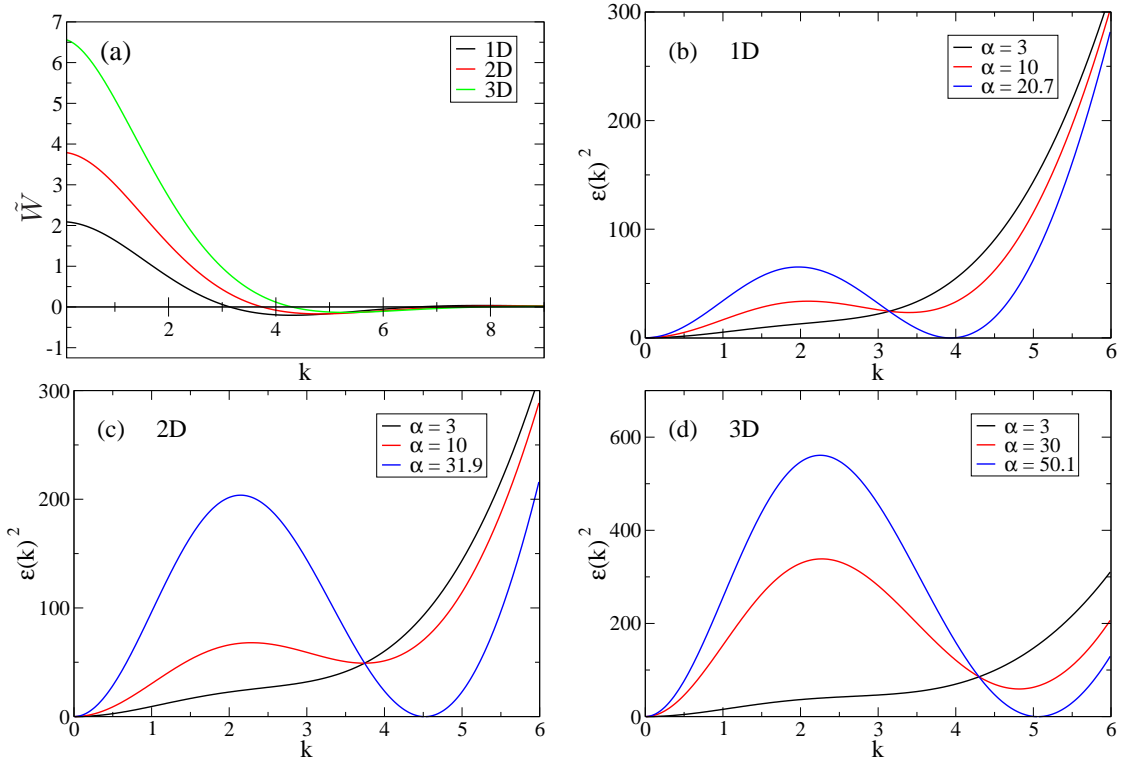


**Figure 5.1.:** (a) One, two and three dimensional Fourier transforms (5.7)–(5.9) of the dressing interaction. It is clearly visible that, independently of the dimension,  $\tilde{W}$  is negative in a certain  $k$ -range.

(b)–(d) Bogoliubov spectra for different values of  $\alpha$  in (b) one dimension, (c) two dimensions, (d) three dimensions. In each panel, one spectrum is shown where  $\alpha$  is so low that the spectrum does not yet have roton-maxon form, one spectrum where the roton-maxon form is evident and one where the roton minimum touches zero and the instability sets in.

$\alpha$  is sufficiently large. Furthermore, for every such interaction it is always possible to find a sufficiently large interaction strength  $\alpha_{\text{inst}}$  for which the roton minimum touches zero at the roton momentum  $k_{\text{roton}}$  (“roton-softening”). Beyond this critical strength, in the so-called “roton-unstable” regime ( $\alpha > \alpha_{\text{inst}}$ ), the evaluation of Eq. (5.4) yields imaginary values  $\varepsilon(k) = i\eta$  with  $\eta \in \mathbb{R}$  for  $k$  sufficiently close to the roton minimum. If those values are substituted into the expression for an elementary excitation, this yields two contributions ( $\pm$ ) proportional to

$$e^{\pm(i\mathbf{k}\cdot\mathbf{r} - i\varepsilon(\mathbf{k})t)} = e^{\pm i\mathbf{k}\cdot\mathbf{r}} e^{\pm\eta t}, \quad (5.10)$$

one of which which diverges for  $t \rightarrow \infty$ .

This implies that the magnitudes of perturbations that correspond to excitations around  $k_{\text{rot}}$  will grow exponentially in time (with the rate  $|\eta| = |\text{Im}\varepsilon(k)|$ ) leading to growing density modulations with the length scale  $l = 2\pi/k_{\text{rot}}$ . This phenomenon is called roton

instability.

By evaluating Eq. (5.6) with Eqs. (5.7), (5.8) and (5.9), we can analytically calculate the values  $\alpha_{\text{rot}}(0)$  and  $\alpha_{\text{inst}}(0)$ , where the roton minimum and the roton instability first appear, for a vanishing short-range interaction ( $\gamma = 0$ ). They are shown in table 5.1. In the presence of a repulsive short-range interaction ( $\gamma > 0$ ) they can also be calculated, as shown in Figs. 5.2 and 5.3. The relation  $\alpha_{\text{inst}}(\gamma)$  turns out to be approximately linear, with parameters that are also shown in table 5.1.

dimension	$\alpha_{\text{rot}}(0)$	$\alpha_{\text{rot}}(\gamma)$	$\alpha_{\text{inst}}(0)$	$\alpha_{\text{inst}}(\gamma)$
1	6.2	$6.2 + 1.60\gamma$	20.7	$20.7 + 5.21\gamma$
2	5.9	$5.9 + 1.28\gamma$	31.9	$31.9 + 6.16\gamma$
3	4.8	$4.8 + 1.00\gamma$	50.1	$50.1 + 7.75\gamma$

**Table 5.1.:** Critical values  $\alpha_{\text{rot}}$  and  $\alpha_{\text{inst}}$  for the long-range interaction strength as predicted from the Bogoliubov spectrum. The results for  $\gamma \neq 0$  are obtained by a fit of the exact results (Fig. 5.2 and 5.3).

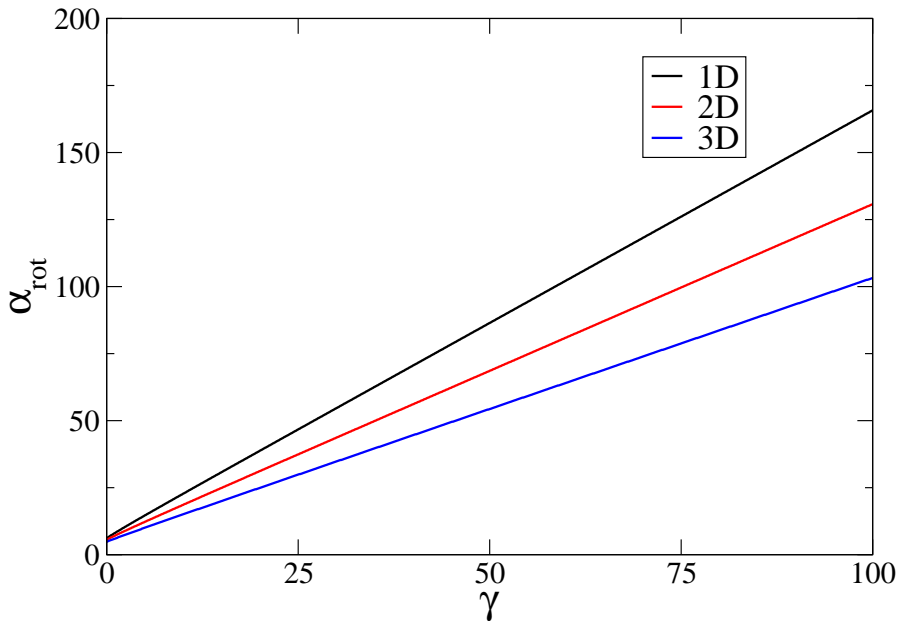


**Figure 5.2.:** Onset of the roton minimum in various dimensions. Shown is the dependence of the critical value  $\alpha_{\text{rot}}$  (where the roton minimum first appears) on the short-range interaction strength  $\gamma$ .

From a physical point of view, the roton instability can be interpreted as an implication of “attraction in momentum space”. As we pointed out already, it occurs for every interaction  $W$  if and only if its Fourier transform  $\tilde{W}$  is negative in any region  $K$  in momentum space. Physically, it can be understood as roton states (i.e., states that ex-

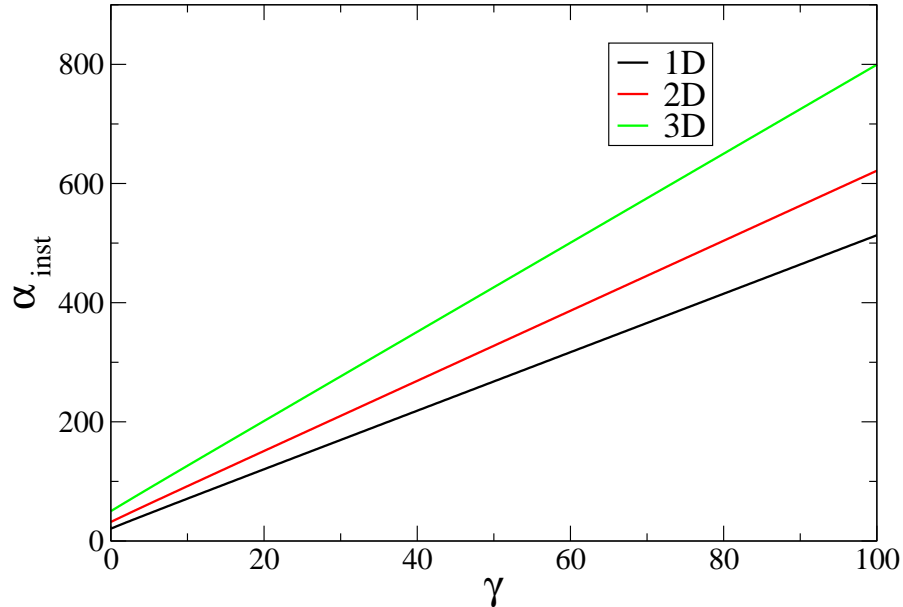


**Figure 5.3.:** Instability diagram in various dimensions. Shown is the dependence of the critical value  $\alpha_{\text{inst}}$  (where the roton instability sets in) on the short-range interaction strength  $\gamma$ .

hibit excitations with  $k = k_{\text{rot}}$ ) being energetically favorable. These states have density modulations with the length scale  $2\pi/k$ . In position space, the instability can also be understood qualitatively: due to the soft-core nature of the interaction ( $W(0) < \infty$ ), particles can approach each other very closely without additional energy cost (as soon as their distance is already smaller than  $R_c$ ). This will lead to clustering of atoms into small droplets. The droplets repel each other, and therefore a so-called “droplet crystal” [40, 165] is formed.

Roton-maxon spectra have also been discovered in dipolar BECs [21, 81, 114, 176, 204]. There, the roton-maxon spectrum arises from the partially attractive nature of the interaction. But the same attraction also leads to collapse of the condensate [56, 74, 109, 177]. It is possible to suppress the collapse by tightly confining the BEC in the attractive direction [33, 141], but then the diverging nature of the repulsive  $r^{-3}$  interaction makes the ground state a classical solid where superfluidity vanishes [165].

The dressing-interaction, on the other hand, is repulsive in all directions and does not diverge. There, the roton-maxon spectrum is an implication of the soft core ( $W(0) < \infty$ ). We will demonstrate that this avoids the problem of collapse altogether.

An unstable state cannot be the ground state of a system because, due to energy conservation, there is no state that it can destabilize towards. Hence, the roton instability we found shows that (for  $\alpha > \alpha_{\text{inst}}$ ) the homogeneous state cannot be the ground state. This raises the question what the ground state actually is.

### 5.3. Supersolid ground states

To address the question what the ground state of a dressed gas is, we will numerically solve the GPE (5.1) on a grid. One possibility of calculating the ground state is the imaginary time evolution (ITE) (see Appendix A.4). For a linear Schrödinger equation, it allows to choose an arbitrary initial state and then propagate it in imaginary time. The method will converge to the ground state, provided that the initial state has a non-zero overlap with the ground state. However, this does not hold for the GPE because its solutions do not obey the superposition principle. Therefore, the GPE has very many metastable states. Depending on the chosen initial state, the ITE can converge to any of those metastable states. Hence, unlike in the linear case, the final steady state now strongly depends on a reasonable choice of the initial state. To solve this problem, we precede the ITE by a variational calculation to find a suitable initial state.

From the preceding discussion, we expect that the ground state might have regular density modulations. Therefore, we make the ansatz

$$\psi_{\sigma,R}(\mathbf{r}) = \sum_i \varphi_{\sigma}(\mathbf{r} - \mathbf{R}_i), \quad (5.11)$$

where the  $\mathbf{R}_i$  define a lattice with a lattice constant  $a$  and a given structure. We consider simple cubic (sc), body-centered cubic (bcc), face-centered cubic (fcc) and hexagonally closest packed (hcp). Localized on each lattice site we assume a Gaussian wave function

$$\varphi_{\sigma}(\mathbf{r}) = c \exp\left(-\frac{r^2}{2\sigma^2}\right). \quad (5.12)$$

The factor  $c$  is determined such that the average density

$$\lim_{V \rightarrow \mathbb{R}^3} \frac{1}{|V|} \int_V d\mathbf{r} |\psi(\mathbf{r})|^2 \quad (5.13)$$

is unity, conforming to our definition of  $\psi$  in section 4.4.

First, we consider states of the form given by Eqs. (5.11) and (5.12). The energy of a state  $|\psi\rangle$  is

$$E(V) = -\frac{1}{2} \int_V d\mathbf{r}' \overline{\psi(\mathbf{r}')} \nabla^2 \psi(\mathbf{r}') + \frac{\gamma}{2} \int_V d\mathbf{r} |\psi(\mathbf{r})|^4 + \frac{\alpha}{2} \int_V d\mathbf{r} \int_V d\mathbf{r}' \frac{|\psi(\mathbf{r}')|^2 |\psi(\mathbf{r})|^2}{1 + |\mathbf{r} - \mathbf{r}'|^6} \quad (5.14)$$

$$= E_{\text{kin}} + E_{\text{contact}} + E_{\text{dressing}} \quad (5.15)$$

in a large box of the volume  $V$ .

Thus, given a certain lattice structure, there are two variational parameters for the state; the lattice constant  $R$  and the width  $\sigma$  of each droplet. Now, for every value of  $\alpha$  and

$\gamma$  (and a given lattice structure), we can vary  $R$  and  $\sigma$  to find the minimal energy

$$E_{\min}(\alpha, \gamma) = E(\alpha, \gamma; R_{\min}, \sigma_{\min}) \quad (5.16)$$

and the corresponding approximate ground state  $|\psi_{\sigma_{\min}, R_{\min}}\rangle$ .

The simple assumption that the density profile on each site is Gaussian is removed by performing the ITE on  $|\psi_{\sigma_{\min}, R_{\min}}\rangle$  which decreases the energy further. This yields an enhanced approximation  $|\psi^{\min}\rangle$  of the ground state.

### Three dimensions

In order to find the phase transition between a homogeneous state (superfluid) and a modulated state (supersolid), we calculated the minimal energy densities  $\varepsilon_{\min}$  of the sc, bcc, fcc and hcp crystal structures for the case of  $\gamma = 0$ . The transition point is found by comparing the energy  $\varepsilon_{\min}$  of the numerically obtained modulated states to the energy  $\varepsilon_{\text{hom}}$  of the homogeneous state  $\psi_{\text{hom}}(\mathbf{r}) = 1$ . The latter one can be calculated analytically:

$$\varepsilon_{\text{hom}} = \lim_{V \rightarrow \mathbb{R}^3} \frac{1}{|V|} E(V) \quad (5.17)$$

$$= \lim_{V \rightarrow \mathbb{R}^3} \frac{1}{|V|} \left( \frac{\gamma}{2} \int_V d\mathbf{r} |\psi_{\text{hom}}(\mathbf{r})|^4 + \frac{\alpha}{2} \int_V d\mathbf{r} \int_V d\mathbf{r}' \frac{|\psi_{\text{hom}}(\mathbf{r}')|^2 |\psi_{\text{hom}}(\mathbf{r})|^2}{1 + |\mathbf{r} - \mathbf{r}'|^6} \right) \quad (5.18)$$

$$= \lim_{V \rightarrow \mathbb{R}^3} \frac{1}{|V|} \left( \frac{\gamma}{2} \int_V d\mathbf{r} 1 + \frac{\alpha}{2} \int_V d\mathbf{r} \int_V d\mathbf{r}' \frac{1}{1 + |\mathbf{r} - \mathbf{r}'|^6} \right) \quad (5.19)$$

$$= \frac{\gamma}{2} + \lim_{V \rightarrow \mathbb{R}^3} \frac{\alpha}{2} \int_V d\mathbf{r} \frac{1}{1 + r^6} = \frac{\gamma}{2} + \frac{\alpha}{2} 4\pi \int_0^\infty dr \frac{r^2}{1 + r^6} \quad (5.20)$$

$$= \frac{\gamma}{2} + \frac{\pi^2}{3} \alpha. \quad (5.21)$$

The resulting differences  $\varepsilon_{\text{hom}} - \varepsilon_{\min}$  (for  $\gamma = 0$ ) are shown in Fig. 5.4. We find that for  $\alpha < \alpha_{\text{suso}} \approx 30$ , the homogeneous state  $\psi_{\text{hom}}$  is energetically lower than all of the investigated modulated states. At  $\alpha_{\text{suso}}$ , the phase transition from a homogeneous to a modulated state takes place. At this point, the hcp-, fcc-, and bcc-states fall below  $\psi_{\text{hom}}$ . These three states have *almost* the same energy, with the hcp-state being the lowest. At the transition point, the derivative  $\partial_\alpha \varepsilon_{\min}(\alpha)$  is discontinuous, marking the phase transition as one of first-order. This also manifests itself in an instantaneous change of the ground state from  $|\psi_{\text{hom}}\rangle$  to one with finite density modulations. Hence, exactly at the transition point,  $|\psi_{\text{hom}}\rangle$  is degenerate with this particular modulated state. Modulated states with lower peak densities, however, have a higher energy. The transition takes place at a finite roton gap. In other words, it occurs at strictly

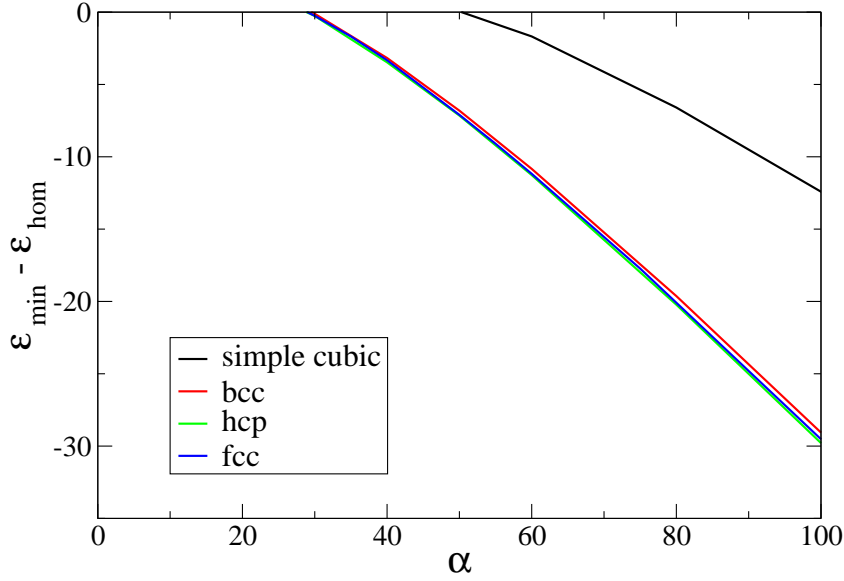


**Figure 5.4.:** Relative energy density  $\varepsilon_{\min}$  of the lowest-lying state with a given symmetry (sc, bcc, fcc, hcp) as a function of the interaction strength  $\alpha$  with  $\gamma = 0$ .  $\varepsilon_{\min}$  is shown relative to the energy density  $\varepsilon_{\text{hom}} = \frac{\gamma}{2} + \frac{\pi^2}{3}\alpha$  (Eq. (5.21)) of the homogeneous state. The transition to a modulated ground state happens at  $\alpha \approx 29$  where the hcp crystal structure becomes energetically most favorable. The hcp state remains the lowest state for all investigated  $\alpha$ , but the fcc state is always extremely energetically close. The bcc state's energy density lies slightly higher.

dimension	$\alpha_{\text{rot}}(0)$	$\alpha_{\text{inst}}(0)$	$\alpha_{\text{suso}}(0)$
1	6.2	20.7	20.7
2	5.9	31.9	26.7
3	4.8	50.1	30.0

**Table 5.2.:** Critical values for  $\alpha$  for  $\gamma \in [0..100]$  as predicted from the Bogoliubov spectrum (repeated from table 5.1) and transition point to a supersolid state, all for  $\gamma = 0$ .

lower interaction strength than the roton instability ( $\alpha_{\text{suso}} < \alpha_{\text{inst}}$ ). This is related to the first-order nature of the transition as will be discussed after showing the results for two- and one-dimensional systems.

## Two dimensions

In two dimensions, the lowest energy state corresponds to a triangular lattice. Apart from this, the situation is qualitatively identical to the three-dimensional case. Again, we find a first-order phase transition, this time at  $\alpha_{\text{suso}} = 26.7$ . This, again, locates the phase transition at a finite roton gap. The exact same behavior was previously found for the model of a step-function interaction  $U(\mathbf{r}) = U_0\vartheta(|a - r|)$ , where  $\vartheta$  is the Heaviside-function [97, 160].

**One dimension**

The one-dimensional case differs significantly from the higher-dimensional ones. We find a *second-order* phase transition at  $\alpha_{\text{suso}} = 20.7$ . Beyond that point, the homogeneous state  $|\psi_{\text{hom}}\rangle$  is replaced as the ground state by a state with infinitesimal modulations. Notably, the situation differs from the other dimensionalities in another important aspect: the phase transition occurs at zero roton gap, i.e., at the same interaction strength as the roton instability. We can understand this different behavior by considering that the Bogolioubov spectrum (5.6) makes a statement about the stability of *plane-wave* excitations. These correspond exactly to the symmetry of the only regular structure in one dimension, an equidistant lattice. In contrast, in higher dimensions the ground states we found exhibit more complicated lattice structures that do not correspond to a simple plane wave. Hence, in those cases, there is no reason why the phase transition and the onset of the roton instability should coincide.

**Connection between phase transition order and roton instability**

We now understand why roton instability and phase transition coincide in one dimension but not in higher dimensions. Furthermore, we observe the following implications for the order of the phase transition:

- (1) If a quantum phase transition coincides with a roton instability, the transition is of second order.
- (2) If a quantum phase transition occurs at a finite roton gap, the transition is of first order.

This connection can be understood:

If a roton-unstable system is arbitrarily weakly perturbed this leads to a growth of density modulations in real time. Since this growth is continuous in time, the time evolution must pass through states with arbitrarily small density modulations. Since the GPE conserves energy, these small-modulation states must have the same energy as the initial state. But for a first-order transition this is not the case. There, at the transition point, a state with finite modulations is degenerate with the initial state but more weakly modulated states are higher in energy. Hence, they are not accessible by a real-time evolution. Therefore, the transition must be of second order, proving statement (1).

In conclusion, we have found that in all dimensions there is a transition from an unmodulated, homogeneous (“liquid”) state to a modulated (“solid”) state at a critical value  $\alpha_{\text{suso}}$ .

In the mean-field approximation, the wave-function, by definition, has long-range phase coherence and the condensate fraction is 100%, so that all of the solid states are also superfluid. Hence, they are indeed *supersolid* states.

Whether the solid states are also supersolid in reality must be checked by moving beyond

the mean-field approximation. This question will be addressed in Section 5.5, where we will perform Monte-Carlo simulations. We will also discuss superfluidity and its dependence on the system parameters in more detail.

## 5.4. Time evolution

It still needs to be established how exactly the instability found in section 5.2 takes place and what the time evolution of a state *after* the destabilization is. To this end, we performed numerical simulations of the time evolution of a dressed, almost homogeneous gas in one to three dimensions. This also allows us to check our prediction of the roton instability. The initial state will be homogeneous except for a small, random phase which is necessary to induce the instability.

First, we simply consider time evolutions with constant values of  $\alpha$  around  $\alpha_{\text{inst}}(0)$  (and with  $\gamma = 0$ ) to check whether the instability occurs at the predicted value. Since the maximum growth rate of the modulations is proportional to  $\text{Im}(\varepsilon(k_{\text{max}}))$  and  $\varepsilon(k_{\text{max}}) \rightarrow 0$  as  $\alpha \rightarrow \alpha_{\text{inst}}$ , it is not possible to verify the prediction to arbitrary accuracy since the times needed for the instability to develop (and hence, the CPU time needed to calculate the time evolution) diverges. Nevertheless, as far as we can tell, the agreement between analytics and numerics is quite good. We show this in Figs. 5.5–5.7, where we plot the time evolution of the kinetic energy density  $\varepsilon_{\text{kin}}$  for one to three dimensions and for several values of  $\alpha$ . We use the same initial state for every value of  $\alpha$  to ensure comparability. Since  $\varepsilon_{\text{kin}}$  is zero only for the homogeneous state and becomes larger for stronger modulated states, it can be used to characterize the real-time transition from the homogeneous state to a modulated one. In our calculations, the initial kinetic energy is not exactly zero, but a small value because of the random phase in the initial state.

### Three dimensions

In three dimensions, we find excellent agreement between analytics and numerics, the critical value is  $\alpha_{\text{inst}} = 50.1$  (see Fig. 5.5(a)). To visualize the resulting soliton state, we show a two-dimensional cut through the 3D-system (Fig. 5.5(b), taken at  $t = 8$ ). No state with long-range symmetry is formed. This is due to a competition between the various lattice symmetries (bcc, fcc, hcp; see the discussion in the preceding section), that have very similar energies and can form small domains. Hence, the resulting state is not crystalline (as in two dimensions), but a self-assembled “glas” state, since it has no crystalline long-range order. At the same time at which the roton instability manifests itself visibly in the density, a self-assembled lattice of vortices and anti-vortices is formed in the low-density regions. The vortices stabilize the supersolid state so that no recurrence towards the homogeneous state occurs. Therefore, the time evolution eventually leads to an approximately steady state that only exhibits a small breathing motion due to excess energy.

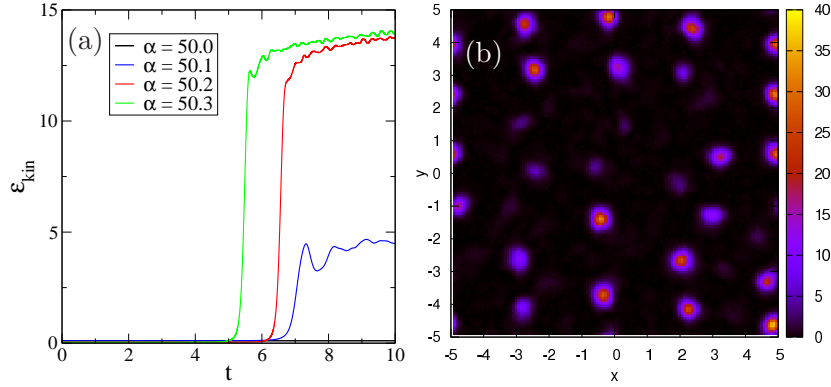


**Figure 5.5.:** 3D, (a) Kinetic energy density  $\varepsilon_{\text{kin}}$  depending on the time, (b), resultant density  $|\psi|^2$  for  $\alpha = 50.1$  at  $t = 8$ .

## Two dimensions

In two dimensions, the numerical result fits the analytical prediction perfectly, too. With both methods we find  $\alpha = 31.9$  as the critical value, which can be seen in Fig. 5.6(a). The time evolution is similar to the three-dimensional one, including the appearance of vortices that stabilize the supersolid state. A difference lies in the long-range triangular lattice that is reached in two dimensions. This is possible because the triangular lattice symmetry is the only energetically relevant one so that domains of different symmetries (as in three dimensions) cannot occur.

In Fig. 5.6(b) we show the density for  $\alpha = 31.9$  at  $t = 20$ , after the steady state has been reached.

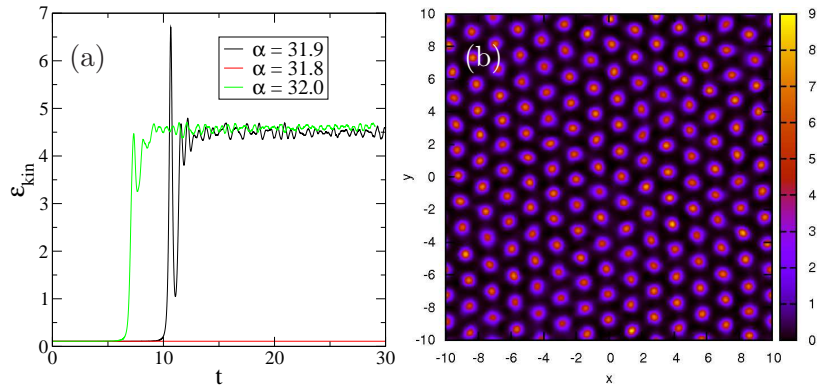


**Figure 5.6.:** 2D, (a) Kinetic energy density  $\varepsilon_{\text{kin}}$  depending on the time, (b), resultant (area) density  $|\psi|^2$  for  $\alpha = 31.9$  at  $t = 20$ .

### One dimension

Again, the one-dimensional case turns out to be different than the others. We find that the smallest value of  $\alpha$  where an instability can clearly be seen is about 21.1, deviating about 2% from the analytically predicted value  $\alpha = 20.7$  (see Fig. 5.7(a)). This apparent deviation can be explained by the coincidence of the roton instability (at  $\alpha = 20.7$ ) with the second-order supersolid phase transition. Close to the transition point, strongly modulated states are non-accessible through a real-time evolution since this would violate energy conservation. Hence, the roton instability can drive the homogeneous state only towards weakly modulated states. Furthermore, the instability would occur very slowly as the growth rate of the modulations vanishes at the critical value  $\alpha_{\text{inst}}$ . While it is likely that the modulational instability also exists in the range  $20.7 \leq \alpha \leq 21.1$ , we did not see it in the numerical simulations.

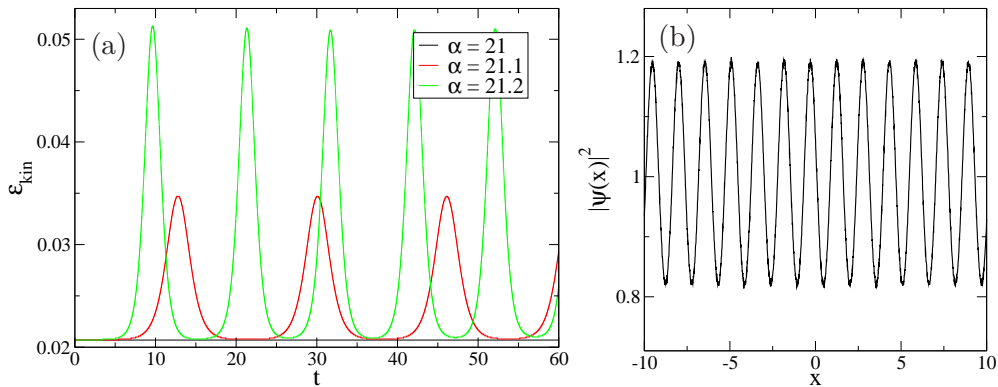


**Figure 5.7.:** 1D, (a) Kinetic energy density  $\varepsilon_{\text{kin}}$  depending on the time, (b), resultant (line) density  $|\psi|^2$  for  $\alpha = 21.1$  at  $t = 30$ .

Fig 5.7(b) shows the density  $|\psi|^2$  at a time where the kinetic energy, and hence, the modulations are maximal. Notably, the system undergoes several cycles of decay and revival of the kinetic energy. This corresponds to recurring revivals of both the homogeneous state and the supersolid state and marks another significant difference of the one-dimensional system. The behavior is due to the absence of the stabilization mechanism in 2D and 3D, namely vortices. Since there are no vortices in 1D, no energy can be shifted into them, making the revivals possible.

### Creation of an ordered crystal in three dimensions

We now consider a somewhat more complicated scheme (see Fig. 5.8 (a)) in order to create a crystalline state in three dimensions. First, we set  $\alpha = 60$ , which quickly introduces the roton instability. The system then evolves into a glassy state (Fig. 5.8 (b)) like the one in Fig. 5.5 (b).

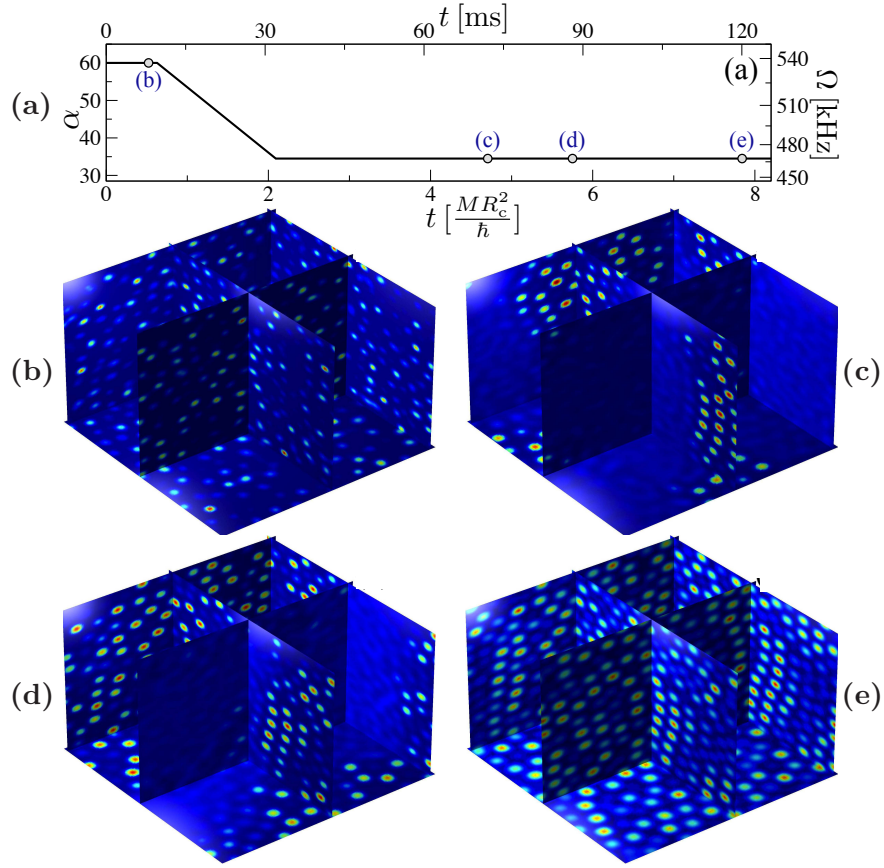


**Figure 5.8.:** Snapshots of the BEC dynamics for a time-varying interaction parameter  $\alpha(t)$  shown in (a). Panels (b)-(e) show the density along orthogonal slices through the simulation box at times indicated in (a). The upper and right axes in (a) show the actual time and Rabi frequency for a  $^{87}\text{Rb}$  BEC with  $n = 60$ ,  $\Delta = 50$  MHz and  $\rho_0 = 2 \cdot 10^{20} \text{ m}^{-3}$ . Figure reprinted from [91]

Afterwards, we decrease the value of  $\alpha$  slowly to a value just above the supersolid phase transition  $\alpha_{\text{suso}} = 30$ . This leads to a partial “melting” (Fig. 5.8 (c)) of the crystal, where the modulated state gives way to a homogeneous “liquid”. Furthermore, it allows the density droplets to move with respect to each other, so that, in the places where there remains a crystal, a more regular lattice is formed after some time (Fig. 5.8 (d)). The system then continues to recrystallize slowly, until all fluid domains have vanished. The resulting lattice (Fig. 5.8 (e)) is significantly more regular than the one created directly by the Roton instability. It exhibits extended domains of regular crystals. For Fig. 5.8, we have assumed a BEC with an average density  $\rho_0 = 2 \cdot 10^{20} \text{ m}^{-3}$ , dressed to the 60s-state with a detuning  $\Delta/2\pi = 50$  MHz. The change in  $\alpha$  then corresponds to two-photon Rabi frequencies from 540 kHz to 450 kHz. According to section 4.2.6, the

lifetime of the dressed states used in this scheme is around

$$\tau \sim 0.5 \text{ s}, \quad (5.22)$$

so that the time evolution should not be influenced by decay of the dressed state.

## 5.5. Beyond mean-field

We have now seen that the type of solid states we found in section 5.3 can, indeed, be prepared in real time by starting from a homogeneous state. However, all investigations so far have used the mean-field (MF) approximation, which we have not yet shown to be appropriate for our system at all. In particular, MF does not take into account thermal and quantum fluctuations which decrease the superfluidity. Hence, we have not yet shown that the modulated ground states we found are superfluid.

While we investigated bulk systems in the previous sections, we will now consider externally trapped finite systems because these are the kind of systems that can be studied experimentally [130]. For the same reason, we will restrict ourselves to quasi-two-dimensional systems, i.e. systems that are very tightly confined in one direction. If the trap is harmonic, this means that the trapping frequency in the tightly confined direction  $\omega_z$  is much larger than the trap frequency  $\omega$  in the directions perpendicular to that. Once the reduction to two dimensions has been performed, the rescaled Hamiltonian is of the form

$$\hat{H} = \frac{1}{2} \sum_{i=1}^N \hat{\mathbf{p}}_i^2 + \sum_{i<j} \frac{\alpha_1}{1 + |\hat{\mathbf{r}}_i - \hat{\mathbf{r}}_j|^6} + \gamma_1 \sum_{i<j} \delta(\hat{\mathbf{r}}_i - \hat{\mathbf{r}}_j) + \frac{1}{2} \omega^2 r^2 \quad (5.23)$$

with the interaction strengths

$$\alpha_1 = \frac{\tilde{C}_6 m}{\hbar^2 R_c^4}, \quad (5.24)$$

$$\gamma_1 = \frac{m}{\hbar^2 R_c} g = \frac{4\pi a_s}{R_c}. \quad (5.25)$$

For the Monte-Carlo simulations, we use the Path-Integral Monte-Carlo (PIMC) method [36] based on the continuous-space Worm algorithm [26, 28]. It allows to calculate the partition function  $Z$  of a system of  $N$  particles and with the Hamiltonian  $\hat{H}$  at a finite inverse temperature  $\beta = 1/k_B T$ :

$$Z = \text{Tr} \left( e^{-\beta \hat{H}} \right). \quad (5.26)$$

This is performed in a position basis, i.e.,

$$Z = \int d^{3N} r \rho(\mathbf{r}, \mathbf{r}, \beta), \quad (5.27)$$

where  $\rho$  is the density matrix

$$\rho(\mathbf{r}, \mathbf{r}', \beta) = \langle \mathbf{r} | e^{-\beta \hat{H}} | \mathbf{r}' \rangle. \quad (5.28)$$

It can be decomposed into imaginary time-steps:

$$e^{-(\beta_1 + \beta_2) \hat{H}} = e^{-\beta_2 \hat{H}} e^{-\beta_1 \hat{H}}, \quad (5.29)$$

or equivalently:

$$\rho(\mathbf{r}_1, \mathbf{r}_2, \beta_1 + \beta_2) = \int d^{3N} r' \rho(\mathbf{r}_1, \mathbf{r}', \beta_1) \rho(\mathbf{r}', \mathbf{r}_2, \beta_2). \quad (5.30)$$

More generally,  $\rho$  can be split into a large number  $M$  of imaginary time-steps:

$$\rho(\mathbf{r}_0, \mathbf{r}_M, \beta) = \int d^{3N} r_1 \dots d^{3N} r_{M-1} \rho(\mathbf{r}_0, \mathbf{r}_1, \tau) \dots \rho(\mathbf{r}_{M-1}, \mathbf{r}_M, \tau) \quad (5.31)$$

with the increment  $\tau = \beta/M$ . The discrete imaginary-time path  $(r_0, r_1, \dots, r_M)$  is called a world-line .

Now, the partition function can be written as

$$Z = \int d^{3N} r \int d^{3N} r_1 \dots d^{3N} r_{M-1} \rho(\mathbf{r}, \mathbf{r}_1, \tau) \dots \rho(\mathbf{r}_{M-1}, \mathbf{r}, \tau) \quad (5.32)$$

with  $\mathbf{r} = \mathbf{r}_0 = \mathbf{r}_M$ . This means that the world line describes a closed path. This integral is then evaluated with a Monte-Carlo procedure, i.e., by randomly sampling a large number of world lines [36]. This yields the partition function, from which many equilibrium properties of the system can be calculated<sup>1</sup>.

### 5.5.1. Calculation of superfluidity: Monte-Carlo and mean-field

Examples of equilibrium properties that can be deduced from the numerically calculated partition function include the one-particle density  $\rho(\mathbf{r})$  as well as the superfluid fraction  $f_s$ . For sufficiently large  $\beta$  (i.e., low temperatures), the results approximate the ground state well. Therefore, a comparison to the mean-field results (which are inherently zero temperature results) is possible although PIMC is a finite temperature method.

In order to make a statement about the validity of the mean-field approximation, we will compare the Monte-Carlo results to those of the corresponding GPE

$$E\psi(\mathbf{r}) = \left( -\frac{1}{2} \nabla^2 + \gamma |\psi(\mathbf{r})|^2 + \alpha \int d\mathbf{r}' \frac{|\psi(\mathbf{r}')|^2}{1 + |\mathbf{r} - \mathbf{r}'|^6} + \frac{1}{2} \omega^2 r^2 \right) \psi(\mathbf{r}) \quad (5.33)$$

---

<sup>1</sup>In principle, perfect knowledge of the function  $Z$  implies knowledge of all properties, but in practice, only numerical values for  $Z$  are calculated.

with the interaction strengths

$$\alpha = \frac{\tilde{C}_6 m N}{\hbar^2 R_c^4}, \quad (5.34)$$

$$\gamma = \frac{m N}{\hbar^2 R_c} g = \frac{4\pi a_s N}{R_c}. \quad (5.35)$$

These were derived in chapter 4 (Eqs. (4.127) and (4.138)), except that we have now added an additional trapping potential. The rescaled trap frequency  $\omega$  can be obtained from the unscaled one  $\omega_{\text{unsc}}$  as

$$\omega = \frac{m R_c^2}{\hbar} \omega_{\text{unsc}} \quad (5.36)$$

(corresponding to the time/energy scaling we introduced in chapter 4).

Comparing the interaction parameters in the Hamiltonian ( $\alpha_1$  and  $\gamma_1$ ) with those in the GPE ( $\alpha$  and  $\gamma$ ) immediately yields an important insight. Since  $\alpha = N\alpha_1$  and  $\gamma = N\gamma_1$ , the effective interaction strengths scale linearly with the particle number  $N$  in the regime where MF is valid.

In order to judge the validity of the MF approximation, it would be useful to be able to also calculate the superfluidity in MF. Indeed, this is possible using Leggett's estimator for the superfluid fraction [120]. This estimator allows to calculate a radially resolved superfluid fraction  $f_s(r)$ , which describes how a particle at a distance  $r$  from the center of the system rotates around the center. It reads

$$f_s(r) = \frac{4\pi^2}{\left(\int_0^{2\pi} d\vartheta \rho(r, \vartheta)^{-1}\right) \left(\int_0^{2\pi} d\vartheta \rho(r, \vartheta)\right)}, \quad (5.37)$$

where  $\rho(r, \vartheta) = |\psi(r, \vartheta)|^2$  is the one-particle density in polar coordinates. Since  $f_s$  depends only on  $\rho$ , the estimator can be used within the MF method. The derivation of this formula as well as a generalization to bulk systems is given in Appendix C.

The formula has a very intuitive physical interpretation: if the density is constant with respect to  $\vartheta$  for a given  $r$  (i.e.,  $\rho(r, \vartheta) = \rho_0(r)$ ), we find  $f_s(r) = 1$ , a perfect superfluid. Following the discussion of section 2.5, this is what we would expect for a weakly interacting, non-modulated gas at zero temperature. However, when modulations occur, the situation changes: any deviation from the constant density leads to a decrease of  $f_s$ , according to Eq. (5.37). This can be understood as the probability for any one particle to pass through a region of low density being lower than the probability to pass through a given region of higher density. The flow of particles through these low-density regions is suppressed, decreasing superfluidity. In the extreme case, where there is an extended  $\vartheta$ -region with  $\rho(r, \vartheta) = 0$ , we find  $f_s(r) = 0$ .

Note that, strictly speaking, the above formula for  $f_s$  is only an upper bound of the actual superfluid fraction. It takes into account the decrease in  $f_s$  through density modulations (as explained above) but not that through quantum fluctuations. As such, it is not clear, a priori, whether the formula is actually useful in the present context. How-

ever, we will see that for a weakly dressed gas it yields results that agree very well with Quantum Monte-Carlo Simulations.

### 5.5.2. Comparison between Monte-Carlo and mean-field results

We performed Monte-Carlo (MC) simulations for numerous values of  $\alpha, \gamma$  and  $\omega$  and found very good agreement between the MC results at low temperature and the MF predictions. The agreement between the methods extends beyond the one-particle density to the superfluid fraction, validating Leggett's estimator.

A specific example that we now discuss in some detail is given in Figs. 5.9, 5.10 and 5.11 for  $\alpha = 500$ ,  $\gamma = 0$  and  $\omega = 7$ . In this example, a *mesoscopic* supersolid is formed, i.e., a structure that is modulated and superfluid but has an extension of only a few lattice constants. It is evident from the density plots (Fig. 5.9) that the state is modulated.

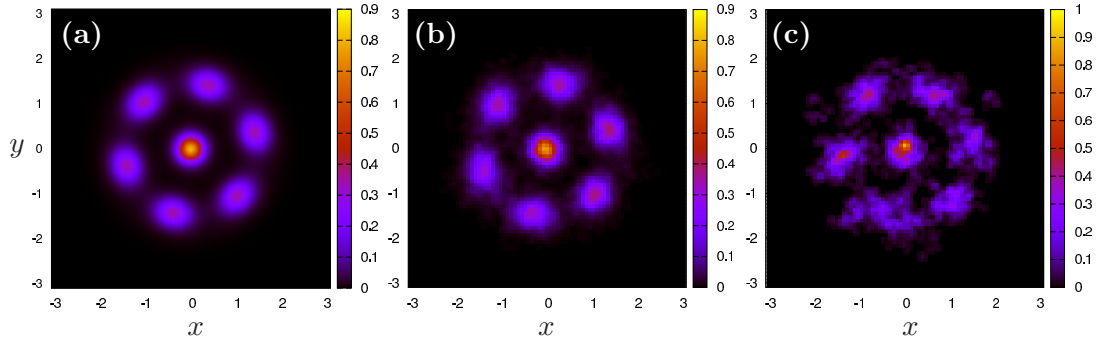


**Figure 5.9.:** Density plots of a system with  $\alpha = 500$ ,  $\gamma = 0$  and  $\omega = 7$ . (a) MF result, (b),(c) MC results for  $T = 1$  and  $T = 10$ . The MC calculations use  $N = 400$  particles.

Panel (a) shows the MF result, (b) and (c) show MC results at scaled temperatures  $T = 1$  and  $T = 10$ . The low-temperature result obviously confirms the MF result. At the higher temperature, thermal fluctuations become evident, which tend to wash out the modulated structure. At sufficiently high temperature, the modulations are expected to vanish, i.e. the crystal melts.

Let us now take a closer look at the superfluidity (Fig. 5.10). Panel (a) shows the dependence of the superfluid fraction  $f_s$  (calculated in the MC simulation) on the temperature  $T$  and the particle number  $N$  for constant values of  $\alpha$ ,  $\gamma$  and  $\omega$  (see above).

Having seen the validity of the MF approximation, we can use the insight that  $\alpha = N\alpha_1$  is the effective interaction strength. Therefore, the MC interaction parameter  $\alpha_1$  that goes into the numerical calculation needs to be chosen differently depending on  $N$ .

For  $T \rightarrow 0$ ,  $f_s(T)$  converges to a value  $f_s(0) \approx 0.6$  independently of  $N$ . As one would expect,  $f_s$  drops as the temperature increases because thermal fluctuations inhibit superfluid flow. However, for higher particle numbers, the drop in  $f_s$  is less pronounced. More precisely, if the temperature is scaled by the particle number, i.e.  $f_s$  plotted as a function of  $T/N$ , then all curves collapse onto a single one. Hence, the superfluidity

depends not on  $N$  and  $T$  separately, but only on  $T/N$ . This is consistent with the linear density scaling of the critical temperature shown by a Berezinskii-Kosterlitz-Thouless transition [17, 111] in the weak-coupling limit [65]. This scaling is useful to predict the superfluidity of systems with higher particle numbers – which, according to the scaling, should remain superfluid at higher temperatures.

An experimental setup that yields the interaction and trap strengths that we considered would be a gas of  $N = 14000$  Rubidium-87 atoms, dressed to the  $60s$ -state with a Rabi frequency  $\Omega = 2\pi \cdot 750$  kHz and a detuning of  $\Delta = 2\pi \cdot 50$  MHz. This yields a length scale of  $R_c = 3.7 \mu\text{m}$  and a temperature scale of  $T_0 = 0.4$  nK. So, the ground state we showed in Fig. 5.9 has a size of about  $20 \mu\text{m}$ . The scaled temperature of  $T = 10$  where there is still significant superfluidity for  $N = 400$  corresponds to a physical temperature of about 4 nK. At first glance, this temperature seems quite discouraging since it is extremely low (see section 2.2 for typical experimentally feasible temperatures). However, if we take the Kosterlitz-Thouless-like scaling of the critical temperature into account, the higher particle number (14000 as opposed to 400) should increase the critical temperature by a factor of 35, so that significant superfluidity should still be observable at around 140 nK. This is much more in line with current experimental capabilities [23].

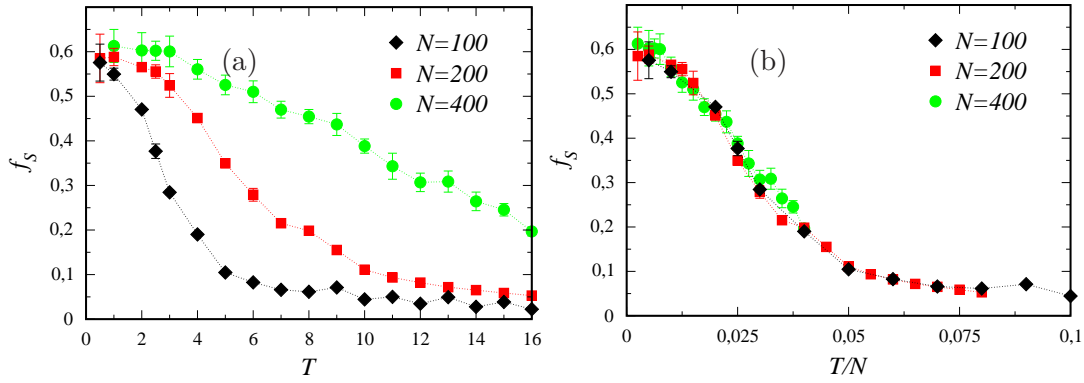


**Figure 5.10.:** (a) Dependence of the superfluidity on the particle number  $N$  and the temperature  $T$ . (b) Dependence of the superfluidity on the particle number and the particle-number-scaled temperature  $T/N$ . All curves collapse to one single curve, showing that the superfluidity depends not on  $N$  and  $T$  separately, but only on  $T/N$ .

### 5.5.3. Validity of the mean-field approximation

We will now check whether the MF simulations can properly predict not only the one-particle density but the superfluid fraction as well. In Fig. 5.11(a), we show the radial density  $\rho(r)$ , i.e., the two-dimensional density  $|\psi|^2$  integrated over the angle  $\vartheta$ :

$$\rho(r) = \frac{N}{2\pi} \int_0^{2\pi} d\vartheta |\psi(r, \vartheta)|^2. \quad (5.38)$$

Since MC and MF agree on the two-dimensional density, it is already clear that they also have to agree on  $\rho(r)$ . More importantly, we also show the superfluid radial density  $\rho_s(r) = f_s(r)\rho(r)$ , where  $f_s(r)$  is the radially resolved superfluid fraction as calculated in MC and MF. Notably, we also see excellent agreement for this important observable. The result conforms to our intuitive understanding of how superfluidity is inhibited through density modulations: around  $r = 0$  we have perfect superfluidity, since this part of the gas is within the central droplet. This is essentially a small trapped BEC where the long-range nature of the dressing-interaction is not relevant, so we would assume it to be perfectly superfluid at sufficiently low temperature. The region around  $r \approx 1.5$  corresponds to the outer shell consisting of 6 droplets. There, we find  $f_s(r) \approx 0.5$ . Since this value is also predicted by the MF calculation, we can conclude that the partial inhibition of the superfluidity in this region comes about through the density modulations, not through thermal or quantum fluctuations which, after all, Leggett's estimator does not take into account.

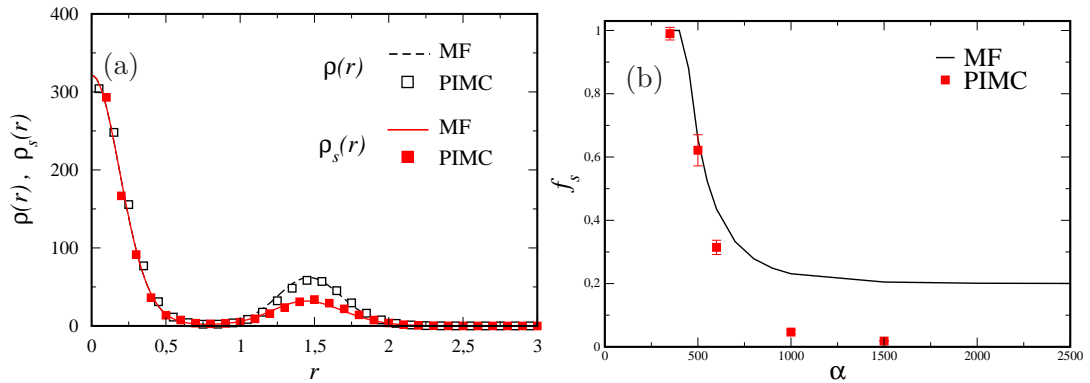


**Figure 5.11.:** Comparison of the superfluidity results from MC and MF calculations. (a) radially resolved superfluid density for  $N = 400$  and  $\alpha = 500$ . The MF and MC calculations agree very well. (b) Dependence of the global superfluidity  $f_s$  on the interaction strength  $\alpha$ . MF and MC agree very well for relatively small strengths but deviate for high strengths. The agreement extends to the regime  $\alpha \sim 500$  where supersolidity is found.

However, it is plausible that Leggett's estimator will fail at a sufficient interaction strength. Indeed, Fig. 5.11(b) shows the global superfluid fraction at various interaction strengths  $\alpha$ . Evidently, the MF prediction is good only in a certain regime. The MF calculation clearly overestimates  $f_s$  at large  $\alpha$ ; and predicts that  $f_s$  converges to a nonzero value. This is clearly wrong and easy to explain: in all the situations in the plot, the ground state density still looks qualitatively like the one for  $\alpha = 500$  (Fig. 5.9). In particular, there is the central droplet around  $r = 0$ . According to Leggett's estimator,  $f_s(r)$  is always unity in that region since there are no modulations in the angular direction. In reality, however, strong interactions will suppress superfluidity. Here, it becomes evident that Eq. (5.37) in general only gives an upper bound on the superfluid fraction.

#### 5.5.4. The physical mechanism of supersolidity

Intuitively, the appearance of superfluidity in a modulated state can be understood as a consequence of the large number of atoms in every droplet. Every single particle in a droplet only contributes a small part of the droplet's total interaction energy. Therefore, only a small energy cost is associated with a jump of this particle from one droplet to another. Such jumps provide for superfluid flow. In contrast, in a classical crystal there is only one atom per lattice site. There, the energy cost of a jump is very high so that superfluid flow is inhibited.

Hence, the superfluidity of the modulated states is a result of the soft core of the dressing interaction. Since this in turn arises from the interaction blockade the supersolidity of the dressed gas can be understood as an implication of the blockade.

### 5.6. Supersolid crystals and Abrikosov lattices in rotating dressed gases

In BEC experiments, superfluidity is measured by rotating a container and observing whether vortices are created [2]. Furthermore, Leggett's idea [120] to experimentally measure superfluidity is also based on placing a gas into a container and then slowly rotating the container. The theoretical ways to calculate the superfluid fraction are also based on this idea. Since we have discussed the superfluidity of a Rydberg-dressed gas in some detail in this chapter, it is a natural extension to ask what the exact effects of faster rotation on the ground state is. Therefore, we will now consider higher rotation frequencies  $\Omega$ .

The existence of so-called Abrikosov vortex lattices (i.e., a triangular lattice of vortices in two dimensions) in a gas with short-range interactions has been established before theoretically [192] and experimentally [167]. They have been predicted for dipolar interactions as well [44, 109].

In the following, we will show that the dressing interaction also leads to an Abrikosov lattice. Furthermore, it enters into a non-trivial competition with the supersolid lattice that we have seen to exist in the previous sections if the interaction is sufficiently strong. We can describe the rotating system by the Hamiltonian [118] (see Appendix A.3 for the derivation)

$$\hat{H} = \hat{H}_0 - \Omega \hat{L}_z, \quad (5.39)$$

where  $\hat{H}_0$  is the dressing-Hamiltonian (without rotation) and  $\hat{L}_z = -i\hbar(x\partial_y - y\partial_x)$  is the angular momentum operator. Since we have seen that the mean-field approximation

is valid for weak dressing, we will use it so that we have to solve the corresponding GPE

$$E\psi(\mathbf{r}) = \left( -\frac{\hbar^2}{2m}\nabla^2 + g^{2\text{D}}|\psi(\mathbf{r})|^2 + \int d^3r' \frac{\tilde{C}_6|\psi(\mathbf{r}')|^2}{R_c^6 + |\mathbf{r} - \mathbf{r}'|^6} + \frac{1}{2}m\omega^2r^2 - \Omega\hat{L}_z \right) \psi(\mathbf{r}). \quad (5.40)$$

While before, we scaled lengths with  $R_c$  and energies with  $\hbar^2/mR_c^2$ , we now choose a different scaling, which is somewhat more convenient for this problem: we scale lengths with the oscillator length

$$l = \sqrt{\frac{\hbar}{m\omega}}$$

and the corresponding energy

$$\frac{\hbar^2}{ml^2} = \hbar\omega.$$

This yields the scaled equation (with  $r_c = R_c/l$ )

$$E\psi(\mathbf{r}) = \left( -\frac{1}{2}\nabla^2 + \tilde{\gamma}|\psi(\mathbf{r})|^2 + \tilde{\alpha} \int d^3r' \frac{|\psi(\mathbf{r}')|^2}{r_c^6 + |\mathbf{r} - \mathbf{r}'|^6} + \frac{1}{2}r^2 - \Omega\hat{L}_z \right) \psi(\mathbf{r}). \quad (5.41)$$

$\Omega$  is now in multiples of  $\omega$ , and the interaction strengths are

$$\tilde{\alpha} = \frac{\tilde{C}_6 m N}{\hbar^2 l^4} = \alpha r_c^4, \quad (5.42)$$

$$\tilde{\gamma} = \frac{mN}{\hbar^2} g^{2\text{D}} = \gamma. \quad (5.43)$$

At fast rotation ( $\Omega > 1$ , or  $\Omega > \omega$  before scaling), the rotation term makes extended states energetically more favorable than trapped states. Hence, we are constrained to  $\Omega \in [0 \dots 1)$  if we want to consider only trapped self-states. This can be seen by considering the eigenstates of a two-dimensional harmonic oscillator with

$$\hat{H}_0 = -\frac{1}{2}\nabla^2 + \frac{1}{2}\hat{\mathbf{r}}^2 \quad (5.44)$$

These are  $|n, l\rangle$  ( $l \in \{-n \dots n\}$ ) with the ( $l$ -degenerate) energies

$$E_{n,l} = n + 1. \quad (5.45)$$

However, since

$$\langle n, l | \hat{L}_z | n, l \rangle = l + 1 \quad (5.46)$$

$$\Rightarrow \langle n, l | \hat{H}_0 - \Omega \hat{L}_z | n, l \rangle = n + 1 - \Omega(l + 1). \quad (5.47)$$

Hence, if  $\Omega > 1$ , the eigenenergies decrease as  $l$  is increased so  $|0, 0\rangle$  ceases to be the ground state. Indeed, there is no ground state since, for every state, there is another state (with larger size) with lower energy. For the same reason, every state will expand ad infinitum in a real-time evolution.

In total, we have a four-dimensional parameter space spanned by  $(\Omega, \tilde{\alpha}, \tilde{\gamma}, r_c)$ . This gives rise to a quite complicated and rich phase-diagram that we will now investigate. Since a complete scan of the whole parameter space is computationally much too expensive, we have to constrict ourselves to a small part of the parameter space. We will proceed in the following way:

We will choose a fixed value for  $\gamma (\neq 0)$ . We will scan slices of the phase diagram by first calculating the ground state with  $\alpha = 0$ , the chosen value of  $\gamma$  and various values of  $(\Omega, r_c)$  (again with the same scheme as above). Then, we perform an imaginary time evolution in whose course we adiabatically change  $\alpha$  to larger values so that in any given imaginary time-step, the system is approximately in a stationary state of the GPE with the  $\alpha$  at that time. Note that, a priori, we do not know whether this stationary state is actually the ground state of the system. Indeed, we will see that in a certain regime it is not, so that our phase diagram is not the ground state phase diagram. But we will also see that our result is highly experimentally relevant, even more so than the ground state phase diagram.

The result of the scheme described above is shown in Fig. 5.12. We investigated a few values of  $r_c$  (1, 3, 5) and rotation frequencies  $\Omega \in [0 \dots 0.9]$  (at  $\Omega = 1$ , the system would become untrapped). As in the previous sections, the relevant parameter for the effective

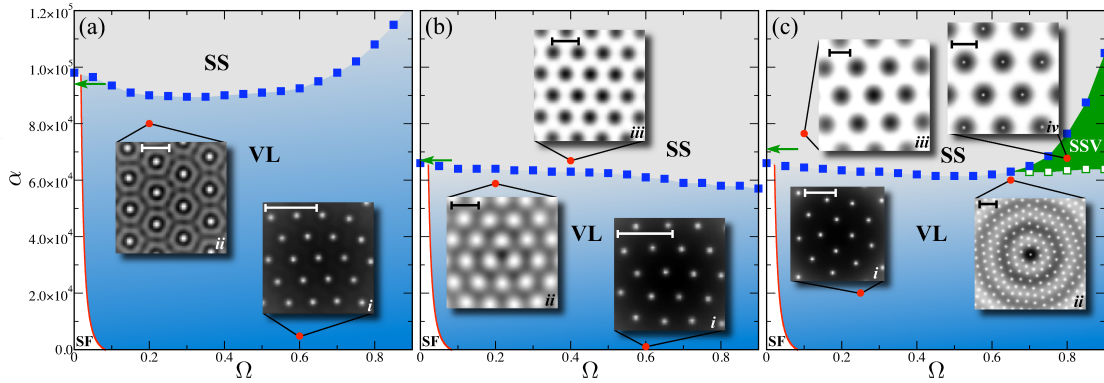


**Figure 5.12.:** Phase diagram for  $\gamma = 10^4$  and various values of  $r_c$ : (a)  $r_c = 1$ , (b)  $r_c = 3$ , (c)  $r_c = 5$ . The ground state depends on the rotation frequency  $\Omega$  and the effective dressing interaction strength  $\alpha = \tilde{\alpha} r_c^{-4}$ . The insets show the one-particle density  $|\psi|^2$  for a few examples. The green arrow represents the point where, at  $\Omega = 0$ , the roton instability sets in in the bulk limit (see section 5.2). The horizontal bar corresponds to a length of  $5l$  and shows the dimension of each inset.

Figure reprinted from [90].

dressing interaction strength is still  $\alpha = \tilde{\alpha} r_c^{-4}$  so that it is reasonable to plot the phase diagram depending on this value instead of  $\tilde{\alpha}$ .

First, for small  $\alpha$  the phase diagram shows the same behavior for all  $r_c$ : below a critical value  $\Omega_{\text{vortex}}$  (which depends on the interaction strengths) the ground state is an unmodulated, vortex-less, superfluid Thomas-Fermi profile (labeled “SF”). Its width depends on the interaction strengths  $\alpha$  and  $\gamma$ . More precisely: as long as  $\alpha$  is sufficiently small that it does not lead to a vortex spectrum, the combination of contact interaction and dressing interaction can be approximated very well by an effective short-range interaction with the strength

$$\gamma' = \gamma + \frac{2\pi^2\tilde{\alpha}}{3^{3/2}r_c^4} = \gamma + 3.80\alpha.$$

This can be seen by considering the MF potential under the assumption that the interaction does not introduce density modulations, i.e.,  $|\psi|^2$  is constant on the length scale of  $r_c$ :

$$\tilde{\alpha} \int d^3r' \frac{|\psi(\mathbf{r}')|^2}{r_c^6 + |\mathbf{r} - \mathbf{r}'|^6} \approx \tilde{\alpha} |\psi(\mathbf{r})|^2 \int d^3r' \frac{1}{r_c^6 + |\mathbf{r} - \mathbf{r}'|^6} = \frac{2\pi^2}{3^{3/2}r_c^4} \tilde{\alpha}. \quad (5.48)$$

When the critical rotation frequency  $\Omega_{\text{vortex}}(\gamma')$  is exceeded, the Thomas-Fermi profile gives way to a one-vortex state, i.e., a state with one single central vortex. Yet higher  $\Omega$  lead to the formation of more vortices which form a regular triangular Abrikosov lattice if their number is sufficient. Examples in the diagram 5.12 are the insets (a)i, (b)i and (c)i in all of which a triangular lattice of vortices can be seen. All states with one or more vortices are labeled “VL” (vortex lattice) in the diagram.

For  $r_c = 1$ , the system is already quite close to the bulk limit and all states within the VL regime differ only by the vortex density. However, for  $r_c \in \{3, 5\}$ , there is still a recognizable finite size effect: when  $\alpha$  becomes sufficiently large, but is still too small to yield a full supersolid lattice, the nonlocal interaction leads to the formation of rings. That means that the system is still spherically symmetric (except for the vortices), but modulated in the radial direction. An example is shown in inset (c)ii.

The second very important transition is the one to a supersolid lattice (from either the vortex lattice or the superfluid, depending on  $\Omega$ ). It occurs when, for given  $r_c$  and  $\Omega$ ,  $\alpha$  exceeds a critical value  $\alpha_c$ . By invoking a local density approximation (LDA) it should be possible to link this value to our bulk limit results from sections 5.2 and 5.3. According to table 5.1, in two dimensions, the critical dressing-interaction strength for the roton instability is

$$\alpha_{\text{inst}} = \frac{31.9 + 6.16\gamma}{|\psi(\mathbf{0})|^2}, \quad (5.49)$$

where  $|\psi(\mathbf{0})|^2$  is the peak density (in the sections about the bulk limit we had assumed that the average density is 1 so that the scaling factor  $|\psi(\mathbf{0})|^2$  must be used in order to apply the LDA). Specifically, for the parameters in the figure, the critical values should be

- in (a)  $\alpha_{\text{inst}} = 9.3 \cdot 10^4$ ,

- in (b)  $\alpha_{\text{inst}} = 6.7 \cdot 10^4$ ,
- in (c)  $\alpha_{\text{inst}} = 7.2 \cdot 10^4$ .

The differences between (a), (b) and (c) come about because of different peak densities. As can be clearly seen, the transition that we actually found is well-predicted by the roton-instability condition so that  $\alpha_c = \alpha_{\text{inst}}$ . The supersolid transition should have occurred earlier. Note that the LDA is best for  $r_c = 1$  and becomes worse at higher  $r_c$  (due to finite size effects becoming important) which might explain the deviation in (c). From an experimental point of view, the roton-instability transition is more important than the supersolid transition because this is what occurs in a real-time evolution starting from an unmodulated state (as it is usually created in BEC experiments). Since for all  $r_c$ , this instability transition occurs at roughly the same value of  $\alpha = \tilde{\alpha} r_c^{-4}$ , it is once again confirmed that indeed  $\alpha$  is the relevant parameter for the interaction strength.

However, in detail, we now find that the position of the transition point is non-trivial and depends explicitly on  $r_c$ . For  $r_c = 1$ ,  $\alpha_{\text{inst}}$  first decreases slowly with increasing  $\Omega$ , then increases again due to the decreasing peak density. This occurs because the rotation partially counteracts the trapping, leading to a weaker confinement. While the supersolid state exhibits vortices, they are pushed into the low-density regions as the roton instability occurs, so that they cannot be seen in the density plots. This is also true for larger  $r_c$  but only at low rotation frequencies (insets (b)iii and (c)iii).

At higher  $r_c$  and high  $\Omega$ , there is an interesting competition between the supersolid and the vortex lattice. When the vortex density exceeds some critical value, it becomes energetically favorable for some of them to form in the high-density regions of the supersolid lattice (inset (c)iv).

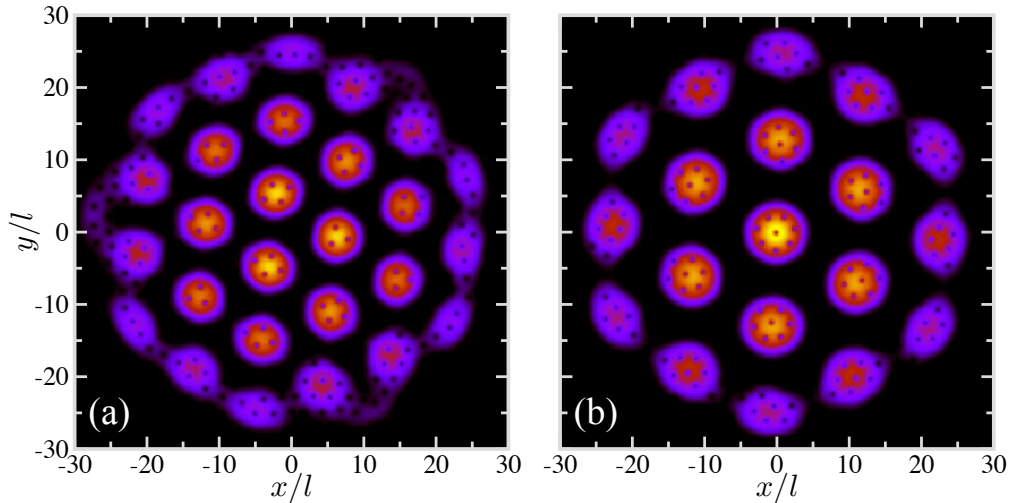


**Figure 5.13.:** Densities for  $\Omega = 0.8$  and (a)  $r_c = 7$ ,  $\alpha = 7.5 \cdot 10^4$ , (b)  $r_c = 9$ ,  $\alpha = 9 \cdot 10^4$ . Figure reprinted from [90]

When  $r_c$  becomes significantly higher than the length scale of the Abrikosov lattice, coexistence between an Abrikosov lattice and a supersolid can be seen very clearly. Two such situations are depicted in Fig. 5.13. Since vortices are a way to experimentally measure superfluidity [2], such states could be used to unambiguously prove the existence of a supersolid state in experiment.

## 6. Solitons and matter-wave bullets of a dressed-gas

Solitons have fascinated researchers for many decades. A very early observation by Russell dates back to 1834 and concerns a water wave traveling in a canal without changing its shape [174]. In this spirit, a soliton or “solitary wave” is defined as a wave-packet that retains its shape over time [106]. In most physical settings there are dispersive effects, i.e., the phase velocity of a wave depends on its frequency. These effects tend to widen wave packets. Hence, solitons can exist only if there is another effect counteracting the dispersion. An important step in the theoretical understanding of solitons was made in 1895, when it was shown that this counteracting effect is a nonlinearity in the differential equation governing the time evolution of the wave [110]. In BEC physics as well as optics, nonlinearities arise from internal interactions, not from external trapping. Therefore, a soliton can also be understood as a “self-trapped” state since it is the interaction of the wave with itself that keeps it from spreading.

Hence, in this thesis, we will use the expressions “soliton” and “solitary wave” synonymously. We define them as a wave packet that, while moving through a dispersive medium, retains its shape due to a nonlinearity. This is a common definition across many fields [106]. It is somewhat less strict than the definition commonly used in the mathematical literature [1, 208].

The kind of soliton described above is also called “bright soliton” in order to differentiate it from “dark solitons”. These are shape-retaining intensity holes on a stable continuous-wave background [107] (cf. Fig. 6.1).

In the last decades, solitons were found in many physical system, ranging from cold matter [186, 187] over plasma physics [49, 161], astrophysics [156] and optics [3] to biology [39].

A specific, long sought-after case of solitons are three-dimensional solitons of light which have been termed light-bullets [132, 181]. While solitons of light were achieved in two dimensions [43] and in discrete waveguide arrays [142], the realization of stable *continuous* light-bullets has so far remained elusive. The most important obstacle in their creation is collapse of the wave-function [18] brought about by the same interaction that is responsible for the self-trapping.

In this chapter, we will be concerned with the matter-wave-analogue of light-bullets. The formation of solitons in BECs has been the subject of intense study in recent years [46]. Condensates with a positive scattering length have a repulsive local nonlinearity which stabilizes the condensate and leads to stable dark solitons [53]. A negative scattering length implies an attractive local nonlinearity which may support bright solitons [186], but collapse occurs if more than one spatial dimension is considered [201].

In a BEC, long-range interatomic interaction of atoms can induce a nonlocal nonlinearity. In [77], nonlocal dipolar interactions were theoretically studied, motivated by the successful condensation of Chromium atoms [81]. While dipolar interactions can in prin-

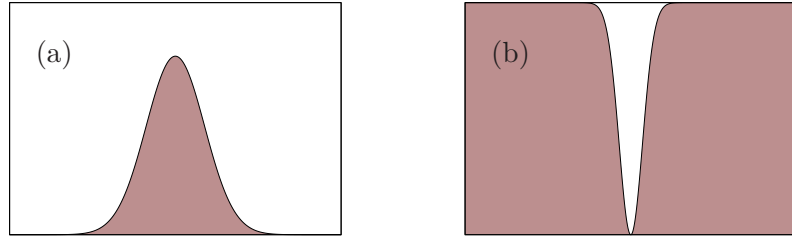


**Figure 6.1.:** Generic examples of one-dimensional solitons. A bright soliton (a) is a self-confined state either in free space or on a constant background. A dark soliton (b) is a hole on a homogeneous background.

principle be used to stabilize solitons, they are not attractive in all spatial directions. Thus, three-dimensional matter-wave solitons – *matter-wave bullets* – have remained just as elusive as light-bullets.

In this chapter, we will show that the dressing interaction derived in chapter 4 leads to the formation of matter-wave bullets. We will first discuss why typical interactions lead to collapse of the BEC in three dimensions. Here, we will show that the dressing-interaction does not suffer from this problem. Thus, it is sensible to explicitly calculate the phase diagram of self-trapping or soliton existence. Finally, we will numerically calculate the time evolution of a soliton under realistic experimental conditions, thus demonstrating the feasibility of experimentally creating a stable soliton.

## 6.1. Self-trapping and collapse-instability

A self-trapped state can be defined as a state with finite width that is bound (its energy is smaller than zero, the vacuum energy) despite the absence of an external potential [18]. Following the discussion in the introduction, we call it a soliton if it is stable, i.e., if it is not subject to instabilities. It is the latter condition that is the main obstacle for the creation of solitons [18]. In particular, any bound state ( $E < 0$ ) that is subject to a power-law interaction  $W(r) \propto -r^{-n}$  with  $n \geq 2$  will suffer a collapse-instability [129,138], i.e., the state collapses to a single point. This can be shown by calculating the second time derivative of the virial [197]

$$V(t) = \langle \psi | \hat{r}^2 | \psi \rangle = \int d^D r r^2 |\psi(r)|^2, \quad (6.1)$$

where  $D$  is the dimension of the system. The virial describes the width of the wave function. In particular  $V \rightarrow 0$  signals collapse. For a power-law interaction

$$W(r) = -1/r^n, \quad (6.2)$$

it can be shown that [138]

$$\partial_t^2 V(t) = 8E - 2(n-2) \int d^D r \int d^D r' \frac{|\psi(\mathbf{r})|^2 |\psi(\mathbf{r}')|^2}{|\mathbf{r} - \mathbf{r}'|^n} = 8E + 4(n-2)E_{\text{int}}, \quad (6.3)$$

where

$$E_{\text{int}} = \frac{1}{2} \int d^D r \int d^D r' W(\mathbf{r} - \mathbf{r}') |\psi(\mathbf{r}')|^2 |\psi(\mathbf{r})|^2 \quad (6.4)$$

is the interaction energy of the system. If  $n = 2$ , this yields  $\partial_t^2 V(t) = 8E$ , which we can integrate, finding

$$V(t) = V(0) + ct + 4Et^2, \quad (6.5)$$

with a constant  $c$  that depends on the initial state and is not relevant for the following argument. If  $E < 0$ , we find that  $V(t_c) = 0$  for a finite collapse time  $t_c$ . This means that every bound state collapses in finite time.

For  $n > 2$ , since  $E_{\text{int}} < 0$ , we have the estimate

$$\partial_t^2 V(t) = 8E + 4(n-2)E_{\text{int}} \leq 8E. \quad (6.6)$$

Hence, the previous argument applies and also here every bound state collapses in finite time. Furthermore, there are even unbound ( $E > 0$ ) states that will collapse, as long as  $8E + 4(n-2)E_{\text{int}} < 0$ .

Similar arguments show that a contact interaction  $\propto \delta(\mathbf{r})$  also leads to collapse in two dimensions if it is sufficiently strong and in three dimensions for any non-zero interaction strength [201].

This rules out the use of the most common interactions in BECs (dipolar interaction  $\propto r^{-3}$ , van-der-Waals interaction  $\propto r^{-6}$  and contact interaction) for the creation of matter-wave bullets.

The dressing interaction derived in chapter 4, on the other hand, does not lead to collapse due to its soft-core nature. Indeed, collapse is avoided [138] by any interaction  $W$  with a finite maximum norm

$$\|W\|_{\infty} = \max_{\mathbf{r} \in \mathbb{R}^D} |W(\mathbf{r})| < \infty. \quad (6.7)$$

This can be shown [138] by considering the interaction energy (recall that it is negative):

$$E_{\text{int}} = \frac{1}{2} \int d^D r \int d^D r' W(\mathbf{r} - \mathbf{r}') |\psi(\mathbf{r}')|^2 |\psi(\mathbf{r})|^2 \quad (6.8)$$

$$\geq -\frac{1}{2} \|W\|_{\infty} \int d^D r \int d^D r' |\psi(\mathbf{r}')|^2 |\psi(\mathbf{r})|^2 \quad (6.9)$$

$$= -\frac{1}{2} \|W\|_{\infty}. \quad (6.10)$$

Hence, the interaction energy is bounded below. Since the total energy  $E = E_{\text{kin}} + E_{\text{int}}$  is conserved the kinetic energy is bounded above:

$$E_{\text{kin}} = E - E_{\text{int}} \leq E + \frac{1}{2} \|W\|_{\infty}. \quad (6.11)$$

But whenever collapse occurs,  $E_{\text{kin}}$  diverges. Hence, a system with the dressing interaction is safe from collapse.

Another interaction that theoretically promotes stable self-trapping in two and three dimensions is the gravity-like interaction  $W(r) = 1/r$ . More generally, if  $n < \min(2, D)$  then the power-law interaction  $W(r) = 1/r^n$  does not lead to collapse. The proof [138] works by showing that the interaction energy is bounded below. Indeed, a way of creating gravity-like interactions has been proposed [73, 147]. However, an experimental realization of the proposed scheme has not yet been achieved.

Notably, the above results can also be understood by considering the scaling of the energies. The interaction energy of a BEC with the width<sup>1</sup>  $\sigma$ , governed by an attractive van-der-Waals interaction  $W(r) \propto r^{-n}$  scales as  $\sigma^{-n}$ . The kinetic energy scales as  $\sigma^{-2}$ , independently of the interaction. So the total energy can be written as

$$E(\sigma) = \frac{A}{\sigma^2} - \frac{B}{\sigma^n}. \quad (6.12)$$

where  $A, B > 0$  are constants. Hence, if  $n > 2$

$$\lim_{\sigma \rightarrow 0} E(\sigma) = -\infty, \quad (6.13)$$

so there is no ground state. More precisely, if  $n > 2$ , for any state with the width  $\sigma$  there is a state with a width  $\sigma' < \sigma$ , that has a lower energy. It seems plausible that then, any initial state will collapse towards one with zero width.

If  $n = 2$ ,

$$E(\sigma) = \frac{A - B}{\sigma^2}. \quad (6.14)$$

If the initial state is bound, we have  $A < B$ , so that again  $\lim_{\sigma \rightarrow 0} E(\sigma) = -\infty$ .

For  $n < 2$  we find

$$\lim_{\sigma \rightarrow 0} E(\sigma) = \infty. \quad (6.15)$$

We see that collapse occurs for exactly those situations where the total energy is not bounded below.

Again, the argument can be extended to contact interactions whose interaction energy scales as  $\sigma^{-D}$  in  $D$  dimensions.

---

<sup>1</sup>For example, the wave-function can be Gaussian. However, the exact form does not matter for the scaling argument, as long as the width  $\sigma$  is the only free parameter of the wave-function.

## 6.2. Physical realization of an attractive dressing-interaction

As we showed in chapter 3, for  $n \geq 59$  all  $d_{3/2}$ -eigenspaces of Rubidium are fully attractive, i.e., all  $4^2 = 16$  interaction curves corresponding to the  $m$ -degenerate  $d_{3/2}$ -states with  $m \in \{-3/2, -1/2, 1/2, 3/2\}$  are attractive. Furthermore, the  $s$ -states of Strontium are also attractive [144, 195]. On the one hand, the theoretical situation is simpler for singlet  $s$ -states due to their spherical symmetry which makes the interactions isotropic. On the other hand, Rubidium BECs are more commonly experimentally created than Strontium BECs, so that we will consider both situations.

Just as in chapter 5, we will describe the atomic dynamics by a rescaled three-dimensional Gross-Pitaevskii equation. In both  $s$ -state dressing and  $d$ -state dressing, the GPE can be written as

$$E\psi(\mathbf{r}) = \left( -\frac{1}{2}\nabla^2 + \gamma|\psi(\mathbf{r})|^2 + V_{MF}[\psi](\mathbf{r}) \right) \psi(\mathbf{r}). \quad (6.16)$$

In an  $s$ -state dressing scheme, the mean-field potential  $V_{MF}$  is identical to the one in the previous chapter, except that we will change the sign in front of the long-range interaction term, so that a positive  $\alpha$  now represents an attractive interaction:

$$V_{MF}[\psi](\mathbf{r}) = -\alpha \int d^3r' \frac{|\psi(\mathbf{r}')|^2}{1 + |\mathbf{r} - \mathbf{r}'|^6}. \quad (6.17)$$

The interaction parameters are (cf. Eqs. (4.130) and (4.131))

$$\alpha = -\frac{\tilde{C}_6 m N}{\hbar^2 R_c^4}, \quad (6.18)$$

$$\gamma = \frac{4\pi a_s N}{R_c}. \quad (6.19)$$

For  $d$ -state dressing, the situation is somewhat more complicated. For fixed quantum numbers  $n$ ,  $l$  and  $j$ , there are  $n_d = 2j + 1$  degenerate eigenstates labeled by  $m$ . For two atoms with a distance vector  $\mathbf{r}$  this yields  $n_d^2$  molecular two-body states  $|\mu_\beta(\mathbf{r})\rangle$  (cf. section 4.3). Since multiple length scales exist, there is no length scaling that removes all of them. Hence, we have to use the unscaled potential from Eq. (4.142)

$$V_{MF}[\psi](\mathbf{r}) = \sum_{\beta=1}^{n_d^2} \int d^3r' |\langle ee|\mu_\beta(\mathbf{r} - \mathbf{r}')\rangle|^2 \frac{\tilde{C}_6^{(\beta)}}{\left(R_c^{(\beta)}\right)^6 + |\mathbf{r} - \mathbf{r}'|^6}. \quad (6.20)$$

However, it is possible to approximate the anisotropic potential by an isotropic one. To this end, we define the angular dependent FWHM of the interaction  $R_c(\vartheta)$  and the

effective parameters (see section 4.4.2 for the details)

$$R_c = \frac{1}{2\pi} \int_0^{2\pi} d\vartheta \sin(\vartheta) R_c(\vartheta), \quad (6.21)$$

$$C_6 = -2\hbar\Delta R_c^6, \quad (6.22)$$

where  $\vartheta$  is the angle between the quantization axis, defined by the laser polarization and the distance vector  $\mathbf{r}$  (the “molecular axis” of the two-atom problem).

We will show in section 6.4 that the isotropic MF potential (6.17) indeed yields a good approximation for the ground states of a dressed BEC.

### 6.3. Self-trapped ground states

Since the GPE (6.16) with the isotropic MF potential (6.17) can be used both to describe dressing to Strontium  $s$ -states exactly and to Rubidium  $d$ -states approximately, we will start by considering this simplified situation.

As we discussed above, a soliton or self-trapped state is a bound state, i.e., a state with an energy lower than that of the vacuum (here: zero), which is trapped solely due to its internal interaction. Hence, we can simply characterize a self-trapped state as any normalized state  $|\psi\rangle$  with a negative energy

$$\begin{aligned} E[\psi] &= -\frac{1}{2} \int d^3r' \overline{\psi(\mathbf{r})} \nabla^2 \psi(\mathbf{r}) + \frac{\gamma}{2} \int d^3r |\psi(\mathbf{r})|^4 - \frac{\alpha}{2} \int d^3r \int d^3r' \frac{|\psi(\mathbf{r}')|^2 |\psi(\mathbf{r})|^2}{1 + |\mathbf{r} - \mathbf{r}'|^6} \\ &= E_{\text{kin}} + E_{\text{cont}} + E_{\text{dressing}} < 0. \end{aligned} \quad (6.23)$$

We have already shown in section 6.1 that any bounded interaction is not prone to collapse. It is clear that the dressing interaction

$$W(r) = -\frac{\alpha}{1 + r^6} \quad (6.24)$$

is bounded by  $\|W\|_{\infty} = \alpha$ . This also means that the total energy  $E[\psi]$  is bounded below because

$$E_{\text{kin}} = -\frac{1}{2} \sum_{j=1}^3 \int d^3r' \overline{\psi(\mathbf{r})} \partial_i (\partial_i \psi(\mathbf{r})) = \frac{1}{2} \sum_{j=1}^3 \int d^3r' \partial_i \overline{\psi(\mathbf{r})} \partial_i \psi(\mathbf{r}) \quad (6.25)$$

$$= \frac{1}{2} \sum_{j=1}^3 \int d^3r' |\partial_i \psi(\mathbf{r})|^2 > 0, \quad (6.26)$$

$$E_{\text{cont}} > 0, \quad (6.27)$$

$$E_{\text{dressing}} = -\frac{\alpha}{2} \int d^3r \int d^3r' \frac{|\psi(\mathbf{r}')|^2 |\psi(\mathbf{r})|^2}{1 + |\mathbf{r} - \mathbf{r}'|^6} \quad (6.28)$$

$$\geq -\frac{\alpha}{2} \int d^3r \int d^3r' |\psi(\mathbf{r}')|^2 |\psi(\mathbf{r})|^2 = -\frac{\alpha}{2}. \quad (6.29)$$

Hence, the energy is bounded below:

$$E[\psi] \geq -\frac{\alpha}{2}. \quad (6.30)$$

Therefore, it is sensible to look for the ground state of a dressed gas. In contrast, systems with power law-potentials  $1/r^n$  with  $n > 2$  do not have a ground state since their energy is not bounded below. Instead they always suffer collapse.

Thus, we have demonstrated that every state is stable with respect to collapse under the dressing interaction. Hence, if there are any self-trapped states they are stable. But we still have to establish the existence of self-trapped states. To this end, we use a variational procedure. We consider Gaussian trial states

$$\psi_\sigma(\mathbf{r}) = \frac{1}{\pi^{\frac{3}{4}} \sigma^{\frac{3}{2}}} \exp\left(-\frac{r^2}{2\sigma^2}\right). \quad (6.31)$$

These have the energies

$$E_{\text{kin}}(\sigma) = \frac{3}{4\sigma^2} \quad (6.32)$$

$$E_{\text{cont}}(\gamma, \sigma) = \frac{\sqrt{2}}{8\pi^{\frac{3}{2}}} \frac{\gamma}{\sigma^3} \quad (6.33)$$

and the dressing-induced interaction energy

$$E_{\text{dressing}}(\alpha, \sigma) = -\frac{\alpha}{2\pi^3 \sigma^6} \int d^3r \int d^3r' \frac{\exp\left(-\frac{r^2+r'^2}{\sigma^2}\right)}{1 + |\mathbf{r} - \mathbf{r}'|^6} \quad (6.34)$$

$$\stackrel{\mathbf{s}=\mathbf{r}-\mathbf{r}'}{=} -\frac{\alpha}{2\pi^3 \sigma^6} \int d^3s \frac{\exp\left(-\frac{s^2}{\sigma^2}\right)}{1 + s^6} \int d^3r \exp\left(-\frac{2r^2 - 2\mathbf{r} \cdot \mathbf{s}}{\sigma^2}\right) \quad (6.35)$$

$$\begin{aligned} &= -\frac{\alpha}{2\pi^3 \sigma^6} \int d^3s \frac{\exp\left(-\frac{s^2}{\sigma^2}\right)}{1 + s^6} \times \\ &\times \left[ 2\pi \int_0^\infty dr r^2 \int_{-1}^1 d(\cos \vartheta) \exp\left(-\frac{2r^2 - 2rs \cos \vartheta}{\sigma^2}\right) \right] \quad (6.36) \end{aligned}$$

$$= -\frac{\alpha}{2\pi^3\sigma^6} \int d^3s \frac{\exp\left(-\frac{s^2}{\sigma^2}\right)}{1+s^6} \left[ \frac{(2\pi)^{3/2}}{8} \sigma^3 \exp\left(\frac{s^2}{2\sigma^2}\right) \right] \quad (6.37)$$

$$= -\frac{\sqrt{2\pi}\alpha}{8\pi^2\sigma^3} \int d^3s \frac{\exp\left(-\frac{s^2}{2\sigma^2}\right)}{1+s^6} \quad (6.38)$$

$$= -\frac{\alpha}{\sqrt{2\pi}} \int_0^\infty dx \frac{x^2 \exp\left(-\frac{1}{2}x^2\right)}{1+\sigma^6 x^6}. \quad (6.39)$$

Then, we can calculate the total energy  $E(\sigma, \alpha, \gamma) = E_{\text{kin}} + E_{\text{cont}} + E_{\text{dressing}}$  for any given values of the attractive strength  $\alpha$ , the repulsive strength  $\gamma$  and the width of the wave function  $\sigma$ . Fig. 6.2 shows exemplarily the relation  $E(\sigma)$  for  $\gamma = 0$  and a few values of

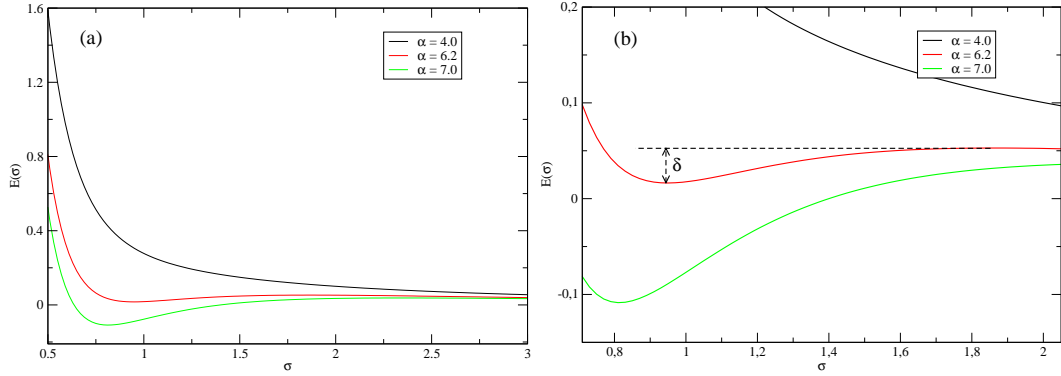


**Figure 6.2.:** (a) Energy  $E(\sigma)$  of a Gaussian wave-function with the width  $\sigma$  for a few values of the effective interaction strength  $\alpha$ . For  $\alpha = 4.0$  neither meta-stable nor self-trapped states exist, for  $\alpha = 6.2$ , there is a meta-stable state with  $\sigma = 0.95$ . At  $\alpha = 7$ , all states with  $0.65 \leq \sigma \leq 1.39$  are self-trapped. (b) Enlarged view of the most important regime.  $\delta$  denotes the energy gap between the local minimum and maximum of the energy in the meta-stable case  $\alpha = 6.2$ .

$\alpha$ . For  $\alpha = 4$ , the energy is monotonically decreasing with  $\sigma$ . For any given state with the width  $\sigma$ , all states with widths  $\sigma' > \sigma$  have lower energies. Hence, there is no soliton state and any initial state will spread out without bounds.

For  $\alpha = 6.2$ ,  $E(\sigma)$  has a local minimum at  $\sigma = 0.95$ . While this implies the existence of a metastable soliton, it is not the ground state. It remains self-confined only for a finite time  $\tau \sim 1/(\delta)$ , where  $\delta$  is the energy gap between local minimum and maximum (see Fig. 6.2(b)).

For  $\alpha = 7.0$ , we finally find self-trapped states for  $\sigma \in [0.65, 1.39]$ , with the local and global minimum of the energy at  $\sigma = 0.81$ .

In order to calculate the full self-trapping phase diagram in Fig. 6.3, we performed a variational scheme for a broad range of values for  $\alpha$  and  $\gamma$ . For given  $\alpha$  and  $\gamma$ , we consider the zeros of the derivative with respect to  $\sigma$  of the energy:

$$\partial_\sigma E(\sigma, \alpha, \gamma) = 0, \quad (6.40)$$

in order to find local minima and maxima of the energy. If there are none, this corresponds to the case  $\alpha = 4.0$  in Fig. 6.2 and there is no self-trapping.

If a local minimum  $\sigma_{\min}$  exists and the corresponding energy

$$E_{\min}(\alpha, \gamma) = E(\sigma_{\min}, \alpha, \gamma) = \min_{\sigma} (E(\sigma, \alpha, \gamma)). \quad (6.41)$$

is positive, there is a metastable soliton like the one we found for  $\alpha = 6.2$  and the point  $(\alpha, \gamma)$  is in the meta-stable phase. The phase boundary between the non-trapped and the metastable phase is denoted by  $\alpha_{\text{ms}}(\gamma)$ , which is the smallest value of  $\alpha$  for the given  $\gamma$  such that  $(\alpha, \gamma)$  is in the meta-stable phase.

If  $E_{\min}(\alpha, \gamma) < 0$ , the corresponding state is self-trapped and in the phase diagram, the point  $(\alpha, \gamma)$  is in the self-trapped phase. The phase boundary between the metastable and the self-trapped phase is denoted by  $\alpha_{\text{st}}(\gamma)$ .

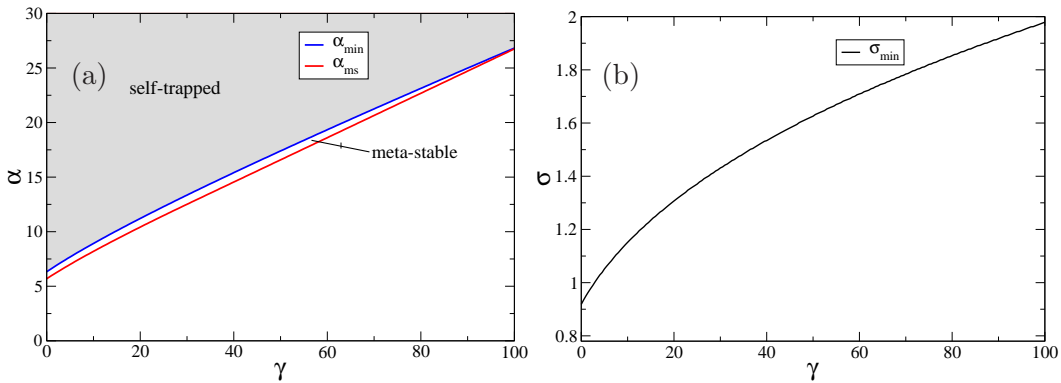


**Figure 6.3.:** (a) ground state phase diagram.  $\alpha_{\text{st}}(\gamma)$  is the smallest dressing interaction strength for which self-trapping can be achieved if the short-range repulsion strength is  $\gamma$ .  $\alpha_{\text{ms}}$  is the smallest value of  $\alpha$  where a meta-stable state exists. (b) BEC ground state width  $\sigma$  for  $\alpha = \alpha_{\text{st}}(\gamma)$  depending on  $\gamma$ .

We find that for all investigated  $\gamma$ , self-trapping can always be found for sufficiently large  $\alpha$ . This can easily be extended to larger values of  $\gamma$ . In particular, for  $\gamma \rightarrow \infty$ , the kinetic energy can be ignored (Thomas-Fermi limit [157]), so that the GPE can be simplified to

$$E\psi(\mathbf{r}) = \left( \gamma |\psi(\mathbf{r})|^2 - \alpha \int d^3r' \frac{|\psi(\mathbf{r}')|^2}{1 + |\mathbf{r} - \mathbf{r}'|^6} \right) \psi(\mathbf{r}), \quad (6.42)$$

and the only remaining parameter determining the eigenstates is  $\frac{\alpha}{\gamma}$ . Hence, in this limit,

$$\alpha_{\text{st,ms}}(\gamma) \propto \gamma. \quad (6.43)$$

Hence,  $\alpha_{\text{st}}$  remains finite for all  $\gamma$ .

However, an analogous statement is not true for the meta-stable phase: at  $\alpha \gtrsim 100$ , we

find  $\alpha_{\text{st}} = \alpha_{\text{ms}}$ , i.e., the meta-stable phase vanishes.

Strictly speaking, the phase boundary that we calculated by the variational approach is only an upper bound of the true phase boundary: when there is a self-trapped Gaussian state  $|\psi\rangle$ , the real ground state  $|\psi_0\rangle$  must also be self-trapped since it cannot be energetically higher than the found Gaussian state. However, it is possible that for a given point  $(\alpha, \gamma)$  in parameter space there is a self-trapped state but no Gaussian self-trapped state. In other words, it is guaranteed that in all cases where our variational ansatz yields the existence of a self-trapped state, this state is also self-trapped in reality.

In order to check the validity of our variational ansatz, we performed a numerical analysis. For given values of  $\alpha$  and  $\gamma$ , we performed an imaginary time evolution (ITE) and checked whether it led to a bound state. The obtained phase diagram recovers the variational result Fig. 6.3 virtually perfectly, proving the validity of the variational calculation.

A further approximation that we have used throughout this chapter is the mean-field approximation. It enters via the assumption that the BEC can be described with a single-particle wave-function. In other words, we have assumed that the many-body state  $|\Psi\rangle$  of the BEC can be approximated as a product of identical single-particle states:

$$\Psi(\mathbf{r}_1 \dots \mathbf{r}_N) = \prod_i \psi(\mathbf{r}_i). \quad (6.44)$$

Qualitatively, the MF approximation has the same effect as our assumption of Gaussian wave-function. For given interaction strengths it is possible that there is no self-trapped product state, but that a self-trapped *correlated* state  $|\Psi\rangle$  exists. Our analysis would miss this correlated state. However, in all cases where we find a self-trapped product state it is certain that the true ground state is also self-trapped.

As far as dressing to  $s$ -states is concerned, this concludes the analysis of the ground state phase diagram. For  $d$ -state dressing, however, we still have to investigate the effects of the anisotropy of the interaction (6.20).

## 6.4. Anisotropy of trapped states

For dressing to  $d$ -states of any element the true interaction is anisotropic. It depends on the angle  $\vartheta$  between the quantization axis which is given by the laser polarization and the distance vector between the atoms (Fig. 6.4).

Therefore, we ought to investigate the impact of the anisotropy. First, we checked the validity of the phase diagram calculated in the isotropic approximation. For a few values of  $\gamma$ , we performed ITE using the GPE (6.16) with the anisotropic potential (6.20). For each  $\gamma$ , we increased  $\alpha$  until a self-confined state was found. The results are shown as red dots in the phase diagram Fig. 6.5. Notably, they coincide virtually exactly with the variational results for the meta-stable states. This behavior is consistent with a property of the ITE, we already commented on in the previous chapter. In the presence of a meta-stable state, it can converge to that state instead of the ground state. Hence,

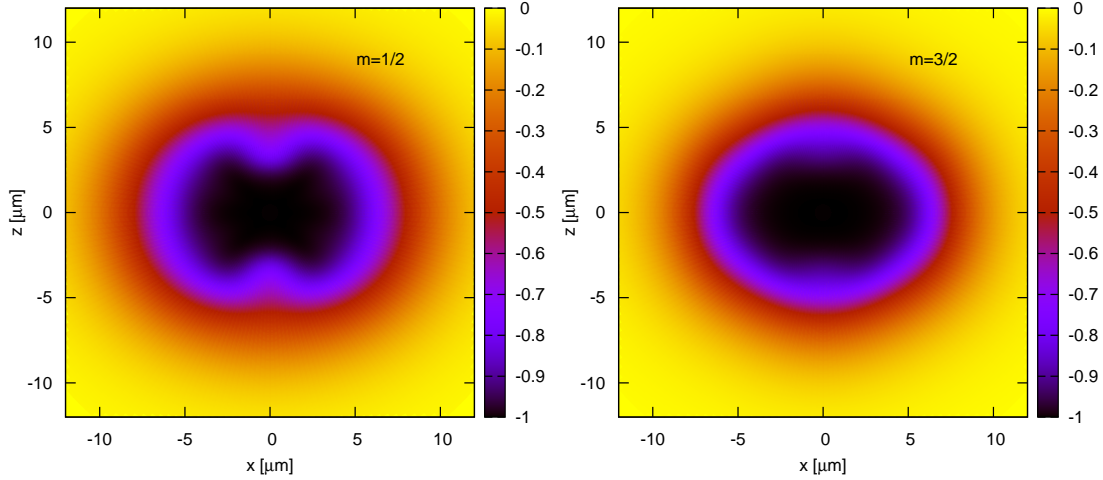


**Figure 6.4.:** Interaction potential  $U(\mathbf{r})$  for dressing to the  $65d$ -state of rubidium (left:  $m = 1/2$ , right:  $m = 3/2$ ), with  $\Delta = 2\pi \cdot 32\text{MHz}$ ; scaled by its maximum absolute value  $|U(0)| = \frac{\hbar\Omega^4}{8\Delta^3}$ . The quantization axis is the  $z$ -axis. Shown is a cut through the  $xz$ -plane which determines the whole interaction since it is symmetric w.r.t. rotation around the  $z$ -axis. Figure repeated from Fig. 4.6.

the validity of the isotropic approximation for the calculation of the phase boundary is confirmed, meaning that the variationally calculated phase diagram is a very good approximation of the true one.

Furthermore, we performed ITE simulations for a number of different situations and calculated the aspect ratio of the obtained ground states. Fig. 6.6 shows the results. The parameters in the figure correspond to a short-range repulsion strength

$$\gamma = 9.0 \quad (6.45)$$

and dressing interaction strengths in the range

$$\alpha \in [10 \dots 100]. \quad (6.46)$$

The smaller values of  $\alpha$  correspond to a relatively weakly trapped soliton, the higher values to a very strongly trapped one. The aspect ratio increases with increasing  $\alpha$  because the effect of the anisotropy becomes more relevant relative to that of the kinetic energy operator and the short-range repulsion (both of which are isotropic). For small  $\alpha$ , the latter tend to round out the soliton, whereas, for larger  $\alpha$ , they are not strong enough to overcome the anisotropy of the dressing-interaction.

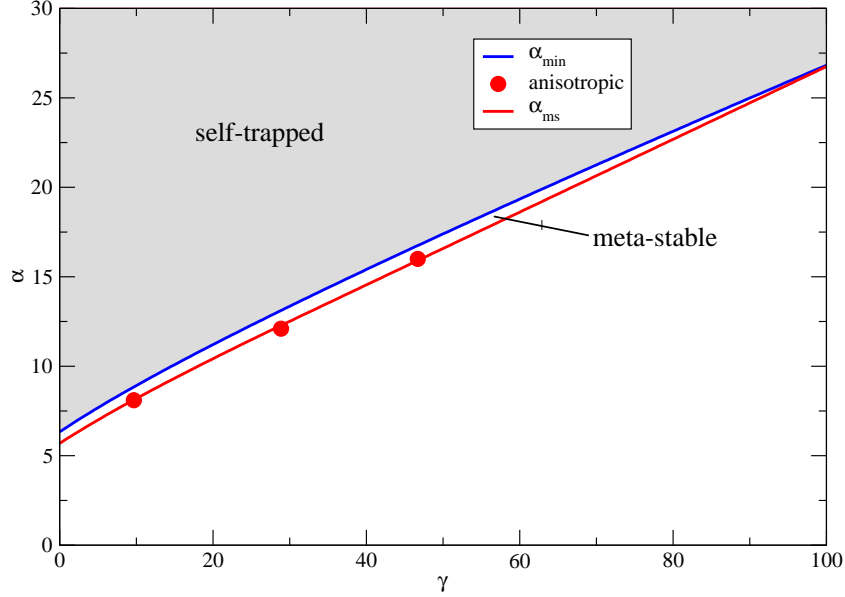


**Figure 6.5.:** Ground state phase diagram reproduced from Fig. 6.3. Additionally, the red dots show the results of the ITE with the exact anisotropic potential. The parameters  $\alpha$  and  $\gamma$  for the anisotropic results were obtained via the isotropic approximation (Eqs. (6.22) and (6.21)).

## 6.5. Physical mechanism of self-trapping

We can understand the physical mechanism behind the self-trapping better by considering the Rydberg-pair density

$$\rho_R(\mathbf{r}_1, \mathbf{r}_2) \quad (6.47)$$

of the condensate. It is the probability density of finding one Rydberg atom at  $\mathbf{r}_1$  and another one at  $\mathbf{r}_2$ . It can be deduced from the second order contribution to the many-body ground state in perturbation theory (which proceeds similar to our perturbative calculation of the dressing interaction in chapter 4). For  $N$  particles with positions  $\mathbf{r}_i$ , the second-order contribution is

$$|G^{(2)}(\mathbf{r}_1 \dots \mathbf{r}_N)\rangle = \frac{\Omega^2}{2\Delta} \sum_{i < j} \sum_{\beta} \frac{\hbar \langle \mu_{\beta}(\mathbf{r}_{ij}) | ee \rangle}{2\hbar\Delta - V^{(\beta)}(r_{ij})} |\mu_{\beta}(\mathbf{r}_{ij})\rangle, \quad (6.48)$$

where  $V^{(\beta)}(r_{ij}) = C_6^{(\beta)}/r_{ij}^6$  are the van-der-Waals interactions and  $|\mu_{\beta}(\mathbf{r}_{ij})\rangle$  are the two-body eigenstates of two atoms with the relative position  $\mathbf{r}_{ij} = \mathbf{r}_i - \mathbf{r}_j$ . Hence, the probability that both the particle at  $\mathbf{r}_1$  and the particle at  $\mathbf{r}_2$  are excited is

$$p(\mathbf{r}_1, \mathbf{r}_2) = \left| \frac{\Omega^2}{2\Delta} \sum_{\beta} \frac{\hbar \langle \mu_{\beta}(\mathbf{r}_{12}) | ee \rangle}{2\hbar\Delta - V^{(\beta)}(r_{12})} \right|^2. \quad (6.49)$$

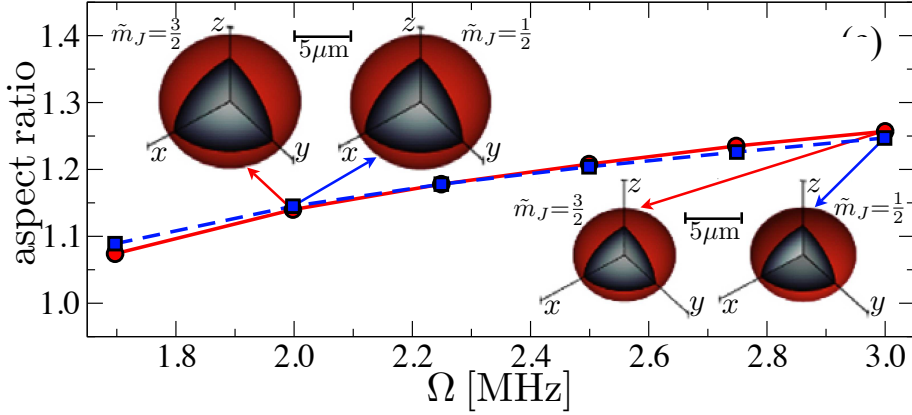


**Figure 6.6.:** Aspect ratios of ground state solitons obtained by dressing  $N = 1000$  atoms to the  $65d_{3/2}(m = 1/2)$  state, with  $\Delta = 2\pi \cdot 32$  MHz and various  $\Omega$ . Simulations were performed for both  $\tilde{m} = 3/2$  (red circles) and  $\tilde{m} = 1/2$  (blue squares). The insets show respective 3D soliton profiles for  $\Omega = 2\pi \cdot 0.3$  MHz and  $2\pi \cdot 0.5$  MHz. Figure reprinted from [137]

Then, if the atoms are distributed according to the condensate wave-function  $\psi$ , the Rydberg pair density becomes

$$\rho_R(\mathbf{r}_1, \mathbf{r}_2) = |\psi(\mathbf{r}_1)|^2 |\psi(\mathbf{r}_2)|^2 p(\mathbf{r}_1, \mathbf{r}_2). \quad (6.50)$$

In order to visualize  $\rho_R$ , we integrate it over one of the coordinates, obtaining the reduced pair density

$$\rho_R(\mathbf{r}) = \int d^3 r_2 \rho_R(\mathbf{r}, \mathbf{r}_2). \quad (6.51)$$

It is shown in Fig. 6.7 together with the total BEC density  $|\psi(\mathbf{r})|^2$ .  $|G^{(2)}\rangle$  is a coherent superposition of pairs of Rydberg excitations. The two-excitation probability  $p(\mathbf{r}_1, \mathbf{r}_2)$  drops to zero on a length-scale  $\sim R_c$  because  $V_{\text{ryd}}^{(\beta)}(R_c) \approx -2\hbar\Delta$ .  $R_c$  is also the size of the soliton, so the excitation probability is highest for two atoms on opposite sides of the BEC. This is due to the interaction blockade where one excited atom blocks the excitations of all atoms in its vicinity. This results in a shell of Rydberg excitations<sup>2</sup> (blue shell in Fig. 6.7). The entire BEC of  $N \sim 1000$  particles is confined by a very small number  $N_R \sim 0.1$  of average excitations that are coherently shared throughout the condensate.

<sup>2</sup>Note that the average number of Rydberg excitations is always  $\ll 1$ . However, due to the extremely strong interaction between Rydberg atoms, this small number is sufficient for self-trapping.

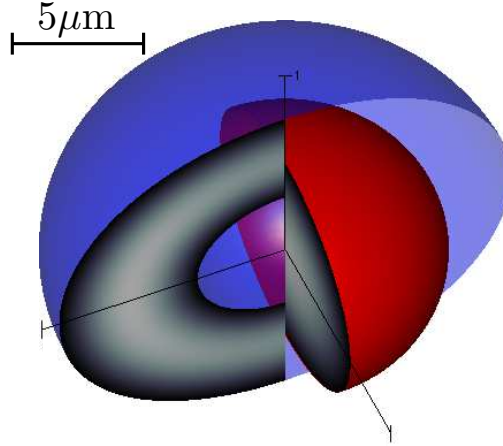


**Figure 6.7.:** Numerically calculated self-trapped ground state (soliton) of a Rubidium BEC dressed to the  $65d_{3/2}(m = 1/2)$  Rydberg state with a Rabi frequency  $\Omega = 2\pi \cdot 0.5$  MHz and laser detuning  $\Delta = 2\pi \cdot 32$  MHz. The red sphere represents the half-maximum iso-density surfaces of the BEC and the blue shell represents the reduced Rydberg-pair density. The gray-scales give the corresponding interior densities.

## 6.6. Soliton robustness

Experimentally, cold gases with Rydberg excitations are now routinely created [69, 89, 168, 194]. Typically, the states created in experiments are roughly spherically symmetric, in contrast to the ground states found in the previous sections. Their width is determined by their effective short-range interaction strength  $\gamma$  and the strength of the external optical trap used to trap the BEC. Therefore, it would be useful for an experimental realization to demonstrate that robust self-trapping does not depend on the exact form of the initial state.

We envision a scenario where a BEC of ground state atoms is created in an external trap in, so that the initial state roughly exhibits a Thomas-Fermi profile

$$\psi(\mathbf{r}) \propto 1 - \frac{r^2}{R_{tf}^2}, \quad (6.52)$$

where  $R_{tf}$  is the Thomas-Fermi radius. Then, simultaneously, the trap is switched off and the dressing lasers are switched on. Hence, the (external) optical trapping is replaced by the self-interaction term from the GPE (6.16). We performed numerical time evolutions of this scheme. One such evolution is depicted in Fig. 6.8. As the initial state, we chose the ground state of a gas with  $N = 825$  Rubidium ground state atoms, leading to

$$\gamma = 7.5, \quad (6.53)$$

in a harmonic trap with the frequency

$$\omega = 170 \text{ Hz}, \quad (6.54)$$

corresponding to a rescaled trap frequency  $\tilde{\omega} = 12.6$ . This state has a width (FWHM) of  $\sigma = 2.9 \mu\text{m}$ . Immediately after release from the trap, the gas is dressed to the state  $|65d_{3/2}(m = 1/2)\rangle$  with the Rabi frequency

$$\Omega = 2.2 \text{ MHz} \quad (6.55)$$

and a detuning  $\Delta = 2\pi \cdot 32 \text{ MHz}$ . Hence, the interaction potential is exactly the one shown in Fig. 6.7. The angle-averaged range of this potential is

$$R_c = 7.4 \mu\text{m}. \quad (6.56)$$

Hence, the effective interaction strength in the isotropic approximation is

$$\alpha = 22.4. \quad (6.57)$$

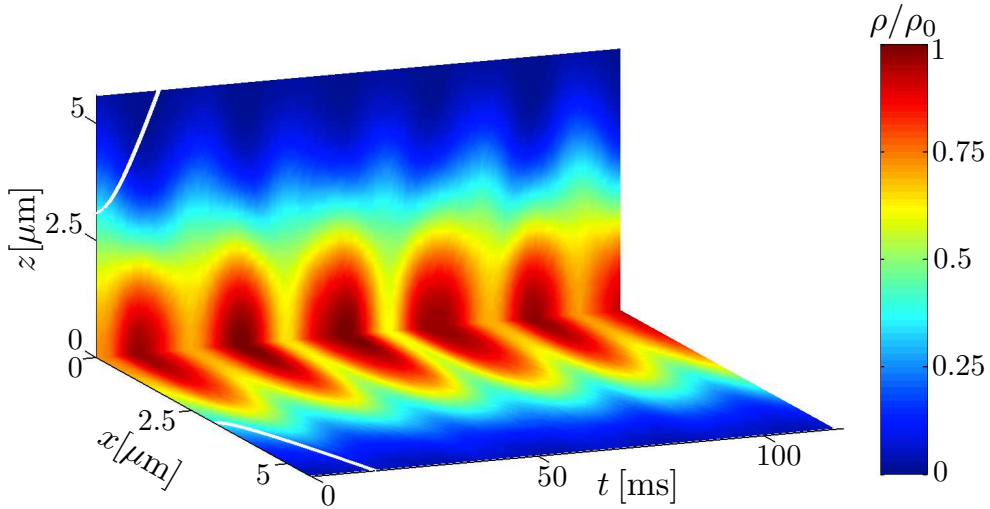


**Figure 6.8.:** Time evolution of a BEC of  $N = 825$  Rubidium atoms, prepared in a harmonic trap ( $\omega = 170 \text{ Hz}$ ). The BEC is released from the trap and, at the same time, dressing lasers driving the transition to the state  $|65d_{3/2}(m = 1/2)\rangle$  with  $\Delta = 2\pi \cdot 32 \text{ MHz}$  and  $\Omega = 2.2 \text{ MHz}$  are activated. The color code shows the density  $|\psi(x, y, z, t)|^2$  (with  $y = 0$ ;  $\psi$  is symmetric in the  $xz$ -plane). The state undergoes multiple revivals and remains self-trapped all the time. The white line represents the time evolution of a BEC *without* dressing interaction. A difference between the two situations becomes evident within  $\sim 20 \text{ ms}$ .

Figure reprinted from [137].

The ground state soliton for these interaction strengths  $(\alpha, \gamma)$  has a size of  $\sigma = 0.57R_c = 4.2 \mu\text{m}$  so that it is almost 50% larger than the initial state. This by itself would lead to a breathing motion. Furthermore, the soliton is strongly self-trapped:

$$22.4 = \alpha > \alpha_{\text{st}}(\gamma = 7.5) = 8.6. \quad (6.58)$$

As we saw in section 6.4 (Fig. 6.5), the anisotropy of the interaction becomes more relevant at strong trapping. Hence, the strength of the breathing motion will be different at different angles.

The time evolution is shown in Fig. 6.7. At  $t = 0$ , the initial state is the ground state in the external trap (without dressing interaction). This state is released from the trap and the dressing interaction is switched on. This leads to breathing oscillations in all directions. They are stronger in the  $x$ -direction (and in the  $y$ -direction, which is identical due to the cylindrical symmetry of the dressing interaction) than in the  $z$ -direction due to the anisotropy. The oscillations remain robust over multiple revivals each of which occurs over a timescale  $\sim 20\text{ms}$ . Hence, the trapping remains robust for at least  $\sim 100\text{ms}$ . Without the dressing interaction, the BEC would expand freely. This expansion is shown by the white line. A significant difference between the self-trapped and the free evolution becomes evident within one revival, i.e. within  $\sim 20\text{ms}$ . According to section 4.2.6, the lifetime of the dressed states we considered for this chapter is around

$$\tau \sim 0.1 \text{ s} \quad (6.59)$$

if the  $6p$ -state is used as intermediate state. Since the time to see the effects of self-trapping is only  $\sim 10\text{ms}$  the effect should be observable well within the lifetime of the Rydberg-dressed BEC.

## 7. Rydberg-dressing beyond perturbation theory

Thus far, we have treated the effective dressing interaction under the assumption that the dressing is sufficiently weak to use fourth-order perturbation theory (see chapter 4). More specifically, we considered the perturbative expansion

$$U(\mathbf{r}_1 \dots \mathbf{r}_N) = \sum_{l=1}^{\infty} \left( \frac{\Omega}{2\Delta} \right)^l U^{(l)}(\mathbf{r}_1 \dots \mathbf{r}_N), \quad (7.1)$$

of the  $N$ -body Born-Oppenheimer potential (4.79) which we truncated at  $l = 4$ . Since all odd orders in the expansion vanish and the  $(2l)$ -th order describes the effects of  $l$ -fold excitation, this neglects all effects that go beyond a pure two-body interaction. In this chapter, we will identify the relevant perturbation parameter that determines the validity of this approximation and we will investigate the consequences of its breakdown. As we will see, this parameter is the average number of Rydberg excitations in a non-interacting gas within one blockade sphere

$$N_R = \left( \frac{\Omega}{2\Delta} \right)^2 N_{\text{loc}}, \quad (7.2)$$

where  $N_{\text{loc}} = \frac{4}{3}\rho R_c^3$  is the number of particles within one blockade sphere. Then, the perturbation theory is valid if

$$N_R \ll 1. \quad (7.3)$$

From an experimental point of view this is a serious constraint on the achievable effective interaction strength since it depends strongly on  $N_R$ .

Hence, going beyond the two-body interaction and even completely beyond perturbation theory is not only of fundamental interest but will also be very important for future experiments. In [93], a dressed gas was investigated beyond perturbation theory based on mean-field theory for the electron dynamics (and thus the Born-Oppenheimer potential) and a local density approximation for the atomic dynamics. The latter implies that the potential is treated as short-ranged. The results showed that the perturbative treatment overestimates the true interaction potential and suggest a significant deviation even at relatively low values of  $N_R$  on the order of 0.05.

We will take the long-range nature into account and we will calculate the true many-body interaction exactly.

First, we will briefly discuss the next-higher term in the perturbation expansion (7.1). However, this term turns out to be insufficient to extend our previous results to higher  $N_R$ .

In the remainder of this chapter we will thus go beyond our perturbative expansion. We will revisit our derivation of the Born-Oppenheimer Hamiltonian (4.76). However, we will not treat it perturbatively. Instead we will calculate the BO potential by exactly

diagonalizing the electronic many-body Hamiltonian. This will be illustrated by the example of self-trapping that was introduced in the previous chapter.

## 7.1. Higher-order perturbation theory terms

As a first step beyond our two-body theory, we extend the perturbative treatment to the next-higher order. In chapter 4, we considered the fourth-order perturbation expansion and found a two-body interaction. The next non-zero term is found in the sixth order:

$$\begin{aligned}
 E^{(6)}(\mathbf{r}_1 \dots \mathbf{r}_N) = & \\
 & \left(\frac{\hbar\Omega}{2}\right)^6 \left( \frac{2N^3}{\hbar^5\Delta^5} - \frac{6N}{\hbar^4\Delta^4} \sum_{i=1}^N \sum_{j \neq i} \frac{1}{2\hbar\Delta - W_{ij}} - \frac{2N}{\hbar^3\Delta^3} \sum_{i=1}^N \sum_{j \neq i} \frac{1}{(2\hbar\Delta - W_{ij})^2} \right. \\
 & + \frac{2}{\hbar^2\Delta^2} \sum_{(i,j,k) \neq} \frac{1}{3\hbar\Delta - W_{ij} - W_{ik} - W_{jk}} \frac{1}{2\hbar\Delta - W_{ij}} \times \\
 & \times \left( \frac{1}{2\hbar\Delta - W_{ij}} + \frac{1}{2\hbar\Delta - W_{ik}} + \frac{1}{2\hbar\Delta - W_{jk}} \right) \\
 & \left. + \frac{1}{\hbar^3\Delta^3} \sum_i \sum_{j \neq i} \frac{1}{2\hbar\Delta - W_{ij}} \left( \sum_{k \neq i} \frac{2}{2\hbar\Delta - W_{ik}} + \sum_{k \neq j} \frac{2}{2\hbar\Delta - W_{jk}} \right) \right), \quad (7.4)
 \end{aligned}$$

where  $W_{ij} = W(r_{ij}) = C_6/r_{ij}^6$  is the van-der-Waals interaction.

At first glance, Eq. (7.4) seems like a nonphysical result due to the appearance of terms proportional to  $N$ . This makes it seem as if adding a particle at an infinite distance would change the interaction energy. However, a closer look reveals that the formula yields physically correct results.

First, the correct light-shift is recovered for non-interacting atoms because Eq. (7.4) yields for  $W_{ij} = 0$ :

$$E^{(6)} = N \frac{\hbar\Omega^6}{32\Delta^5}, \quad (7.5)$$

which is the third-order light-shift of  $N$  particles (cf. Eq. (4.85)).

Second, we can explicitly calculate the additional energy imparted to a pair of  $N = 2$  particles when a third particle is added at an infinite distance. For two particles we find

$$E^{(6)}(\mathbf{r}_1, \mathbf{r}_2) = \left(\frac{\hbar\Omega}{2}\right)^6 \left( \frac{16}{(\hbar\Delta)^5} - \frac{24}{(\hbar\Delta)^4} \frac{1}{2\hbar\Delta - W_{12}} \right). \quad (7.6)$$

For three particles, one of which is at infinite distance, Eq. (7.4) yields

$$E^{(6)}(\mathbf{r}_1, \mathbf{r}_2, \infty) = \left(\frac{\hbar\Omega}{2}\right)^6 \left( \frac{18}{(\hbar\Delta)^5} - \frac{24}{(\hbar\Delta)^4} \frac{1}{2\hbar\Delta - W_{12}} \right) \quad (7.7)$$

The ensuing difference  $\hbar\Omega^6/32\Delta^5$  is precisely the light-shift of the additional atom and the interaction energy

$$\left(\frac{\hbar\Omega}{2}\right)^6 \frac{1}{2\hbar\Delta - W_{12}} \quad (7.8)$$

remains unchanged.

Third, in the general case of  $N_{\text{loc}}$  particles at low distances (such that the interaction is relevant) and  $N_0 = N - N_{\text{loc}}$  additional particles beyond the reach of any interactions, one expects that the energy (apart from the light-shift) depends only on the  $N_{\text{loc}}$  particles. This is indeed the case as an explicit evaluation of Eq. (7.4) under the above assumption reveals; omitting constant terms, we obtain

$$\begin{aligned} E^{(6)}(\mathbf{r}_1 \dots \mathbf{r}_{N_{\text{loc}}}; \mathbf{r}_{N_{\text{loc}}+1} \dots \mathbf{r}_N) &= E^{(6)}(\mathbf{r}_1 \dots \mathbf{r}_{N_{\text{loc}}}; \infty \dots \infty) = \\ &\left(\frac{\hbar\Omega}{2}\right)^6 \left( -\frac{6N_{\text{loc}}}{\hbar^4\Delta^4} \sum_{i=1}^{N_{\text{loc}}} \sum_{j \neq i} \frac{1}{2\hbar\Delta - W_{ij}} - \frac{2N_{\text{loc}}}{\hbar^3\Delta^3} \sum_{i=1}^{N_{\text{loc}}} \sum_{j \neq i} \frac{1}{(2\hbar\Delta - W_{ij})^2} \right. \\ &+ \frac{2}{\hbar^2\Delta^2} \sum_{(i,j,k) \neq} \frac{1}{3\hbar\Delta - W_{ij} - W_{ik} - W_{jk}} \frac{1}{2\hbar\Delta - W_{ij}} \times \\ &\times \left( \frac{1}{2\hbar\Delta - W_{ij}} + \frac{1}{2\hbar\Delta - W_{ik}} + \frac{1}{2\hbar\Delta - W_{jk}} \right) \\ &\left. + \frac{1}{\hbar^3\Delta^3} \sum_i \sum_{j \neq i} \frac{1}{2\hbar\Delta - W_{ij}} \left( \sum_{k \neq i} \frac{2}{2\hbar\Delta - W_{ik}} + \sum_{k \neq j} \frac{2}{2\hbar\Delta - W_{jk}} \right) \right), \quad (7.9) \end{aligned}$$

Hence, particles that are widely separated from the rest do not contribute to the interaction and can be ignored. Using Eq. (7.4), we can calculate the energy of  $N_{\text{loc}}$  particles, for the case where they are infinitesimally close together:

$$E^{(6)}(0) = \left(\frac{\hbar\Omega}{2}\right)^6 \frac{2N_{\text{loc}}^3}{\hbar^5\Delta^5} = \hbar\Delta \left(\frac{\Omega}{2\Delta}\right)^6 N_{\text{loc}}^3 = \hbar\Delta N_R^3. \quad (7.10)$$

Finally, the total height  $U^{(6)}(0)$  of the interaction potential of  $N_{\text{loc}}$  particles can be determined as the difference between  $E^{(6)}(0)$  and the third-order light-shift (7.5), hence,

$$U^{(6)}(0) = \hbar\Delta N_R^3 - N \frac{\hbar\Omega^6}{32\Delta^5} = \hbar\Delta \left( N_R^3 - N \left(\frac{\Omega}{2\Delta}\right)^6 \right), \quad (7.11)$$

which is simplified to

$$U^{(6)}(0) = \hbar\Delta N_R^3 \quad (7.12)$$

if  $N_{\text{loc}} \gg 1$ . Thus, we see that  $N_R$  is, indeed, the parameter governing the interaction strength.

One might now try to include the three-body interaction into the non-local GPE (2.51).

To this end, one would define the three-body mean-field potential

$$V_{MF}^{(3)}[\psi](\mathbf{r}) = \rho^2 \int d\mathbf{r}' \int d\mathbf{r}'' U_{123}(\mathbf{r}, \mathbf{r}', \mathbf{r}'') |\psi(\mathbf{r}')|^2 |\psi(\mathbf{r}'')|^2, \quad (7.13)$$

where  $U_{ijk}(\mathbf{r}_i, \mathbf{r}_j, \mathbf{r}_k)$  is the three-body contribution to the interaction energy of three particles, such that

$$U^{(6)}(\mathbf{r}_1 \dots \mathbf{r}_N) = \sum_{(i,j,k) \neq} U_{ijk}(\mathbf{r}_i, \mathbf{r}_j, \mathbf{r}_k). \quad (7.14)$$

$V_{MF}^{(3)}$  would then be added to the usual GPE which includes the two-body mean-field potential  $V_{MF}^{(2)} = V_{MF}$ :

$$i\hbar\partial_t\psi(\mathbf{r}) = \left( -\frac{\hbar^2}{2m}\nabla^2 + V_{\text{ext}}(\mathbf{r}) + Ng|\psi(\mathbf{r})|^2 + V_{MF}^{(2)}[\psi](\mathbf{r}) + V_{MF}^{(3)}[\psi](\mathbf{r}) \right) \psi(\mathbf{r}). \quad (7.15)$$

However, there are two problems. The three-body mean-field potential (7.13) is a  $2d$ -dimensional integral if the system in question is  $d$ -dimensional. The computational cost for its calculation on a discrete grid with  $N$  points per dimension is  $\mathcal{O}(N^{2d} \log(N))$  if the convolution theorem is used (compared to  $\mathcal{O}(N^d \log(N))$  for the case of a two-body interaction)<sup>1</sup>. This makes the numerical calculation of the integral an extremely challenging problem.

More importantly, the inclusion of the three-body interaction term in the GPE does not solve the fundamental limitation of any perturbative treatment. The condition for the validity of the perturbation theory that

$$N_R \ll 1 \quad (7.16)$$

can be slightly relaxed when higher terms are included but it is still not clear how small exactly  $N_R$  needs to be. In fact it was suggested in [93] that the perturbation theory breaks down already at relatively small values of  $N_R \sim 0.05$ . In the following, we will answer this question via numerical calculation of the  $N$ -body Born-Oppenheimer potential without approximations.

## 7.2. The Born-Oppenheimer approximation beyond perturbation theory

The full Hamiltonian of a dressed gas of  $N$  atoms is (see section 4.2.5, in particular Eq. (4.73))

$$\hat{H} = \hat{T} + \hat{H}_{\text{el}} \quad (7.17)$$

---

<sup>1</sup>Without the convolution theorem, the corresponding costs would be  $\mathcal{O}(N^{3d})$  and  $\mathcal{O}(N^{2d})$ .

where the electron dynamics is described by

$$\hat{H}_{\text{el}} = \sum_{i < j} \hat{W}_{ij} \otimes \hat{\sigma}_{ee}^i \hat{\sigma}_{ee}^j - \hbar\Delta \sum_{i=1}^N \sigma_{ee}^i + \frac{\hbar\Omega}{2} \sum_{i=1}^N (\sigma_{ge}^i + \sigma_{eg}^i). \quad (7.18)$$

with  $\hat{W}_{ij} = W(\hat{r}_{ij}) = C_6/\hat{r}_{ij}^6$  and  $\hat{r}_{ij} = |\hat{\mathbf{r}}_i - \hat{\mathbf{r}}_j|$ .

In section 4.2.4 we justified the use of the Born-Oppenheimer (BO) approximation for the dressing scheme. We found that it is valid even for large values of  $\Omega/2\Delta$ , and hence of  $N_R$ . Hence, the atomic dynamics still takes place on a BO potential which, however, has to be calculated exactly if  $N_R$  is too large. To this end, we have to solve the eigenvalue problem

$$\hat{H}_{\text{el}}(\mathbf{r}_1 \dots \mathbf{r}_N) |\Psi_n(\mathbf{r}_1 \dots \mathbf{r}_N)\rangle = E_n(\mathbf{r}_1 \dots \mathbf{r}_N) |\Psi_n(\mathbf{r}_1 \dots \mathbf{r}_N)\rangle. \quad (7.19)$$

For each set of atom positions  $(\mathbf{r}_1 \dots \mathbf{r}_N)$  this equation yields  $2^N$  eigenvalues or in other words, it yields  $2^N$  potential surfaces  $U_n$ . The atomic dynamics then take place on one of those surfaces. Here, we consider the situation where all atoms are initially in the ground state  $|g\rangle$  and the dressing-laser is then switched on slowly. Hence, we need the single eigenenergy

$$E_G = E_G(N, N_R) = E_G(N, N_R; (\mathbf{r}_1 \dots \mathbf{r}_N)) \quad (7.20)$$

that corresponds to the eigenstate  $|\Psi_0(\mathbf{r}_1 \dots \mathbf{r}_N)\rangle = |G(\mathbf{r}_1 \dots \mathbf{r}_N)\rangle$  which adiabatically connects to the state  $|G_0\rangle = |g \dots g\rangle$  as  $\Omega \rightarrow 0$ . The BO potential is then found by subtracting from  $E_G$  the corresponding light-shift:

$$U_G(N, N_R) = E_G(N, N_R; \mathbf{r}_1 \dots \mathbf{r}_N) - E_{\text{LS}}(N, N_R), \quad (7.21)$$

where  $E_{\text{LS}}(N, N_R) = E_G(N, N_R; \infty \dots \infty)$  (where the interactions  $W_{ij}$  vanish).

We diagonalize  $\hat{H}_{\text{el}}$  numerically for every set of atom positions  $(\mathbf{r}_1 \dots \mathbf{r}_N)$  using the full  $2^N$ -dimensional basis

$$(|g \dots g\rangle, |eg \dots g\rangle, |geg \dots g\rangle, \dots, |e \dots e\rangle), \quad (7.22)$$

Since the number of states  $2^N$  scales exponentially with the number of particles  $N$ , a straightforward diagonalization quickly becomes prohibitively demanding. However, the interaction drastically limits the number of accessible many-body states. This allows to truncate the Hilbert space which significantly reduces the size of the matrix. Since there are  $\binom{N}{n}$  states with exactly  $n$  excitations, the reduced dimension of the truncated Hilbert space is

$$D = \sum_{n=0}^{N_{\text{exc}}} \binom{N}{n}. \quad (7.23)$$

We performed calculations for various values of  $N_{\text{exc}}$ , until convergence was reached. Our most demanding computations used  $N = 25$ ,  $N_{\text{exc}} = 5$ , so that there are

$$D = 68406. \quad (7.24)$$

many-body states. This is a significant reduction from the  $2^{25} = 3.4 \cdot 10^7$  states in the full Hilbert space and leads to a feasible computational cost of the diagonalization. Since each many-body state is coupled to only  $\sim N$  other many-body states, the matrix is sparse. It is useful to exploit this by using a diagonalization algorithm geared towards sparse matrices. We used a subroutine from the ARPACK library [13].

### 7.3. Application to self-trapping

The previous section allows us to calculate the interaction energy of a gas of particles with fixed positions exactly. We now come back to the question of self-trapping which we will investigate using this approach. In chapter 6, we considered self-trapping using the perturbatively obtained interaction potential and found that for a sufficient interaction strength, self-trapped solitons, i.e., states that remain confined solely due to internal interactions (in this case the dressing interaction). Now, we will investigate whether the inclusion of many-body interactions jeopardizes self-trapping as  $N_R$  is increased. We start from the total many-body Hamiltonian of the dressed gas in the BO approximation:

$$\hat{H} = -\frac{\hbar^2}{2m} \sum_i \nabla_i^2 + U_G(\hat{\mathbf{r}}_1 \dots \hat{\mathbf{r}}_N). \quad (7.25)$$

If energies are again scaled with  $\frac{\hbar^2}{mR_c^2}$  and lengths with  $R_c$  we obtain

$$\hat{H}^{\text{sc}} = -\frac{1}{2} \sum_i \nabla_i^2 + \beta U_G(\hat{\mathbf{r}}_1 \dots \hat{\mathbf{r}}_N). \quad (7.26)$$

Using the scaled variables,  $U_G$  is given by

$$\hat{H}_{\text{el}}^{\text{sc}}(\mathbf{r}_1 \dots \mathbf{r}_N) |G(\mathbf{r}_1 \dots \mathbf{r}_N)\rangle = U_G(\mathbf{r}_1 \dots \mathbf{r}_N) |G(\mathbf{r}_1 \dots \mathbf{r}_N)\rangle \quad (7.27)$$

with

$$\hat{H}_{\text{el}}^{\text{sc}} = -\sum_{i<j} \frac{2}{\hat{r}_{ij}^6} \otimes \hat{\sigma}_{ee}^i \hat{\sigma}_{ee}^j - \sum_{i=1}^N \sigma_{ee}^i + \frac{\Omega}{2\Delta} \sum_{i=1}^N (\sigma_{ge}^i + \sigma_{eg}^i). \quad (7.28)$$

The prefactor

$$\beta = -\frac{C_6 m}{2\hbar^2 R_c^4} \quad (7.29)$$

is closely related to our earlier effective interaction strength (6.18)

$$\alpha = -\frac{\tilde{C}_6 m N}{\hbar^2 R_c^4} = -\left(\frac{\Omega}{2\Delta}\right)^4 \frac{C_6 m N}{\hbar^2 R_c^4} \quad (7.30)$$

introduced in chapter 6. Their relation can be written as

$$\alpha = 2 \frac{N_R^2}{N} \beta. \quad (7.31)$$

The parameters  $\alpha$  and  $\beta$  differ because in chapter 6, the perturbative treatment combined with the mean-field approximation allowed to fully incorporate the parameters  $(\Omega/2\Delta)^4$  and  $N$  directly into  $\alpha$ , while now their effects are more complicated and enter through the fully correlated many-body potential  $U_G(\hat{\mathbf{r}}_1 \dots \hat{\mathbf{r}}_N)$ . However, in order to simplify comparisons to chapter 6, we will give all of our results in terms of  $\alpha$ .

According to Eq. (7.28),  $U_G$  depends only on  $\Omega/2\Delta$  and  $N$ . Since  $N_R = N(\Omega/2\Delta)^2$ , it can alternatively be written as depending only on  $N_R$  and  $N$  which is the notation we will use in the following:

$$U_G(\hat{\mathbf{r}}_1 \dots \hat{\mathbf{r}}_N) = U_G(N_R, N | \hat{\mathbf{r}}_1 \dots \hat{\mathbf{r}}_N). \quad (7.32)$$

### 7.3.1. Interaction energy of a BEC

While we now have a numerically exact description of the internal many-body states; the motional dynamics of the atoms on the resulting BO potential can still be described within the mean-field approximation. Hence, we can consider product states of the form

$$|\Psi(\mathbf{r}_1 \dots \mathbf{r}_N)\rangle = \bigotimes_i |\psi(\mathbf{r}_i)\rangle^i, \quad (7.33)$$

where all particles are described by the same BEC wave-function  $\psi$ . As in section 6.3, we use a variational method with Gaussian trial states

$$\psi(\mathbf{r}) = \frac{1}{\pi^{\frac{3}{4}} \sigma^{\frac{3}{2}}} \exp\left(-\frac{r^2}{2\sigma^2}\right). \quad (7.34)$$

Using the scaled Hamiltonian (7.26) including the fully correlated potential  $U_G$ , the energy of a BEC with the wave-function  $\psi$  is

$$\begin{aligned} E(\sigma) &= E_{\text{kin}}(\sigma) + E_{\text{dress}}(\sigma, N, N_R, \alpha) \quad (7.35) \\ &= -\frac{N}{2} \int d^3r \overline{\psi(\mathbf{r})} \nabla^2 \psi(\mathbf{r}) + \frac{1}{2} \beta \int d^3r_1 \dots \int d^3r_N \prod_{i=1}^N |\psi_\sigma(\mathbf{r}_i)|^2 U_G(\mathbf{r}_1 \dots \mathbf{r}_N) \\ &= -\frac{N}{2} \int d^3r \overline{\psi(\mathbf{r})} \nabla^2 \psi(\mathbf{r}) + \frac{1}{2} \beta \int d^3r_1 |\psi_\sigma(\mathbf{r}_1)|^2 \dots \int d^3r_N |\psi_\sigma(\mathbf{r}_N)|^2 U_G(\mathbf{r}_1 \dots \mathbf{r}_N). \end{aligned}$$

The kinetic energy can be calculated analytically:

$$E_{\text{kin}}(\sigma) = \frac{3N}{4\sigma^2}, \quad (7.36)$$

while for the potential energy

$$E_{\text{dress}}(\sigma, N, N_R, \alpha) = \frac{1}{2}\beta \int d^3r_1 |\psi_\sigma(\mathbf{r}_1)|^2 \dots \int d^3r_N |\psi_\sigma(\mathbf{r}_N)|^2 U_G(N_R, N | \mathbf{r}_1 \dots \mathbf{r}_N)$$

we need to evaluate a  $3N$ -dimensional integral. This can be done efficiently by Monte-Carlo sampling the  $3N$ -dimensional position space [145]. We use the Marsaglia polar method [135] to generate Gaussian distributed atomic positions  $\mathbf{r}_i$  that yield configurations

$$\mathbf{R} = (\mathbf{r}_1 \dots \mathbf{r}_N) \quad (7.37)$$

We then calculate  $U_G(\mathbf{R})$  for each  $\mathbf{R}$  as described in section 7.2. The potential energy is obtained by averaging the results over a large number of configurations:

$$E_{\text{dress}}(\sigma, N, N_R, \alpha) = \frac{1}{N_c} \sum_{\mathbf{R}} \beta U_G(\mathbf{R}). \quad (7.38)$$

We will compare the results to those obtained from perturbation theory where  $U_G$  reduces to

$$U_G^{\text{pert}}(\mathbf{r}_1 \dots \mathbf{r}_N) = - \left( \frac{\Omega}{2\Delta} \right)^4 \sum_{i < j} \frac{2\beta}{1 + |\mathbf{r}_i - \mathbf{r}_j|^6}, \quad (7.39)$$

leading to the potential energy

$$E_{\text{dress}}^{\text{pert}}(\sigma, N, N_R, \alpha) = - \underbrace{\frac{1}{2} 2\beta \left( \frac{\Omega}{2\Delta} \right)^4}_{=\alpha N} N^2 \int d^3r_1 \int d^3r_2 \frac{|\psi_\sigma(\mathbf{r}_1)|^2 |\psi_\sigma(\mathbf{r}_2)|^2}{1 + |\mathbf{r}_1 - \mathbf{r}_2|^6} \quad (7.40)$$

that we already calculated in Eq. (6.39). For  $\sigma \rightarrow 0$  it simplifies to

$$E_0 = E_{\text{dress}}(0, N, N_R, \alpha) = -\frac{1}{2}\alpha N = -\beta N_R^2. \quad (7.41)$$

Fig. 7.1 shows some results for  $N = 20$  including a comparison to the fourth-order perturbative result. We scaled the results for  $E_{\text{dress}}$  from our exact calculations with the perturbative energy  $|E_0| = \beta N_R^2$  in order to compare them to the perturbative prediction. If this prediction were valid over the whole range of  $N_R$ , all curves would be identical. We find that, for  $N_R \ll 1$ , our calculations perfectly recover the perturbative result, as was to be expected. For larger  $N_R$ , deviations appear. The potential is weaker than predicted, consistent with the findings in [93]. This weakening can be qualitatively understood within the interaction blockade picture. Recall that  $N_R$  is defined as the

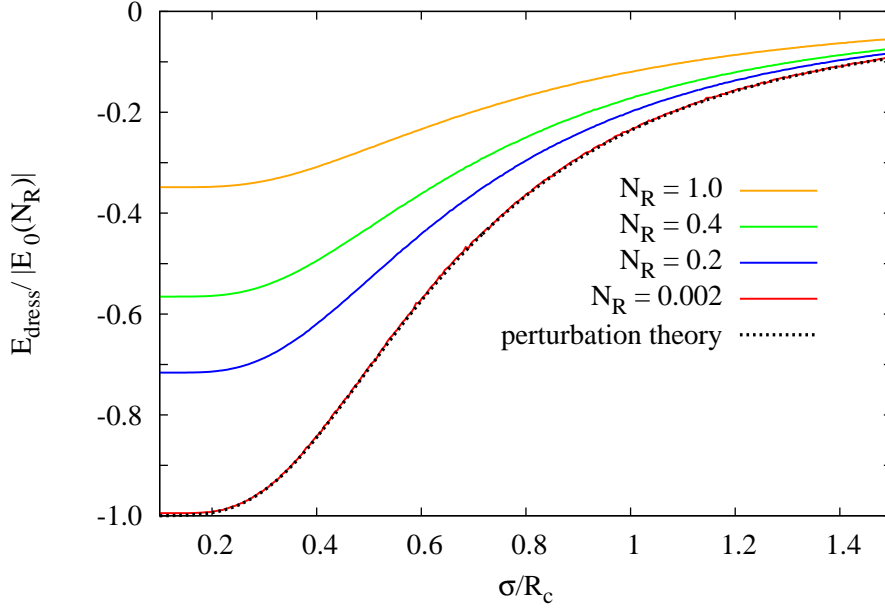


**Figure 7.1.:** Potential energies of condensates with size  $\sigma$  for various values of the perturbation parameter  $N_R$ . Energies are scaled by  $|E_0(N_R)| = \beta N_R^2$ , which is the scaling predicted by the perturbation theory

average number of Rydberg excitations in the absence of interactions. Since interactions limit the actual number of excitations below this value, the effects of the blockade become more pronounced as  $N_R$  increases.

In particular, the potential energy per particle of a fully blockaded gas (e.g., a gas of particles at very low distance) is non-extensive and increases much slower than linear in  $N$ . This can be illustrated by considering a simple situation where all atoms are within one blockade radius:

As we discussed earlier (Eq. (4.84)), the light shift of  $N$  non-interacting atoms is

$$E_L(N) = \frac{1}{2} N \hbar \Delta \left( -1 + \sqrt{1 + 4 \left( \frac{\Omega}{2\Delta} \right)^2} \right). \quad (7.42)$$

$N$  fully blockaded particles can be described using only the two states  $|g \dots g\rangle$  and

$$\frac{1}{\sqrt{N}} (|eg \dots g\rangle + |geg \dots g\rangle + \dots + |g \dots geg\rangle + |g \dots ge\rangle) \quad (7.43)$$

because excitation of more than one particle is inhibited. The Hamiltonian in that basis is

$$\hat{H}_{\text{bl}} = \hbar \begin{pmatrix} 0 & \frac{\Omega}{2}\sqrt{N} \\ \frac{\Omega}{2}\sqrt{N} & -\Delta \end{pmatrix} \quad (7.44)$$

and the eigenvalue adiabatically corresponding to  $|g \dots g\rangle$ , and thus the light-shift, is

$$E_L^{\text{bl}}(N) = \frac{1}{2}\hbar\Delta \left( -1 + \sqrt{1 + 4N \left( \frac{\Omega}{2\Delta} \right)^2} \right) = \frac{1}{2}\hbar\Delta \left( -1 + \sqrt{1 + 4N_R} \right). \quad (7.45)$$

These light-shifts determine the energy of a BEC with infinite width ( $E_L$ ) and one with zero width, where all atoms are located at the same position ( $E_L^{\text{bl}}$ ). Hence, the total height of the interaction potential is given by the difference between them. It is

$$\Delta E_L(N) = E_L^{\text{bl}}(N) - E_L(N) = \frac{\hbar\Delta}{2} \left( -1 + \sqrt{1 + 4N_R} + N - \sqrt{N^2 + 4N_R N} \right). \quad (7.46)$$

In the thermodynamical limit  $N \rightarrow \infty$ , with  $\Omega/2\Delta \rightarrow 0$  such that  $N_R = \text{const}$ , the difference becomes

$$\Delta E_L(\infty) = \lim_{N \rightarrow \infty} \left( E_L^{\text{bl}}(N) - E_L(N) \right) = \frac{\hbar\Delta}{2} \left( -1 + \sqrt{1 + 4N_R} - 2N_R \right). \quad (7.47)$$

For large  $N_R$ , this expression depends less than quadratically on  $N_R$ , thus leading to non-extensivity and the observed weakening of the dressing potential. This is in contrast to the perturbative regime  $N_R \ll 1$  where we find

$$\Delta E_L(N) = -\hbar\Delta(1 - N^{-1})N_R^2 + \mathcal{O}(N_R^4), \quad (7.48)$$

$$\Delta E_L(\infty) = -\hbar\Delta N_R^2 + \mathcal{O}(N_R^4), \quad (7.49)$$

making the energy extensive for  $N_R \ll 1$ .

Despite the quantitative deviations, the order of magnitude of the potential still conforms to the perturbative prediction in the whole investigated regime of  $N_R \in [0, 1]$ . Furthermore, the dependence of  $E_{\text{dress}}$  on  $\sigma$  remains very similar. Hence, the nonlocal character of the interaction persists in the many-body interaction regime.

We now investigate the implications of the weakening of the interaction on self-trapping. To this end we plot the total energy in Fig. 7.2, including the kinetic energy. For this example we assume a fixed effective interaction strength  $\alpha = 10$ . In the perturbative regime, this yields a sufficiently strong potential to ensure self-trapping (cf. Fig. 6.3) as indicated by the negative minimum of the corresponding curve in Fig. 7.2.

We observe that the energy minimum becomes shallower for increasing  $N_R$  and vanishes completely between  $N = 0.4$  and  $N = 1.0$ . Hence, the corrections to the perturbative prediction that occur at higher  $N_R$  can indeed inhibit self-trapping for a fixed effective interaction strength  $\alpha$ . In the following, we will therefore have a closer look at the effects of the many-body interactions onto the conditions for self-trapping.

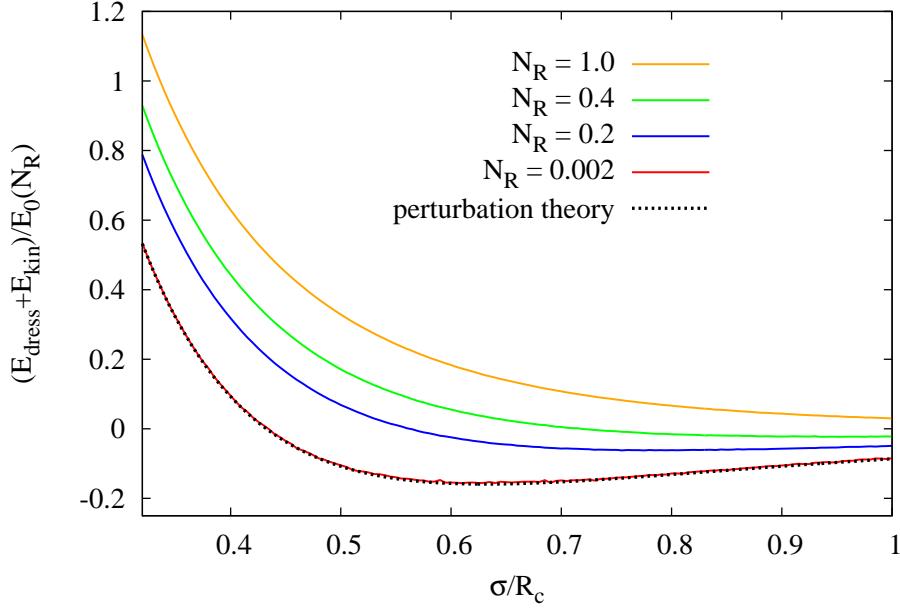


**Figure 7.2.:** Total energies of condensates with size  $\sigma$  and for  $\alpha = 10$ , for various values of the perturbation parameter  $N_R$ . Energies are scaled by  $E_0(N_R) = -\frac{1}{2}\beta N_R^2$ . For small  $N_R$ , the interaction leads to a negative minimum of the energy functional and thus to a self-trapped state. For sufficiently high  $N_R$  the self-trapping vanishes.

### 7.3.2. Variational method for minimization of the energy

Analogous to the variational procedure of chapter 6, we minimize the total energy (including also the short-range-interaction energy  $E_{\text{cont}}$ )

$$E(\sigma, N, N_R, \alpha, \gamma) = E_{\text{kin}}(\sigma) + E_{\text{cont}}(\sigma, N, \gamma) + E_{\text{dress}}(\sigma, N, N_R, \alpha) \quad (7.50)$$

for fixed values of  $\alpha$ ,  $N_R$  and  $N$  with respect to  $\sigma$ . This yields an approximate ground state  $|\psi_{\sigma_{\min}}\rangle$  with the energy

$$E_{\min}(N, \tilde{\Omega}, \alpha, \gamma) = \min_{\sigma} E(\sigma, N, \tilde{\Omega}, \alpha, \gamma). \quad (7.51)$$

In the same way as in chapter 6, we define the critical interaction strength for self-trapping  $\alpha_{\text{st}}(N, \tilde{\Omega}, \gamma)$  as the smallest  $\alpha$  such that

$$E_{\min}(N, \tilde{\Omega}, \alpha, \gamma) < 0. \quad (7.52)$$

With this method, we can recalculate the conditions for self-trapping beyond perturbation theory (see Fig. 6.3 for the perturbative result).

## 7.4. Modification of the self-trapping condition

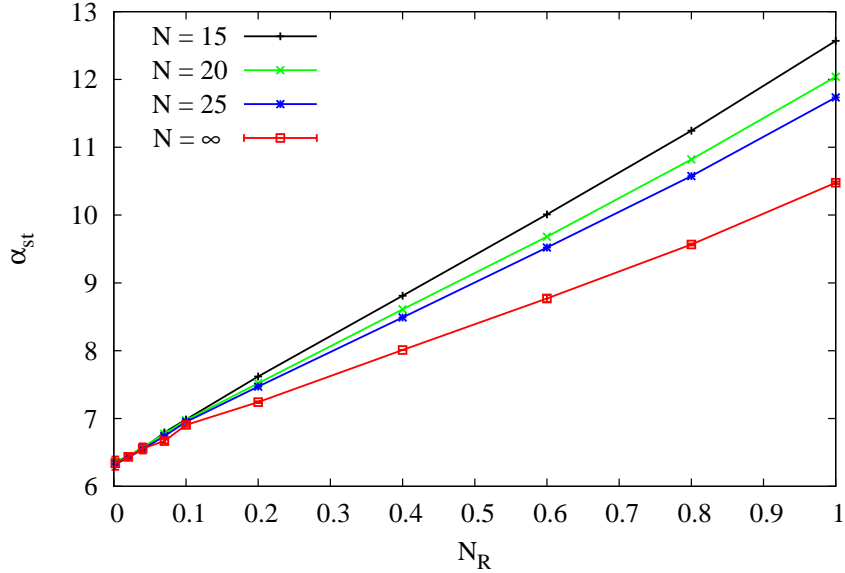


**Figure 7.3.:** Value of the minimal interaction strength for self-trapping  $\alpha_{st}$  depending on  $N_R$ , explicitly calculated for  $N \in \{15, 20, 25\}$ . The curve labeled “ $N = \infty$ ” was obtained by a finite-size scaling as explained in the main text.  $s$ -wave scattering has been neglected for these results ( $\gamma = 0$ ).

Fig. 7.3 shows our results for the dependence of  $\alpha_{st}$  on  $N_R$  for a few values of the particle number  $N$  and for the simplest case of  $\gamma = 0$ . For  $N_R \rightarrow 0$ , the perturbative result of  $\alpha_{st}^{\text{pert}} = 6.3$  is recovered perfectly. For  $N_R > 0$ , we find deviations towards higher critical  $\alpha$ , which are due to the weakening of the dressing induced interactions compared to the perturbative result. The strength of the deviations also depends on the total number of particles  $N$ . The higher  $N$ , the weaker the deviations from the perturbative prediction. This dependence is not surprising since the light-shift difference  $\Delta E_L(N)$  (Eq. (7.46)) and its deviation from its perturbative approximation (7.48) depend explicitly on  $N$ . As mentioned before, the considered particle numbers are too low to make predictions for typical experimental situations and the result needs to be extrapolated to much higher particle numbers. In order to do this, we perform a finite-size-scaling. For every  $N_R$  we consider the relation  $\alpha_{st}(N_R, N)$ . At sufficiently high  $N$ , this can be approximated by a Taylor series in  $N^{-1}$ , yielding

$$\alpha_{st}(N_R, N) = A(N_R) + B(N_R)N^{-1}, \quad (7.53)$$

where  $A(N_R) =: \alpha_{st}(N_R, \infty)$  and  $B(N_R)$  are fitting parameters. The result is shown as

the curve labeled “ $N = \infty$ ” in Fig. 7.3. We find that this curve consists approximately of two linear regions given by

$$\alpha_{\text{st}}(N_R, \infty) = \begin{cases} 6.3 + 5.5N_R & \text{for } N_R \leq 0.1 \\ 6.5 + 4.0N_R & \text{for } N_R \geq 0.1 \end{cases} \quad (7.54)$$

For low  $N_R$ , the linear behavior can be understood as follows.  $\alpha_{\text{st}}(0, \infty)$  simply corresponds to the fourth order perturbation theory result  $\alpha_{\text{st}}^{\text{pert}} = 6.3$ . The fourth-order term in the perturbation expansion scales with  $N_R^2$ , the sixth-order term with  $N_R^3$ . Hence, for small  $N_R$  the total dressing-interaction energy per particle scales as

$$\frac{E_{\text{dress}}}{N} = \frac{N_R^2}{N} (A + BN_R) \propto \alpha (A + BN_R), \quad (7.55)$$

with constants  $A < 0$  and  $B > 0$ . The critical value  $\alpha_{\text{st}}$  is reached when

$$\frac{E_{\text{dress}}}{N} + E_{\text{kin}} = 0, \quad (7.56)$$

or

$$\alpha (A + BN_R) + E_{\text{kin}} = 0. \quad (7.57)$$

Thus, we find

$$\alpha_{\text{st}}(N_R) = \frac{E_{\text{kin}}}{A + BN_R} \approx \frac{E_{\text{kin}}}{A} \left(1 - \frac{B}{A}N_R\right) = \alpha_{\text{st}}(0) \left(1 - \frac{B}{A}N_R\right). \quad (7.58)$$

### Inclusion of $s$ -wave scattering

Up to now we have set  $\gamma = 0$  for simplicity, i.e., we have neglected the contact interaction through  $s$ -wave scattering. In experiments, however,  $s$ -wave scattering is typically present, unless switched off by Feshbach resonances [60, 94, 136]. Therefore, we now consider the effect of a short-range interaction, i.e.,  $\gamma \neq 0$  in Eq. (7.50). The short-range interaction energy (Eq. 6.33) is

$$E_{\text{cont}}(\gamma, \sigma) = \frac{\sqrt{2}}{8\pi^{\frac{3}{2}}} \frac{\gamma}{\sigma^3}. \quad (7.59)$$

Including it into our variational procedure is straightforward. Again, we consider the particle numbers  $N \in \{15, 20, 25\}$  and then extrapolate the results to  $N = \infty$  via a finite-size-scaling. The results are shown in Fig. 7.4. For  $N_R \rightarrow 0$  we again recover the perturbative result from Fig. 6.3 and for higher  $N_R$  the critical value  $\alpha_{\text{st}}$  is shifted to higher values. The critical value for self-trapping can be approximated as

$$\alpha_{\text{st}}(\gamma, N_R) = 6.3 + (0.20 + 0.05N_R)\gamma + 4N_R. \quad (7.60)$$

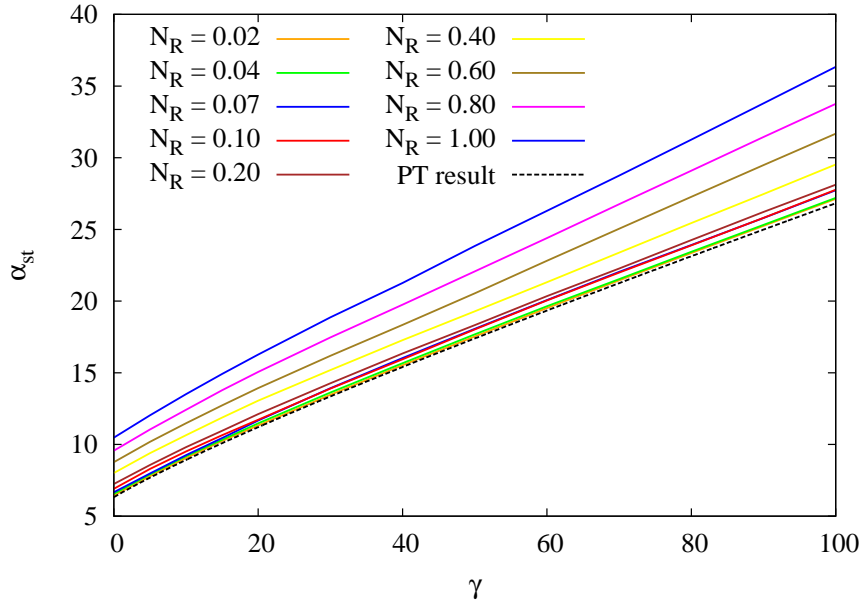


**Figure 7.4.:** Value of the transition point  $\alpha_{\text{st}}$ , for  $N = \infty$  (obtained by a finite size scaling, see main text), depending on the short-range interaction strength  $\gamma$  and for various values of  $N_R$ . For  $N_R \ll 1$ , the perturbative result (from Fig. 6.3) is recovered. For larger  $N_R$ , the critical value  $\alpha_{\text{st}}$  is shifted to higher values. This effect is relatively smaller for larger values of  $\gamma$ .

In relative terms the deviations are less pronounced at larger  $\gamma > 0$  than at  $\gamma = 0$ . This is the case because a larger  $\gamma$  leads to a larger size of the self-trapped state. Hence, atoms are further apart on average so that the blockade effect which is responsible for the weakening of the dressing interaction is effectively less pronounced for a given  $N_R$ .

## 7.5. Implications for experiments

We have seen that, as the perturbation parameter  $N_R$  is increased from 0 to 1, the critical interaction strength  $\alpha_{\text{st}}$  increases. For  $\gamma = 0$  it almost doubles from 6.3 to 11, for  $\gamma = 100$  the effect is considerably weaker in relative terms:  $\alpha_{\text{st}}$  increases roughly from 27 to 37. However, increasing  $N_R$  can still lead to the vanishing of self-trapping if  $\alpha$  is kept fixed.

However, the possibility of using high values of  $N_R$  also drastically increases the range of values for  $\alpha$  that can be achieved:

$$\alpha = - \left( \frac{\Omega}{2\Delta} \right)^4 \frac{C_6 m N}{\hbar^2 R_c^4} = - \frac{N_R^2}{N} \frac{C_6 m}{\hbar^2 R_c^4}. \quad (7.61)$$

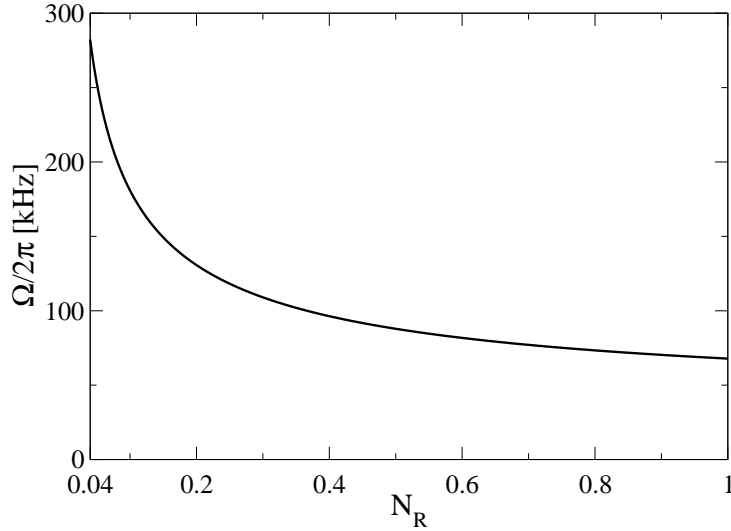


**Figure 7.5.:** Necessary Rabi frequency  $\Omega$  in order to achieve the self-trapping of a BEC dressed to the  $|65d_{3/2}\rangle$  state with  $\Delta = 2\pi \cdot 32$  MHz and for a given  $N_R$ .

As a baseline for our considerations we use a Rubidium BEC of  $N = 1700$  atoms dressed to the  $|65d_{3/2}\rangle$  state with  $\Omega = 2\pi \cdot 0.28$  MHz and  $\Delta = 2\pi \cdot 32$  MHz. This is similar to the situations considered in chapter 6 and yields an approximate<sup>2</sup> blockade radius of  $R_c = 5 \mu\text{m}$  which corresponds to a van-der-Waals coefficient  $C_6 = -6.6 \cdot 10^{-58} \text{Jm}^6$ . This yields the parameters

$$\alpha = 11.3, \quad (7.62)$$

$$\gamma = 22.6, \quad (7.63)$$

$$N_R = 0.04, \quad (7.64)$$

such that perturbation theory is valid. Furthermore, the necessary strength for self-trapping at  $\gamma = 13.3$  is

$$\alpha_{\text{st}} = 10.8, \quad (7.65)$$

according to the phase diagram in Fig. 6.5. Hence, a BEC with these parameters is self-trapped. However, the necessary Rabi frequency of  $\Omega = 2\pi \cdot 0.3$  MHz is difficult to achieve experimentally.

We now move beyond perturbation theory and consider how the necessary  $\Omega$  changes if higher values of  $N_R$  are allowed. According to Eq. (7.60),  $\alpha_{\text{st}}$  can be approximated as

$$\alpha_{\text{st}}(N_R) = 6.3 + (0.20 + 0.05N_R)\gamma + 4N_R \quad (7.66)$$

<sup>2</sup>cf. the discussion about the isotropic approximation of  $d$ -state interactions in section 4.4.2

for  $N_R \geq 0.1$ . Therefore, the condition for self-trapping becomes

$$6.3 + (0.20 + 0.05N_R)\gamma + 4N_R = -\left(\frac{\Omega}{2\Delta}\right)^4 \frac{C_6 m N}{\hbar^2 R_c^4} \quad (7.67)$$

$$\Leftrightarrow \quad \Omega = \frac{2\Delta \hbar R_c^2}{\sqrt{-m C_6}} \sqrt{\frac{6.3}{N_R} + 4 + \left(\frac{0.20}{N_R} + 0.05\right)\gamma} \quad (7.68)$$

$$= 2\pi \cdot 17 \text{ kHz} \cdot \sqrt{\frac{6.3}{N_R} + 4 + \left(\frac{0.20}{N_R} + 0.05\right)\gamma} \quad (7.69)$$

$$= 2\pi \cdot 17 \text{ kHz} \cdot \sqrt{\frac{10.8}{N_R} + 5.13}. \quad (7.70)$$

$$(7.71)$$

As shown in Fig. 7.5, the necessary Rabi frequency  $\Omega$  is decreased by a factor of 2.5 from  $2\pi \cdot 280$  kHz to  $2\pi \cdot 110$  kHz as  $N_R$  is increased from 0.04 to 0.3. A further increase of  $N_R$  to 1 reduces  $\Omega$  to  $2\pi \cdot 70$  kHz. In the first case  $N$  would need to be increased from 1700 to 100000 in order to reach the desired value of  $N_R = 0.3$  and in the second case to 300000 to reach  $N_R = 1$ . Such atom numbers are within current experimental capabilities [125]. Furthermore, the decrease of  $\Omega$  by a factor of 4 increases the lifetime of the dressed BEC by a factor of 16. This should further simplify an experimental verification of the predicted self-trapping effect, and make the first creation of a three-dimensional “matter-wave bullet” possible.

## 8. Conclusions

The aim of this thesis was to devise a viable scheme to realize long-range atomic interactions in a Bose-Einstein condensate (see chapter 2). As a source of such interactions we considered Rydberg atoms, which are atoms excited to high-lying atomic states. Rydberg atoms have a number of remarkable properties, such as extremely strong van-der-Waals interactions and long radiative lifetimes on the order of  $100 \mu\text{s}$ . The interactions give rise to the so-called interaction blockade where the excitation of a single atom inhibits the excitation of any other atoms in its vicinity [96]. The blockade has enabled a range of fascinating applications in quantum information science [175] and quantum optics [78, 158]. These important applications are based on the fast (microsecond) electron-dynamics, exploiting the long lifetimes of Rydberg atoms in order to conserve coherence. In contrast, we were primarily interested in the much slower millisecond dynamics of atomic motion. In this case, Rydberg decay is still too fast and would lead to decoherence before any interesting phenomena could be observed.

In chapter 4, we introduced a method to overcome this problem by off-resonant coupling of the atomic ground state to Rydberg states as an alternative to resonant excitation. This so-called Rydberg dressing scheme (see section 4.1) admixes a small fraction of Rydberg character to the ground state. Consequently, the dressed ground state has a significantly enhanced lifetime on the order of 100 milliseconds. Even though the admixed Rydberg character is weak, the resulting ground state interaction is still sufficiently strong. We derived the dressing interaction within the Born-Oppenheimer approximation using perturbation theory. We started from the simple case of coupling to a single Rydberg state (see section 4.2) and extended the derivation to the general case of coupling to a degenerate Rydberg manifold (section 4.3). It turned out that the total interaction energy can be written as a sum of two-body interactions that are asymptotically van-der-Waals like but have a soft core due to the interaction blockade, i.e., they do not diverge at small distances but instead flatten off. Importantly, the scheme relies on the condition that all interaction curves in the relevant Rydberg manifold have the same sign.

This issue is addressed in chapter 3, where we performed extensive calculations of the interaction curves of numerous Rydberg manifolds of Rubidium-87 in chapter 3. In particular, we found that all  $s$ -states are repulsive and that all  $d_{3/2}$ -states with a principal quantum number  $n \geq 59$  are attractive. These two examples open up the opportunity to realize repulsive as well as attractive interactions via Rydberg dressing. In both cases, the peculiar soft-core form of the interaction combined with the extended lifetime leads to distinct behavior and gives rise to a number of interesting effects which we investigated in chapters 5 and 6.

In chapter 5, we considered a Rubidium BEC with a repulsive dressing interaction (as realized by dressing to  $s$ -states). First, we applied a mean-field approximation and

found that the elementary excitations of a homogeneous dressed BEC exhibit a roton-maxon spectrum (see section 5.2). Once the interaction becomes sufficiently strong, the roton-minimum touches zero, leading to a dynamical roton-instability. The resulting time evolution transforms the initially homogeneous state into a state with broken continuous translational symmetry. This new state consists of an ordered arrangement of droplets that are as large as the Rydberg blockade radius. In one and two dimensions, the droplets form a regular crystal structure, i.e., the underlying lattice has a discrete symmetry. On the other hand, in three dimensions the instability leads to a glass-like state due to several competing lattice symmetries with nearly degenerate energies.

In section 5.3, the static properties of a dressed BEC were considered. We found a quantum phase transition between the superfluid and the modulated droplet-crystal phase. In three and two dimensions, the phase transition is of first order and occurs at a lower interaction strength than the roton instability, i.e., at a non-zero roton gap. Notably, the situation is different in one dimension where the transition is of second order and coincident with the roton instability, illustrating the important role of the roton minimum for the phase transition.

Dynamical simulations for realistic parameters (see section 5.4) showed that droplet crystals can form on a sufficiently short timescale (smaller than the lifetime of the dressed states), thus enabling the possibility of their experimental observation.

Since the mean-field approximation implicitly assumes a finite superfluid fraction, we performed path-integral Monte-Carlo simulations in section 5.5 in order to investigate the superfluidity of the droplet crystal. In order to be close to possible future experiments, we considered finite-size BECs in a harmonic trap. The Monte-Carlo results are in excellent agreement with those from the mean-field approximation, both for the density profile of the droplet crystal and for its superfluidity. Importantly, the superfluidity was found to persist up to relatively high temperatures on the order of 100 nK that are accessible by current experiments.

Being both crystalline and superfluid makes the droplet state a supersolid, an exotic state of matter that has been intensively pursued since its very first conjecture forty years ago [10, 37]. Supersolidity has mostly been investigated in the context of pressurized helium, but recent theoretical and experimental evidence suggests that it is not supersolid [25, 101]. Hence, the finding of an alternative candidate for supersolidity is of great relevance.

In experiments, superfluidity is typically measured by setting the BEC into rotation and observing the creation of vortices, which are a signature of superfluidity. Whether this approach is viable in the present case has been investigated in section 5.6. We found that vortices tend to be located between the droplets for low rotation frequencies, making them hard to detect experimentally. However, if the rotation frequency is increased, the vortex density increases as well. Once it rises to sufficient values, it becomes favorable for vortices to appear within the high-density droplets. This would make them experimentally observable and would enable the first unambiguous creation and observation of a supersolid state.

---

In chapter 6, the effects of an attractive dressing interaction were investigated. Such an interaction can be generated by using Rubidium  $d$ -states (see section 6.2). In section 6.3, we used a variational ansatz and found that the interaction leads to the existence of stable self-trapped ground states. Three-dimensional self-trapped states of light, so-called light bullets and their material counterparts, matter-wave bullets or self-trapped solitons, have fascinated researchers for a long time [18]. There have been numerous theoretical studies, but an experimental realization has remained elusive thus far. The major obstacle has been that interactions are either too weak, or diverge for low distances, causing collapse of the wave function. The present interaction, however, is sufficiently strong to confine a BEC, while its soft core prevents collapse.

In addition to the variational calculations, we also performed numerical simulations of the static (section 6.4) and dynamic (section 6.6) properties of the system. Here we found good agreement with the simplified variational ansatz and showed that three-dimensional self-trapping can indeed be demonstrated for realistic experimental parameters. In fact, it turned out that typical Rydberg-Rydberg atom interactions are so strong that a shell of only one single pair of coherently shared excitations can trap the entire BEC with  $\sim 10^3$  atoms.

In the final chapter 7, we went beyond the perturbative approach for calculating the effective interactions. This approximation is expected to break down if the optical coupling becomes strong, i.e., if the corresponding Rabi frequency is on the order of the detuning. In section 7.1, we started by considering the next higher-order term in the perturbation series, which yields a genuine three-body interaction, which tends to lower the total interaction energy. This raised the question whether the phenomena of super-solidity and self-trapping revealed in chapter 6 and 5 would persist at stronger dressing. So far, we have addressed this question for the simpler scenario of self-trapping. To this end, we developed an approach for the exact calculation of the underlying many-body potential energy surface, which is outlined in section 7.2 and applied to the self-trapping problem in section 7.3. In the limit of weak dressing, the new method recovered the perturbative result (of section 6.3) perfectly. At stronger dressing, deviations appear due to the lowering of the total interaction strength. However, since the constraints on the dressing parameters can be relaxed outside of the perturbative regime, our results show that the proper inclusion of genuine many-body interactions in fact relaxes the conditions for soliton formation, rather than diminishing the effect.

## Future perspectives

The previously discussed results have generated new questions and ideas that call for further investigation. While thus far the focus has been on situations accessible by simplified mean-field approaches, the regime where this approximation breaks down might feature additional interesting physics concerning correlated many-body systems

and nonlinear quantum optics. Below, a few specific ideas are outlined, which might provide promising avenues of research.

### **Roton instability and supersolids in a collectively interacting BEC**

In chapter 7, we investigated self-trapping in the regime of strong dressing to attractive Rydberg states, where the perturbative calculation of the dressing potential from chapter 4 breaks down. An equivalent break-down takes place when repulsive interactions are considered. Studying the effects of the resulting many-body interactions on supersolidity may prove interesting and important for several reasons. First, the experimental demonstration of the supersolid phase transition, currently pursued in several laboratories, sets high demands on the laser parameters required to induce sufficiently strong interactions. While the required parameters appear to be within reach they are still very challenging for current setups. The condition of weak dressing in particular sets strict constraints on the achievable interaction strength. Therefore, the theoretical demonstration of supersolidity in the collective interaction regime could greatly facilitate corresponding experiments and thereby pave the way for the first demonstration of continuous-space supersolidity in such systems. Second, the study of genuine many-body interactions in continuous-space quantum systems appears to be very interesting from a fundamental point of view. This question has attracted considerable interest in the context of lattice-confined polar molecules [34, 179], but it has not been addressed in continuous space.

A promising starting point to tackle this problem could be to consider a mean-field description for the spatial atomic degrees of freedom but use the fully correlated internal many-body states of the laser-driven atoms. This should allow to derive an excitation spectrum that generalizes the standard Bogoliubov spectrum to the case of  $N$ -body interactions and that could be evaluated via Monte-Carlo sampling.

One may take the idea of strong dressing further and consider resonant excitation to Rydberg states. The key point now is that for a sufficiently strong interaction blockade each atom still carries only a small fraction of Rydberg-state character, so that one may find conditions for that the overall lifetime of a resonantly driven BEC is still high enough to observe coherent motional dynamics. To start out simple, one may first consider excitation of attractive Rydberg states in a small blockaded BEC, which may form a self-bound state confined by a collective surface excitation of Rydberg atom pairs. This situation differs dramatically from the off-resonant case and soliton stability may be dependent on an interesting interplay between coherent generation of internal-state entanglement, correlated atomic motion and dissipation.

### **Dissipation in interacting quantum systems**

While the above discussion treats spontaneous decay as an undesired side effect and a point of worry, several recent works (e.g. [54]) suggest that dissipation can instead be

---

useful. In the present context, such a situation may be encountered by considering the dressing scheme of chapter 4 with reversed signs, i.e., by using a blue-detuned dressing laser and repulsively interacting Rydberg states (or vice versa). For two atoms, this leads to an interaction-induced pair resonance and thus to an avoided crossing between the two-atom ground state and the doubly excited state. Interactions increase tremendously once the atoms are transferred to their excited states. On the other hand, this also leads to strong dissipation. Importantly, this situation can no longer be treated quasi-statically but needs to be approached as a two-channel dissipative collision problem. One of the interesting questions will be whether the strong decay will lead to reflection due to the quantum Zeno effect or whether it will lead to enhanced non-adiabatic transitions of the atoms through the avoided crossings with minimal dissipation. The latter scenario would result in largely coherent interactions, which may be greatly enhanced with respect to the standard off-resonant dressing scheme. In contrast, the former case will imply an effective hard-core interaction and lead to quasi-bound molecular states, for incoming and outgoing scattering, respectively.

### **Integrated description of matter and light**

All of the above ideas concern the effect of a laser field on an ultracold gas or BEC. In an additional work that was performed in the course of this thesis but that has not been explicitly discussed here, we showed that the light propagation is also influenced by the presence of a gas, given an appropriate excitation scheme. In particular, we explored the effects an excitation scheme that features electromagnetically induced transparency (EIT) [180]. We found that this induces an effective photon-photon interaction very similar to the atomic dressing interaction derived in chapter 4. Therefore, the fast light propagation dynamics features similar phenomena as the dressed gas, such as a roton-maxon spectrum and a roton instability, as well as formation of self-assembled modulated states and self-trapping [180].

Interesting effects may also occur on the slower timescale of the atomic motion, as the system consists of two components (light and matter) that can not be treated independently anymore. The atoms are governed by an effective interaction whose properties are given by the laser intensity. At the same time, the photons exhibit an effective interaction that depends on the gas density.

Here, one could first consider the regime where only two-body effects are relevant, both in the gas and in the light. The light field can be described by a non-linear Schrödinger equation which is identical to a non-local Gross-Pitaevskii equation. If the mean-field approximation is used for the gas, it can also be described by a Gross-Pitaevskii equation. Hence, the coupled system is fully described by two coupled Gross-Pitaevskii equations. This should already yield valuable insights into the mutual interaction of light and matter. Furthermore, it will be interesting to explore the effect of atom-atom and/or photon-photon correlations in the regime where the respective mean-field treatments of gas and light break down. In this regime, the many-body nature of the dressing interaction might also become relevant and could lead to interesting collective effects.



# A. Solving the Gross-Pitaevskii equation on a discrete spatial grid

## A.1. Split-operator method

We are interested in a Gross-Pitaevskii equation in of the form

$$\left(\hat{T} + \hat{V}(t) + \hat{V}_{\text{MF}}[\psi]\right) |\psi\rangle = i\partial_t |\psi\rangle \quad (\text{A.1})$$

with an external potential  $\hat{V}$ , the mean-field potential

$$V_{\text{MF}}[\psi](\mathbf{r}) = \int d\mathbf{r}' W(\mathbf{r} - \mathbf{r}') |\psi(\mathbf{r}')|^2 \quad (\text{A.2})$$

which describes the interaction between particles and the initial condition  $|\psi(0)\rangle = |\psi_0\rangle$ . We would like to solve this equation on a discrete spatial grid. The formal solution is

$$|\psi(t)\rangle = \hat{O} \exp\left(\int_0^t dt' \left(\hat{T} + \hat{U}(t')\right)\right) |\psi_0\rangle, \quad (\text{A.3})$$

where  $\hat{O}$  is the time ordering operator and  $\hat{U}(t) = \hat{V}(t) + \hat{V}_{\text{MF}}[\psi(t)]$ . This solution can also be written as

$$|\psi(t)\rangle = \lim_{\Delta \rightarrow 0} \prod_{n=0}^{t/\Delta} e^{-i\Delta(\hat{T} + \hat{U}(n\Delta))} |\psi_0\rangle. \quad (\text{A.4})$$

For the numerical solution we use a non-zero but small value for  $\Delta$  and discretize time accordingly, using  $t = N\Delta$ . This yields

$$|\psi_N\rangle = \prod_{n=0}^N e^{-i\Delta(\hat{T} + \hat{V}_n + \hat{U}_n)} |\psi_0\rangle, \quad (\text{A.5})$$

where the index  $n$  denotes that the corresponding object is to be taken at time  $n\Delta$ .

We now need a way to calculate the single time step  $e^{-i\Delta(\hat{T} + \hat{U})}$ . Since  $[\hat{T}, \hat{U}] \neq 0$ , the propagator cannot simply be split as  $e^{-i\Delta\hat{T}} e^{-i\Delta\hat{U}}$ , in which case both partial propagators could be applied one at a time since they are simply multiplication operators in spatial or momentum representation, respectively. However we can still use this first-order-splitting as an approximation:

$$e^{-i\Delta(\hat{T} + \hat{U})} = e^{-i\Delta\hat{U}} e^{-i\Delta\hat{T}} + \mathcal{O}(\Delta^2), \quad (\text{A.6})$$

which can be shown by Taylor-expanding all exponentials. This guarantees that for any fixed  $t = N\Delta$  the approximation becomes arbitrarily good if  $\Delta$  is small enough:

$$\begin{aligned} |\psi_N\rangle - |\psi_N^{\text{split}}\rangle &= \prod_{n=0}^N e^{-i\Delta(\hat{T}+\hat{U}_n)} |\psi_0\rangle - \prod_{n=0}^N e^{-i\Delta\hat{U}_n} e^{-i\Delta\hat{T}} |\psi_0\rangle \\ &= \left( \prod_{n=0}^N e^{-i\Delta(\hat{T}+\hat{U}_n)} - \underbrace{\prod_{n=0}^N [e^{-i\Delta(\hat{T}+\hat{U}_n)} + \mathcal{O}(\Delta^2)]}_{= [\prod_{n=0}^N e^{-i\Delta(\hat{T}+\hat{U}_n)}]_{+N\mathcal{O}(\Delta^2)}} \right) |\psi_0\rangle. \end{aligned}$$

Hence the total error in  $|\psi_N\rangle$  vanishes like  $N\mathcal{O}(\Delta^2) = \mathcal{O}(\Delta)$ . We see that it is important that the error in Eq. A.6 is  $\mathcal{O}(\Delta^2)$ , since  $\mathcal{O}(\Delta)$  would not have been sufficient.

We can further improve the behavior by splitting the propagator in second order:

$$e^{-i\Delta(\hat{T}+\hat{U})} = e^{-\frac{1}{2}i\Delta\hat{U}} e^{-i\Delta\hat{T}} e^{-\frac{1}{2}i\Delta\hat{U}} + \mathcal{O}(\Delta^3), \quad (\text{A.7})$$

which makes the total error vanish like  $\mathcal{O}(\Delta^3)$ . This is the splitting we use in our actual numerical calculations. In principle, arbitrarily high splitting orders can be constructed, but they are of little use to us here.

Finally, the split operator can be applied to a state by piecewise applying the potential and kinetic parts as if  $[\hat{T}, \hat{U}] = 0$ , assuming the time-step is small enough:

$$\psi(\mathbf{r}, t + \Delta) = e^{-\frac{1}{2}i\Delta U(\mathbf{r})} \mathcal{F}_{\mathbf{p} \rightarrow \mathbf{r}}^{-1} \left[ e^{-i\Delta \frac{p^2}{2}} \mathcal{F}_{\mathbf{r} \rightarrow \mathbf{p}} \left( e^{-\frac{1}{2}i\Delta U(\mathbf{r})} \psi(\mathbf{r}, t) \right) \right]. \quad (\text{A.8})$$

$\mathcal{F}$  denotes the Fourier transform:

$$\tilde{\psi}(\mathbf{p}) = (\mathcal{F}_{\mathbf{r} \rightarrow \mathbf{p}} \psi)(\mathbf{p}) = \int d^3r e^{-i\mathbf{p} \cdot \mathbf{r}} \psi(\mathbf{r}), \quad (\text{A.9})$$

$$\psi(\mathbf{r}) = (\mathcal{F}_{\mathbf{p} \rightarrow \mathbf{r}}^{-1} \tilde{\psi})(\mathbf{r}) = \frac{1}{(2\pi)^3} \int d^3p e^{i\mathbf{p} \cdot \mathbf{r}} \tilde{\psi}(\mathbf{p}). \quad (\text{A.10})$$

## A.2. Mean-field potential, convolution theorem and periodicity

In the preceding section we saw how to perform one time-step, assuming the potential  $\hat{U} = \hat{V} + \hat{V}_{\text{MF}}[\psi]$  is known. So, we still need to calculate the mean-field potential

$$V_{\text{MF}}[\psi](\mathbf{r}) = \int dr' W(\mathbf{r} - \mathbf{r}') |\psi(\mathbf{r}')|^2. \quad (\text{A.11})$$

This is trivial if  $W$  can be approximated as short-ranged as described in Chapter 2.3.2. If  $W(r) = g\delta(r)$ , then

$$V_{\text{MF}}[\psi](\mathbf{r}) = g|\psi(\mathbf{r})|^2 \quad (\text{A.12})$$

and no integral needs to be evaluated.

The situation is more difficult if  $W$  has a finite range such that the integral must explicitly be calculated numerically. In  $d$  dimensions, using a discrete and finite spatial grid with  $N$  grid points per dimension, the simple quadrature calculation of (A.11) costs  $\mathcal{O}(N^{2d})$  operations, since it needs to be performed for  $N^3$  values of  $\mathbf{r}$  and for each  $\mathbf{r}$ ,  $N^3$  values of  $W(\mathbf{r} - \mathbf{r}')|\psi(\mathbf{r}')|^2$  must be added up. This high cost can be improved upon by using the Fourier transform and the convolution theorem. Let

$$\tilde{W}(\mathbf{p}) = \int d\mathbf{r} e^{-i\mathbf{p}\cdot\mathbf{r}}W(\mathbf{r}) \quad (\text{A.13})$$

be the Fourier transform of  $W$  and  $\tilde{\rho}$  the Fourier transform of the density  $|\psi|^2$ , then the convolution theorem leads to

$$V_{\text{MF}}[\psi](\mathbf{r}) = \int d\mathbf{p} e^{i\mathbf{p}\cdot\mathbf{r}}\tilde{W}(\mathbf{p})\tilde{\rho}(\mathbf{p}), \quad (\text{A.14})$$

such that  $V_{\text{MF}}$  can be calculated by one Discrete Fourier transform (DFT), one pointwise multiplication between  $\tilde{W}$  and  $\tilde{\rho}$  and one inverse DFT. The cost of the multiplication is  $\mathcal{O}(N^d)$ , the cost of each DFT is  $\mathcal{O}(N^d \ln(N))$  if it is performed using a Fast Fourier Transform (FFT) algorithm<sup>1</sup>. Note that if one would not use an FFT algorithm but would calculate the DFT in a naive way, the total cost would be  $\mathcal{O}(N^{2d})$  just as with the naive quadrature calculation.

In the previous discussion we have switched freely between the continuous (integral) representation of the system and the numerically relevant discrete representation. For the most part this is unproblematic. However, there are two small complications when the continuous Fourier transform is replaced by the DFT: The discrete version of the convolution theorem implies periodicity of the density. This problem applies to the calculation of the mean-field potential. An equivalent problem exists with the application of the kinetic energy operator in Eq. (A.8). We will explicitly consider the ramifications for the mean-field potential; for the kinetic energy an equivalent result can be found.

Let  $\{\rho_n\}$  and  $\{W_n\}$  be infinite series representing the density and the interaction with  $\rho_n = W_n = 0 \forall n \notin [0, N + 1]$ . Then

$$\tilde{W}_k \tilde{\rho}_k = \sum_{n=0}^{N-1} \sum_{m=0}^{N-1} W_n \rho_m e^{-2\pi i \frac{k(n+m)}{N}} = \sum_{n=-\infty}^{\infty} \sum_{l=-\infty}^{\infty} W_n \rho_{l-n} e^{-2\pi i \frac{kl}{N}}$$

---

<sup>1</sup>In practice, we use the C subroutine library FFTW [68]

$$\begin{aligned}
 \Rightarrow \mathcal{F}_{k \rightarrow m}^{-1}(\tilde{W}_k \tilde{\rho}_k) &= \frac{1}{N} \sum_{k=0}^{N-1} e^{\frac{2\pi i k m}{N}} \sum_{n=-\infty}^{\infty} \sum_{l=-\infty}^{\infty} W_n \rho_{l-n} e^{-2\pi i \frac{k l}{N}} \\
 &= \frac{1}{N} \sum_{n=-\infty}^{\infty} \sum_{l=-\infty}^{\infty} W_n \rho_{l-n} \sum_{k=0}^{N-1} e^{-2\pi i \frac{k(l-m)}{N}} \\
 &= \sum_{n=-\infty}^{\infty} \sum_{l=-\infty}^{\infty} W_n \rho_{l-n} \sum_{j=-\infty}^{\infty} \delta_{l, m+jN} \\
 &= \sum_{n=-\infty}^{\infty} W_n \sum_{j=-\infty}^{\infty} \rho_{m+jN-n}.
 \end{aligned}$$

This means that any simulation using the convolution theorem will actually simulate an infinite number of systems that interact with each other. For the investigation of infinite systems this is a useful feature since it means that periodic boundary conditions apply automatically. For finite systems it is necessary to make the box so large that the interactions between the unit cells can be neglected.

### A.3. Generalization to rotating systems

In section 5.6 we investigated rotating systems by considering a Hamiltonian where the angular momentum operator  $\hat{L}_z$  appeared in the form

$$\hat{H} = \hat{T} + \hat{V} - \Omega \hat{L}_z, \quad (\text{A.15})$$

where  $\hat{V}$  summarizes all external and mean-field potentials. In the following it will be explained how this Hamiltonian is derived, what kind of rotation it exactly describes and how we can numerically implement it within the split-step-method described above.

#### A.3.1. Derivation of the Hamiltonian

The following derivation can also be found in [118], where it originates.

We consider a two-dimensional system with the Hamiltonian  $\hat{H} = \hat{T} + \hat{V}(t)$ .  $\hat{V}$  could be a mean-field potential, i.e. non-linear. For this derivation, this does not matter. The corresponding TDSE or GPE is

$$\hat{H} |\psi(t)\rangle = i\hbar \partial_t |\psi(t)\rangle. \quad (\text{A.16})$$

We will transform this equation into a frame that is rotating with an angular velocity  $\Omega$  that is perpendicular to the system (i.e. if the system is in the  $xy$ -plane,  $\Omega$  is in the  $z$ -direction):

The index  $i$  denotes a quantity in the inertial frame,  $r$  in the rotating frame. We have

$$\mathbf{v}_i = \mathbf{v}_r + \boldsymbol{\Omega} \times \mathbf{r}_r. \quad (\text{A.17})$$

The Lagrangian is

$$L = \frac{m}{2} v_i^2 - V = \frac{m}{2} (\mathbf{v}_r + \boldsymbol{\Omega} \times \mathbf{r}_r)^2 - V \quad (\text{A.18})$$

$$\begin{aligned} \mathbf{p}_r &= \frac{\partial L}{\partial \mathbf{v}_r} = m (\mathbf{v}_r + \boldsymbol{\Omega} \times \mathbf{r}_r) \\ \Rightarrow L &= \frac{p_r^2}{2m} - V \\ \text{and } \mathbf{v}_r &= \frac{\mathbf{p}_r}{m} - \boldsymbol{\Omega} \times \mathbf{r}_r \\ \Rightarrow v_r^2 &= \frac{p_r^2}{m^2} + (\boldsymbol{\Omega} \times \mathbf{r}_r)^2 - 2 \frac{\mathbf{p}_r}{m} \cdot (\boldsymbol{\Omega} \times \mathbf{r}_r). \end{aligned}$$

So, we find for the Hamiltonian:

$$\begin{aligned} H &= \mathbf{p}_r \cdot \mathbf{v}_r - L = m (\mathbf{v}_r + \boldsymbol{\Omega} \times \mathbf{r}_r) \cdot \mathbf{v}_r - \frac{p_r^2}{2m} + V \\ &= m (v_r^2 + \mathbf{v}_r \cdot (\boldsymbol{\Omega} \times \mathbf{r}_r)) - \frac{p_r^2}{2m} + V \\ &= m \left( \frac{p_r^2}{m^2} + (\boldsymbol{\Omega} \times \mathbf{r}_r)^2 - 2 \frac{\mathbf{p}_r}{m} \cdot (\boldsymbol{\Omega} \times \mathbf{r}_r) + \mathbf{v}_r \cdot (\boldsymbol{\Omega} \times \mathbf{r}_r) \right) - \frac{p_r^2}{2m} + V \\ &= \frac{p_r^2}{2m} + m (\boldsymbol{\Omega} \times \mathbf{r}_r)^2 - 2 \mathbf{p}_r \cdot (\boldsymbol{\Omega} \times \mathbf{r}_r) + m \left( \frac{\mathbf{p}_r}{m} - \boldsymbol{\Omega} \times \mathbf{r}_r \right) \cdot (\boldsymbol{\Omega} \times \mathbf{r}_r) + V \\ &= \frac{p_r^2}{2m} + m (\boldsymbol{\Omega} \times \mathbf{r}_r)^2 - \mathbf{p}_r \cdot (\boldsymbol{\Omega} \times \mathbf{r}_r) - m (\boldsymbol{\Omega} \times \mathbf{r}_r)^2 + V \\ &= \frac{p_r^2}{2m} - \mathbf{p}_r \cdot (\boldsymbol{\Omega} \times \mathbf{r}_r) + V \\ &= \frac{p_r^2}{2m} - \boldsymbol{\Omega} \cdot (\mathbf{r}_r \times \mathbf{p}_r) + V. \end{aligned}$$

Since the system is supposed to rotate around the  $z$ -axis, we have  $\boldsymbol{\Omega} = (0, 0, \Omega)$ . In the formula we recognize the angular momentum  $\mathbf{L}_z = \mathbf{r}_r \times \mathbf{p}_r$ . Hence, we find

$$H = \frac{p_r^2}{2m} - \Omega L_z + V,$$

which we can quantize, yielding the Hamiltonian

$$\hat{H} = \frac{\hat{p}^2}{2m} - \Omega \hat{L}_z + \hat{V},$$

q.e.d.

### A.3.2. Numerical implementation

First, since  $[\hat{T}, \hat{L}_z] = 0$  the additional term  $-\Omega \hat{L}_z$  can be incorporated in the split step method simply by

$$e^{-i\hat{H}t} \approx e^{-\frac{1}{2}i\hat{U}t} e^{-i\hat{T}t} e^{-\Omega \hat{L}_z t} e^{-\frac{1}{2}i\hat{U}t}. \quad (\text{A.19})$$

Now, we still need an efficient way to apply  $e^{-i\Omega \hat{L}_z t}$ . There are two possible ways of doing this:

- In polar coordinates  $(r, \varphi)$  the angular momentum is  $\hat{L}_z = -i\partial_\varphi$ . Therefore,  $\hat{L}_z$  is a multiplication operator in angular momentum space and  $e^{-\frac{1}{2}i\hat{L}_z t}$  can be applied by transforming the wavefunction into polar coordinates, Fourier transforming and multiplying. Unfortunately, this works well only if the wavefunction is rotational symmetric, in which case  $\hat{L}_z |\psi\rangle = 0$ , anyway. In other cases the rounding errors when transforming to polar coordinates tend to destabilize the numerics.
- in Cartesian coordinates it is  $\hat{L}_z = i(y\partial_x - x\partial_y)$ . We can again split

$$e^{-i\Omega \hat{L}_z t} \approx e^{\frac{\Omega t}{2} y \partial_x} e^{-\Omega t x \partial_y} e^{\frac{\Omega t}{2} y \partial_x}.$$

Then,  $e^{-\Omega t x \partial_y}$  can be applied by performing a 1D Fourier transform (with respect to  $y$ ) and a multiplication and  $e^{\frac{\Omega t}{2} y \partial_x}$  analogously. This method turned out to work very well and it is what we used in practice.

### A.4. Imaginary time evolution

The imaginary time evolution is a method to calculate the ground state of a Hamiltonian. It works by solving the imaginary-time Schrödinger equation

$$\partial_t |\psi(t)\rangle = \hat{H} |\psi(t)\rangle. \quad (\text{A.20})$$

If the initial state is  $|\psi(0)\rangle = |\psi_0\rangle$ , it can formally be solved by the propagation equation

$$|\psi(t)\rangle = e^{-\hat{H}t} |\psi_0\rangle. \quad (\text{A.21})$$

We assume that the eigenstates and -values of  $\hat{H}$  are  $|i\rangle$  and  $E_i$  with  $|0\rangle$  the ground state. We write the initial state in that basis:

$$|\psi_0\rangle = \sum_i c_i |i\rangle, \quad (\text{A.22})$$

then Eq. (A.21) becomes

$$|\psi(t)\rangle = \sum_i c_i e^{-E_i t} |i\rangle. \quad (\text{A.23})$$

For  $t \rightarrow \infty$ , all summands with  $E_i > 0$  vanish, all with  $E_i < 0$  diverge. These divergences can be removed by renormalizing the state<sup>2</sup>, i.e., by using the modified equation

$$|\psi(t)\rangle = \frac{\sum_i c_i e^{-E_i t} |i\rangle}{\sqrt{\langle \psi(t) | \psi(t) \rangle}} = \frac{\sum_i c_i e^{-E_i t} |i\rangle}{\sqrt{\sum_i |c_i e^{-E_i t}|^2}} = \frac{\sum_i c_i e^{-(E_i - E_0)t} |i\rangle}{\sqrt{\sum_i |c_i e^{-(E_i - E_0)t}|^2}}. \quad (\text{A.24})$$

Then, we see that

$$\lim_{t \rightarrow \infty} |\psi(t)\rangle = |0\rangle, \quad (\text{A.25})$$

unless  $c_0 = 0$ . Hence, unless the ground state has no overlap with the initial state, the procedure will converge to the ground state. More generally, it will always converge to the lowest-lying state  $|i\rangle$  such that  $c_i \neq 0$ .

If the Hamiltonian has degenerate ground states, the procedure will converge to *a* ground state, i.e., a state from the ground state vector space. The precise form of the final state depends on the initial state.

In general, the method does not work for a Gross-Pitaevskii equation. Because it is non-linear, the superposition principle does not hold and the above proof fails. The nonlinearity also manifests itself in the existence of a large number of meta-stable states which the method can converge to. Such states do not exist within the framework of a Schrödinger equation.

However, even for a GPE, the method still decreases the energy. Hence, it can be used for a GPE, provided that a suitable initial state can be chosen, thus avoiding convergence to a metastable state.

---

<sup>2</sup>In practice, this should be done by normalizing the state  $|\psi(t)\rangle$  after every discrete time step.



## B. Clebsch-Gordan coefficients

The Clebsch-Gordan coefficients (3.61)

$$\mathbf{C}_0^a = \mathbf{C}_{l_0, j_0, m_0}^{l_a, j_a, m_a} = \int d\varphi d(\cos \vartheta) \overline{\mathcal{Y}_{l_0 j_0 m_0}(\vartheta, \varphi)} \begin{pmatrix} \sin \vartheta \cos \varphi \\ \sin \vartheta \sin \varphi \\ \cos \vartheta \end{pmatrix} \mathcal{Y}_{l_a j_a m_a}(\vartheta, \varphi), \quad (\text{B.1})$$

are the angular integrals used to calculate dipole matrix elements (and subsequently van-der-Waals interaction between Rydberg states) in chapter 3 (Eq. (3.61)). For convenience we write  $d\Omega = d\varphi d(\cos \vartheta)$ . As before,  $s_a = 2(j_a - l_a) \in \{-1, 1\}$ . We use the basis

$$(\mathbf{e}_1, \mathbf{e}_2, \mathbf{e}_3) = \left( \frac{\mathbf{e}_x + i\mathbf{e}_y}{\sqrt{2}}, \frac{\mathbf{e}_x - i\mathbf{e}_y}{\sqrt{2}}, \mathbf{e}_z \right)$$

as the basis of position space. Then, we can evaluate the coefficients by using the relation between spherical harmonics and Wigner-3j-symbols:

$$\begin{aligned} & \int d\Omega Y_{l_1}^{m_1}(\vartheta, \varphi) Y_l^m(\vartheta, \varphi) Y_{l_2}^{m_2}(\vartheta, \varphi) \\ &= \sqrt{\frac{(2l_1 + 1)(2l + 1)(2l_2 + 1)}{4\pi}} \begin{pmatrix} l_1 & l & l_2 \\ 0 & 0 & 0 \end{pmatrix} \begin{pmatrix} l_1 & l & l_2 \\ m_1 & m & m_2 \end{pmatrix} \end{aligned}$$

We calculate the contributions of each dimension separately, with the abbreviation  $\lambda_{\pm} = \sqrt{(l_0 + \frac{1}{2} \pm s_0 m_0)(l_a + \frac{1}{2} \pm s_a m_a)}$ :

$$\begin{aligned} & \mathbf{e}_3 \cdot \mathbf{C}_{l_0, j_0, m_0}^{l_a, j_a, m_a} \\ &= \int d\Omega \overline{\mathcal{Y}_{l_0 j_0 m_0}} \cos(\vartheta) \mathcal{Y}_{j_a m_a l_a} = \sqrt{\frac{4\pi}{3}} \int d\Omega \overline{\mathcal{Y}_{l_0 j_0 m_0}} Y_1^0 \mathcal{Y}_{j_a m_a l_a} \\ &= \sqrt{\frac{4\pi}{3}} \frac{1}{(2l_0 + 1)(2l_a + 1)} \int d\Omega Y_1^0 \left[ s_0 s_a \lambda_+ \overline{Y_{l_0}^{m_0 - \frac{1}{2}}} Y_{l_a}^{m_a - \frac{1}{2}} + \lambda_- \overline{Y_{l_0}^{m_0 + \frac{1}{2}}} Y_{l_a}^{m_a + \frac{1}{2}} \right] \\ &= \sqrt{\frac{4\pi}{3}} \frac{1}{(2l_0 + 1)(2l_a + 1)} \int d\Omega Y_1^0 \left[ s_0 s_a \lambda_+ (-1)^{m_0 - \frac{1}{2}} Y_{l_0}^{-m_0 + \frac{1}{2}} Y_{l_a}^{m_a - \frac{1}{2}} \right. \\ & \quad \left. + \lambda_- (-1)^{m_0 + \frac{1}{2}} Y_{l_0}^{-m_0 - \frac{1}{2}} Y_{l_a}^{m_a + \frac{1}{2}} \right] \end{aligned}$$

$$\begin{aligned}
 &= \frac{\sqrt{\pi}(-1)^{m_0+\frac{1}{2}}}{\sqrt{3}(l_0+\frac{1}{2})(l_a+\frac{1}{2})} \left[ s_0 s_a \lambda_+ \sqrt{\frac{(2l_0+1)3(2l_a+1)}{4\pi}} \begin{pmatrix} l_0 & 1 & l_a \\ \frac{1}{2}-m_0 & 0 & m_a-\frac{1}{2} \end{pmatrix} \right. \\
 &\quad \left. - \lambda_- \sqrt{\frac{(2l_0+1)3(2l_a+1)}{4\pi}} \begin{pmatrix} l_0 & 1 & l_a \\ \frac{1}{2}-m_0 & 0 & m_a-\frac{1}{2} \end{pmatrix} \right] \begin{pmatrix} l_0 & 1 & l_a \\ 0 & 0 & 0 \end{pmatrix} \\
 &= (-1)^{m_0+\frac{1}{2}} \begin{pmatrix} l_0 & 1 & l_a \\ 0 & 0 & 0 \end{pmatrix} \left[ s_0 s_a \lambda_+ \begin{pmatrix} l_0 & 1 & l_a \\ \frac{1}{2}-m_0 & 0 & m_a-\frac{1}{2} \end{pmatrix} \right. \\
 &\quad \left. - \lambda_- \begin{pmatrix} l_0 & 1 & l_a \\ -m_0-\frac{1}{2} & 0 & m_a+\frac{1}{2} \end{pmatrix} \right].
 \end{aligned}$$

The calculation of the other components proceeds in the same way:

$$\begin{aligned}
 &\mathbf{e}_1 \cdot \mathbf{C}_{l_0, j_0, m_0}^{l_a, j_a, m_a} \\
 &= \int d\Omega \frac{\overline{\mathcal{Y}_{l_0 j_0 m_0}} \sin \vartheta \cos \varphi + i \sin \vartheta \sin \varphi}{\sqrt{2}} \mathcal{Y}_{j_a m_a l_a} = -\sqrt{\frac{4\pi}{3}} \int d\Omega \overline{\mathcal{Y}_{l_0 j_0 m_0}} Y_1^1 \mathcal{Y}_{j_a m_a l_a} \\
 &= -(-1)^{m_0+\frac{1}{2}} \begin{pmatrix} l_0 & 1 & l_a \\ 0 & 0 & 0 \end{pmatrix} \left[ s_0 s_a \lambda_+ \begin{pmatrix} l_0 & 1 & l_a \\ \frac{1}{2}-m_0 & 1 & m_a-\frac{1}{2} \end{pmatrix} \right. \\
 &\quad \left. - \lambda_- \begin{pmatrix} l_0 & 1 & l_a \\ -m_0-\frac{1}{2} & 1 & m_a+\frac{1}{2} \end{pmatrix} \right],
 \end{aligned}$$

$$\begin{aligned}
 &\mathbf{e}_2 \cdot \mathbf{C}_{l_0, j_0, m_0}^{l_a, j_a, m_a} \\
 &= \int d\Omega \frac{\overline{\mathcal{Y}_{l_0 j_0 m_0}} \sin \vartheta \cos \varphi - i \sin \vartheta \sin \varphi}{\sqrt{2}} \mathcal{Y}_{j_a m_a l_a} = \sqrt{\frac{4\pi}{3}} \int d\Omega \overline{\mathcal{Y}_{l_0 j_0 m_0}} Y_1^{-1} \mathcal{Y}_{j_a m_a l_a} \\
 &= (-1)^{m_0+\frac{1}{2}} \begin{pmatrix} l_0 & 1 & l_a \\ 0 & 0 & 0 \end{pmatrix} \left[ s_0 s_a \lambda_+ \begin{pmatrix} l_0 & 1 & l_a \\ \frac{1}{2}-m_0 & -1 & m_a-\frac{1}{2} \end{pmatrix} \right. \\
 &\quad \left. - \lambda_- \begin{pmatrix} l_0 & 1 & l_a \\ -m_0-\frac{1}{2} & -1 & m_a+\frac{1}{2} \end{pmatrix} \right].
 \end{aligned}$$

Summarizing, all components can be written as

$$\begin{aligned}
 &\mathbf{e}_i \cdot \mathbf{C}_{l_0, j_0, m_0}^{l_a, j_a, m_a} \\
 &= c_i (-1)^{m_0+\frac{1}{2}} \begin{pmatrix} l_0 & 1 & l_a \\ 0 & 0 & 0 \end{pmatrix} \left[ s_0 s_a \lambda_+ \begin{pmatrix} l_0 & 1 & l_a \\ \frac{1}{2}-m_0 & \mu_i & m_a-\frac{1}{2} \end{pmatrix} \right. \\
 &\quad \left. - \lambda_- \begin{pmatrix} l_0 & 1 & l_a \\ -m_0-\frac{1}{2} & \mu_i & m_a+\frac{1}{2} \end{pmatrix} \right], \quad (\text{B.2})
 \end{aligned}$$

with  $\mu_1 = 1, \mu_2 = -1, \mu_3 = 0$  and  $c_1 = -1, c_2 = c_3 = 1$ .

## C. Superfluidity

### C.1. Leggett's estimator for rotating motion

Following the idea of Leggett [120], one can calculate an estimate of the superfluid fraction based on only the one-particle density. Hence, this method is suitable for use within the mean-field approximation. Consider a gas in a container which has the form of a ring of with a very small width  $d$  and hence almost identical inner and outer Radii  $R_1 \approx R_2 =: R$  (see Fig. C.1). If we write the ground state wave function  $\psi'$  using the

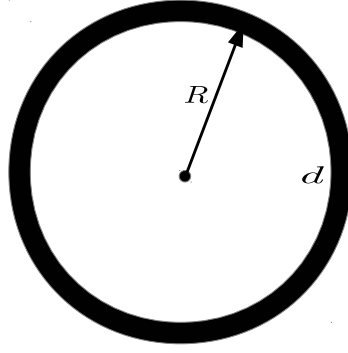


Figure C.1.: Ring of Radius  $R$  and width  $d \ll R$ .

polar coordinate  $\vartheta'$ , it obeys the dimensionless GPE and periodicity condition

$$\left( \frac{1}{R^2} \partial_{\vartheta'}^2 + V_{ext}(\vartheta') + V_{MF}[\psi'](\vartheta') \right) \psi'(\vartheta') = E \psi'(\vartheta') \quad (\text{C.1})$$

$$\psi'(\vartheta' + 2\pi) = \psi'(\vartheta') \quad (\text{C.2})$$

if no rotation is involved. Note that  $\psi'$  can always be assumed to be real. We now consider rotation by assuming that the container (and hence, the external potential) is rotating with an angular velocity  $\omega$ , i.e.  $V_{ext}(t, \vartheta') = V_{ext}(0, \vartheta' - \omega t)$ . We now move to the corresponding rotating frame where the potential is constant. This is done by the transformation

$$\vartheta' = \vartheta + \omega t \quad (\text{C.3})$$

$$\psi'(\vartheta') = \psi(\vartheta) e^{-i\omega R^2 \vartheta}. \quad (\text{C.4})$$

The transformed wave function  $\psi$  then obeys the modified condition

$$\psi(\vartheta + 2\pi) = \psi(\vartheta) e^{-2\pi i \omega R^2}. \quad (\text{C.5})$$

### C. Superfluidity

---

We can define a quantum mechanical moment of inertia  $I_{qm}$  by calculating the energy in the rest frame

$$E(\omega) = E(0) + \frac{1}{2}I_{qm}\omega^2. \quad (\text{C.6})$$

If the system is classical, then we have  $I_{qm} = I_{cl} = R^2 \int d\vartheta \rho(\vartheta)$  with  $\rho(\vartheta) = |\psi(\vartheta)|^2$ . However, in general we will find that  $I_{qm} = I_{cl} - I_{sfl} \leq I_{cl}$ , because (due to superfluidity) not all particles participate in the rotation of the container. The superfluid fraction can be calculated as

$$f_s = \frac{I_{qm}}{I_{cl}} = \frac{\partial_\omega^2 E(\omega)}{R^2 \int d\vartheta \rho(\vartheta)}. \quad (\text{C.7})$$

Furthermore, at small rotation frequencies  $\omega$ , the density  $\rho$  of the gas is not changed with respect to  $\omega = 0$ . Hence, the difference in energies between the two corresponding ground states is only due to the phase difference  $\varphi$ :

$$E(\omega) = E(0) + \frac{1}{2R^2} \int d\vartheta (\partial_\vartheta \varphi(\vartheta))^2 \rho(\vartheta) \quad (\text{C.8})$$

$\varphi$  is that phase that obeys the periodicity condition  $\varphi(2\pi) = \varphi(0) - 2\pi R^2 \omega$  and at the same time minimizes  $E(\omega)$ . To find this phase, we introduce a Lagrangian multiplier  $\lambda$  and consider

$$\tilde{E}(\omega) = \int d\vartheta (\partial_\vartheta \varphi(\vartheta))^2 \rho(\vartheta) + \lambda(\varphi(2\pi) + \varphi(0) + 2\pi m R^2 \omega) \quad (\text{C.9})$$

and its functional derivative

$$0 \stackrel{!}{=} \frac{\delta E(\omega)}{\delta(\varphi(\vartheta))} = \frac{\partial}{\partial \vartheta} \frac{\delta E(\omega)}{\delta(\partial_\vartheta \varphi(\vartheta))} = \frac{\partial}{\partial \vartheta} [2\rho(\vartheta) \partial_\vartheta \varphi(\vartheta)]. \quad (\text{C.10})$$

Hence,

$$\partial_\vartheta \varphi(\vartheta) = \frac{c}{\rho(\vartheta)} \quad (\text{C.11})$$

with a constant  $c$  that we can determine:

$$2\pi R^2 \omega = \varphi(2\pi) - \varphi(0) = \int_0^{2\pi} d\vartheta \partial_\vartheta \varphi(\vartheta) = c \int_0^{2\pi} \frac{d\vartheta}{\rho(\vartheta)} \quad (\text{C.12})$$

$$\Rightarrow c = \frac{2\pi R^2 \omega}{\int_0^{2\pi} d\vartheta \rho(\vartheta)^{-1}}. \quad (\text{C.13})$$

With this, we find for the energy

$$E(\omega) = E(0) + \frac{1}{2R^2} \int d\vartheta \left( \frac{c}{\rho(\vartheta)} \right)^2 \rho(\vartheta) \quad (\text{C.14})$$

$$= E(0) + \frac{2\pi^2 m^2 R^2 \omega^2}{\int_0^{2\pi} d\vartheta \rho(\vartheta)^{-1}}, \quad (\text{C.15})$$

so that finally

$$f_s = \frac{4\pi^2}{\left( \int_0^{2\pi} d\vartheta \rho(\vartheta)^{-1} \right) \left( \int_0^{2\pi} d\vartheta \rho(\vartheta) \right)}. \quad (\text{C.16})$$

This is the result that we claimed in section 5.5.1. Leggett's estimator can also be generalized to linear motion (as opposed to rotation). This makes it suitable for the calculation of superfluidity in bulk systems. The derivation is given in the next section.

## C.2. Leggett's estimator for linear motion

The same idea as before can be applied to an infinite system that is subjected to a linear acceleration. This time, we consider a wave function with a discrete translational periodicity.

If we write the 1D ground state wave function  $\psi'$  using the single coordinate  $x'$ , it obeys GPE and periodicity condition

$$\psi'(x' + L) = \psi'(x') \quad (\text{C.17})$$

if no rotation is involved. The external potential is moving with a velocity  $v$ , i.e.  $V_{ext}(t, x') = V_{ext}(0, x' - vt)$ . We transform to the frame where the potential is constant by the transformation

$$x' = x + vt \quad (\text{C.18})$$

$$\psi'(x') = \psi(x) e^{-ivx}. \quad (\text{C.19})$$

The transformed wave function obeys

$$\psi(x + L) = \psi(x) e^{-iLv}. \quad (\text{C.20})$$

Analogously to the quantum mechanical moment of inertia  $I_{qm}$  from before, we can define a quantum mechanical inert mass by calculating the energy in the rest frame

$$E(\omega) = E(0) + \frac{1}{2} m_{qm} v^2. \quad (\text{C.21})$$

The superfluid fraction can be calculated as

$$f_s = \frac{m_{qm}}{m} = \frac{\partial_v^2 E(v)}{\int dx \rho(x)}. \quad (\text{C.22})$$

The difference in energies between the two corresponding ground states is, again, only due to the phase difference  $\varphi$ :

$$E(\omega) = E(0) + \frac{1}{2} \int_{-\infty}^{\infty} dx (\partial_x \varphi(x))^2 \rho(x) \quad (\text{C.23})$$

where  $\varphi$  obeys  $\varphi(L) = \varphi(0) - mLv$  and minimizes  $E(\omega)$ . We apply the same Lagrangian method as before and obtain after an equivalent calculation:

$$f_s = f_s^{(L)} = \frac{L^2}{\left(\int_0^L dx \rho(x)^{-1}\right) \left(\int_0^L dx \rho(x)\right)}. \quad (\text{C.24})$$

Note that  $L$  can be any length with respect to which  $\psi$  is periodic. In particular, if  $\psi$  is  $L$ -periodic, it is also  $mL$ -periodic for any  $m \in \mathbb{Z}$ . The formula is consistent with this since we easily see

$$f_s^{(mL)} = f_s^{(L)}. \quad (\text{C.25})$$

We have not used this result for linear motion in the context of this thesis, but it might be useful for later studies.

# Bibliography

- [1] M. J. Ablowitz and P. A. Clarkson. *Solitons, Nonlinear Evolution Equations and Inverse Scattering*. London Mathematical Society Lecture Note Series, 1991.
- [2] J. R. Abo-Shaeer, C. Raman, J. M. Vogels, and W. Ketterle. Observation of Vortex Lattices in Bose-Einstein Condensates. *Science* **292**, (5516) 476–479, 2001. doi: 10.1126/science.1060182.
- [3] G. P. Agrawal. *Nonlinear Fiber Optics*. Academic Press, San Diego, third edition, 2001.
- [4] K. Aikawa, A. Frisch, M. Mark, S. Baier, A. Rietzler, R. Grimm, and F. Ferlaino. Bose-Einstein Condensation of Erbium. *Phys. Rev. Lett.* **108**, 210401, 2012. doi: 10.1103/PhysRevLett.108.210401.
- [5] J. F. Allen and A. D. Misener. Flow Phenomena in Liquid Helium II. *Nature* **142**, 643–644, 1938. doi: 10.1038/142643a0.
- [6] E. Anderson, Z. Bai, C. Bischof, S. Blackford, J. Demmel, J. Dongarra, J. Du Croz, A. Greenbaum, S. Hammarling, A. McKenney, and D. Sorensen. *LAPACK Users' Guide*. Society for Industrial and Applied Mathematics, Philadelphia, PA, third edition, 1999. doi: 10.1137/1.9780898719604.
- [7] M. H. Anderson, J. R. Ensher, M. R. Matthews, C. E. Wieman, and E. A. Cornell. Observation of Bose-Einstein Condensation in a Dilute Atomic Vapor. *Science* **269**, 198–201, 1995. doi: 10.1126/science.269.5221.198.
- [8] P. W. Anderson. A Gross-Pitaevskii Treatment for Supersolid Helium. *Science* **324**, (5927) 631–632, 2009. doi: 10.1126/science.1169456.
- [9] A. F. Andreev, K. Keshishev, L. Mezhev-Deglin, and A. Shal'nikov. Attempts at observing vacancies in He crystals. *Sov. Phys. JETP Lett.* **9**, 306, 1969.
- [10] A. F. Andreev and I. M. Lifshitz. Quantum Theory of Defects in Crystals. *Soviet Physics Uspekhi* **13**, 670, 1971. doi: 10.1070/PU1971v013n05ABEH004235.
- [11] P. Arnold and G. Moore. BEC Transition Temperature of a Dilute Homogeneous Imperfect Bose Gas. *Phys. Rev. Lett.* **87**, 120401, 2001. doi: 10.1103/PhysRevLett.87.120401.
- [12] R. A. Aziz, V. P. S. Nain, J. S. Carley, W. L. Taylor, and G. T. McConville. An accurate intermolecular potential for helium. *The Journal of Chemical Physics* **70**, (9) 4330–4342, 1979. doi: 10.1063/1.438007.
- [13] L. R. B., S. D. C., and Y. C. *ARPACK Users' Guide*. Society for Industrial and Applied Mathematics, 1998. doi: 10.1137/1.9780898719628.

- [14] S. Balibar. The enigma of supersolidity. *Nature* **464**, 176–182, 2010. doi: 10.1038/nature08913.
- [15] V. Bendkowsky, B. Butscher, J. Nipper, J. B. Balewski, J. P. Shaffer, R. Löw, T. Pfau, W. Li, J. Stanojevic, T. Pohl, and J. M. Rost. Rydberg Trimers and Excited Dimers Bound by Internal Quantum Reflection. *Phys. Rev. Lett.* **105**, 163201, 2010. doi: 10.1103/PhysRevLett.105.163201.
- [16] V. Bendkowsky, B. Butscher, J. Nipper, J. P. Shaffer, R. Löw, and T. Pfau. Observation of ultralong-range Rydberg molecules. *Nature* **458**, 1005–1008, 2009. doi: 10.1038/nature07945.
- [17] V. Berezinskii. Destruction of long-range order in one-dimensional and two-dimensional systems with a continuous symmetry group. *Sov. Phys. JETP* **32**, 493, 1971.
- [18] L. Bergé. Wave collapse in physics: principles and applications to light and plasma waves. *Physics Reports* **303**, 259 – 370, 1998. doi: 10.1016/S0370-1573(97)00092-6.
- [19] I. I. Beterov, I. I. Ryabtsev, D. B. Tretyakov, and V. M. Entin. Quasiclassical calculations of blackbody-radiation-induced depopulation rates and effective lifetimes of Rydberg nS, nP, and nD alkali-metal atoms with  $n \leq 80$ . *Phys. Rev. A* **79**, 052504, 2009. doi: 10.1103/PhysRevA.79.052504.
- [20] D. J. Bishop, M. A. Paalanen, and J. D. Reppy. Search for superfluidity in hcp  $^4\text{He}$ . *Phys. Rev. B* **24**, 2844–2845, 1981. doi: 10.1103/PhysRevB.24.2844.
- [21] P. B. Blakie, D. Baillie, and R. N. Bisset. Roton spectroscopy in a harmonically trapped dipolar Bose-Einstein condensate. *Phys. Rev. A* **86**, 021604, 2012. doi: 10.1103/PhysRevA.86.021604.
- [22] I. Bloch. Ultracold quantum gases in optical lattices. *Nature Physics* **1**, 23–30, 2005. doi: 10.1038/nphys138.
- [23] I. Bloch, J. Dalibard, and W. Zwerger. Many-body physics with ultracold gases. *Rev. Mod. Phys.* **80**, 885–964, 2008. doi: 10.1103/RevModPhys.80.885.
- [24] H. M. J. M. Boesten, C. C. Tsai, J. R. Gardner, D. J. Heinzen, and B. J. Verhaar. Observation of a shape resonance in the collision of two cold  $^{87}\text{Rb}$  atoms. *Phys. Rev. A* **55**, 636–640, 1997. doi: 10.1103/PhysRevA.55.636.
- [25] M. Boninsegni, N. Prokof'ev, and B. Svistunov. Superglass Phase of  $^4\text{He}$ . *Phys. Rev. Lett.* **96**, 105301, 2006. doi: 10.1103/PhysRevLett.96.105301.
- [26] M. Boninsegni, N. Prokof'ev, and B. Svistunov. Worm Algorithm for Continuous-Space Path Integral Monte Carlo Simulations. *Phys. Rev. Lett.* **96**, (7) 070601, 2006. doi: 10.1103/PhysRevLett.96.070601.

- 
- [27] M. Boninsegni and N. V. Prokof'ev. *Colloquium: Supersolids: What and where are they?* *Rev. Mod. Phys.* **84**, 759–776, 2012. doi: 10.1103/RevModPhys.84.759.
- [28] M. Boninsegni, N. V. Prokof'ev, and B. V. Svistunov. Worm algorithm and diagrammatic Monte Carlo: A new approach to continuous-space path integral Monte Carlo simulations. *Phys. Rev. E* **74**, (3) 036701, 2006. doi: 10.1103/PhysRevE.74.036701.
- [29] M. Born and V. Fock. Beweis des Adiabatenatzes. *Zeitschrift für Physik A Hadrons and Nuclei* **51**, 165–180, 1928.
- [30] S. N. Bose. Plancks Gesetz und Lichtquantenhypothese. *Zeitschrift für Physik* **26**, 178, 1924. doi: 10.1007/BF01327326.
- [31] C. C. Bradley, C. A. Sackett, J. J. Tollett, and R. G. Hulet. Evidence of Bose-Einstein Condensation in an Atomic Gas with Attractive Interactions. *Phys. Rev. Lett.* **75**, 1687–1690, 1995. doi: 10.1103/PhysRevLett.75.1687.
- [32] D. B. Branden, T. Juhasz, T. Mahlokozera, C. Vesa, R. O. Wilson, M. Zheng, A. Kortyna, and D. A. Tate. Radiative lifetime measurements of rubidium Rydberg states. *Journal of Physics B: Atomic, Molecular and Optical Physics* **43**, (1) 015002, 2010. doi: 10.1088/0953-4075/43/1/015002.
- [33] H. P. Büchler, E. Demler, M. Lukin, A. Micheli, N. Prokof'ev, G. Pupillo, and P. Zoller. Strongly Correlated 2D Quantum Phases with Cold Polar Molecules: Controlling the Shape of the Interaction Potential. *Phys. Rev. Lett.* **98**, 060404, 2007. doi: 10.1103/PhysRevLett.98.060404.
- [34] H. P. Büchler, A. Micheli, and P. Zoller. Three-body interactions with cold polar molecules. *Nature Physics* **3**, 726–731, 2007. doi: 10.1038/nphys678.
- [35] B. Butscher, V. Bendkowsky, J. Nipper, J. B. Balewski, L. Kukota, R. Löw, T. Pfau, W. Li, T. Pohl, and J. M. Rost. Lifetimes of ultralong-range Rydberg molecules in vibrational ground and excited states. *Journal of Physics B: Atomic, Molecular and Optical Physics* **44**, (18) 184004, 2011. doi: 10.1088/0953-4075/44/18/184004.
- [36] D. M. Ceperley. Path integrals in the theory of condensed helium. *Rev. Mod. Phys.* **67**, 279–355, 1995. doi: 10.1103/RevModPhys.67.279.
- [37] G. V. Chester. Speculations on Bose-Einstein Condensation and Quantum Crystals. *Phys. Rev. A* **2**, 256–258, 1970. doi: 10.1103/PhysRevA.2.256.
- [38] H. Choi, D. Takahashi, K. Kono, and E. Kim. Evidence of Supersolidity in Rotating Solid Helium. *Science* **330**, (6010) 1512–1515, 2010. doi: 10.1126/science.1196409.

- [39] P. L. Christiansen and S. Alwyn. *Davydov's soliton revisited: self-trapping of vibrational energy in protein*. Plenum Press, 1990.
- [40] F. Cinti, P. Jain, M. Boninsegni, A. Micheli, P. Zoller, and G. Pupillo. Supersolid Droplet Crystal in a Dipole-Blockaded Gas. *Phys. Rev. Lett.* **105**, 135301, 2010. doi: 10.1103/PhysRevLett.105.135301.
- [41] B. K. Clark and D. M. Ceperley. Off-Diagonal Long-Range Order in Solid  $^4\text{He}$ . *Phys. Rev. Lett.* **96**, 105302, 2006. doi: 10.1103/PhysRevLett.96.105302.
- [42] C. Cohen-Tannoudji, B. Diu, and F. Laloë. *Quantenmechanik, Band 2*. de Gruyter, Berlin, 2008.
- [43] C. Conti, M. Peccianti, and G. Assanto. Observation of Optical Spatial Solitons in a Highly Nonlocal Medium. *Phys. Rev. Lett.* **92**, 113902, 2004. doi: 10.1103/PhysRevLett.92.113902.
- [44] N. R. Cooper, E. H. Rezayi, and S. H. Simon. Vortex Lattices in Rotating Atomic Bose Gases with Dipolar Interactions. *Phys. Rev. Lett.* **95**, 200402, 2005. doi: 10.1103/PhysRevLett.95.200402.
- [45] S. L. Cornish, N. R. Claussen, J. L. Roberts, E. A. Cornell, and C. E. Wieman. Stable  $^{85}\text{Rb}$  Bose-Einstein Condensates with Widely Tunable Interactions. *Phys. Rev. Lett.* **85**, 1795–1798, 2000. doi: 10.1103/PhysRevLett.85.1795.
- [46] F. Dalfovo, S. Giorgini, L. P. Pitaevskii, and S. Stringari. Theory of Bose-Einstein condensation in trapped gases. *Rev. Mod. Phys.* **71**, 463–512, 1999. doi: 10.1103/RevModPhys.71.463.
- [47] J. Dalibard and C. Cohen-Tannoudji. Laser cooling and trapping of neutral atoms. In R. Campargue, editor, *Atomic and Molecular Beams, The State of the Art 2000*, pages 43–62. Springer, 2001.
- [48] K. B. Davis, M. O. Mewes, M. R. Andrews, N. J. van Druten, D. S. Durfee, D. M. Kurn, and W. Ketterle. Bose-Einstein Condensation in a Gas of Sodium Atoms. *Phys. Rev. Lett.* **75**, 3969–3973, 1995. doi: 10.1103/PhysRevLett.75.3969.
- [49] T. Davydova and A. Fishchuk. Upper hybrid nonlinear wave structures. *Ukr. J. Phys.* **40**, 487, 1995.
- [50] J. Day and J. Beamish. Low-temperature shear modulus changes in solid He-4 and connection to supersolidity. *Nature* **450**, 853–856, 2007. doi: 10.1038/nature06383.
- [51] Y. N. M. de Escobar, P. G. Mickelson, M. Yan, B. J. DeSalvo, S. B. Nagel, and T. C. Killian. Bose-Einstein Condensation of  $^{84}\text{Sr}$ . *Phys. Rev. Lett.* **103**, 200402, 2009. doi: 10.1103/PhysRevLett.103.200402.

- 
- [52] E. Demler and F. Zhou. Spinor Bosonic Atoms in Optical Lattices: Symmetry Breaking and Fractionalization. *Phys. Rev. Lett.* **88**, 163001, 2002. doi: 10.1103/PhysRevLett.88.163001.
- [53] J. Denschlag, J. E. Simsarian, D. L. Feder, C. W. Clark, L. A. Collins, J. Cubizolles, L. Deng, E. W. Hagley, K. Helmerson, W. P. Reinhardt, S. L. Rolston, B. I. Schneider, and W. D. Phillips. Generating Solitons by Phase Engineering of a Bose-Einstein Condensate. *Science* **287**, (5450) 97–101, 2000. doi: 10.1126/science.287.5450.97.
- [54] S. Diehl, A. Micheli, A. Kantian, B. Kraus, H. P. Büchler, and P. Zoller. *Nature Physics* **4**, 878–883, 2008. doi: 10.1038/nphys1073.
- [55] O. W. Dietrich, E. H. Graf, C. H. Huang, and L. Passell. Neutron Scattering by Rotons in Liquid Helium. *Phys. Rev. A* **5**, 1377–1391, 1972. doi: 10.1103/PhysRevA.5.1377.
- [56] O. Dutta, R. Kanamoto, and P. Meystre. Fermionic Stabilization and Density-Wave Ground State of a Polar Condensate. *Phys. Rev. Lett.* **99**, 110404, 2007. doi: 10.1103/PhysRevLett.99.110404.
- [57] N. Dyumin, S. Svatko, and V. Grigor'ev. *Sov. J. Low Temp. Phys.* **15**, 295.
- [58] A. Einstein. Quantentheorie des einatomigen idealen Gases. *Sitzungsberichte der Preussischen Akademie der Wissenschaften* **1**, 261, 1924. doi: 10.1002/3527608958.ch27.
- [59] A. Einstein. Quantentheorie des einatomigen idealen Gases, zweite Abhandlung. *Sitzungsberichte der Preussischen Akademie der Wissenschaften* **1**, 3, 1925. doi: 10.1002/3527608958.ch28.
- [60] P. O. Fedichev, Y. Kagan, G. V. Shlyapnikov, and J. T. M. Walraven. Influence of Nearly Resonant Light on the Scattering Length in Low-Temperature Atomic Gases. *Phys. Rev. Lett.* **77**, 2913–2916, 1996. doi: 10.1103/PhysRevLett.77.2913.
- [61] P. O. Fedichev, M. W. Reynolds, and G. V. Shlyapnikov. Three-Body Recombination of Ultracold Atoms to a Weakly Bound  $s$  Level. *Phys. Rev. Lett.* **77**, 2921–2924, 1996. doi: 10.1103/PhysRevLett.77.2921.
- [62] R. P. Feynman. Superfluidity and Superconductivity. *Rev. Mod. Phys.* **29**, 205–212, 1957. doi: 10.1103/RevModPhys.29.205.
- [63] R. P. Feynman. The Messenger Lectures. 1964.
- [64] R. P. Feynman and M. Cohen. Energy Spectrum of the Excitations in Liquid Helium. *Phys. Rev.* **102**, 1189–1204, 1956. doi: 10.1103/PhysRev.102.1189.

- [65] D. S. Fisher and P. C. Hohenberg. Dilute Bose gas in two dimensions. *Phys. Rev. B* **37**, 4936–4943, 1988. doi: 10.1103/PhysRevB.37.4936.
- [66] D. G. Fried, T. C. Killian, L. Willmann, D. Landhuis, S. C. Moss, D. Kleppner, and T. J. Greytak. Bose-Einstein Condensation of Atomic Hydrogen. *Phys. Rev. Lett.* **81**, 3811–3814, 1998. doi: 10.1103/PhysRevLett.81.3811.
- [67] H. Friedrich. *Theoretical Atomic Physics*. Springer, Berlin, 1994.
- [68] M. Frigo and S. Johnson. The Design and Implementation of FFTW3. *Proceedings of the IEEE* **93**, (2) 216–231, 2005. doi: 10.1109/JPROC.2004.840301.
- [69] A. Gaëtan, Y. Miroshnychenko, T. Wilk, A. Chotia, M. Viteau, D. Comparat, P. Pillet, A. Browaeys, and P. Grangier. Observation of collective excitation of two individual atoms in the Rydberg blockade regime. *Nature Physics* **5**, 115–118, 2009. doi: 10.1038/nphys1183.
- [70] T. F. Gallagher. *Rydberg Atoms*. Cambridge University Press, Cambridge, 2005.
- [71] D. E. Galli and L. Reatto. Solid  $^4\text{He}$  and the Supersolid Phase: from Theoretical Speculation to the Discovery of a New State of Matter? A Review of the Past and Present Status of Research. *Journal of the Physical Society of Japan* **77**, (11) 111010, 2008. doi: 10.1143/JPSJ.77.111010.
- [72] C. Gardiner and P. Zoller. *Quantum Noise*. Springer, Berlin, 2000.
- [73] S. Giovanazzi, D. O’Dell, and G. Kurizki. Self-binding transition in Bose condensates with laser-induced “gravitation”. *Phys. Rev. A* **63**, 031603, 2001. doi: 10.1103/PhysRevA.63.031603.
- [74] S. Giovanazzi, D. O’Dell, and G. Kurizki. Density Modulations of Bose-Einstein Condensates via Laser-Induced Interactions. *Phys. Rev. Lett.* **88**, 130402, 2002. doi: 10.1103/PhysRevLett.88.130402.
- [75] Y. Gnedin, A. Mihajlov, L. Ignjatović, N. Sakan, V. Srećković, M. Zakharov, N. Bezuglov, and A. Klycharev. Rydberg atoms in astrophysics. *New Astronomy Reviews* **53**, (7–10) 259 – 265, 2009. doi: 10.1016/j.newar.2009.07.003.
- [76] E. Gomez, S. Aubin, L. A. Orozco, and G. D. Sprouse. Lifetime and hyperfine splitting measurements on the 7s and 6p levels in rubidium. *J. Opt. Soc. Am. B* **21**, (11) 2058–2067, 2004. doi: 10.1364/JOSAB.21.002058.
- [77] K. Góral, K. Rzażewski, and T. Pfau. Bose-Einstein condensation with magnetic dipole-dipole forces. *Phys. Rev. A* **61**, 051601, 2000. doi: 10.1103/PhysRevA.61.051601.

- 
- [78] A. V. Gorshkov, J. Otterbach, M. Fleischhauer, T. Pohl, and M. D. Lukin. Photon-Photon Interactions via Rydberg Blockade. *Phys. Rev. Lett.* **107**, 133602, 2011. doi: 10.1103/PhysRevLett.107.133602.
- [79] M. Greiner, O. Mandel, T. Esslinger, T. W. Hänsch, and I. Bloch. Quantum phase transition from a superfluid to a Mott insulator in a gas of ultracold atoms. *Nature* **415**, 39–44, 2002. doi: 10.1038/415039a.
- [80] D. S. Greywall. Search for superfluidity in solid  $^4\text{He}$ . *Phys. Rev. B* **16**, 1291–1292, 1977. doi: 10.1103/PhysRevB.16.1291.
- [81] A. Griesmaier, J. Werner, S. Hensler, J. Stuhler, and T. Pfau. Bose-Einstein Condensation of Chromium. *Phys. Rev. Lett.* **94**, 160401, 2005. doi: 10.1103/PhysRevLett.94.160401.
- [82] A. Griffin. Conserving and gapless approximations for an inhomogeneous Bose gas at finite temperatures. *Phys. Rev. B* **53**, 9341–9347, 1996. doi: 10.1103/PhysRevB.53.9341.
- [83] E. P. Gross. Unified Theory of Interacting Bosons. *Phys. Rev.* **106**, 161–162, 1957. doi: 10.1103/PhysRev.106.161.
- [84] E. P. Gross. Classical theory of boson wave fields. *Annals of Physics* **4**, (1) 57 – 74, 1958. doi: 10.1016/0003-4916(58)90037-X.
- [85] K. Gross, C. P. Search, H. Pu, W. Zhang, and P. Meystre. Magnetism in a lattice of spinor Bose-Einstein condensates. *Phys. Rev. A* **66**, 033603, 2002. doi: 10.1103/PhysRevA.66.033603.
- [86] R. F. Gutterres, C. Amiot, A. Fioretti, C. Gabbanini, M. Mazzoni, and O. Dulieu. Determination of the  $^{87}\text{Rb}$   $5p$  state dipole matrix element and radiative lifetime from the photoassociation spectroscopy of the  $\text{Rb}_2 0_g^-(P_{3/2})$  long-range state. *Phys. Rev. A* **66**, 024502, 2002. doi: 10.1103/PhysRevA.66.024502.
- [87] Z. Hadzibabic, P. Krüger, M. Cheneau, B. Battelier, and J. Dalibard. Berezinskii-Kosterlitz-Thouless crossover in a trapped atomic gas. *Nature* **441**, 1118–1121, 2006. doi: 10.1038/nature04851.
- [88] J. Han, Y. Jamil, D. V. L. Norum, P. J. Tanner, and T. F. Gallagher. Rb  $nf$  quantum defects from millimeter-wave spectroscopy of cold  $^{85}\text{Rb}$  Rydberg atoms. *Phys. Rev. A* **74**, 054502, 2006. doi: 10.1103/PhysRevA.74.054502.
- [89] R. Heidemann, U. Raitzsch, V. Bendkowsky, B. Butscher, R. Löw, and T. Pfau. Rydberg Excitation of Bose-Einstein Condensates. *Phys. Rev. Lett.* **100**, 033601, 2008. doi: 10.1103/PhysRevLett.100.033601.

- [90] N. Henkel, F. Cinti, P. Jain, G. Pupillo, and T. Pohl. Supersolid Vortex Crystals in Rydberg-Dressed Bose-Einstein Condensates. *Phys. Rev. Lett.* **108**, 265301, 2012. doi: 10.1103/PhysRevLett.108.265301.
- [91] N. Henkel, R. Nath, and T. Pohl. Three-Dimensional Roton Excitations and Supersolid Formation in Rydberg-Excited Bose-Einstein Condensates. *Phys. Rev. Lett.* **104**, 195302, 2010. doi: 10.1103/PhysRevLett.104.195302.
- [92] D. G. Henshaw and A. D. B. Woods. Modes of Atomic Motions in Liquid Helium by Inelastic Scattering of Neutrons. *Phys. Rev.* **121**, 1266–1274, 1961. doi: 10.1103/PhysRev.121.1266.
- [93] J. Honer, H. Weimer, T. Pfau, and H. P. Büchler. Collective Many-Body Interaction in Rydberg Dressed Atoms. *Phys. Rev. Lett.* **105**, 160404, 2010. doi: 10.1103/PhysRevLett.105.160404.
- [94] S. Inouye, M. R. Andrews, J. Stenger, H.-J. Miesner, D. M. Stamper-Kurn, and W. Ketterle. Observation of Feshbach resonances in a Bose-Einstein condensate. *Nature* **392**, 151–154, 1998. doi: 10.1038/32354.
- [95] D. Jaksch, C. Bruder, J. I. Cirac, C. W. Gardiner, and P. Zoller. Cold Bosonic Atoms in Optical Lattices. *Phys. Rev. Lett.* **81**, 3108–3111, 1998. doi: 10.1103/PhysRevLett.81.3108.
- [96] D. Jaksch, J. I. Cirac, P. Zoller, S. L. Rolston, R. Côté, and M. D. Lukin. Fast Quantum Gates for Neutral Atoms. *Phys. Rev. Lett.* **85**, 2208–2211, 2000. doi: 10.1103/PhysRevLett.85.2208.
- [97] C. Josserand, Y. Pomeau, and S. Rica. Coexistence of Ordinary Elasticity and Superfluidity in a Model of a Defect-Free Supersolid. *Phys. Rev. Lett.* **98**, 195301, 2007. doi: 10.1103/PhysRevLett.98.195301.
- [98] P. Kapitza. Viscosity of Liquid Helium below the  $\lambda$ -Point. *Nature* **141**, 74, 1938. doi: 10.1038/141074a0.
- [99] V. A. Kashurnikov, N. V. Prokof'ev, and B. V. Svistunov. Critical Temperature Shift in Weakly Interacting Bose Gas. *Phys. Rev. Lett.* **87**, 120402, 2001. doi: 10.1103/PhysRevLett.87.120402.
- [100] W. Ketterle. Nobel lecture: When atoms behave as waves: Bose-Einstein condensation and the atom laser. *Rev. Mod. Phys.* **74**, 1131–1151, 2002. doi: 10.1103/RevModPhys.74.1131.
- [101] D. Y. Kim and M. H. W. Chan. Absence of Supersolidity in Solid Helium in Porous Vycor Glass. *Phys. Rev. Lett.* **109**, 155301, 2012. doi: 10.1103/PhysRevLett.109.155301.

- 
- [102] E. Kim and M. H. W. Chan. Probable observation of a supersolid helium phase. *Nature* **427**, 225–227. doi: 10.1038/nature02220.
- [103] E. Kim and M. H. W. Chan. Observation of Superflow in Solid Helium. *Science* **305**, (5692) 1941–1944, 2004. doi: 10.1126/science.1101501.
- [104] E. Kim and M. H. W. Chan. Supersolid Helium at High Pressure. *Phys. Rev. Lett.* **97**, 115302, 2006. doi: 10.1103/PhysRevLett.97.115302.
- [105] T. Kinoshita, T. Wenger, and D. S. Weiss. Observation of a One-Dimensional Tonks-Girardeau Gas. *Science* **305**, (5687) 1125–1128, 2004. doi: 10.1126/science.1100700.
- [106] Y. S. Kivshar and G. Agrawal. *Optical Solitons: From Fibers to Photonic Crystals*. Academic Press, San Diego, 2003.
- [107] Y. S. Kivshar and B. Luther-Davies. Dark optical solitons: physics and applications. *Phys. Rep.* **298**, 81–197, 1998. doi: 10.1016/S0370-1573(97)00073-2.
- [108] J. Klaers, J. Schmitt, F. Vewinger, and M. Weitz. Bose-Einstein condensation of photons in an optical microcavity. *Nature* **468**, 545–548, 2010. doi: 10.1038/nature09567.
- [109] S. Komineas and N. R. Cooper. Vortex lattices in Bose-Einstein condensates with dipolar interactions beyond the weak-interaction limit. *Phys. Rev. A* **75**, 023623, 2007. doi: 10.1103/PhysRevA.75.023623.
- [110] D. J. Korteweg and G. de Vries. XLI. On the change of form of long waves advancing in a rectangular canal, and on a new type of long stationary waves. *Philosophical Magazine Series 5* **39**, 422–443, 1895.
- [111] J. M. Kosterlitz and D. J. Thouless. Ordering, metastability and phase transitions in two-dimensional systems. *Journal of Physics C: Solid State Physics* **6**, (7) 1181, 1973. doi: 10.1088/0022-3719/6/7/010.
- [112] S. Kraft, F. Vogt, O. Appel, F. Riehle, and U. Sterr. Bose-Einstein Condensation of Alkaline Earth Atoms:  $^{40}\text{Ca}$ . *Phys. Rev. Lett.* **103**, 130401, 2009. doi: 10.1103/PhysRevLett.103.130401.
- [113] V. I. Kruglov and M. J. Collett. Roton Excitation Spectrum in Liquid Helium II. *Phys. Rev. Lett.* **87**, 185302, 2001. doi: 10.1103/PhysRevLett.87.185302.
- [114] T. Lahaye, C. Menotti, L. Santos, M. Lewenstein, and T. Pfau. The physics of dipolar bosonic quantum gases. *Reports on Progress in Physics* **72**, (12) 126401, 2009. doi: 10.1088/0034-4885/72/12/126401.
- [115] L. Landau. Zur Theorie der Energieübertragung. II. *Phys. Z. Sowjetunion* **2**, 46, 1932.

- [116] L. Landau. The theory of superfluidity of helium II. *J. Phys. USSR* **5**, 71, 1941.
- [117] L. Landau. On the Theory of Superfluidity. *Phys. Rev.* **75**, 884–885, 1949. doi: 10.1103/PhysRev.75.884.
- [118] L. Landau and E. Lifshitz. *Quantum mechanics*. Pergamon, 1977.
- [119] A. Leggett. *Quantum liquids*. Oxford Univ. Press, 1938.
- [120] A. J. Leggett. Can a Solid Be "Superfluid"? *Phys. Rev. Lett.* **25**, 1543–1546, 1970. doi: 10.1103/PhysRevLett.25.1543.
- [121] H. A. Leth, L. B. Madsen, and K. Mølmer. Monte Carlo wave packet approach to dissociative multiple ionization in diatomic molecules. *Phys. Rev. A* **81**, 053409, 2010. doi: 10.1103/PhysRevA.81.053409.
- [122] P. D. Lett, R. N. Watts, C. I. Westbrook, W. D. Phillips, P. L. Gould, and H. J. Metcalf. Observation of Atoms Laser Cooled below the Doppler Limit. *Phys. Rev. Lett.* **61**, 169–172, 1988. doi: 10.1103/PhysRevLett.61.169.
- [123] W. Li, I. Mourachko, M. W. Noel, and T. F. Gallagher. Millimeter-wave spectroscopy of cold Rb Rydberg atoms in a magneto-optical trap: Quantum defects of the *ns*, *np*, and *nd* series. *Phys. Rev. A* **67**, 052502, 2003. doi: 10.1103/PhysRevA.67.052502.
- [124] W. Li, T. Pohl, J. M. Rost, S. T. Rittenhouse, H. R. Sadeghpour, J. Nipper, B. Butscher, J. B. Balewski, V. Bendkowsky, R. Löw, and T. Pfau. A Homonuclear Molecule with a Permanent Electric Dipole Moment. *Science* **334**, (6059) 1110–1114, 2011. doi: 10.1126/science.1211255.
- [125] R. Loew, U. Raitzsch, R. Heidemann, V. Bendkowsky, B. Butscher, A. Grabowski, and T. Pfau. Apparatus for excitation and detection of Rydberg atoms in quantum gases. arXiv:0706.2639.
- [126] F. London. *Superfluids: Macroscopic theory of superfluid helium*. Wiley, 1954.
- [127] M. Lu, N. Q. Burdick, S. H. Youn, and B. L. Lev. Strongly Dipolar Bose-Einstein Condensate of Dysprosium. *Phys. Rev. Lett.* **107**, 190401, 2011. doi: 10.1103/PhysRevLett.107.190401.
- [128] M. D. Lukin, M. Fleischhauer, R. Cote, L. M. Duan, D. Jaksch, J. I. Cirac, and P. Zoller. Dipole Blockade and Quantum Information Processing in Mesoscopic Atomic Ensembles. *Phys. Rev. Lett.* **87**, 037901, 2001. doi: 10.1103/PhysRevLett.87.037901.
- [129] P. M. Lushnikov. Collapse and stable self-trapping for Bose-Einstein condensates with  $1/r^b$ -type attractive interatomic interaction potential. *Phys. Rev. A* **82**, 023615, 2010. doi: 10.1103/PhysRevA.82.023615.

- 
- [130] R. Löw, H. Weimer, J. Nipper, J. B. Balewski, B. Butscher, H. P. Büchler, and T. Pfau. An experimental and theoretical guide to strongly interacting Rydberg gases. *Journal of Physics B: Atomic, Molecular and Optical Physics* **45**, (11) 113001, 2012. doi: 10.1088/0953-4075/45/11/113001.
- [131] E. Majorana. Atomi orientati in campo magnetico variabile. *Il Nuovo Cimento (1924-1942)* **9**, 43–50, 1932.
- [132] B. A. Malomed, D. Mihalache, F. Wise, and L. Torner. Spatiotemporal optical solitons. *Journal of Optics B: Quantum and Semiclassical Optics* **7**, (5) R53, 2005. doi: 10.1088/1464-4266/7/5/R02.
- [133] M. Marinescu, H. R. Sadeghpour, and A. Dalgarno. Dispersion coefficients for alkali-metal dimers. *Phys. Rev. A* **49**, 982–988, 1994. doi: 10.1103/PhysRevA.49.982.
- [134] H. J. Maris. Effect of elasticity on torsional oscillator experiments probing the possible supersolidity of helium. *Phys. Rev. B* **86**, 020502, 2012. doi: 10.1103/PhysRevB.86.020502.
- [135] G. Marsaglia and T. A. Bray. A Convenient Method for Generating Normal Variables. *Soc. Ind. Appl. Math. Rev.* **6**, (3) 260–264, 1964. doi: 10.1137/1006063.
- [136] A. Marte, T. Volz, J. Schuster, S. Dürr, G. Rempe, E. G. M. van Kempen, and B. J. Verhaar. Feshbach Resonances in Rubidium 87: Precision Measurement and Analysis. *Phys. Rev. Lett.* **89**, 283202, 2002. doi: 10.1103/PhysRevLett.89.283202.
- [137] F. Maucher, N. Henkel, M. Saffman, W. Królikowski, S. Skupin, and T. Pohl. Rydberg-Induced Solitons: Three-Dimensional Self-Trapping of Matter Waves. *Phys. Rev. Lett.* **106**, 170401, 2011. doi: 10.1103/PhysRevLett.106.170401.
- [138] F. Maucher, S. Skupin, and W. Krolikowski. Collapse in the nonlocal nonlinear Schrödinger equation. *Nonlinearity* **24**, 1987–2001, 2011. doi: 10.1088/0951-7715/24/7/005.
- [139] C. Meijer. Über Whittakersche bzw. Besselsche Funktionen und deren Produkte. *Nieuw Archief voor Wiskunde* (2) **18**, (4) 10–39, 1936.
- [140] M. W. Meisel. Supersolid  $^4\text{He}$ : an overview of past searches and future possibilities. *Physica B: Condensed Matter* **178**, (1–4) 121–128, 1992. doi: 10.1016/0921-4526(92)90186-V.
- [141] A. Micheli, G. Pupillo, H. P. Büchler, and P. Zoller. Cold polar molecules in two-dimensional traps: Tailoring interactions with external fields for novel quantum phases. *Phys. Rev. A* **76**, 043604, 2007. doi: 10.1103/PhysRevA.76.043604.

- [142] S. Minardi, F. Eilenberger, Y. V. Kartashov, A. Szameit, U. Röpke, J. Kobelke, K. Schuster, H. Bartelt, S. Nolte, L. Torner, F. Lederer, A. Tünnermann, and T. Pertsch. Three-Dimensional Light Bullets in Arrays of Waveguides. *Phys. Rev. Lett.* **105**, 263901, 2010. doi: 10.1103/PhysRevLett.105.263901.
- [143] G. Modugno, G. Ferrari, G. Roati, R. J. Brecha, A. Simoni, and M. Inguscio. Bose-Einstein Condensation of Potassium Atoms by Sympathetic Cooling. *Science* **294**, 1320–1322, 2001. doi: 10.1126/science.1066687.
- [144] R. Mukherjee, J. Millen, R. Nath, M. P. A. Jones, and T. Pohl. Many-body physics with alkaline-earth Rydberg lattices. *Journal of Physics B: Atomic, Molecular and Optical Physics* **44**, (18) 184010, 2011.
- [145] M. E. J. Newman and G. T. Barkema. *Monte Carlo Methods in Statistical Physics*. Clarendon Press, 1999. doi: 10.1137/1.9780898719628.
- [146] P. Nozières. In A. Griffin, D. Snoke, and S. Stringari, editors, *Bose-Einstein Condensation*. Cambridge University Press, 1995.
- [147] D. O’Dell, S. Giovanazzi, G. Kurizki, and V. M. Akulin. Bose-Einstein Condensates with  $1/r$  Interatomic Attraction: Electromagnetically Induced “Gravity”. *Phys. Rev. Lett.* **84**, 5687–5690, 2000. doi: 10.1103/PhysRevLett.84.5687.
- [148] M. Olshanii. Atomic Scattering in the Presence of an External Confinement and a Gas of Impenetrable Bosons. *Phys. Rev. Lett.* **81**, 938–941, 1998. doi: 10.1103/PhysRevLett.81.938.
- [149] H. Palevsky, K. Otnes, and K. E. Larsson. Excitation of Rotons in Helium II by Cold Neutrons. *Phys. Rev.* **112**, 11–18, 1958. doi: 10.1103/PhysRev.112.11.
- [150] B. Paredes, A. Widera, V. Murg, O. Mandel, S. Fölling, I. Cirac, G. V. Shlyapnikov, T. W. Hänsch, and I. Bloch. Tonks-Girardeau gas of ultracold atoms in an optical lattice. *Nature* **429**, 277–281, 2004. doi: 10.1038/nature02530.
- [151] O. Penrose and L. Onsager. Bose-Einstein Condensation and Liquid Helium. *Phys. Rev.* **104**, 576–584, 1956. doi: 10.1103/PhysRev.104.576.
- [152] F. Pereira Dos Santos, J. Léonard, J. Wang, C. J. Barrelet, F. Perales, E. Rasel, C. S. Unnikrishnan, M. Leduc, and C. Cohen-Tannoudji. Bose-Einstein Condensation of Metastable Helium. *Phys. Rev. Lett.* **86**, 3459–3462, 2001. doi: 10.1103/PhysRevLett.86.3459.
- [153] D. S. Petrov. Three-Boson Problem near a Narrow Feshbach Resonance. *Phys. Rev. Lett.* **93**, 143201, 2004. doi: 10.1103/PhysRevLett.93.143201.
- [154] D. S. Petrov, G. V. Shlyapnikov, and J. T. M. Walraven. Regimes of Quantum Degeneracy in Trapped 1D Gases. *Phys. Rev. Lett.* **85**, 3745–3749, 2000. doi: 10.1103/PhysRevLett.85.3745.

- 
- [155] T. Peyronel, O. Firstenberg, Q.-Y. Liang, S. Hofferberth, A. V. Gorshkov, T. Pohl, M. D. Lukin, and V. Vuletic. Quantum nonlinear optics with single photons enabled by strongly interacting atoms. *Nature* **488**, 57, 2012. doi: 10.1038/nature11361.
- [156] T. G. Philbin, C. Kuklewicz, S. Robertson, S. Hill, F. König, and U. Leonhardt. Fiber-Optical Analog of the Event Horizon. *Science* **319**, (5868) 1367–1370, 2008. doi: 10.1126/science.1153625.
- [157] L. Pitaevskii and S. Stringari. *Bose-Einstein Condensation*. Clarendon Press, Oxford, 2003.
- [158] T. Pohl, E. Demler, and M. D. Lukin. Dynamical Crystallization in the Dipole Blockade of Ultracold Atoms. *Phys. Rev. Lett.* **104**, 043002, 2010. doi: 10.1103/PhysRevLett.104.043002.
- [159] T. Pohl, D. Vrinceanu, and H. R. Sadeghpour. Rydberg Atom Formation in Ultracold Plasmas: Small Energy Transfer with Large Consequences. *Phys. Rev. Lett.* **100**, 223201, 2008. doi: 10.1103/PhysRevLett.100.223201.
- [160] Y. Pomeau and S. Rica. Dynamics of a model of supersolid. *Phys. Rev. Lett.* **72**, 2426–2429, 1994. doi: 10.1103/PhysRevLett.72.2426.
- [161] M. Porkolab and M. V. Goldman. Upper hybrid solitons and oscillating two-stream instabilities. *Phys. Fluids* **19**, 872, 1976. doi: 10.1063/1.861553.
- [162] E. J. Pratt, B. Hunt, V. Gadagkar, M. Yamashita, M. J. Graf, A. V. Balatsky, and J. C. Davis. Interplay of Rotational, Relaxational, and Shear Dynamics in Solid  $^4\text{He}$ . *Science* **332**, (6031) 821–824, 2011. doi: 10.1126/science.1203080.
- [163] J. D. Pritchard, K. J. Weatherill, and C. S. Adams. Non-linear optics using cold Rydberg atoms. arXiv:1205.4890.
- [164] N. Prokof'ev and B. Svistunov. Supersolid State of Matter. *Phys. Rev. Lett.* **94**, 155302, 2005. doi: 10.1103/PhysRevLett.94.155302.
- [165] G. Pupillo, A. Micheli, M. Boninsegni, I. Lesanovsky, and P. Zoller. Strongly Correlated Gases of Rydberg-Dressed Atoms: Quantum and Classical Dynamics. *Phys. Rev. Lett.* **104**, 223002, 2010. doi: 10.1103/PhysRevLett.104.223002.
- [166] G. Racah. Theory of Complex Spectra. II. *Phys. Rev.* **62**, 438–462, 1942. doi: 10.1103/PhysRev.62.438.
- [167] C. Raman, J. R. Abo-Shaeer, J. M. Vogels, K. Xu, and W. Ketterle. Vortex Nucleation in a Stirred Bose-Einstein Condensate. *Phys. Rev. Lett.* **87**, (21) 210402, 2001. doi: 10.1103/PhysRevLett.87.210402.

- [168] M. Reetz-Lamour, T. Amthor, J. Deiglmayr, and M. Weidemüller. Rabi Oscillations and Excitation Trapping in the Coherent Excitation of a Mesoscopic Frozen Rydberg Gas. *Phys. Rev. Lett.* **100**, 253001, 2008. doi: 10.1103/PhysRevLett.100.253001.
- [169] A. Reinhard, T. C. Liebisch, B. Knuffman, and G. Raithel. Level shifts of rubidium Rydberg states due to binary interactions. *Phys. Rev. A* **75**, 032712, 2007. doi: 10.1103/PhysRevA.75.032712.
- [170] J. D. Reppy. Nonsuperfluid Origin of the Nonclassical Rotational Inertia in a Bulk Sample of Solid  $^4\text{He}$ . *Phys. Rev. Lett.* **104**, 255301, 2010. doi: 10.1103/PhysRevLett.104.255301.
- [171] X. Rojas, A. Haziot, V. Bapst, S. Balibar, and H. J. Maris. Anomalous Softening of  $^4\text{He}$  Crystals. *Phys. Rev. Lett.* **105**, 145302, 2010. doi: 10.1103/PhysRevLett.105.145302.
- [172] S. Ronen and J. L. Bohn. Dipolar Bose-Einstein condensates at finite temperature. *Phys. Rev. A* **76**, 043607, 2007. doi: 10.1103/PhysRevA.76.043607.
- [173] R. Rota and J. Boronat. Path Integral Monte Carlo Calculation of Momentum Distribution in Solid  $^4\text{He}$ . *J. Low. Temp. Phys.* **162**, 146, 2011. doi: 10.1007/s10909-010-0249-5.
- [174] J. S. Russel. Report on Waves. *Report of the 14th Meeting of the British Association for the Advancement of Science* **1**, 311–390, 1844.
- [175] M. Saffman, T. G. Walker, and K. Mølmer. Quantum information with Rydberg atoms. *Rev. Mod. Phys.* **82**, 2313–2363, 2010. doi: 10.1103/RevModPhys.82.2313.
- [176] L. Santos, G. V. Shlyapnikov, and M. Lewenstein. Roton-Maxon Spectrum and Stability of Trapped Dipolar Bose-Einstein Condensates. *Phys. Rev. Lett.* **90**, 250403, 2003. doi: 10.1103/PhysRevLett.90.250403.
- [177] L. Santos, G. V. Shlyapnikov, P. Zoller, and M. Lewenstein. Bose-Einstein Condensation in Trapped Dipolar Gases. *Phys. Rev. Lett.* **85**, 1791–1794, 2000. doi: 10.1103/PhysRevLett.85.1791.
- [178] M. Schlesinger, M. Mudrich, F. Stienkemeier, and W. Strunz. Evidence for Landau’s critical velocity in superfluid helium nanodroplets from wave packet dynamics of attached potassium dimers. arXiv:0909.4691.
- [179] K. Schmidt, J. Dorier, and A. Läuchli. Solids and Supersolids of Three-Body Interacting Polar Molecules on an Optical Lattice. *Phys. Rev. Lett.* **101**, 150405, 2008. doi: 10.1103/PhysRevLett.101.150405.

- 
- [180] S. Sevinçli, N. Henkel, C. Ates, and T. Pohl. Nonlocal Nonlinear Optics in Cold Rydberg Gases. *Phys. Rev. Lett.* **107**, 153001, 2011. doi: 10.1103/PhysRevLett.107.153001.
- [181] Y. Silberberg. Collapse of optical pulses. *Opt. Lett.* **15**, (22) 1282–1284, 1990. doi: 10.1364/OL.15.001282.
- [182] K. Singer, J. Stanojevic, M. Weidemüller, and R. Côté. Long-range interactions between alkali Rydberg atom pairs correlated to the  $ns - ns$ ,  $np - np$  and  $nd - nd$  asymptotes. *J. Phys. B* **38**, (2) S295, 2005. doi: 10.1088/0953-4075/38/2/021.
- [183] R. P. Smith, R. L. D. Campbell, N. Tammuz, and Z. Hadzibabic. Effects of Interactions on the Critical Temperature of a Trapped Bose Gas. *Phys. Rev. Lett.* **106**, 250403, 2011. doi: 10.1103/PhysRevLett.106.250403.
- [184] S. Stellmer, M. K. Tey, B. Huang, R. Grimm, and F. Schreck. Bose-Einstein Condensation of Strontium. *Phys. Rev. Lett.* **103**, 200401, 2009. doi: 10.1103/PhysRevLett.103.200401.
- [185] S. V. Stepkin, A. A. Konovalenko, N. G. Kantharia, and N. Udaya Shankar. Radio recombination lines from the largest bound atoms in space. *Mon. Not. Roy. Astron. Soc.* **374**, 852–856, 2007. doi: 10.1111/j.1365-2966.2006.11190.x.
- [186] K. E. Strecker, G. B. Partridge, A. G. Truscott, and R. G. Hulet. Formation and propagation of matter-wave soliton trains. *Nature* **417**, 150–153, 2002. doi: 10.1038/nature747.
- [187] K. E. Strecker, G. B. Partridge, A. G. Truscott, and R. G. Hulet. Bright matter wave solitons in Bose–Einstein condensates. *New Journal of Physics* **5**, (1) 73, 2003. doi: 10.1088/1367-2630/5/1/373.
- [188] E. Stükelberg. Theorie der unelastischen Stöße zwischen Atomen. *Helvetica Physica Acta* **5**, 24, 1932. doi: 10.5169/seals-110177.
- [189] H. Suzuki. Plastic Flow in Solid Helium. *Journal of the Physical Society of Japan* **35**, (5) 1472–1479, 1973. doi: 10.1143/JPSJ.35.1472.
- [190] Y. Takasu, K. Maki, K. Komori, T. Takano, K. Honda, M. Kumakura, T. Yabuzaki, and Y. Takahashi. Spin-Singlet Bose-Einstein Condensation of Two-Electron Atoms. *Phys. Rev. Lett.* **91**, 040404, 2003. doi: 10.1103/PhysRevLett.91.040404.
- [191] G. Taubes. Hot on the Trail of a Cold Mystery. *Science* **265**, (5169) 184–186, 1994. doi: 10.1126/science.265.5169.184.
- [192] M. Tsubota, K. Kasamatsu, and M. Ueda. Vortex lattice formation in a rotating Bose-Einstein condensate. *Phys. Rev. A* **65**, (2) 023603, 2002. doi: 10.1103/PhysRevA.65.023603.

- [193] V. Tsympalenko. *Sov. Phys. JETP Lett.* **23**, 653, 1976.
- [194] E. Urban, T. A. Johnson, T. Henage, L. Isenhower, D. D. Yavuz, T. G. Walker, and M. Saffman. Observation of Rydberg blockade between two atoms. *Nature Physics* **5**, 110–114, 2009. doi: 10.1038/nphys1178.
- [195] C. L. Vaillant, M. P. A. Jones, and R. M. Potvliege. Long-range Rydberg–Rydberg interactions in calcium, strontium and ytterbium. *Journal of Physics B: Atomic, Molecular and Optical Physics* **45**, (13) 135004, 2012. doi: 10.1088/0953-4075/45/13/135004.
- [196] G. Vitrant, J. M. Raimond, M. Gross, and S. Haroche. Rydberg to plasma evolution in a dense gas of very excited atoms. *Journal of Physics B: Atomic and Molecular Physics* **15**, (2) L49, 1982. doi: 10.1088/0022-3700/15/2/004.
- [197] S. N. Vlasov, V. A. Petrishchev, and V. I. Talanov. Averaged description of wave beams in linear and nonlinear media (the method of moments). *Radiophysics and Quantum Electronics* **14**, 1062–1070, 1971. doi: 10.1007/BF01029467.
- [198] T. G. Walker and M. Saffman. Zeros of Rydberg–Rydberg Förster interactions. *Journal of Physics B: Atomic, Molecular and Optical Physics* **38**, (2) S309, 2005. doi: 10.1088/0953-4075/38/2/022.
- [199] T. G. Walker and M. Saffman. Consequences of Zeeman degeneracy for the van der Waals blockade between Rydberg atoms. *Phys. Rev. A* **77**, 032723, 2008. doi: 10.1103/PhysRevA.77.032723.
- [200] T. Weber, J. Herbig, M. Mark, H.-C. Nägerl, and R. Grimm. Bose-Einstein Condensation of Cesium. *Science* **299**, (5604) 232–235, 2003. doi: 10.1126/science.1079699.
- [201] M. I. Weinstein. Nonlinear Schrödinger equations and sharp interpolation estimates. *Communications in Mathematical Physics* **87**, 567–576, 1983.
- [202] P. Westphal, S. Koch, A. Horn, J. Schmand, and H. J. Andrä. Low-velocity elastic scattering of Rb–Rb. *Phys. Rev. A* **56**, 2784–2787, 1997. doi: 10.1103/PhysRevA.56.2784.
- [203] N. K. Wilkin and J. M. F. Gunn. Condensation of “Composite Bosons” in a Rotating BEC. *Phys. Rev. Lett.* **84**, 6–9, 2000. doi: 10.1103/PhysRevLett.84.6.
- [204] R. M. Wilson, S. Ronen, J. L. Bohn, and H. Pu. Manifestations of the Roton Mode in Dipolar Bose-Einstein Condensates. *Phys. Rev. Lett.* **100**, 245302, 2008. doi: 10.1103/PhysRevLett.100.245302.
- [205] C. N. Yang. Concept of Off-Diagonal Long-Range Order and the Quantum Phases of Liquid He and of Superconductors. *Rev. Mod. Phys.* **34**, 694–704, 1962. doi: 10.1103/RevModPhys.34.694.

- [206] J. L. Yarnell, G. P. Arnold, P. J. Bendt, and E. C. Kerr. Excitations in Liquid Helium: Neutron Scattering Measurements. *Phys. Rev.* **113**, 1379–1386, 1959. doi: 10.1103/PhysRev.113.1379.
- [207] C.-D. Yoo and A. T. Dorsey. Theory of viscoelastic behavior of solid  $^4\text{He}$ . *Phys. Rev. B* **79**, 100504, 2009. doi: 10.1103/PhysRevB.79.100504.
- [208] N. J. Zabusky and M. D. Kruskal. Interaction of “Solitons” in a Collisionless Plasma and the Recurrence of Initial States. *Phys. Rev. Lett.* **15**, 240–243, 1965. doi: 10.1103/PhysRevLett.15.240.
- [209] C. Zener. Non-Adiabatic Crossing of Energy Levels. *Proc. R. Soc. Lond. A* **137**, 696, 1932. doi: 10.1098/rspa.1932.0165.



# Acknowledgements/Danksagung

Während meiner Doktorarbeit wurde ich von vielen Menschen auf unterschiedlichste Art und Weise hervorragend unterstützt, wofür ich mich hier recht herzlich bedanken möchte.

Zunächst danke ich meinem Doktorvater, Prof. Jan-Michael Rost für die Aufnahme in seine Abteilung und viel hilfreichen Rat.

Ganz besonders möchte ich meinem Betreuer, Dr. Thomas Pohl, für seine unermüdliche Betreuung von früh bis spät, innerhalb und außerhalb der Physik, danken. Ich gelobe, dass ich weder deine physikalische Intuition noch die Überlegenheit von echter Thüringer Bratwurst jemals wieder in Zweifel ziehen werde (bei den Äpfeln bin ich aber noch nicht überzeugt).

Viele Mitglieder und Ehemalige der Abteilung haben mir durch (oft laut, manchmal kontrovers geführte) Diskussionen sehr bei der Erarbeitung meiner Dissertation geholfen. Insbesondere möchte ich erwähnen: Stefan Skupin, Fabian Maucher, Sevilay Sevinçli, Fabio Cinti, Tommaso Macri, Rejish Nath, Weibin Li, Michael Genkin und Cenap Ates.

Ferner danke ich Sebastian Wüster, Ulf Saalman, Stefan Skupin, Zachary Walters und Jörg Götte für das Korrekturlesen meiner Arbeit und Hilfe im Umgang mit den Tücken der englischen Sprache.

Für viele höchst interessante und lehrreiche, wenn auch gelegentlich an den Haaren herbeigezogene, außerphysikalische Diskussionen sowie für die Förderung des sportlichen Wettstreits danke ich allen regelmäßigen Mitgliedern der Mittagsrunde: Thomas „Random“ „Propeller“ Pohl, Ulf „Der Bomber der Nation“ Saalman, Gerhard „Übersteiger“ Ritschel, Fabian „Da war alles offen“ Maucher, Laura „Old Surehand“ Gil, Sebastian „Catenaccio“ Möbius, Adrian „Slowhand“ Sanz Mora und Georg „Volles Rohr“ Bannasch.

Meinem Bürogenossen Abraham Camacho danke ich für mehrere Jahre tolle Büroatmosphäre, friedliche Koexistenz sowie interkulturelle Diskussionen über das lateinamerikanische Verständnis von (den in gewisser Weise ja physikalisch relevanten Themen) Temperatur und Zeit. Speziell danke ich ihm für die Einführung in richtiges mexikanisches Essen (es war nicht wirklich zu scharf, das waren Freudentränen).

Für viele Jahre der Freundschaft danke ich Jan Metje. Und denk dran: Nicht mit dem verbleibenden Auge in den Laser sehen.

Ganz besonders danke ich meiner lieben Freundin Ulrike Georgi für ihre ständige Unterstützung in einer manchmal stressigen Zeit.

Meiner ganzen Familie, insbesondere meinen Eltern Heike und Klaus, danke ich herzlich dafür, dass sie mich immer unterstützt und hinter mir gestanden haben.



# Versicherung

Hiermit versichere ich, dass ich die vorliegende Arbeit ohne unzulässige Hilfe Dritter und ohne Benutzung anderer als der angegebenen Hilfsmittel angefertigt habe; die aus fremden Quellen direkt oder indirekt übernommenen Gedanken sind als solche kenntlich gemacht. Die Arbeit wurde bisher weder im Inland noch im Ausland in gleicher oder ähnlicher Form einer anderen Prüfungsbehörde vorgelegt.

Die Arbeit wurde von Mai 2009 bis Januar 2013 am Max-Planck-Institut für Physik komplexer Systeme in der Abteilung Endliche Systeme angefertigt und von Prof. Dr. Jan-Michael Rost betreut.

Es haben keine früheren erfolglosen Promotionsverfahren stattgefunden.

Ich erkenne die Promotionsordnung der Fakultät Mathematik und Naturwissenschaften der Technischen Universität Dresden vom 23.02.2011 an.

---

Nils Henkel